ANNUAL REPORTS ON NMR SPECTROSCOPY

Volume 10A

ANNUAL REPORTS ON

NMR SPECTROSCOPY

This Page Intentionally Left Blank

ANNUAL REPORTS ON
NMR SPECTROSCOPY

Edited by

G. A. WEBB

Department of Chemical Physics, University of Surrey, Guildford, Surrey, England

VOLUME 10A

1980

ACADEMIC PRESS

A Subsidiary of Harcourt Brace Jovanovich, Publishers

London • New York • Toronto • Sydney • San Francisco

ACADEMIC PRESS INC. (LONDON) LTD.
24–28 Oval Road,
London, NW1 7DX

U.S. Edition Published by

ACADEMIC PRESS INC.
111 Fifth Avenue
New York, New York 10003

British Library Cataloguing in Publication Data

Annual reports on *NMR* spectroscopy.
Vol. 10A
1. Nuclear magnetic resonance spectroscopy
I. Webb, Graham Alan
541'.28 QD96.N8 68–17678

ISBN 0–12505310–X
ISSN 0066–4103

Printed in Great Britain by J. W. Arrowsmith Ltd.
Bristol BS3 2NT

LIST OF CONTRIBUTORS

ISAO ANDO, *Department of Polymer Chemistry, Tokyo Institute of Technology, Ookayama, Tokyo, Japan.*

TETSUO ASAKURA, *Department of Polymer Chemistry, Tokyo Institute of Technology, Ookayama, Tokyo, Japan.*

R. GARTH KIDD, *Department of Chemistry, University of Western Ontario, London, Ontario, Canada.*

I. K. O'NEILL, *Laboratory of the Government Chemist, Cornwall House, Stamford Street, London, SE1 9NQ, U.K.* (*Present address*: *RTZ Services Ltd., York House, Bond Street, Bristol, BS1 3PE, U.K.*)

C. P. RICHARDS, *Laboratory of the Government Chemist, Cornwall House, Stamford Street, London, SE1 9NQ, U.K.*

This Page Intentionally Left Blank

PREFACE

The widespread application of the NMR spectroscopy of "other nuclei" is clearly reflected in the contributions to this volume. As with some earlier members of this series of reports, the present volume is split into two parts.

Volume 10B is the more specific one, dealing with the ^{19}F NMR parameters of various series of compounds. It comprises extensive tabulations of ^{19}F NMR data and serves to update reports in earlier volumes of this series.

The range of topics covered in volume 10A indicates some of the numerous areas of science which are dependent upon NMR as a primary investigative tool. The areas covered include transition metal NMR, ^{13}C NMR applications to synthetic polymers, and some uses of ^{31}P NMR in biochemistry.

All the authors writing for volume 10 are new to Annual Reports and, in welcoming their contributions, I wish to thank all of them for their efforts and patience both in the preparation of their manuscripts and of this volume.

University of Surrey,
Guildford, Surrey,
England

G. A. WEBB
December 1979

This Page Intentionally Left Blank

CONTENTS

Nuclear Shielding of the Transition Metals

R. GARTH KIDD

NMR Chemical Shift Calculations and Stereochemical Structures of Synthetic Polymers

ISAO ANDO AND TETSUO ASAKURA

Biological ^{31}P NMR Spectroscopy

I. K. O'NEILL AND C. P. RICHARDS

CONTENTS OF VOLUME 10B

Fluorine-19 Nuclear Magnetic Resonance Spectroscopy (1976–1978)

V. WRAY

Nuclear Shielding of the Transition Metals

R. GARTH KIDD

Department of Chemistry, University of Western Ontario, London, Ontario, Canada

I. INTRODUCTION

The structures and chemical behaviour of compounds containing metal atoms comprise a major portion of that broad field of human endeavour which still goes under the designation of inorganic chemistry. While the first generation of commercial NMR spectrometers proved to be of greatest utility to the organic chemist because of the emphasis on proton detection, the current generation of pulsed Fourier transform (FT) instruments brings the routine detection of metal atom resonances within the realm of reality. During the developing years of NMR spectroscopy starting about 1950, the proton was the focus of attention because of its high detection sensitivity. Its

limited shielding range of 10 ppm in typical organic compounds, later extended to 25–30 ppm by the hydridic protons in metal hydrides, precluded a simple theoretical interpretation for observed shieldings and led to the development of empirical correlations between structure and chemical shift.

In 1950, Ramsey (111) adapted Van Vleck's quantum-mechanical model (203) for magnetic susceptibility to provide a general theoretical formulation for nuclear shielding, and the appearance of ^{19}F and ^{59}Co spectra with chemical shift ranges of 750 ppm and 14 000 ppm provided an opportunity to test Ramsey's shielding theory on systems sufficiently sensitive to reveal the effects of subtle changes in chemical bonding. While the initial NMR focus on protons with their largely s-orbital* participation in bonding led to the association of increased shielding with increased electron density through a diamagnetic mechanism, the Ramsey treatment of ^{19}F shieldings, where p-orbital participation dominates the chemical bonding, attributed 90% of the observed shielding variation to the paramagnetic term σ_p which measures the orbital angular momentum. The other 10% was attributed to the diamagnetic term σ_d which measures the spherically symmetrical part of the electron distribution and is the putative source of non-hydridic proton chemical shifts.

Transition metals are, by definition, those elements for which the d-orbitals play a significant, if not a dominating, role in chemical bonding. This role becomes manifest in those physical properties sensitive to variations in orbital angular momentum, and nuclear shielding is one of these. Other manifestations are temperature-independent paramagnetism and spin–orbit coupling, both of which are larger for transition metal compounds than for compounds of the Main Group elements. Thus, although other factors enter the picture, it is the d-orbital participation with its large orbital angular momentum contribution that is fundamental to the large chemical shifts undergone both by transition metals themselves and by other atoms covalently bonded to them. The ^{59}Co shielding range of 18 000 ppm reflects the combination of all factors, including d-orbital participation, working together to maximize the variation in nuclear shielding.

The Ramsey theory has been successfully applied to the task of calculating nuclear shieldings in some small molecules. At the stage where even modest molecular dimensions are reached, however, the direct application of the Ramsey theory is made impractical by a number of serious drawbacks summarized recently by Webb. (205) The result has been the adoption of different semi-empirical theoretical models for each nucleus studied, most of them based on the average excitation energy (AEE) method discussed in detail in Section VIII in connection with ^{59}Co shieldings. Jameson and

* Recall that the s, p, and d orbital designations reflect 0, 1, and 2 units of orbital angular momentum.

Gutowsky (204) have provided the only theoretical model to be broadly applied across a range of elements, and it too makes use of the AEE formalism. While it is reasonably successful in rationalizing the observed periodicity in chemical shift ranges for the Main Group elements, it has not been applied with any degree of success to a series of transition metals, nor has its efficacy been tested in the cause of rationalizing the incidence of normal versus inverse halogen dependence.

The value of a theoretical model is directly proportional to the number of different systems to which it can be successfully applied, and hence to the generality of the insight it provides. By this measure, no chemical shift theory has been found to apply more broadly than for two or three elements in atomic number sequence or for three or four elements within a Periodic Group. As more broadly based theories of nuclear shielding begin to take form, the body of chemical shift data for the transition metals must inevitably form the anvil upon which these theories are wrought. The body of data here drawn together and analysed has been selected with this end in view. Relaxation data and coupling constants have been included only where they serve this end or where they comprise the only NMR parameters available on a particular element.

A comprehensive review of the transition metal NMR literature to early 1977 is available. (207) Wehrli (206) has surveyed the recent literature on quadrupolar nuclei, many of which are transition metals, to early 1978. The literature to early 1979 has been surveyed for the present report. During the past two years, the transition metals that have received most study are ^{113}Cd and ^{199}Hg; this interest stems from their relationship to biologically active molecules, and they have received more detailed coverage than some of the other elements such as ^{59}Co where NMR knowledge is more extensive but less recent.

A. Magnitude of the paramagnetic term

Any theoretical approach to nuclear shielding which rests on a perturbation treatment will involve a diamagnetic (σ_d) and a paramagnetic term (σ_p), with the paramagnetic term being inversely proportional to one or more electronic energy separations in the molecule under consideration. In the absence of sufficiently detailed knowledge of excited-state wavefunctions and energies to enable evaluation of the orbital angular momentum matrix elements between ground and excited states, recourse is had to the AEE approximation which casts the shielding equation in the form:

$$\sigma = \sigma_d + \sigma_p = A - B/\Delta E \tag{1}$$

where ΔE is taken as the value of the AEE. Differences in the theoretical approaches adopted by different workers reside in the method used to

calculate the orbital angular momentum matrix elements contained in the B factor; Ramsey, (111) Griffith and Orgel, (99) Jameson and Gutowsky, (204) and Pople (208) have each introduced different ways of tackling the problem. All these methods have an outcome common to the extent that, as the size of the atom increases, an increasing fraction of its shielding *variation* resides in the paramagnetic term, and for all atoms heavier than lithium σ_p accounts for at least 90% of the observed chemical shift range.* Thus the theory of nuclear shielding for all but the lightest elements must be addressed through the paramagnetic term.

The development of a more broadly based shielding theory requires a homgeneous set of experimental data which compare analogous shielding environments for a range of elements. The first such data set to be assembled was the 1963 shielding ranges observed for Main Group elements and used by Jameson and Gutowsky. (204) While useful in its time, this compilation had two severe limitations. The transition metals, with the highest inherent shielding sensitivities, are not represented. The data set also lacks homogeneity in that paucity of experimental shift data precludes the comparison of analogous environments. The intervening 15 years has seen a growth in shielding data for "other nuclei" to the extent that both of these deficiencies can now be rectified.

In searching for a pair of shielding values with which to measure the sensitivities of different elements, one discovers that chemical combinations with the halogens provide a more extensive set of data than any other. The MCl_4–MI_4 pairs are particularly useful in that their chemical shifts span a significant proportion of the total shielding range for most elements. The M^{n+}(aq)–M (free atom) pair provides another comparison which, although more limited in extent, provides the benefit of involving an "absolute" shielding reference. Both of these are discussed if data are available in the subsequent sections dealing with the individual elements.

B. Metal atom shielding sensitivities

It has been known for some time that the chemical shifts for analogous compounds of two different elements from the same Periodic Group correlate reasonably well with one another. The plot (210) of $\delta(^{207}Pb)$ *vs.* $\delta(^{119}Sn)$ for 15 compounds has a slope of 3·0, and the $\delta(^{125}Te)$ *vs.* $\delta(^{77}Se)$ plot (85) for 14 compounds has a slope of 1·8. A similar comparison (8) shows ^{199}Hg to have a shielding sensitivity 2·9 times that of ^{113}Cd. These comparisons indicate that there is some merit in the concept of an inherent shielding sensitivity for each element.

* The atom-dipole model suggested by Flygare, (209) which gives to σ_d a larger fraction of σ, is not based upon the electronic wavefunctions for the molecule and is therefore incapable of evaluating the explicit contribution of the orbital angular momentum.

The Cl–I shift data presented in Fig. 1 represent an initial attempt at evaluation of relative shielding sensitivities for the transition metals and for some of the other elements where comparable data are available. The Cl–I shifts are presented in ppm on a per halogen basis. Where the chloride–iodide separation is taken from molecules containing 2, 4, or 6 halogens, the molecular shift has been divided by 2, 4, or 6 to obtain the numbers in Fig. 1.

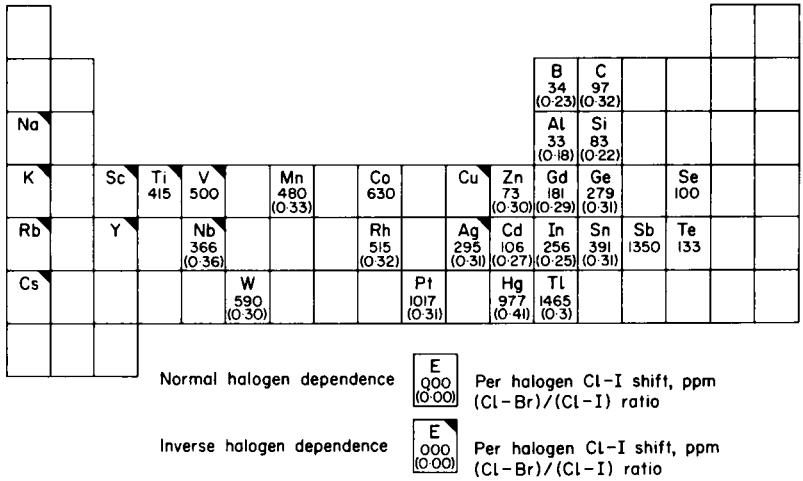

FIG. 1. Shielding sensitivities, halogen shielding patterns, and halogen dependences for the elements.

Where data for the appropriate iodide compound are missing, the Cl–Br separation has been divided by 0·3 as representative of the typical (Cl–Br)/(Cl–I) ratio. While it would be too much to expect other measures of relative sensitivity to coincide precisely with these values, they provide a more comprehensive set than any other measure, and in most cases comparisons with M^{n+}(aq)–M(free atom) or with particular ligand substituent constants agree within ±20%.

C. Halogen dependence of metal atom shieldings

The shieldings of all atoms are particularly sensitive to halogen substitution. The ^{13}C shielding patterns for the halogenomethanes received early attention (202) from NMR spectroscopists, and CH_3I was at one stage adopted as the reference compound for ^{13}C chemical shifts because of its position at the extreme low frequency end of the shielding range. The fact that iodine substitution causes large low frequency shifts becomes increasingly obtrusive as the shieldings of additional atoms come under study. Compounds of the type EX_4^{2-}, EX_4^-, EX_4, and EX_4^+ are formed by

elements from Groups II, III, IV, and V respectively, and for those elements where the data are available, the ECl_4–EI_4 chemical shift is over half the total shielding range for the element, with the EI_4 compound at or close to the top of the shielding range in every case. The uniformity of this pattern extends to the relative position of the EBr_4 compound which lies to low frequency of ECl_4, 1/4 to 1/3 of the distance to EI_4. The relative positions of the resonances for the chloride, bromide, and iodide compounds can be expressed in terms of the (Cl–Br)/(Cl–I) ratio which generally adopts values in the range 0·25 to 0·33. The halogen shielding order $Cl < Br \ll I$ holds for ^{11}B, ^{27}Al, ^{71}Ga, ^{115}In, ^{13}C, ^{29}Si, ^{73}Ge, and ^{119}Sn, and is sufficiently pervasive in other regions of the Periodic Table for compounds containing only one E–X bond, that it has come to be designated the normal halogen dependence (NHD).

For elements where shielding information for the analogous fluoride compound is available, the fluoride shielding pattern is much less consistent. This is not too surprising when one considers the prevalence of anomalous behaviour for the first-row element in each of the Periodic Groups. The fluorides of the Main Group elements generally absorb to low frequency of the chlorides. For ^{11}B the shielding order is $Cl < F < Br$, while for ^{27}Al, ^{29}Si, and ^{119}Sn the order is $Br < F < I$. The normal halogen dependence designation carries with it no implication about the fluoride chemical shift.

Most of the transition metals display normal halogen dependence. In 1971, however, Buslaev reported that the ^{93}Nb nucleus in $NbCl_6^-$ is more highly shielded than that in $NbBr_6^-$. Shortly thereafter, Kidd, Matthews, and Spinney reported that a similar situation prevails for ^{47}Ti and ^{49}Ti in $TiCl_4$ and $TiBr_4$; this led to speculation that inverse halogen dependence (IHD) might be a common property of transition metal halides. The information contained in Fig. 1 shows that the incidence of IHD among the transition metals studied to date is restricted to Sc, Ti, V, Nb, Cu, and Ag. The other transition metals to have been tested, W, Mn, Co, Rh, Pt, Zn, Cd, and Hg, all show normal halogen dependence. The distribution of IHD among the transition metals is interesting and may ultimately provide the clue as to the cause of this phenomenon. Adopting the convention that assigns a B-designation to the Sc to Zn Periodic Groups, it is Groups IB, IIIB, IVB, and VB only which show any evidence of IHD. In Group IIB, Zn, Cd, and Hg all show strong evidence of NHD, and in Groups VIB, VIIB, VIIIB, IXB, and XB data for at least one element showing NHD are available.

When we step outside the transition metal area, the situation becomes even more interesting. Groups IIIA, IVA, VA, and VIA all show NHD. In Group IA, however, both the solid alkali halides (154) and the slopes of the concentration plots for aqueous alkali halides (60) show IHD. Little information with which to assess the behaviour of Group IIA elements is available. Some ^9Be shielding studies (51) suggest that beryllium may show

NHD, as do the concentration plots for aqueous $^{43}Ca^{2+}$ and $^{87}Sr^{2+}$ salt solutions, (52) but a definitive answer must await further work.

What causes this peculiar reversal of halogen dependence on moving from group to group across the Periodic Table? Since the full scope of the phenomenon has not previously been traced, the current theories of nuclear shielding make no attempt to explain the reversal. It is also clear, however, that no future theoretical development can be regarded as completely successful until it does. A clue to its origin lies with the manner in which the reversal occurs. As we move across the Periodic Table, the halogen dependence does not start off with one sign, gradually diminish in magnitude until it passes through zero, and then increase in magnitude with the opposite sign. Rather it undergoes abrupt sign reversal on passing from one group to the next with no apparent diminution in magnitude.

The valence-shell electron configurations of those atoms exhibiting IHD are s^1, d^3, d^4, d^5, and $d^{10}s^1$ for the K, Sc, Ti, V, and Cu triads, respectively. These are all electron configurations for which the valence orbital set is *less than half filled.*

The spin–orbit coupling constant is a fundamental atomic parameter the sign of which depends upon whether the valence orbital set is more or less than half filled. (53) For configurations less than half filled, the multiplet resulting from spin–orbit splitting of the term has the component of lowest angular momentum lying lower in energy, while for configurations more than half filled the component of highest angular momentum is more stable. The effect of this magnetic property can be seen in the departure from spin-only value of the magnetic susceptibility of a complex, and in the zero-field splitting observed by ESR spectroscopy. The effect of spin–orbit coupling upon nuclear shielding in diamagnetic compounds has been assessed (116) and has up to now been regarded as relatively unimportant. It is just possible that future considerations of this question may reach a different conclusion.

II. THE SCANDIUM TRIAD

In chemical terms, scandium, yttrium, and lanthanum are considerably more basic than aluminium, and their behaviour resembles that of the alkaline earths rather than that of the transition metals. In chemical combination they form only the M^{III} oxidation state, and the M^{3+} ions show little tendency to form coordination complexes. Their oxides are *not* amphoteric, so the formation of anionic species such as $ScCl_4^-$ is extremely unlikely. Their interactions with counterions in aqueous solution are transitory, and shielding differences which result from these interactions are manifest as variations in the position of a time-averaged resonance line whose position depends upon both the concentration and the static shielding

of the complexed metal ion. All attempts to measure static shieldings for complexes of these metals have been hampered by lack of the appropriate formation constants.

Both ^{45}Sc and ^{139}La have receptivities that make them easier to detect than the alkaline earths. In general their ease of detection is comparable to that of the alkali metals. The information to emerge from the small number of NMR studies carried out on each of these nuclei projects an image similar to that cast by ^{23}Na, ^{39}K, and the other alkali metals, an image based upon concentration dependences, anion effects, preferential solvation, and changes in relaxation times rather than upon chemical shift values assignable to particular metal environments.

TABLE I

Nuclear properties of the scandium triad elements

Nucleus	Spin	Abundance (%)	Quadrupole moment · 10^{28} (m^2)	Usual shielding reference	Receptivity re ^{13}C
^{45}Sc	7/2	100	−0·22	Sc^{3+}(aq)	1710
^{89}Y	1/2	100	0	Y^{3+}(aq)	0·67
^{139}La	7/2	99·9	0·21	—	336

^{89}Y is a spin $I = 1/2$ nucleus and might be expected to yield sharp resonances with relative ease. Its magnetic moment is low, however, so lacking a quadrupolar relaxation mechanism and with only an inefficient magnetic dipolar one, the resonances saturate readily and a special detection technique is used to circumvent this problem.

A. Scandium-45

A precise measurement of the ^{45}Sc magnetic moment has been carried out by Lutz, (193) who identified both the concentration and anion dependence of scandium shieldings and measured the solvent isotope effect between light and heavy water to be $\delta(Sc^{3+}, H_2O) - \delta(Sc^{3+}, D_2O) = 6{\cdot}2$ ppm. Buslaev *et al.* (190) and Melson *et al.* (191, 192) have extended the earlier work of Lutz to put the anion dependence of aqueous Sc^{3+} shieldings on a quantitative basis. The concentration plots for the chloride, bromide, and perchlorate salts all extrapolate to a common origin at infinite dilution which has been adopted as the $\delta = 0$ reference for ^{45}Sc chemical shifts. At concentrations below 1 molar the plots are reasonably linear with slopes $\delta = -3{\cdot}6$ ppm M^{-1} for ClO_4^-, $\delta = -2{\cdot}5$ ppm M^{-1} for Br^-, and $\delta = +0{\cdot}5$ ppm M^{-1} for Cl^-. At higher concentrations, the plots show some

curvature. Although no concentration is given, added SCN^- ion is reported (190) to shift the ^{45}Sc resonance to high frequency by 27 ppm, action similar to its effect on ^{113}Cd where a strong high frequency shift is also observed. (14)

Aqueous solutions of $Sc_2(SO_4)_3$, $Sc(NO_3)_3$, and ScI_3 do not extrapolate to $\delta = 0$, but intersect the shielding axis at $\delta = 9{\cdot}4$, $4{\cdot}3$, and $2{\cdot}3$ respectively. In addition, their linewidths measured at low concentrations are significantly wider than those for the other salts. These differences suggest complex or ion-pair formation even at low concentration, a conclusion supported by a ^1H solvation study of $Sc(NO_3)_3$ in water–acetone mixtures. (43)

A number of environments in which ^{45}Sc is markedly deshielded have been studied, (192) but there is inadequate information from which to draw any general conclusions. $ScCl_3$ dissolved in tetrahydrofuran absorbs at $\delta = 204$, and in water–THF mixtures $\delta = 102$ occurs at a 0·17 mole fraction water composition.

On the question of the ^{45}Sc halogen dependence the evidence is conflicting and further work is required to resolve the issue. Buslaev *et al.* (190) report that $ScCl_3$, in added HCl, absorbs at $\delta = -26$ to low frequency of the aquo cation, and that $ScBr_3$ in 40% HBr absorbs at $\delta = -15$, while Sc^{3+} solutions saturated with KI are unshifted at $\delta = 0$. This would establish IHD for ^{45}Sc, similar to that encountered with the alkali metals. Melson *et al.*, (192) however, report a high frequency shift for $ScCl_3$ in 12 M HCl at $\delta = 144$, and slopes for the $ScBr_3$ and $ScCl_3$ concentration plots with the chloride to high frequency of the bromide, both of which suggest NHD.

B. Yttrium-89

By using the Quadriga-FT detection technique, Hassler, Kronenbitter, and Schwenk (194) have measured a number of ^{89}Y NMR parameters without having to add paramagnetic ions to reduce the inherently long relaxation times of this nucleus. A precise measurement of the magnetic moment has been obtained, and the solvent isotope effect between water and heavy water is $\delta(Y^{3+}, H_2O) - \delta(Y^{3+}, D_2O) = 4{\cdot}3$ ppm, regarded as a normal solvent isotope effect with the D_2O solution being more highly shielded. This value is similar in magnitude and direction to that observed for ^{45}Sc and has been interpreted as indicating the absence of complexing or ion pairing at low concentrations. A sign reversal has been observed with $^{67}Zn^{2+}$ and $^{199}Hg^{2+}$ salts where the fact that H_2O solutions are more highly shielded than D_2O solutions is taken as evidence for complex formation with the halide counterion.

Concentration plots for $Y(NO_3)_3$, $Y(ClO_4)_3$, and YCl_3 are linear at low concentrations and extrapolate to a common origin at infinite dilution which is used as the $\delta = 0$ reference for reporting ^{89}Y chemical shifts. (194) The

slopes of the concentration plots are $-7{\cdot}5$ ppm M^{-1} for NO_3^-, -1 ppm M^{-1} for ClO_4^-, and $+1$ ppm M^{-1} for Cl^-.

The rate of transverse relaxation $1/T_2$ shows a sharp increase above pH 0·6 which is not reflected in a corresponding change in $1/T_1$ or in δ. Rapid chemical exchange between the Y^{3+}(aq) state and a low concentration of a hydroxide-bridged polymeric state has been suggested as the source of this relaxation anomaly.

C. Lanthanum-139

A precise measurement of the ^{139}La magnetic moment in a 0·16 molal D_2O solution of $LaCl_3$ has been carried out by Krüger, Lutz and Oehler. (195) The solvent isotope effect $\delta(^{139}La^{3+}, H_2O) - \delta(^{139}La^{3+}, D_2O) = 1{\cdot}6$ ppm establishes an unusual trend in which the magnitude of this effect decreases along the series $Sc^{3+} > Y^{3+} > La^{3+}$.

The intermediately valued ^{139}La quadrupole moment of $0{\cdot}21 \times 10^{-28}$ m^2 makes its relaxation sensitive to changes in electric field gradient, and this sensitivity has been exploited in the assessment of complex formation by La^{3+}. Linewidth variations with change in counterion have been measured, (197) and the hazards of attempting to extract relaxation times from linewidths have been identified. (196) The relaxation study (196) indicates that NO_3^- forms an inner-sphere complex while ClO_4^- forms an outer-sphere complex with the La^{3+} aquo-cation.

Reuben (198) has given an elegant demonstration of how complex formation between a natural protein and a metal cation can be studied using NMR relaxation times. The introduction of bovine serum albumin (BSA), a protein molecule with about 100 free carboxylate groups, into aqueous $LaCl_3$ solution, produces incremental increases in $1/T_1$ which are linear in protein concentration. The magnitude of the increase is proportional to n/T_1, where n is the number of carboxylate groups on each protein molecule participating in coordination. The normal correlation time τ_c for the rotational motion that modulates the quadrupole coupling is *ca.* 10^{-11} s, making $\omega_0\tau_c \ll 1$ and T_1 independent of observation frequency. Owing to the large size of the protein complex, however, $\tau_c \approx 10^{-8}$ s and $\omega_0\tau_c \geqslant 1$, thereby making T_1 frequency dependent and permitting a separation of n from T_1. The number of protein carboxylate groups involved in complexing La^{3+} ions has been evaluated using this analysis. In the course of solving this problem, Reuben and Luz (199) have worked out a general solution for the relaxation behaviour of an $I = 7/2$ nucleus.

Smith and coworkers (200) have measured ^{139}La and ^{35}Cl resonance positions and linewidths for methanol solutions of $LaCl_3$. The ^{139}La resonance at $\delta = 293$ and all other evidence are consistent with a binuclear 8-coordinate structure with two bridging chlorines which is formulated as

$[Cl(MeOH)_5La(Cl)_2La(MeOH)_5Cl]^{2+}$. A recent study (201) concludes that acetate ion forms inner-sphere complexes with La^{3+} in aqueous solution. The limiting shift for the 1 : 1 complex calculated from formation constant data is $\delta = 100$. Other complexing anions also cause high frequency shifts. In 10 M HCl $\delta \approx 100$, in 5 M SCN^- $\delta = 36$, and the EDTA complex gives a limiting shift of $\delta = 570$. (201)

III. THE TITANIUM TRIAD

It is surprising that only one solution NMR study has been reported for titanium and nothing as yet for zirconium or hafnium. The large quadrupole moments of both hafnium isotopes reduce the probability of their providing structural information of interest to the chemist. The ^{91}Zr quadrupole moment, while unknown at present, is unlikely to be so large that it vitiates direct observation of this nucleus whose receptivity is the highest of the titanium triad and larger than several other quadrupolar nuclei (^{39}K, ^{67}Zn, ^{73}Ge) that have yielded useful signals. Growing interest in zirconium chemistry can be expected to produce some NMR results before too long.

TABLE II

Nuclear properties of the titanium triad elements

Nucleus	Spin	Abundance (%)	Quadrupole moment · 10^{28} (m^2)	Usual shielding reference	Receptivity re ^{13}C
^{47}Ti	5/2	7·28	unknown	TiF_6^{2-}	0·86
^{49}Ti	7/2	5·51	unknown	TiF_6^{2-}	1·18
^{91}Zr	5/2	11·23	unknown	—	6·04
^{177}Hf	7/2	18·50	3	—	0·67
^{179}Hf	9/2	13·75	3	—	0·17

A. Titanium-47 and titanium-49

Several elements have two isotopes that are about equally sensitive to NMR detection. Titanium is unique in that the resonance frequencies for its two isotopes differ by less than 300 ppm while its shielding range is an order of magnitude greater than this difference. All titanium spectra are therefore twinned, with a ^{49}Ti peak 271 ppm to high frequency of every ^{47}Ti peak resulting in overlapping ^{47}Ti and ^{49}Ti spectra. A practical consequence of this is that the spectra have an internal chemical shift calibration.

The only titanium shielding data available are for the halide environments. Kidd, Matthews, and Spinney (186) have observed ^{47}Ti and ^{49}Ti in

TiF_6, $TiCl_4$, and $TiBr_4$. The significance of this modest amount of information is that it establishes titanium among those few elements, all of them metals, whose shieldings exhibit IHD. In addition, the $TiCl_4$–$TiBr_4$ shielding separation can be compared with that for other central elements to provide an estimate of the titanium atom shielding sensitivity.

Titanium–fluorine coupling has been observed in the ^{19}F spectrum of TiF_6^{2-} and is reported to have a value of 33 Hz. (187) This coupling is not resolved in the Ti spectrum of TiF_6^{2-} (0·8 M TiF_4 in 48% aqueous HF) presumably because of F^- exchange in the coordination shell of titanium. The signals observed, however, are *ca.* 220 Hz wide, consistent with an unresolved septet with spacings of 33 Hz. Relative to TiF_6^{2-}, $TiCl_4$ and $TiBr_4$ as neat liquids give spectra that occur at $\delta = 1177$ and $\delta = 1675$ respectively, both less than 25 Hz in width. The lowest-lying electronic transitions for the chloride and the bromide are 34 840 cm^{-1} and 28 680 cm^{-1}.

The chloride–bromide separation of 498 ppm can be compared with the analogous separations in other tetrahedral MX_4 compounds: 22 ppm for ^{27}Al, 188 ppm for ^{71}Ga, 260 ppm for ^{115}In, 125 ppm for ^{13}C, 73 ppm for ^{29}Si, 343 ppm for ^{73}Ge, 485 ppm for ^{119}Sn, 90 ppm for ^{67}Zn, 115 ppm for ^{113}Cd, and 1044 ppm for ^{195}Pt(planar). The Group IV comparison of elements is Ti, Zr, Hf with Ge, Sn, Pb, the difference being a d-orbital valence shell in the first set and an sp-orbital valence shell in the second. The d-orbital participation in the transition metal case, with its higher orbital angular momentum, should make it more susceptible to shielding changes caused by changes in covalent bonding. The Ti with Ge comparison of 498 ppm *vs.* 343 ppm bears this out.

IV. THE VANADIUM TRIAD

The NMR study of ^{51}V shows an interesting historical development. Because of its high receptivity, this nucleus in its chemically stable +5 oxidation state received early attention in 1965 both from Richards (162) and from Schneider, (163) the directors of the two NMR schools responsible for much of the initial work on "other nuclei". This was followed by 10 years during which vanadium received little NMR attention. Then, beginning in 1974, Rehder and his coworkers (164–176) began the ^{51}V study of low oxidation state vanadium carbonyl and cyclopentadienyl compounds which continues to provide a rich source of systematic shielding data. During the past 3 years there has been renewed interest in the study of V^V systems, (173, 177, 178) as the enhanced sensitivity of the FT instruments enables more refined interpretation of the iso- and hetero-polyvanadate spectra.

TABLE III

Nuclear properties of the vanadium triad elements

Nucleus	Spin	Abundance (%)	Quadrupole moment · 10^{28} (m^2)	Usual shielding reference	Receptivity re ^{13}C
^{51}V	7/2	99·76	0·3	$VOCl_3$ (neat)	2160
^{93}Nb	9/2	100	−0·2	$NbCl_6^-$	2740
^{181}Ta	7/2	100	3		204

Niobium-93, because of the narrower range of compounds studied, has received less recent attention although the history of its study also begins in Schneider's laboratory in 1965. (163) Only four ^{93}Nb studies have been published since then, (179–182) and these have been restricted to the niobium(v) halides and oxyhalides. The large quadrupole moment for ^{181}Ta makes its NMR observation in solution unrewarding. Two unsuccessful attempts (163, 183) led in 1973 to the only report of a tantalum resonance. (184)

A. Vanadium-51

The ^{51}V resonance for liquid $VOCl_3$ has been adopted as the reference for reporting vanadium chemical shifts, and since it appears near the high frequency end of the V shielding range, most compounds have negative δ-values. Molecules studied to date span a shielding range of 2450 ppm, with V^V compounds, V^I compounds, and V^{-I} compounds occupying characteristic and distinct regions of the range. Figure 2 shows V^V compounds in the region +440 to −785, V^I compounds in the region −870 to −1540, and V^{-I} compounds in the region −1670 to −1950.

1. Vanadyl halides and esters

Until recently $VOCl_3$ was the only halogen-containing compound to be reported, and the halogen dependence for ^{51}V could not be established. Rehder (173) has recently provided shieldings for $VOBr_3$ and VOF_3 which show the bromide signal to be at 440 ppm to high frequency of the chloride, thereby establishing ^{51}V as one of the metals that shows IHD. In addition, the VOF_3 position at $\delta = -780$ makes vanadium one of the few metals where the shift direction obtained by substituting F for Cl represents a continuation of that obtained by substituting Cl for Br. All three of these oxyhalides show solvent shifts of up to 30 ppm which can be attributed to solvation that does not replace any of the ligands. In addition, $VOCl_3$ in THF gives rise to a

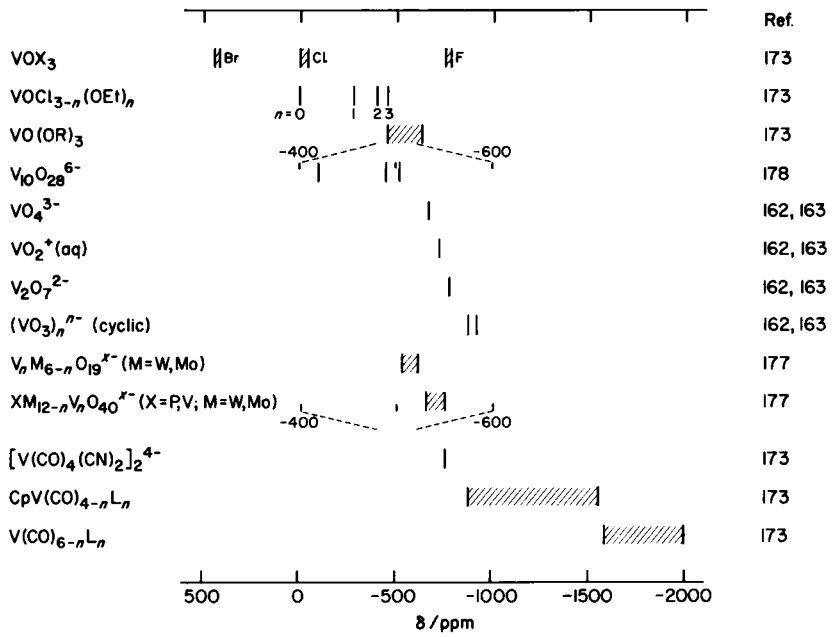

FIG. 2. ^{51}V chemical shift ranges for V^{V}, V^{I}, and V^{-I} in different chemical environments. Note ×5 scale expansion for oxyanions.

second ^{51}V signal at $\delta = -315$ in the VCl_2O_2-coordination region, favouring a $VOCl_2$ THF assignment.

Mixed chloro-ester vanadyl compounds of the type $VOCl_n(OR)_{3-n}$ (R = Me, Et, Pr^i, Bu^t) have been studied; (173) they have shifts intermediate in value between those of the $VOCl_3$ and VO_4 environments. The fact that the vanadyl triesters absorb in the same region as the tetrahedral oxyanions indicates a primary dependence upon the nature of the donor atom.

An attempt has been made (173) to explain the order of halogen shielding in terms of $1/\Delta E$ variations combined with varying amounts of vanadium valence shell orbital expansion. While these arguments provide plausible explanations for the observed variations in ^{51}V shieldings, they provide no basis for addressing the central question of why the halogen shielding order for ^{51}V, along with ^{47}Ti and ^{93}Nb, is the reverse of that for elements found in most other regions of the Periodic Table. This question is raised in Section VIII where some possible causes for this inversion are discussed.

2. *Oxyanions and polyanions*

The aqueous chemistry of vanadium(V) represents a rich variety of iso- and hetero-polyvanadates in which the fundamental structural units are VO_4

tetrahedra and VO_6 octahedra. At pH 14, the mononuclear VO_4^{3-} orthovanadate ion with a V : O ratio of 2·5 is clearly recognizable in solution by its narrow (<40 Hz) ^{51}V resonance at $\delta = -536$. (162. 163) By increasing hydrogen ion concentration and lowering the pH, an environment is created which favours structures with higher V:O ratios; this is achieved by condensation polymer formation. The first two series of polymers to form are the linear ($V_2O_7^{4-}$) and cyclic ($V_3O_9^{3-}$, $V_4O_{12}^{4-}$) structures formed by VO_4 tetrahedra sharing corners. These have been identified (177) in the pH region 9–13, and their resonance positions are shown in the expanded portion of Fig. 2. While the separations between these broad lines can be as little as 20 ppm, they can be located with an uncertainty of ±2 ppm and their positions have been verified by three separate studies. (162, 163, 177)

Below pH 6 the $V_{10}O_{28}^{6-}$ dodecavanadate ion forms with a structure containing 6 VO_6 octahedra sharing edges in a planar 2×3 array, with 2 octahedra top and bottom occupying the valleys between the 6 planar peaks. The three resonances observed (178) for this ion are at $\delta = -420$, -490, -510 with area ratios 2:4:4. The -420 resonance is clearly assignable to the inner 2 vanadiums of the planar array on symmetry grounds, and the -510 resonance has been assigned by Howarth and Jarrold (178) to the outer 4 vanadiums in the planar array on the basis of its pH dependence. The positions of both of the stronger peaks move to higher shielding with decreasing pH while the -420 peak stays relatively constant, indicating that protonation occurs at the apical rather than the bridging oxygens. (178)

Below pH 4 V_2O_5 starts to precipitate. This oxide is amphoteric and redissolves in excess acid. Below pH 1 the VO_2^+ cation in solution yields a ^{51}V resonance at $\delta = -543$.

The heteropolyvanadates (177) are of two general types, the hexametallates with M_6O_{19} stoichiometry and the dodecametallates with $XM_{12}O_{40}$ (X = P or V; M = V, Mo, or W) stoichiometry. The ^{51}V in hexametallates absorbs around $\delta = -515$ and that in the dodecametallates absorbs around $\delta = -540$. These resonances also move to higher shielding on protonation.

3. Low oxidation state vanadium compounds

Vanadium forms two series of low oxidation state compounds: those containing V^I and those containing V^{-1}. All the vanadium(I) compounds to be studied by ^{51}V NMR contain η^5-$C_5H_5^-$ as a 6-electron donor, in combination with various other ligands sufficient to provide vanadium with 18 valence shell electrons. These occupy the shielding region from $\delta = -870$ to $\delta = -1550$. The $CpV(CO)_2L_2$ (L_2 = diphosphine, triphosphine) compounds occupy the high frequency end of this region, (166, 169, 170) and the *cis* isomers are about 100 ppm more shielded than the *trans*. The $CpV(CO)_3L$ compounds occupy the low frequency end of the region (165)

with $CpV(CO)_4$ absorbing at $\delta = -1520$. As-, Sb-, and P-donor ligands have been investigated in place of one CO.

The vanadium(I) compounds studied are all carbonyls of the types $V(CO)_3L_3^-$, $V(CO)_4L_2^-$, and $V(CO)_5L$, and they absorb in the region $\delta = -1580$ to $\delta = -2010$. The $V(CO)_3L_3^-$ series (167) overlaps with the $V(CO)_4L_2^-$ series, (168) while the $V(CO)_5L^-$ series (164, 169, 170) provides a vehicle for testing the ability of a range of ligands to shield ^{51}V. This ligand comparison is discussed in detail in Section X.

B. Niobium-93

Niobium is one of the most favourable elements for NMR detection. Its receptivity of 2740 is third only to ^1H and ^{19}F, and its quadrupole moment of $-0{\cdot}2 \times 10^{-28}$ m^2 is among the lowest of the quadrupolar transition metals. Compounds that have been studied in the few investigations published to date are restricted to the halides and pseudohalides. All are Nb^V compounds and the present range of ^{93}Nb shieldings covers 2300 ppm.

Both NbF_6^- and $NbCl_6^-$ have been adopted as the reference for reporting ^{93}Nb chemical shifts, and both have drawbacks. Although in some solvents NbF_6^- gives a well resolved septet due to coupling with the six fluorines with $^1J(^{93}Nb–^{19}F) = 342$ Hz, (180) in 48% aqueous HF fluoride ion exchange is rapid enough for the ^{93}Nb resonance to be a sharp singlet. (183) There is, however, some question as to whether (180) or not (189) NbF_6^- displays a solvent effect of 60–70 ppm on going from aqueous to acetonitrile solution, and for this reason $NbCl_6^-$ has been chosen as the reference in Fig. 3 in spite of the fact that it falls in the middle of the shielding range.

The most recent ^{93}Nb study to be reported by Buslaev and coworkers (182) is the first to apply FT methodology to this nucleus and provides chemical shifts and assignments for the 10 different niobium environments in the system $NbCl_nBr_{6-n}^-$ which are more precise than those reported in the two previous studies of this system. (179, 181) The regular spacing of the spectral lines is shown in Fig. 3. By assuming a point charge model, the electric field gradient (EFG) for each isomer has been calculated and the low frequency line in each of the closely spaced pairs has been assigned to the *trans* isomer because its greater width corresponds to the larger EFG calculated. It is interesting that in 6-coordinate ^{51}V, ^{59}Co, ^{103}Rh, and ^{195}Pt complexes the *trans* isomers all absorb to high frequency of the corresponding *cis*-isomers. A numerical model for calculating the ^{93}Nb shieldings in these compounds by forming 10 linear combinations of 3 *trans* additivity coefficients is found to give better agreement with observed shieldings than the linear combinations using 3 pairwise additivity coefficients previously reported. (181) The success of the *trans* model over the pairwise model indicates that the second-order shielding effect of a particular ligand

operates through its influence on the *trans* ligand rather than through its influence on the four neighbouring ligands.

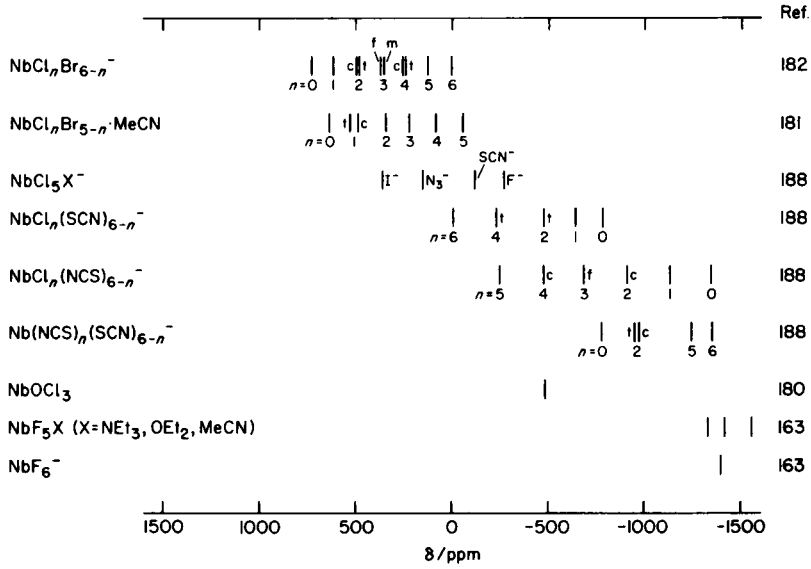

FIG. 3. ^{93}Nb chemical shift ranges for Nb^V in different halogen environments.

The shielding effect of other halide and pseudohalide ligands in combination with niobium is shown in Fig. 3. From the $NbCl_5X$ compounds the order of increasing shielding is:

$$I^- < N_3^- < Br^- < Cl^- < MeCN < \underline{S}CN^- < \underline{N}CS^- < F^-$$

This ordering of I^-, Br^-, and Cl^- is seen to be the inverse of the halogen dependence observed with most other metals, and makes tempting the conclusion that here is an example of $1/\Delta E$ domination of the shielding through the accustomed operation of the Ramsey paramagnetic shielding term. Little satisfaction can be derived from this rationalization, however, without some moderately convincing explanation of why ^{93}Nb, and a few other metals, behaves abnormally. This topic is explored more fully in Section VIII. By re-defining σ_d in a manner different from that adopted by Ramsey, Buslaev and coworkers (182) find that ^{93}Nb σ_p values obtained as the difference between calculated values of σ_d and observed δ-values comprise 70% of the observed ^{93}Nb shielding variation in the mixed $NbCl_nB_{6-n}^-$ hexahalogenoniobates.

C. Tantalum-181

Erich, Gossard, and Hartless (184) in 1973 succeeded in obtaining the first and only ^{181}Ta resonance to be measured in solution. A solution containing tantalum metal dissolved in 1:1 HF–HNO_3 yields a room-temperature resonance 36 kHz in width which narrows to 10 kHz on warming to 80 °C. The solute species is assumed to be the TaF_6^- ion. A nuclear screening of *ca.* 20 ppm is calculated for this ion and the result used as a correction factor in the precise determination of the ^{181}Ta magnetic moment.

V. THE CHROMIUM TRIAD

Table IV shows that all the elements in this group have low receptivities and as a result do little to encourage direct observation. Three studies of ^{53}Cr have been reported and a few more deal with ^{95}Mo which is a little easier to observe. One feature which makes molybdenum particularly interesting from an NMR point of view is the fact that it has two isotopes with $I > 1/2$ whose quadrupole moments differ by a sizeable factor. It therefore provides a unique system for studying the quadrupole contribution to the relaxation process. In spite of having the lowest receptivity of these three elements, ^{183}W provides the widest range of chemical shift and coupling constant data by virtue of the fact that it is a spin $I = 1/2$ nucleus and is accessible by indirect observation.

TABLE IV

Nuclear properties of the chromium triad elements

Nucleus	Spin	Abundance (%)	Quadrupole moment · 10^{28} (m^2)	Usual shielding reference	Receptivity re ^{13}C
^{53}Cr	3/2	9·6	unknown	CrO_4^{2-}	0·49
^{95}Mo	5/2	15·7	0·12	MoO_4^{2-}	2·88
^{97}Mo	5/2	9·5	1·1	MoO_4^{2-}	1·84
^{183}W	1/2	14·4	0	WF_6	0·059

A. Chromium-53

^{53}Cr resonances have been reported for only two chemical environments, CrO_4^{2-} and $Cr(CO)_6$. In the carbonyl environment (127) chromium is 1795 ppm more highly shielded than in the chromate, the direction expected in going from Cr^{VI} to Cr^0. The magnitude of the shift is comparable to the 2325 ppm ^{55}Mn shielding difference between MnO_4^- and $Mn_2(CO)_{10}$.

Although the quadrupole moment for ^{53}Cr is not yet known, the fact that the only two signals to be observed both come from cubic environments would suggest that lower symmetries cause significant broadening as the result of a medium sized quadrupole moment of *ca.* $0{\cdot}5 \times 10^{-28}$ m^2.

Aqueous solutions of CrO_4^{2-} exhibit both cation and concentration dependence. (127) Increasing concentration causes an increase in screening for all counterions, with the slopes to lower frequency, increasing in the order $Na^+ < K^+ < Rb^+ < NH_4^+ < Cs^+$. This order is apparently size-related judging from the position of NH_4^+ in the series. The concentration dependence for Cs_2CrO_4, the highest observed, is roughly linear with a δ-slope of *ca.* -5 ppm/molal. By comparison, the ^{39}K concentration dependence for aqueous K_2CrO_4 is $-0{\cdot}43$ ppm/molal.

The natural ^{53}Cr linewidth for aqueous CrO_4^{2-} is about 10 Hz. Enrichment to 35% in ^{17}O causes shoulders to develop at the base of the resonance which have been analysed to yield a coupling constant $^1J(^{53}Cr–^{17}O) = 10 \pm 2$ Hz. (128)

The ^{53}Cr linewidth in aqueous CrO_4^{2-} has served as the basis for a kinetic study to measure the rate of CrO_3 exchange between chromate and dichromate ions. (129) The rate constant measured is in good agreement with that obtained in an earlier study (130) where the same reaction was monitored through the width of the ^{17}O NMR signal.

B. Molybdenum-95 and molybdenum-97

With the exception of the nice relaxation study carried out by Vold and Vold (131) which capitalizes on the 10-fold quadrupole moment difference between the two isotopes, all the work on molybdenum has been done by members of the Tübingen school. Only a few compounds have been studied, and the rich field of iso- and hetero-polymolybdates remains as yet unexplored, but with at least one example from each of the Mo^{VI}, Mo^{IV}, and Mo^0 oxidation states the shielding range for diamagnetic compounds at present spans 4100 ppm, with shielding increasing on moving to lower oxidation states as expected.

Lutz and coworkers (133) have determined the effect of S^{2-} substitution for O^{2-} in MoO_4^{2-} on molybdenum shielding and find a regular, incremental, screening decrease of 550 ± 55 ppm for each successive oxygen substituted. This marked effect of S-coordination is most pronounced for closed-shell d^0 or d^{10} compounds and has received systematic study via ^{113}Cd NMR. (10) The shielding pattern is one in which the row in the Periodic Table from which the ligating atom is drawn is the prime shielding determinant, and for the chalcogenides the metal shielding increases in the order $S < Se < Te < O$. We recognize here an analogy with normal halogen dependence and also the probability that MoS_4^{2-} marks the limit for

molybdenum shieldings since $MoCl_6$ has never been successfully prepared.

The lower oxidation states, exemplified by $Mo(CN)_8^{4-}$ and $Mo(CO)_6$, are more highly shielded than MoO_4^{2-}, with the enhanced shielding for the carbonyl lying within 3% of the analogous value for $Cr(CO)_6$ as shown in Fig. 4. This comparison alone suggests that the shielding sensitivities for ^{53}Cr and ^{95}Mo are remarkably similar. A minor difference arises, however, when we look at the anion dependence of the molybdate salt concentration plots. (134) Increasing concentration of the Li^+ and NH_4^+ salts increases the ^{95}Mo shielding of MoO_4^{2-} with a δ-slope of *ca.* $-2{\cdot}4$ ppm/molal, a pattern comparable to the CrO_4^{2-} case, but the Na^+ and K^+ salts cause *deshielding* of ^{95}Mo with δ-slopes of *ca.* $+1$ ppm/molal. There may be some significance in the fact that solid Ag_2MoO_4 absorbs at $\delta = 82$, a shift consistent with the extrapolated concentration plots for Na^+ and K^+.

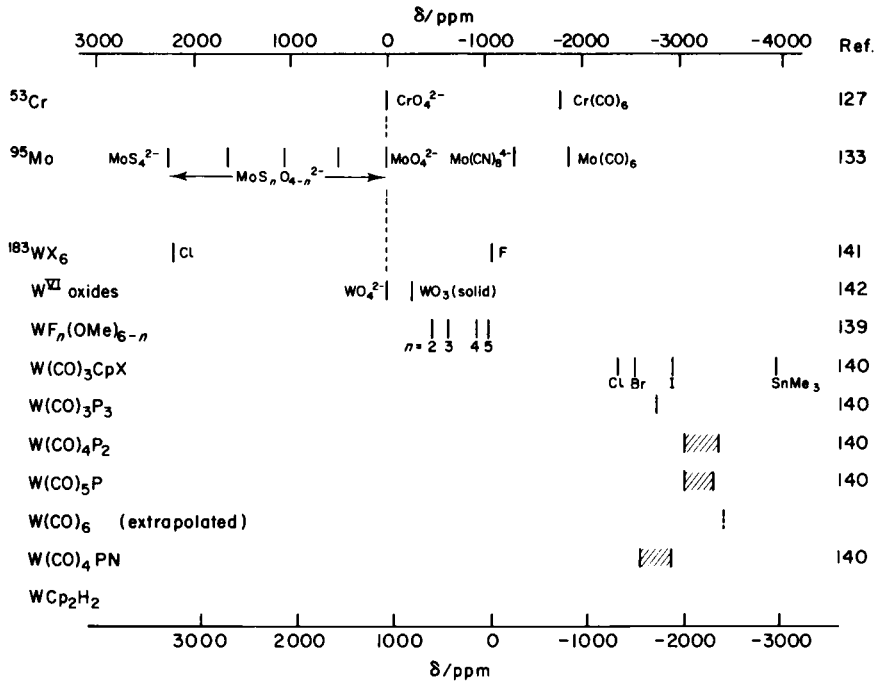

FIG. 4. ^{53}Cr and ^{95}Mo chemical shift ranges. ^{183}W chemical shift ranges plotted to same scale using different reference. MO_4^{2-} shieldings arbitrarily equated.

A start has been made on the isopolyanion problem by studying the pH dependence of the MoO_4^{2-} signal. (134) For basic solutions with pH >6·4, the position and width of the MoO_4^{2-} signal remain unchanged. At pH 5·4,

however, the signal shifts to $\delta = 30$ and the linewidth increases to 170 Hz. At lower pH values, where polyanion formation is known to increase, the signal is no longer detectable owing to excessive broadening. In a sample of MoO_4^{2-} enriched to 11% in ^{17}O a ^{95}Mo sextet is observed (128) due to coupling with the $I = 5/2$ ^{17}O isotopes in the oxyanion. The coupling constant $^1J(^{95}Mo-^{17}O)$ is $40{\cdot}5 \pm 0{\cdot}8$ Hz.

The effects of the heavier isotopes ^{18}O and ^{34}S on the ^{95}Mo shielding in MoO_4^{2-} have both been determined. (135, 136) For MoO_4^{2-} enriched to 72·5% in ^{18}O a ^{95}Mo 5-line multiplet containing resolved signals for different MoO_4^{2-} ions containing 0–4 ^{18}O isotopes is observed. The isotope shift is $0{\cdot}25 \pm 0{\cdot}01$ ppm to higher shielding for each ^{18}O substitution. The analogous experiment with MoS_4^{2-} gives an isotope effect of $0{\cdot}09 \pm 0{\cdot}01$ ppm to higher shielding for each ^{34}S substitution. These isotope effects are consistent with the general theoretical treatment worked out by Lauterbur. (137)

C. Tungsten-183

Shielding studies of ^{183}W are relatively few in number and yet, when taken together with the even more meagre data for ^{35}Cr and ^{95}Mo as is done in Fig. 4, a remarkably complete picture for shielding of the Group VI transition metals can be obtained. For purposes of reporting ^{183}W chemical shifts, the not altogether satisfactory WF_6 having $\Xi(^{183}W) = 4\,161\,733$ Hz (141) has been adopted by those working in the area and δ-values referenced to WF_6 are given at the bottom of Fig. 4. In order to allow comparison with ^{53}Cr and ^{95}Mo shieldings which have been referenced to the MO_4^{2-} oxyanion, the WO_4^{2-} position in Fig. 4 is aligned with its chromium and molybdenum counterparts, and the shielding scale at the top gives $\delta(WO_4^{2-})$ values for ^{183}W.

The present range (140, 141) of ^{183}W shieldings spans 6850 ppm from WCl_6 at $\delta = 3302$ to WCp_2H_2 at $\delta = -3550$, with tungsten(VI) compounds occupying the lower 3300 ppm of the range while the lower oxidation state W^{II} and W^0 compounds occupy the upper 2300 ppm, leaving a gap of about 1200 ppm separating the two groups.

By making use of an estimated $\delta = -2400$ for $W(CO)_6$, (140) it is possible to deduce that the shielding sensitivity of ^{183}W is *ca.* 1·8 times that of ^{97}Mo. This figure comes from the ratio 3500/1900 for the MO_4^{2-}–$M(CO)_6$ separations in each case. Further evidence that this is the right order of magnitude comes from a comparison of the WCl_6–WF_6 separation (3300 ppm) in another part of the range with the MoS_4^{2-}–MoO_4^{2-} separation (2300 ppm) to give a ratio 3300/2300 = 1·4. This comparison turns out to be reasonably valid since adjacent donor atoms coming from different rows of the Periodic Table have similar shielding effects.

Shieldings for the series of mixed ligand complexes (139) $WF_n(OMe)_{6-n}$ show monotonic high frequency shifts in the region between the WO_3 (WO_6 octahedra sharing corners) (142) and WF_6 resonances as F^- is successively substituted by MeO^-. The fact that the WO_3 resonance fits reasonably into this sequence in place of $W(OMe)_6$ indicates that other substituents on a donor atom exercise a relatively minor effect upon ^{183}W shielding. This is further borne out by the narrow ranges over which a variety of $W(CO)_4P_2$ and $W(CO)_5P$ tertiary phosphine complexes absorb. (140)

The halogen dependence of ^{183}W follows the normal pattern with the iodide complex in the $W(CO)_3CpX$ system occupying the low frequency position at $\delta = -1875$ and a (Cl–Br)/(Cl–I) ratio of 0·30. A number of irregular structural and bonding factors make first-row donor atoms unreliable bases for the recognition of trend patterns, and for this reason the WF_6 position, to low frequency of WCl_6, is not unusual for NHD. While fluoride data are not available for all cases where NHD is recognizable, the shielding order $Cl < Br < F < I$ holds for ^{11}B, ^{27}Al, ^{29}Si, and ^{119}Sn, and it would be surprising if WF_6 were *not* to low frequency of WCl_6.

VI. THE MANGANESE TRIAD

The situation with the Group VI transition metals is just the reverse of that encountered with the chromium triad. In this case it is the first member, manganese, that has received the most NMR attention while technetium and rhenium have been the objects of only isolated study, insufficient for the purpose of establishing shielding sensitivities and other chemical shift patterns. The chemistry of manganese is dominated by the stable Mn^{II} and Mn^{III} oxidation states, both of which are paramagnetic, leaving to the NMR spectroscopist only the permanganate ion and the lower oxidation states

TABLE V

Nuclear properties of the manganese triad elements

Nucleus	Spin	Abundance (%)	Quadrupole moment · 10^{28} (m^2)	Usual shielding reference	Receptivity re ^{13}C
^{55}Mn	5/2	100	0·55	MnO_4^-	994
^{99}Tc	9/2	radioactive	0·3	TcO_4^- [a]	2134 [b]
^{185}Re	5/2	37	2·8	ReO_4^- [a]	280
^{187}Re	5/2	63	2·6	ReO_4^- [a]	490

[a] The only compound observed.
[b] Based on 100% ^{99}Tc.

Mn^{I}, Mn^{0}, and Mn^{-I} which are diamagnetic because of their d^0 and spin-paired d^6 and d^8 configurations. Technetium NMR is limited in scope not by any inherent spectroscopic difficulty but by availability of the element with which to study its chemistry. While both isotopes of rhenium have respectable receptivities, their large quadrupole moments in the presence of significant electric field gradients facilitate rapid nuclear relaxation making their signals undetectable because of excessive width.

A. Manganese-55

The MnO_4^- ion is the only Mn^{VII} compound studied and its resonance position has been adopted as the reference for reporting ^{55}Mn chemical shifts in all of the dozen or so studies to be reported. The concentration and anion dependence of aqueous permanganate have been studied (143) in such a way that the results can be compared with those for CrO_4^{2-} and MoO_4^{2-}. Increasing concentrations cause roughly linear low frequency shifts for all cations, with the slopes of the concentration plots increasing in the order $Li^+ < Mg^{2+} < K^+ < Ba^{2+}$. For K^+ the δ-slope is $-1{\cdot}6$ ppm/molal and for Ba^{2+} it is $-9{\cdot}5$ ppm/molal. The zero point for the δ-scale is defined by the infinite dilution extrapolation of these plots.

The effects of different solvents on the ^{55}Mn shielding in MnO_4^- have been investigated by Gudlin and Schneider (150) who find that coordinating solvents move the resonance to higher frequencies, the opposite direction to that for $^{23}Na^+$ resonances (151) and for $^{199}HgMe_2$ resonances. (32) The largest deshielding is 18 ppm for hexamethylphosphoramide, with dimethylformamide and acetone giving lower solvent shifts. A 25 ppm solvent effect for $Ph_3SnMn(CO)_5$ between tetrahydrofuran and dimethylformamide has also been observed, (147) confirming the fact that one can expect solvent effects of up to *ca.* 25 ppm on ^{55}Mn shieldings, but probably no larger.

By dissolving $KMnO_4$ in 99% ^{18}O-water, a 5-line ^{55}Mn spectrum develops over a period of 35 days, from which an isotope effect for ^{18}O substitution of $0{\cdot}599 \pm 0{\cdot}015$ ppm to low frequency for each ^{18}O incorporated into the anion has been obtained. The time constant for the exchange process at room temperature has been estimated to be *ca.* 7 days. (144)

In adopting the MnO_4^- ion as the ^{55}Mn shielding reference it should be recognized that the 690 nm absorption band responsible for its deep violet colour identifies the lowest-lying electronic excited state among all the tetrahedral oxyanions and, indeed, among most compounds generally. This very low excitation energy will, through the $1/\Delta E$ factor, provide MnO_4^- with one of the largest σ_p terms of any compound, resulting in a higher relative deshielding than is found with the other tetrahedral oxyanions. An

obvious manifestation of this σ_p limit status is the 1000 ppm gap between MnO_4^- and all other ^{55}Mn resonances which is much larger than can be accounted for solely on the basis of the difference in oxidation state. No similar gap exists for ^{183}W (Fig. 4) where a comparable body of shielding data is available.

All other manganese compounds for which shielding information is available are low oxidation state carbonyl compounds containing Mn^I, Mn^0, and Mn^{-I}. By comparing the shieldings illustrated in Fig. 5 for $(CO)_5MnL$ compounds as the sixth ligand is changed, the increasing shielding order is:

$$Cl < Br < I < alkyl \approx acyl \approx CO < SnR_3Mn(CO)_5 < H < PF_3$$

The shieldings for these compounds are discussed in greater detail in Section X where they are compared with those for analogous ^{51}V and ^{59}Co compounds.

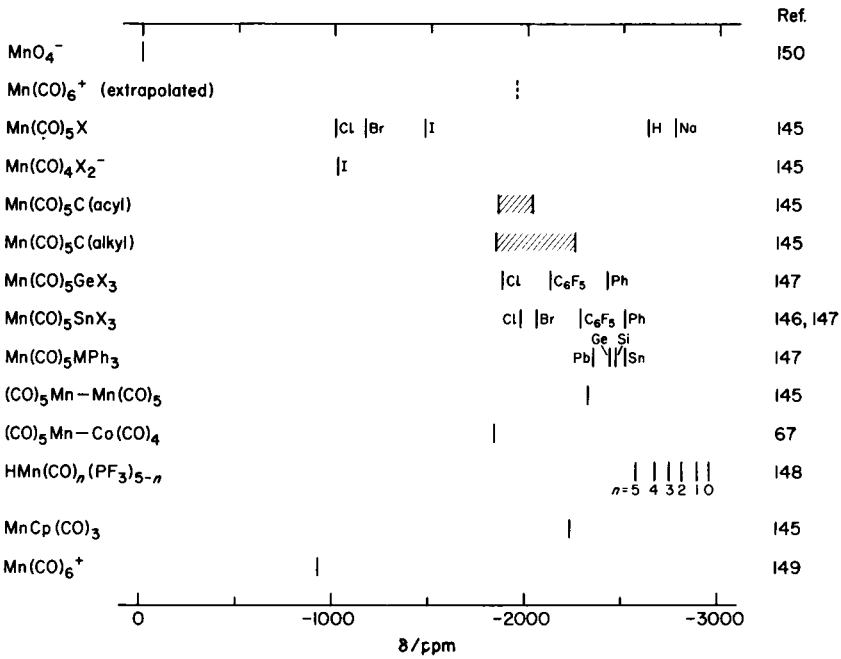

FIG. 5. ^{55}Mn chemical shift ranges for Mn^{VII} and Mn^I in different chemical environments.

The resonance reported (149) at $\delta = -935$ for $Mn(CO)_6^+$ calls for some comment. Not only is the reported linewidth of 0·428 mT inconsistent with the low electric field gradient present in an octahedral complex, but the $\delta = -935$ position places L = CO in the above series lower than Cl^-, a

position totally inconsistent with the shielding properties of CO in combination with this and other transition metals. A more realistic δ-value for $Mn(CO)_6^+$ is obtained by extrapolating from $(CO)_4MnI_2^-$ ($\delta = -1020$) and $(CO)_5MnI$ ($\delta = -1485$) to obtain $\delta \approx -2000$ with probable error limits of no more than ± 200 ppm on this estimated value. The lack of experimental detail in Reference 149 concerning sample preparation makes it difficult to speculate upon alternative assignments for the $\delta = -935$ resonance; a solvate in which acetone has replaced one or more CO groups is a possibility.

B. Technetium-99

Textbooks of inorganic chemistry do not reveal a high degree of interest in or knowledge about technetium compounds, and the NMR literature mirrors this situation. No stable isotopes of technetium exist, and all technetium chemistry has been conducted with ^{99}Tc (0·29 MeV β^-, $t_{\frac{1}{2}}$ 2×10^5 years) isolated from waste fission product solutions after removal of plutonium and uranium. Surprisingly ^{99}Tc, with a receptivity relative to ^{13}C of 2134, ranks fourth among all the elements after ^1H, ^{19}F, and ^{93}Nb.

The most stable form of technetium and the one in which it is normally encountered is the TcO_4^- anion representing Tc^{VII}. The ^{17}O chemical shift for this anion has been reported (152) to show a normal $1/\Delta E$ correlation with the ^{17}O shifts for other d^0 tetrahedral oxyanions. A strong ^{99}Tc resonance for the same solution was observed (153) having a half-height linewidth of 29 Hz measured under high-resolution conditions. By comparison the ^{55}Mn linewidth in MnO_4^- is 17 Hz (202) and the ^{185}Re and ^{187}Re linewidths in ReO_4^- are 8280 Hz and 7820 Hz respectively. (154).

C. Rhenium-185 and rhenium-187

The NMR situation with respect to ^{185}Re and ^{187}Re is the same as that for ^{99}Tc in that the ReO_4^- anion is the only compound to be studied. Although the receptivities for both Re isotopes are reasonably high, their large quadrupole moments (Q) dictate that signals will only be observed from rhenium occupying sites of cubic symmetry, and even then the fact that the signal width is proportional to Q^2 makes it very sensitive to small changes in electric field gradient. Dwek, Luz, and Shporer (73) obtain linewidths of 8280 Hz ($T_2 = 22$ μs) and 7820 Hz ($T_2 = 23{\cdot}5$ μs) for ^{185}Re and ^{187}Re.

VII. THE IRON TRIAD

A. Iron-57

Iron, ruthenium, and osmium offer little prospect of structural information without large expenditures of time and effort by the NMR spectroscopist. There have been two studies of ^{57}Fe, one (155) by direct

TABLE VI

Nuclear properties of the iron triad elements

Nucleus	Spin	Abundance (%)	Quadrupole moment · 10^{28} (m^2)	Usual shielding reference	Receptivity re ^{13}C
^{57}Fe	1/2	2·2	0	$(\eta^5\text{-}C_5H_5)_2Fe$	0·004
^{99}Ru	3/2	12·7	unknown	—	0·14
^{101}Ru	5/2	17·1	unknown	—	1·38
^{187}Os	1/2	1·6	0	—	0·001
^{189}Os	3/2	16·1	0·8	OsO_4(l)	2·13

observation on natural abundance $Fe(CO)_5$ requiring 20 hours of instrument time and $6{\cdot}5 \times 10^6$ pulses to achieve a signal-to-noise ratio above 100, the other (156) by triple resonance indirect observation of substituted ferrocenes with samples enriched to 82% in ^{57}Fe. A precise determination of the ^{57}Fe resonance frequency in $Fe(CO)_5$ relative to that of ^2H in ^2H_2O at the same field (158) enables the ^{57}Fe shieldings from these two studies to be related to each other as shown in Table VII where Fc–X represents η^5-$C_5H_5Fe\eta^5$-C_5H_4X.

TABLE VII

^{57}Fe chemical shifts

Compound	Medium	δ	Field reference $\nu(^{57}Fe)/\nu(^2H_2O)$	Ref.
Fc–C(O)Me		216		156
Fc–CH_2Me		37		156
Fc–CH(OH)Me		0		156
$(\eta^5\text{-}C_5H_5)_2Fe$	CS_2	0	0·211 316	156
$(\eta^5\text{-}C_5H_5)_2FeH^+$	BF_3–H_2O	−1099		156
$Fe(CO)_5$	neat liquid	−1867	0·210 921	158

Although limited in extent, what chemical shift information there is projects a shielding pattern for iron consistent with that of the other transition metals. The 1867 ppm shielding increase from ferrocene to $Fe(CO)_5$ reflects the change expected in going from Fe^{II} to Fe^0, as well as the enhanced shielding that occurs with ^{51}V, ^{55}Mn, and ^{59}Co when η^5-C_5H_5 is replaced by the appropriate number of carbon monoxides. The deshielding caused by acyl and alkyl substitution of one η^5-C_5H_5 however is opposite to the ^{55}Mn change found in similarly substituted manganese compounds

where $\delta[C_5H_5Mn(CO)_3] = -2225$ (145) and $\delta[Ph(MeCO_2)_2C_5H_2Mn(CO)_3] = -2588$. (159)

B. Osmium-187 and osmium-189

The only report of an osmium resonance is by Sahm and Schwenk (157) who have obtained signals from both ^{187}Os and ^{189}Os in OsO_4 which is liquid at room temperature. The pulse technique used for detection yields relaxation times of $T_2 \approx 5$ s for ^{187}Os and $T_2 = 230 \pm 10$ μs for ^{189}Os. The 10^4-fold more rapid relaxation of ^{189}Os results from the operation of an effective quadrupolar mechanism and indicates the presence of a non-zero electric field gradient in OsO_4.

VIII. THE COBALT TRIAD

Cobalt-59 occupies a pivotal point in the field of NMR spectroscopy. The chemical shift phenomenon was first recognized in 1951 as a compound-specific anomaly affecting precise measurements of the ^{59}Co nuclear magnetic moment. (84) The relationship between low-lying electronic excited states and large paramagnetic chemical shifts which now serves as the basis for our theoretical understanding of all nuclear shieldings except those for hydrogen and helium was first observed (100) and rationalized (86) using octahedral complexes of cobalt(III). Finally, the range of cobalt shieldings observed in diamagnetic compounds, at 18 000 ppm is the widest of all the elements.

Within the context of transition metal NMR, cobalt occupies a dominating position with over 50 independent ^{59}Co studies being reported since 1951 and continued steady growth in recent years. By comparison, the approximate number of NMR studies published on other transition metals are 30 for ^{199}Hg, 25 each for ^{113}Cd and ^{51}V, 15 for ^{195}Pt, 10 each for ^{55}Mn, ^{103}Rh, and ^{183}W, and less than 10 in all other cases. The correlation between number of

TABLE VIII

Nuclear properties of the cobalt triad isotopes

Nucleus	Spin	Abundance (%)	Quadrupole moment · 10^{28} (m^2)	Usual shielding reference	Receptivity re ^{13}C
^{59}Co	7/2	100	0·4	$Co(CN)_6^{3-}$	1570
^{103}Rh	1/2	100	0	$\Xi = 3{\cdot}16$ MHz	0·177
^{191}Ir	3/2	37·3	1·5	—	0·054
^{193}Ir	3/2	62·7	1·5	—	0·117

studies published and receptivity of the nucleus is fairly close, and within the cobalt triad a large variation in receptivity is encountered. Thus ^{103}Rh, with a receptivity of 0·177 has never been observed directly in solution. The considerable body of rhodium shielding information condensed into Fig. 8 has been obtained by indirect observation and is available because ^{103}Rh has spin $I = 1/2$. Both isotopes of iridium have even lower receptivities and no NMR studies of this element have yet been reported.

A. Cobalt-59

The $Co(CN)_6^{3-}$ ion which is stable, water soluble, and has a sharp ^{59}Co resonance, absorbs near the low frequency end of the cobalt range and is the preferred reference for the reporting of ^{59}Co chemical shifts. A comprehensive review of the literature to the end of 1976 is available, (87) and the shielding ranges observed for various cobalt environments are summarized in Fig. 6. These are seen to span a total of 18 000 ppm, with cobalt(III) complexes occupying the high frequency 14 000 ppm and cobalt(0)/cobalt(−I) carbonyl and phosphine complexes occupying the low frequency 3400 ppm, with no overlap between the two groups.

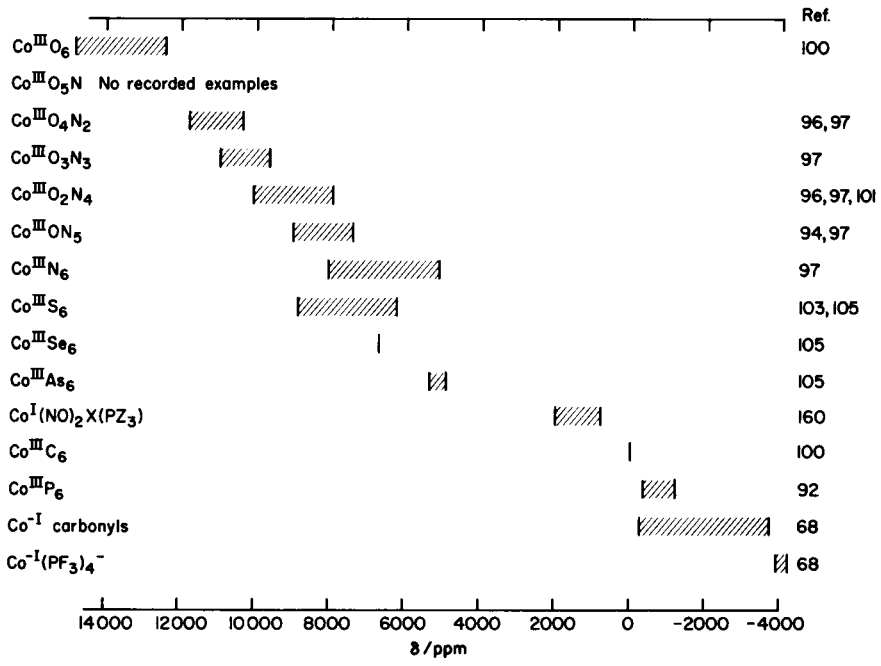

FIG. 6. ^{59}Co chemical shift ranges for Co^{III} and Co^{-I} in different chemical environments.

Recent studies have slightly extended both ends of the cobalt(III) chemical shift range. The central Co in the tetranuclear $[Co_4(OH)_6(NH_3)_{12}]^{6+}$ occupies an octahedral environment of six bridging OH^- ions, and its resonance position of $\delta = 14\,850$ is the most deshielded cobalt shift to be reported. (88) At the other end of the scale, several $Co(phosphite)_6^{3+}$ complexes have been studied, (89, 92) the most highly shielded of which has $\delta = -1243$. In keeping with the current interest in metal complexes in biology, eight glycinato complexes have been studied and their cobalt shieldings enable the identification of different geometric isomers. (90) For $Co(NH_2CH_2COO)_3$ the *fac* isomer is more highly shielded than the *mer* isomer by 293 ppm, while in $Co(C_2O_4)(NH_2CH_2COO)_2^-$ the *cis* isomer is more highly shielded than the *trans* isomer by 419 ppm. The effect of substituting ^2H for ^1H in $Co(en)_3^{3+}$ and $Co(am)_3^{3+}$ is a low frequency shift of 5 ppm in the cobalt resonance. (91)

1. First order shielding effects

Initiated by the pioneering work of Werner at the turn of the century, the preparation of 6-coordinate cobalt(III) complexes has developed into a cottage industry among inorganic chemists and provides the NMR spectroscopist with a larger variety of chemical environments for cobalt than for any other transition metal. While not all of these have received NMR study, the variety is sufficiently wide to provide a clear picture of how different ligands affect the shielding of cobalt. To a first approximation it is the ligating atom bonded to the cobalt that determines the chemical shift; differences in shielding ability among ligands all of which bind through the same atom are less. Figure 6 illustrates the shielding ranges for $Co^{III}L_6$ complexes and for $Co^{III}O_xN_{6-x}$ mixed ligand complexes. Shielding data for specific ligands which may not form CoL_6 complexes are available from a number of systems in which bonding at five coordination positions is held constant while different ligands are successively substituted in the sixth position. LaRossa and Brown (93) have provided data for a consistent set of 13 methyl cobaloximes with $CoCN_4L$ coordination; these are given in Table IX. Data from different authors and therefore less internally consistent are also provided for a series of $Co(NH_3)_5L$ complexes, thereby extending the variety of ligands studied.

As we descend the separate lists in Table IX the ability of the ligand to increase the shielding of cobalt increases. For ligands which bond through a first-row element, the increasing shielding order is $F < O < N < C$, the same as the order with which these ligating atoms appear in the spectrochemical series (98) by virtue of their increasing ability to cause d-orbital splitting in the cobalt. Among N-bonding ligands, bidentate ones such as ethylenediamine, π-acceptor bidentates such as *o*-phenanthroline, and stronger

TABLE IX

^{59}Co chemical shifts for some cobaloxime and pentammine complexes

Compound	δ	Ref.	Compound[a]	δ[b]
$Co(NH_3)_5L^{n+}$			$CH_3Co(dh)_2^-$	
$L = F^-$	9520	94	CH_3OH	4110
$C_2O_4^{2-}$	9130	95	NMe_3	3790
OH^-	9117	94	NC_5H_5	3660
H_2O	9060	94	β-picoline	3660
CO_3^{2-}	9000	96	SMe_2	3190
NO_3^-	8930	95	$AsPh_3$	2950
CH_3COO^-	8910	95	PPh_3	2800
Cl^-	8850	94	$CNCH_3$	2680
Br^-	8820	94	$P(n\text{-}Bu)_3$	2620
I^-	8760	94	$P(OMe)_3$	1580
SCN^-	8760	95	NC_5H_5	5170
N_3^-	8680	97	PPh_3	4790
NCS^-	8200	95	$P(n\text{-}Bu)_3$	4130
NH_3	8150	97	$P(OMe)_3$	3600
NO_2^-	7630	94		

[a] (dh) = dimethylglyoximato monoanion.
[b] Reference 93 converted using $\delta[Co(NH_3)_6]^{3+} = 8150$.

π-acceptors such as NO_2^- cause progressively higher shielding than NH_3 and also occur higher in the spectrochemical series. The reason for this close correlation lies in the theoretical model (99) used to explain the paramagnetic contribution σ_p which dominates ^{59}Co shielding variations,

$$\sigma_p = (\text{constant}/\Delta E)\langle r^{-3}\rangle_d \qquad (2)$$

In equation (2), $\langle r^{-3}\rangle_d$ refers to the inverse cube of the separation of the d electrons from the ^{59}Co nucleus. Provided the size of the cobalt 3d-orbitals remains constant throughout the series of complexes studied, then δ will correlate with $1/\Delta E$ for the optical *d–d* transition on cobalt. This relationship has been observed for C-, N-, O- and F-bonding ligands by Freeman, Murray, and Richards, (100) by Kanekar, (95, 101) and by Biradar. (96, 102)

As the range of cobalt complexes studied has been extended to include P-, As-, S-, and Se-bonding ligands, the fact that they do not fit the same correlation line has become increasingly obtrusive. (92, 103, 105) It is also clear that while Cl^-, Br^-, and I^- appear in the spectrochemical series in the order:

$$I^- < Br^- < Cl^- < F^- < O < N < C$$

their ability to shield cobalt is $F^- < Cl^- < Br^- < I^-$, i.e. the NHD for metal

chemical shifts, and the reverse of the order predicted by $1/\Delta E$ considerations. These two factors taken together lead inexorably to the conclusion that for ligands which bind through atoms lying below the first row of the Periodic Table, $\langle r^{-3}\rangle_d$ does *not* remain constant, but diminishes below its free Co^{3+} ion value by an amount that depends upon the ability of the ligand to increase $\langle r\rangle_d$.

A measure of the abilities of different ligands to accomplish this d-orbital expansion is provided by the nephelauxetic series (106) where, based upon reductions in term separations observed in the electronic spectra of complexes, ligands appear in the order:

$$F^- < H_2O < NH_3 < NCS^- < Cl^- \approx CN^- < Br^- < I^-$$

The most significant difference between the spectrochemical series and the nephelauxetic series is the re-location of Cl^-, Br^-, and I^- from the bottom of the former to the top of the latter, and in the *reverse* order. It was this nephelauxetic ordering of Cl^-, Br^-, and I^- that was first used to explain the halogen dependence of ^{27}Al shielding in the AlX_4^- tetrahalides, (107) and it is this phenomenon, operating through the $\langle r^{-3}\rangle_d$ term in the σ_p expression, equation (2), that is responsible for all cases of NHD.

2. *Second order shielding effects*

The shielding ability of different ligands is determined primarily by the atoms through which they coordinate, and this is seen from Fig. 7 and Table X to increase in the order:

$$F < O \approx Cl \approx Br \approx I < N \approx S \approx Se \approx As < C < P$$

If each ligand contributed to the cobalt shielding a constant increment independent of the nature of its neighbours, then a substituent constant value for each ligand could be determined and the cobalt chemical shift in an octahedral complex would be represented by the sum of six substituent constants. Within this simple theoretical perception of metal shielding, geometrical isomers would all exhibit the same cobalt chemical shift. The fact that systematic shielding differences between geometric isomers are observed (89, 97) indicates that second order effects, dependent upon interactions with neighbouring ligands, also contribute to the metal shielding.

While there are exceptions, it is generally observed that *cis* isomers give higher shieldings than *trans*, and *fac* isomers give higher shieldings than *mer*. (90, 97) The differences range from barely perceptible up to 600 ppm and tend to be larger where chelating ligands are involved. No satisfactory

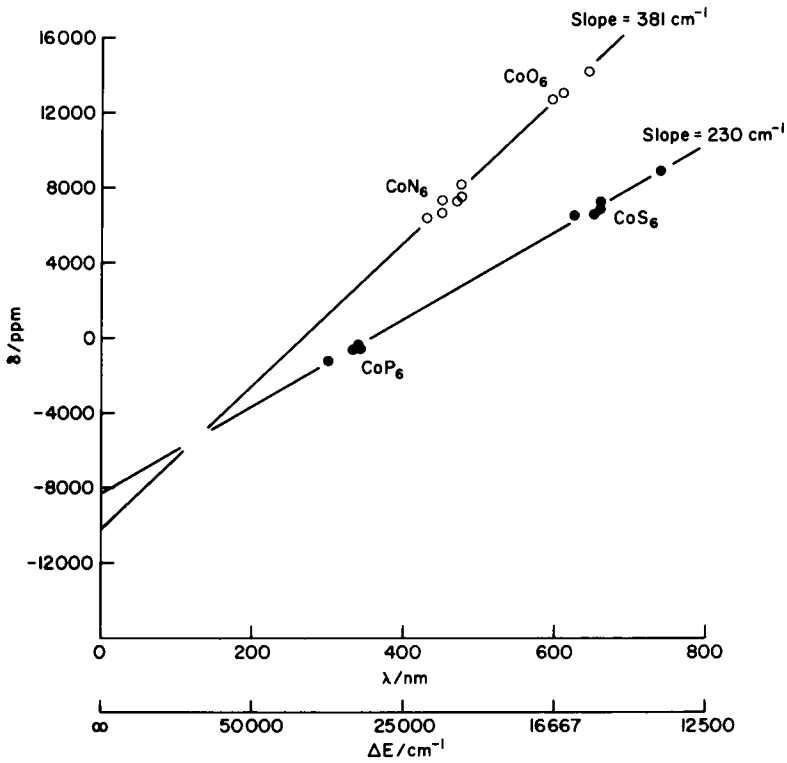

FIG. 7. ^{59}Co chemical shift dependence upon $1/\Delta E$ for octahedral cobalt(III) complexes. CoN_6 data from ref. 100; CoO_6 data from ref. 100; CoP_6 data from ref. 92; CoS_6 data from ref. 105.

theoretical understanding of this has yet been worked out, but the structural dependence is similar to that which has been expressed for a number of other metals in tetrahedral (108, 109) and octahedral (110) environments using empirical pairwise additivity parameters which contain both the first order and the second order shielding information for each ligand.

An elegant study of the second order effects whereby the contribution to the environment of a cobalt atom made by one ligand is influenced by neighbouring ligands has been carried out by LaRossa and Brown. (93) They have succeeded in fractionating the electric field gradient in cobaloximes, as measured by ^{59}Co NQR spectroscopy, into separate contributions from individual ligands. The extent to which variations in the axial ligands affect the partial field gradient contributions of the equatorial ligands has been determined, and a regular monotonic relationship between the ^{59}Co NMR and NQR data has been established. Relationships of this sort result in part from the fact that σ_p and the electric field gradient both depend upon $\langle r^{-3} \rangle_d$.

3. *Theory of cobalt shieldings*

The basic shielding model developed by Ramsey (111) starts with the bare nucleus and formulates a screening constant as the sum of the diamagnetic and paramagnetic terms as shown in equation (1). These represent respectively the diamagnetic field induced at the nucleus by the unhindered motion of the electrons in the free atom, and the paramagnetic field induced at the nucleus by the electronic angular momentum developed through interactions with other atoms. Variations in σ_d from one compound to another are believed to be so small that cobalt shifts are discussed solely in terms of variations in σ_p. Equation (2) may be rewritten:

$$\sigma_p = [\text{constant} \cdot (k')^2/\Delta E]\langle r^{-3}\rangle_d \qquad (3)$$

where k' is referred to as the "orbital reduction factor" after Griffith; the more cumbersome but more specific "orbital momentum reduction factor" would avoid confusion in NMR circles with the complexing effect upon $\langle r^{-3}\rangle_d$ which leads to an *increase* in orbital *size*. The constant is the appropriate proportionality that relates electronic orbital momentum to a magnetic moment at the metal centre which in the case of Co^{3+} takes the value $-32\ \mu_B^2$ where μ_B is the Bohr magneton.

In practice it is difficult, if not impossible, to separate the k' and the $\langle r^{-3}\rangle_d$ effects upon σ_p because both factors become progressively reduced below their free Co^{3+} ion values with increasing covalency. For purposes of plotting experimental data, they are combined into one variable B regarded as the orbital angular momentum variable, and the total shielding is expressed by equation (1). The effects upon cobalt shieldings of each of these variables are now considered in turn.

Linear dependence on $1/\Delta E$. The qualitative correlation between sample colour and large high frequency chemical shift was first observed for ^{59}Co in 1957, and a plot of σ vs. $1/\Delta E$ for 14 different complexes containing C-, N-, and O-bonding ligands turned out to be remarkably linear, (100) to the extent that the past 20 years has seen many attempts to correlate the shieldings of various nuclei with $1/\Delta E$ in circumstances where such a correlation clearly does not exist. It is certainly true, however, that many of the transition metals and some of the other elements obey the correlation. In general, compounds with low-lying electronic excited states giving rise to transitions in the visible and near-ultraviolet regions do show marked NMR deshielding. For compounds characterized by larger ΔE in which the electronic excited states are less accessible we must look elsewhere for a chemical shift rationale.

A δ *vs.* $1/\Delta E$ plot of the type shown in Fig. 7 furnishes both a slope and an intercept value that provide theoretical insight into cobalt shielding. The angular momentum factor B is obtained directly from the slope of the line.

TABLE X

Paramagnetic term dependence of ^{59}Co upon ΔE and B

Cobalt environment	Slope[a] B (cm^{-1})	Intercept[b] $\delta(Co^{3+})$ (ppm)	$\gamma(^{59}Co)/2\pi.10^{-7}$ ($T^{-1}s^{-1}$)	$\langle r^{-3}\rangle_d$ (au)	$(k')^2$	B/B_0[c]	Ref.
Co^{3+} free ion				6·7	1·00	1·00	118
C-, N-, O-ligands	495	−15 395		5·3[d]			99
C-, N-, O-ligands	450	−13 995	0·9963				100
CoSi, $CoSi_2$		−5 000	1·0054(20)				112
$Co(CN)_6^{3-}$ (imputed)		−5 000	1·0054(20)	4·8[e]	0·4	0·29	112
N-, O-ligands	400	−11 000	1·0015(2)			0·64	113
$Co(CN)_6^{3-}$		(−11 000)	1·0015(2)			0·57	113
S-ligands		(−11 000)	1·0015(2)			0·45	113
C-, N-, O-ligands	450	−13 842				0·64	114
S-, Se-, As-ligands	310[g]	(−13 842)				0·45	114
$Co(C_5H_5)_2^+$ solid		−6 800	1·0035		0·7		115
C-, N-, O-ligands	440	−14 000		6·7	0·72[f]	0·72	116
Si-, P-, S-, Cl-ligands	315[g]	(−14 000)		6·7	0·52[f]	0·52	116
As-, Se-, Br-ligands	275[g]	(−14 000)		6·7	0·45[f]	0·45	116
Tris-(β-diketonates)	270	−3 625					117
C-, N-, O-ligands	450	−13 900					92
S-, P-ligands	230	−8 260					92
N-, O-ligands	381	−10 275	1·0011				[h]

[a] Assumes $B \neq f(E)$.
[b] Extrapolated or calculated $\delta[Co(CN)_6^{3-}]$ value for free Co^{3+} ion.
[c] $B/B_0 = (k')^2 \langle r^{-3}\rangle_d$ (complex)/$\langle r^{-3}\rangle_d$(free ion).
[d] Estimated from Co^{2+} ESR studies.
[e] Co^0 value from ref. 118.
[f] Authors incorporate all orbital momentum reduction into k' term.
[g] Slope obtained using intercept for C-, N-, O-ligands.
[h] Re-calculated in this study.

Since $B/\Delta E$ is a dimensionless constant, and since ΔE is normally expressed in cm^{-1}, B is most conveniently reported in cm^{-1}. Because the ΔE^{-1} axis in chemical shift correlation plots is frequently calibrated in nm, the slope conversion factor 1 (ppm/nm) = 10 cm^{-1} should be recognized. The y-intercept at $\Delta E^{-1} = 0$ is of particular interest since it represents the shielding of a Co^{3+} ion with a spherically symmetric charge distribution for which

$\sigma_p = 0$. The δ-value for this point on the shielding axis differs from that for the bare ^{59}Co nucleus by the magnitude of σ_d which has been calculated to be 2166 ppm. (119) Because this state for the cobalt atom is at least hypothetically, if not experimentally, accessible, it provides a chemically unencumbered state for evaluation of the ^{59}Co magnetogyric ratio γ, and some spectroscopists (96, 113) urge its adoption as an "absolute" reference for the reporting of cobalt chemical shifts. As is shown in Table X, however, slope variations coupled with the length of the extrapolation give intercept values which vary between $\delta = -8570$ and $\delta = -15\,395$, an uncertainty range hardly befitting a reference point.

The intercept at $\delta \approx -14\,000$ first measured by Freeman, Murray, and Richards (FMR) (100) and subsequently verified in three other studies (92, 114, 116) was, until 1979, the only extrapolated value upon which any reliance could be placed. All the others available involve a more limited range of ligands and hence greater slope uncertainties. For complexes involving the larger 2nd and 3rd row ligating atoms, the chemical shift range available is so small that only by utilizing the $\delta = -14\,000$ intercept as a fixed point on the line could slopes, and hence B-values, be obtained. An NMR study of CoSi and $CoSi_2$ intermetallic compounds (112) and a study of chemical shift anisotropy in $[Co(C_5H_5)_2]NO_3$ (115) both carried out in the solid state and both directed at evaluating $\gamma(^{59}Co)$ obtained γ-values higher by 9000 ppm and 7200 ppm respectively than the FMR value which convert to $\delta(Co^{3+})$ values of -5000 and -6800 respectively. In both cases these intercept values are considerably higher than the FMR value and have been rationalized by arguing that B does not remain constant even for ligating atoms from the same row and that the linearity obtained by FMR was fortuitous. Given the attitude of most scientists that has Nature behaving in a linear fashion, this rationalization lacks conviction, since B variation for 2nd and 3rd row ligating atoms can already be accommodated by slope variations while retaining the same intercept. In 1979, however, Weiss and Verkade (92) published the first shielding data for CoP_6 environments thereby permitting a slope evaluation for P- and S-ligands independent of the $\delta = -14\,000$ intercept. As shown in Fig. 7, this gives an intercept of $\delta = -8260$, almost within the ± 2000 ppm uncertainty limits on the $\delta = -5000$ value of Walstedt *et al.* (112)

Ignoring the $Co(CN)_6^{3-}$ shift which is the only CoC_6 point available, a least-squares fit of the first-row ligand line to the CoN_6 and CoO_6 data gives an intercept at $\delta = -10\,275$. The mean position for these two intercepts is $\delta = -9265$ giving a $(\gamma/2\pi)(^{59}Co)$ value of $1{\cdot}001 \times 10^7\ T^{-1}\ s^{-1}$. This now represents the most reliable magnetogyric ratio value for ^{59}Co corrected for orbital paramagnetism. The fact that $Co(CN)_6^{3-}$ falls well off the line for first-row ligands is not unexpected. In comparison with N- and O-ligands, CN^- appears near the top of the nephelauxetic series along with ligands such

as Br^- and I^- whose shielding effect is manifest more through the B term than through the ΔE^{-1} term.

Effects of orbital momentum reduction. When the chemical shifts for those complexes formed with second- and third-row ligands are plotted against $1/\Delta E$, the points do not fall on the same correlation line as do those for first-row ligands, but establish a new correlation line having a lower slope. Since the slope, B, is a measure of orbital angular momentum, this indicates a reduction brought about by replacing first-row ligands with second-row ligands. Independent evidence obtained from magnetic susceptibilities and from the electronic spectra of transition metal complexes confirms this reduction. Variations in spin–orbit coupling (as measured by magnetic moments of paramagnetic complexes) and in the inter-electron repulsion (as measured by spectroscopic term separations) of metal ions, as the ligand is changed, both indicate that all ligands increase the radial size of the metal valence orbitals beyond their free-ion value, and that some ligands cause a greater "nephelauxetic effect" than others. The fractions of its free ion value to which different ligands reduce $\langle r^{-3}\rangle_d$ for Co^{3+} are: (106) oxalate ion (0·47), NH_3 (0·49), ethylenediamine (0·53), CN^- (0·30). These data show that, while reasonable constancy of B can be expected among N- and O-ligands, a reduced value is to be expected for CN^- as is born out in Fig. 7. This constitutes the evidence that variations in $\langle r^{-3}\rangle_d$, resulting from varying ligation, affect metal atom chemical shifts even in those cases where the shielding is dominated by the $1/\Delta E$ factor. In cases where $1/\Delta E$ is small, the $\langle r^{-3}\rangle_d$ factor becomes paramount.

Several authors (104, 105) introduce the "orbital reduction factor" k' as a third empirical variable used to rationalize cobalt shieldings. This factor has its origin in the theoretical treatment of magnetic susceptibility and ESR measurements where it provides a measure of reduction in the spin–orbit coupling constant. While the nephelauxetic factor has its origins in electronic spectroscopy, k has its origins in the magnetic properties of complexes, and it is questionable whether they should be regarded as independent phenomena. There has been no experimental demonstration of the one effect operating independently of the other, and since any structural change which affects one is expected to alter the other in the same direction, for NMR purposes the two effects should be regarded as synonymous, with variations in B being attributed to the product $(k')\langle r^{-3}\rangle_d$. This has been done in the B/B_0 column of Table X, and the plots in Fig. 7 reflect in their slopes a pattern of decreases in B on going from first- to second- to third-row ligands.

What emerges from all this with reasonable certainty is the following picture for ^{59}Co shieldings:

(i) The orbital momentum factor B for N- and O-ligands is roughly constant. ^{59}Co chemical shifts for complexes with these ligands

correlate well with their $1/\Delta E$ values and give a Co^{3+} intercept at $\delta = -10\,275$.

(ii) The orbital momentum factor, B, for $Co(CN)_6^{3-}$ is lower than that of the N-, O-ligand value, accounting for its position below the first-row ligand correlation line.

(iii) The slope for the P-, S-ligand second-row correlation line is lower than that for first-row ligands, the reduction being $B_2 = 0{\cdot}6B_1$. This line gives a Co^{3+} intercept value of $\delta = -8260$.

(iv) The intercept values for the two correlation lines establish the outer limits for the resonance position of the free Co^{3+} ion (spin-paired). The mean value at $\delta = -9265$ represents the most probable "measured" value.

B. Rhodium-103

All the ^{103}Rh NMR data to be reported, apart from some Knight shift measurements done on rhodium metal and its alloys in the solid state, (120, 121) have been obtained by indirect observation and necessarily involve compounds in which ^{103}Rh is coupled to another $I = 1/2$ nucleus, the foremost examples being ^{1}H, ^{31}P, and ^{13}C. This requirement makes unavailable at present shielding data for RhX_6^{3-} ($X = Cl^-$, Br^-, I^-), nor do we have anything as yet on the aquo-cation $Rh(H_2O)_6^{3+}$.

The reference which has been adopted by Goodfellow and coworkers (122) for reporting rhodium shieldings is $\Xi(^{103}Rh) = 3{\cdot}16$ MHz, and this is the $\delta = 0$ value to which all the data in Fig. 8 have been converted. This reference frequency is near the low frequency end of the shielding spectrum and results in positive δ-values for most rhodium environments.

The range of rhodium shieldings illustrated in Fig. 8 spans 6300 ppm, a range considerably less than that of both ^{59}Co (19 100 ppm) and ^{195}Pt (13 400 ppm). A comparison in Figs. 6, 8 and 9 of corresponding cobalt, rhodium, and platinum compounds shows the variety of rhodium environments studied to be more restricted than that of the other two metals. Eliminating PtF_6^{2-} and $PtCl_6^{2-}$, for which there are no analogous rhodium data, leaves a ^{195}Pt range of 4500 ppm, indicating the inherent shielding sensitivities of rhodium and platinum to be comparable. In comparison with cobalt, rhodium lacks examples of coordination by O- and N-bonding ligands which dominate the deshielded end of the cobalt spectrum. In addition, since no δ *vs.* $1/\Delta E$ correlations are available for rhodium, no estimate of the δ-value for the free Rh atom can be made. While a clearer picture will emerge when information of both types becomes available, it appears that the shielding sensitivity of rhodium is lower than that of cobalt. The ^{103}Rh shift for RhF_6^{3-}, known to be diamagnetic and distinguished from the high-spin CoF_6^{3-}, which is potentially available by ^{19}F decoupling

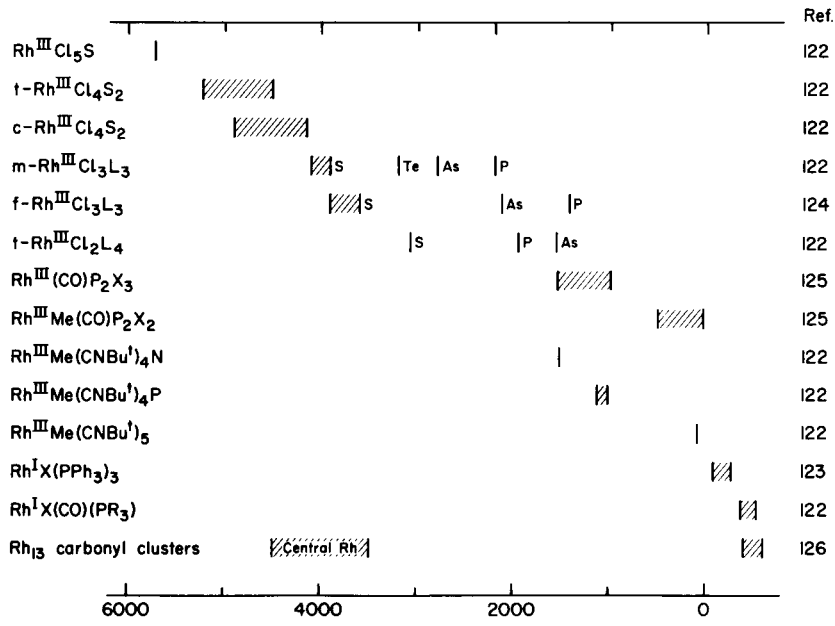

FIG. 8. ^{103}Rh chemical shifts for Rh^{III} and Rh^{I} in different chemical environments.

should settle the question by demarcating the high frequency end of the rhodium spectrum.

The limited range of rhodium compounds to be investigated consists primarily of trihalide complexes of Rh^{III} in which the other three coordination positions are occupied by C-, P-, S-, and As-bonding ligands (122–125) and of 4-coordinate phosphine and carbonyl complexes of Rh^{I} containing one halide ion. (123, 125, 126) The pattern of rhodium shieldings exhibited by these compounds is similar to that displayed by other transition metals. The lower oxidation state phosphine and carbonyl complexes occupy the upper 1500 ppm of the ^{103}Rh shielding range. An interesting feature of the Rh–carbonyl cluster compounds is that both $Rh_{13}(CO)_{24}H_2^{3-}$ and $Rh_{13}(CO)_{24}H_3^{2-}$ have a high frequency rhodium resonance around $\delta = 4000$ which has been assigned to the central rhodium atom in the cluster and whose large shift to high-frequency results from extensive metal–metal bonding. The Rh^{III} compounds occupy the lower 5700 ppm of the range and overlap the Rh^{I} compounds to the extent of about 900 ppm. While there is little or no data with which to assess the effects of N- and O-bonding ligands, and leaving aside the effects of halide ions for the moment, the S-ligands produce the largest high frequency shifts, followed in order of increasing shielding by $S < N < P \approx As < C$. The $RhCl_xS_{6-x}$ complexes in Fig. 8 provide

a set of chemical shifts sufficiently systematic to permit extrapolation in both directions, yielding reasonable estimates for the shielding in $RhCl_6$ and RhS_6 environments of $\delta \approx 2000$ respectively.

Shielding data for a number of comparable chloride, bromide, and iodide complexes establish rhodium as a metal whose chemical shifts show a NHD with iodides absorbing to low frequency. Both octahedral Rh^{III} and planar Rh^{I} complexes follow this pattern, and the (Cl–Br)/(Cl–I) ratio for both planar and octahedral complexes containing one, two, or three halide ions per complex is remarkably constant around 0·32 as shown in Table XI.

TABLE XI

Halogen dependence of ^{103}Rh shieldings

Compound	X =	$\delta(^{103}Rh)$ Cl	Br	I	$\frac{(Cl-Br)}{(Cl-I)}$	Ref.
cis-$RhX_4(SMe_2)_2^-$		4882	4339	3070	0·30	122
trans-$RhX_4(SMe_2)_2^-$		5226	4532	2958	0·31	122
mer-$RhX_3(PMe_3)_3$		2202	1746	809	0·33	122
mer-$RhX_3(AsMe_3)_3$		2806	2276	1191	0·33	123
mer-$RhX_3(SMe_2)_3$		3897	3437	2448	0·32	124
mer-$RhX_3(TeMe_2)_3$		3179	2567	1352	0·33	122
trans-$RhX_2(PMe_3)_4^+$		1564	1154	398	0·35	122
cis,trans-$RhX_2Me(CO)(PMe_2Ph)_2$		499	351	52	0·33	125
trans-$RhXMe(CNBu^t)_4^+$		526	367	107	0·38	122
$RhX(PPh_3)_3$		−81	−142	−268	0·33	123
trans-$RhX(CO)(PMe_2Ph)_2$		−405	−441	−523	0·31	125

Second order shielding effects resulting from geometric isomerism are consistent with the pattern observed in the case of ^{59}Co. *cis*-Isomers are more highly shielded than *trans*-isomers by 344 ppm in the case of $RhCl_4(SMe_2)_2$ and by 361 ppm in the case of $RhCl_4(SOMe_2)_2$. *fac*-Isomers are more highly shielded than *mer*-isomers, by 756 ppm in the case of $RhCl_3(PMe_3)_3$ and by 217 ppm for $RhCl_3(SMePh)_3$. Other examples with differences lying in these ranges are available. (122)

IX. THE NICKEL TRIAD

The NMR characteristics for this triad are in Table XII. Neither nickel nor palladium has yielded any NMR information that might be of interest to the chemist. This situation could be accounted for solely on the basis of their low

TABLE XII

Nuclear properties of the nickel triad isotopes

Nucleus	Spin	Abundance (%)	Quadrupole moment . 10^{28} (m^2)	Usual shielding reference	Receptivity re ^{13}C
^{61}Ni	3/2	1·19	unknown	—	0·24
^{105}Pd	5/2	22·23	unknown	—	1·41
^{195}Pt	1/2	33·8	0	$\Xi = 21{\cdot}4$ MHz	19.1

receptivities which would make the acquisition of signals tedious and time consuming. In addition, however, most nickel compounds that might be of interest are paramagnetic, and palladium probably has a quadrupole moment of sufficient magnitude to broaden beyond recognition the weak signals which might otherwise be detected.

We now have a large and rapidly increasing body of data available for platinum which is the result of two happy coincidences. The ^{195}Pt nucleus has a receptivity about 20 times greater than ^{13}C and is therefore readily amenable to direct observation. In many of its compounds, ^{195}Pt, having $I = 1/2$, is spin coupled to ^{1}H, ^{13}C, or ^{31}P, each of which provides an opportunity for indirect observation of ^{195}Pt through spin decoupling. The INDOR technique has been extensively applied to platinum, and the largest part of our present ^{195}Pt information has been obtained by indirect observation.

A. Platinum-195

A good reference for ^{195}Pt chemical shifts possessing the desirable features of ease of reproducible preparation, low coefficients for temperature, concentration, and counter-ion dependence, and shielding near the low frequency end of the range is not readily apparent, and aqueous $Pt(CN)_6^{2-}$ has been adopted as the best compromise. Its ^{195}Pt Ξ value of 21 414 376 (20) Hz contains an uncertainty of just under 1 ppm. For the reporting of chemical shifts, the $\delta = 0$ has been established at $\Xi(^{195}Pt) = 21{\cdot}4$ MHz which places $Pt(CN)_6^{2-}$ at $\delta = 672$; Goodfellow has outlined the arguments favouring this choice. (70) Although the resonance position for the free, gaseous platinum atom has not been measured, it has been estimated from the δ *vs.* $1/\Delta E = 0$ to be $\delta = -5906$ (71, 106). It would be useful to have a hydration shift value for Pt^{2+} to compare with that for other metallic cations. In the absence of a measured shift for $Pt^{2+}(aq)$ an estimated position of $\delta = -750$ (100) lying between $Pt(CN)_4^{2-}$ and PtI_4^{2-} appears reasonable by analogy with the corresponding ^{67}Zn and ^{113}Cd patterns. The

difference between these two estimated resonance positions gives an estimated hydration shift for Pt^{2+} of *ca.* 5150 ppm.

Figure 9 shows the current range of platinum shifts to cover about 14 000 ppm, with all of the typical platinum environments now accounted for. While among the transition metals this range is second only to that of ^{59}Co, the range for all ligands except F^- can be accommodated within 6000 ppm. For platinum in the zero and negative oxidation states stabilized by phosphine and carbon monoxide ligands, absorption in the highly shielded region with $\delta < 250$ occurs. (71, 76, 77) Most Pt^{II} and Pt^{IV} compounds contain one or more halogens, and where present these dominate the platinum shielding as discussed below. Most combinations of halogen and other ligating atoms in various proportions have now been investigated, and the platinum shift data available are rather extensive. In Fig. 9 only the shielding pattern for $PtCl_3L$ complexes is illustrated as this represents the most complete body of data with which to compare the shielding properties of non-halogen ligands. When substituted for Cl^- in $PtCl_4^{2-}$, N-bonded ligands increase Pt shielding by up to 400 ppm, P-bonded ligands increase the shielding by about 2000 ppm, and chalcogen ligating atoms, Sb, and As all lie between these two extremes.

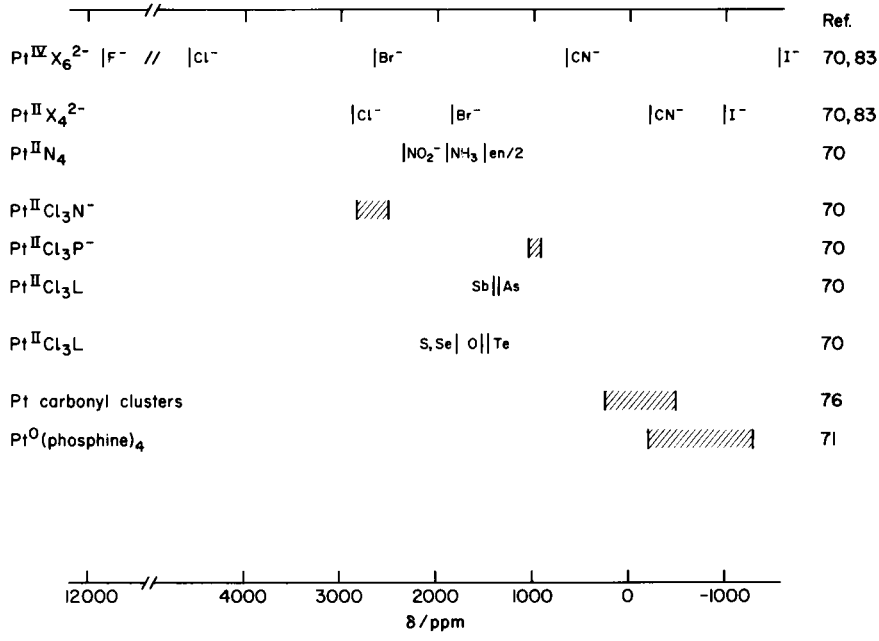

FIG. 9. ^{195}Pt chemical shifts for Pt^{IV}, Pt^{II}, and Pt^0 in different chemical environments.

Those combinations that have undergone recent investigation are with ammonia and glycine, (74) with phosphines, (78, 80) with pentaborane, (80) and with hydride. (78)

1. Halogen environments

The halide complexes of platinum were among the earliest ^{195}Pt resonances to be observed, (82) and their study by several groups of workers (70, 71, 75, 83) has produced an extensive and coherent body of platinum shielding data for both the pure (PtX_4^{2-}, PtX_6^{2-}) and the mixed ($PtX_nY_{4-n}^{2-}$, $PtX_nY_{6-n}^{2-}$) halides of Pt^{II} and Pt^{IV}. In addition to delineating the present range of platinum shifts from the most highly shielded for PtI_6^{2-} to the most deshielded for PtF_6^{2-}, these data will undoubtedly provide the basis for the theoretical understanding of platinum shieldings which has yet to be worked out. For the octahedral PtX_6^{2-} halides, the (Cl–Br)/(Cl–I) ratio is 0·31, a value comparable to that for the tetrahedral halides, and for the square planar PtX_4^{2-} complexes it is 0·27. These complexes represent the limiting case in tetragonal distortion of tetrahedral MX_4 halides, and the ratio value of 0·27, which is only 10% lower than the norm for tetrahedral halides, indicates that the value of this ratio is relatively insensitive to the symmetry of 4-coordinate complexes.

The platinum shieldings in the mixed tetrahalides and hexahalides obtained by successive substitution of Br^- or I^- for Cl^- in $PtCl_4^{2-}$ and $PtCl_6^{2-}$ undergo regular, though not linear, increases with increasing substitution. Thus it is not just the identity of a particular substituent but also the identity of its neighbours, that determines the contribution made to the metal shielding. For 6-coordinate complexes this has the particular advantage of making the platinum shielding sensitive to *cis/trans fac/mer* isomerism, enabling distinctions to be made about isomers in solution, distinctions that are inaccessible by other techniques.

The high frequency shift caused by fluoride ion coordination, which alone extends the platinum shielding range another 7300 ppm beyond that of $PtCl_6^{2-}$, is quite remarkable. While there are other examples of fluoride shielding to high frequency of chloride, e.g. ^{121}Sb and ^{59}Co, in both of these cases the deshielding is only slightly less than that found in the chloride, and the pattern observed for most metals is one in which the fluoride causes *greater* shielding than the chloride; in some cases (e.g. ^{11}B, ^{27}Al) it is almost as great as the iodide. The platinum shielding in PtF_6^{2-} is best compared with the metal shielding in $^{47}TiF_4$ and in $^{93}NbF_6^-$, both of which metals show an IHD. TiF_6^{2-} absorbs 1177 ppm to low frequency of $TiCl_4$, and NbF_6^- absorbs 1490 ppm to low frequency of $NbCl_6^-$; in both cases the low frequency shift is greater than is the shift of the bromide complex to high frequency of the chloride.

X. ^{51}V, ^{55}Mn, ^{59}Co NMR OF ORGANOMETALLICS

Transition metal chemistry divides naturally into two categories. In the first category are the traditional coordination complexes in which a metal atom in an oxidation state of +2 or higher combines with N-donor, O-donor, and halide ion ligands. The basic principle at work in this category is the achievement by the metal ion of a 6-coordinate octahedral structure, and in this process the valence shell electron configuration is a dependent variable determined by the oxidation state of the metal. Thus many of these complexes contain unpaired electrons and the magnetic susceptibility is an important parameter in their characterization. The second category upon which attention has focused in recent years contains the organometallic compounds of metal atoms in their low oxidation states of +1, 0, and −1 combined with C-donor and P-donor ligands which are capable of functioning as π-acceptors thereby stabilizing the low oxidation state. Here the fundamental structural consideration is the "effective atomic number" or "eighteen electron rule" whereby the metal atom binds the appropriate type and number of ligands to achieve a valence shell electron configuration of eighteen. For the later transition metals such as platinum, increasing numbers of compounds obeying a sixteen electron rule are emerging, and it is these elements that have the least tendency to be 6-coordinate. In either case, the compound is almost invariably spin-paired and diamagnetic.

For those transition metals forming compounds in each category, the pattern of metal atom shielding parallels the category of compound with uniform regularity. In every case for which chemical shift data are available, the organometallic compounds occupy the top end of the shielding range while the higher oxidation state complexes are deshielded in comparison. The distinction is sufficiently clear for most metals that little or no overlap occurs between the two regions. Metal atom shielding in the higher oxidation complexes is discussed in the sections dealing with individual metals. The purpose of this discussion is to bring out the features of shieldings in the organometallic compounds that are common among different metals.

For each of ^{51}V, ^{55}Mn, and ^{59}Co we have a considerable body of shielding data on the low oxidation state organometallics which enable the recognition of a general shielding pattern. For some of the other transition metals there are chemical shifts for isolated compounds which can be fitted into the general pattern. The metals under consideration, shown in their periodic relationship to one another, are:

^{51}V	^{53}Cr	^{55}Mn	^{57}Fe	^{59}Co
	^{95}Mo			^{103}Rh
	^{183}W			^{195}Pt

The ligands that stabilize the low oxidation states and whose shielding

characteristics comprise the pattern we seek are:

CN^-, CO, NO^+
CH_3^-(alkyl), COR^-(acyl), H^-
η^5-C_5H_5, η^6-C_6H_6, η^2-C_2H_4
PR_3, PF_3
MX_3^-, MR_3^-(M = Si, Ge, Sn, Pb)
Cl^-, Br^-, I^-

The benchmark compounds from which to begin a discussion of metal shieldings in organometallics are the mononuclear carbonyls from which other compounds can, in concept, be derived through CO substitution by L. With the exception of $Co(PF_3)_4^-$ and the $Co(NO)_2X(PZ_3)$ series, all the low oxidation state organometallics considered here contain one or more carbonyl groups. The $M(CO)_xL_y$ series of compounds provides the most coherent set of compounds involving different L ligands and permits intermetal comparability for the metals listed above. The $CpM(CO)_xL_y$ series in which 2 or 3 CO groups have been replaced by a $C_5H_5^-$ ion provides a smaller but equally systematic set of data.

TABLE XIII

Ligand shielding patterns (ppm) with low oxidation state metals

Carbonyl benchmark	Carbonyl position re MO_4^{n-}	η^5-Cp^- shift re carbonyl	PF_3 shift re carbonyl	PR_3 shift re carbonyl
$^{51}V(CO)_6^-$	−1430	$CpV(CO)_4$ 450		100
$^{53}Cr(CO)_6$	−1760			
$^{95}Mo(CO)_6$	−1855			
$^{183}W(CO)_6$	−3600[a]	Cp_2WH_2 −1100/2		100
$^{55}Mn(CO)_6^+$	−2000[a]	$CpMn(CO)_3$ 250	−100	
$^{57}Fe(CO)_5$		Cp_2Fe	1865/2	
$^{59}Co(CO)_4^-$		$CpCo(CO)_2$ 420	−275	
$^{103}Rh_nCO$ clusters				200
$^{195}Pt_nCO$ clusters				−200

[a] Estimated value.

A. Carbonyls

For ^{51}V, ^{53}Cr, ^{95}Mo, ^{57}Fe, and ^{103}Rh, an unsubstituted carbonyl compound provides the most highly shielded metal environment recorded to date, while in the other cases the pure carbonyl shielding is only marginally exceeded by one involving PF_3 or hydride ion. The theoretical picture which

has metal shieldings determined by σ_p containing a $1/\Delta E$ and a $\langle r^{-3}\rangle_d$ factor provides three reasons why this should be so, listed here in order of decreasing importance:

(i) By virtue of stabilizing a low oxidation state with its reduced effective nuclear charge (Z^*), the CO group increases shielding by reducing $\langle r^{-3}\rangle_d$ and thus reducing σ_p.

(ii) The π-acceptor action of CO has a strong nephelauxetic effect on the metal-atom d-orbitals which make the major contribution to σ_p, thereby reducing $\langle r^{-3}\rangle_d$ and reducing σ_p.

(iii) For d^8 configurations where d–d electronic transitions are possible, the enhanced ligand field splitting of the d-orbitals, caused by π-bonding, increases ΔE and reduces δ. It is questionable whether the $1/\Delta E$ factor makes a significant contribution to *variations* in σ_p when ΔE exceeds *ca* 30 000 cm^{-1}.

For ^{51}V, ^{53}Cr, ^{95}Mo, ^{183}W, and ^{55}Mn, the metal shielding in the $M(CO)_6$ compound can be compared with that in the MO_4^{n-} tetrahedral oxyanions, each of which has low-lying electronic excited states which dominate σ_p through $1/\Delta E$. The shielding differences listed in Table XIII provide a nice measure with which to compare metal atom shielding sensitivities.

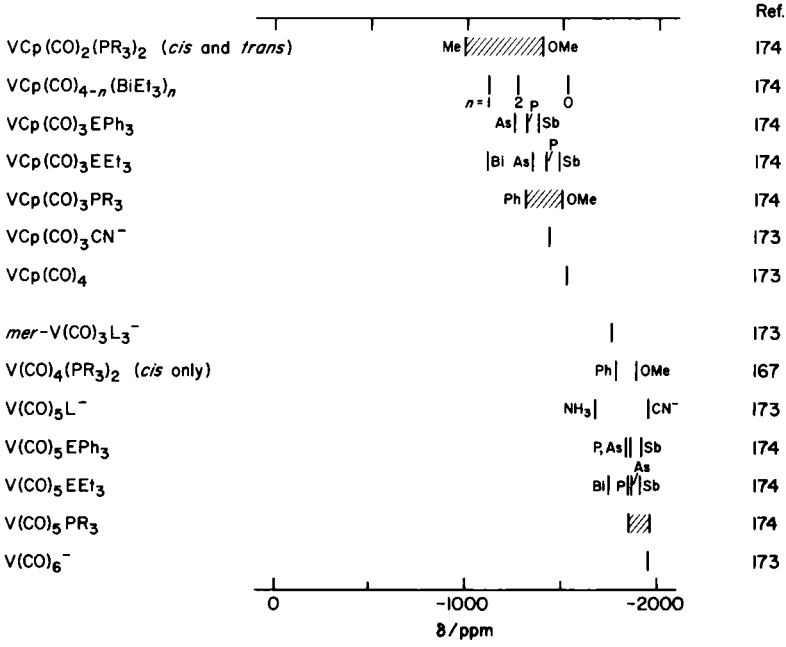

FIG. 10. ^{51}V chemical shifts for some lower oxidation state vanadium compounds.

B. Cyclopentadienides

The sets of compounds in which the cyclopentadienide anion has replaced 2–3 carbonyls are characterized by a shift to lower shielding. In the ^{51}V, ^{57}Fe, and ^{59}Co cases part of this deshielding results from the two-unit increase in the oxidation state of the metal. For ^{51}V and ^{59}Co the deshielding is about 435 ppm while for ^{57}Fe the deshielding is about twice this amount per Cp^-. With ^{55}Mn the deshielding is still 250 ppm on replacement of three CO with no change in oxidation state. The apparent anomaly where the ^{183}W signal moves to low frequency on Cp substitution is understandable in terms of the hydrogen which accompanies the Cp giving Cp_2WH_2. If it is regarded as a W^0 compound then the hydrogen is protonic, and protonation of ferrocene causes a ^{57}Fe low frequency shift of 1099 ppm (Table XIII). If the hydrogen is considered to be hydridic, H^- substitution of CO in $Mn(CO)_6^+$ shifts the ^{55}Mn resonance to low frequency by about 600 ppm (Fig. 5). Considering Cp substitution without oxidation state change to deshield by *ca.* 250 ppm, a hydrogen contribution of −800 ppm to give a net increment of −550 ppm per CpH combination is not unreasonable.

C. Phosphine substituents

^{51}V, ^{55}Mn, ^{59}Co, ^{183}W, ^{103}Rh, and ^{195}Pt all show sufficient incidence of phosphine substitution for a pattern to be recognizable in the shielding range figures. The only phosphine to appear in combination with ^{55}Mn and ^{59}Co is PF_3; in both cases it generates a higher shielding than CO, a not unexpected observation given the high π-acceptor strength of this ligand. With ^{51}V and ^{183}W, PPh_3 deshields by *ca.* 100 ppm per CO substituted; with trialkylphosphines the deshielding is slightly greater and with trialkoxyphosphines slightly less. With ^{103}Rh the deshielding is about 200 ppm per phosphine. ^{195}Pt is the only case where phosphines other than PF_3 shift the metal resonance to low frequency from the carbonyl. Since the reference in this case is not a mononuclear carbonyl, it is probable that the ^{195}Pt shielding in the polynuclear cluster compounds is lower than in the mononuclear benchmark compounds as a result of metal–metal interactions known to lower the metal shielding.

D. Metal substituents

Both ^{55}Mn and ^{59}Co provide extensive sets of data on ligands which bind through a trisubstituted Group IV metal. The Ph_3M ligands (M = Si, Ge, Sn, Pb) generate a 175 ppm range for ^{55}Mn and a 325 ppm range for ^{59}Co which straddles the carbonyl benchmark position in the case of cobalt and in the case of ^{55}Mn occurs 450 ppm to low frequency of the $Mn(CO)_6^+$ position. Substituted transition metals such as $(CO)_5Mn-$, $(CO)_4CoHg-$, and

$(CO)_4Co$–, acting in a similar capacity, show a remarkably uniform shielding reduction below the centre of the MPh_3 range, by the amounts:

	^{55}Mn	^{59}Co
$(CO)_5Mn$–	125 ppm	225 ppm
$(CO)_4CoHg$–		600 ppm
$(CO)_4Co$–	600 ppm	1025 ppm

It is useful to note that the L_3M– metal donor ligands represent a case where the shielding of the central metal is more sensitive to the substituent L than to the donor atom M. For L_3Sn– ligands the shielding range covered by variation in L is 540 ppm for ^{55}Mn and 600 ppm for ^{59}Co compared with 175 ppm and 325 ppm respectively. Comparable metal-donors for which ^{51}V data are available are the Group V atom ligands L_3M– (M = As, Sb, Bi) which absorb over a 350 ppm range centred 150 ppm to high frequency of $V(CO)_6^-$ in the same region as PR_3 ligands.

E. The hydrogen substituent

The bonding of hydrogen, be it hydridic or protonic, to a low oxidation state transition metal results in a marked shielding increase relative to the carbonyl benchmark. The most outstanding example is Cp_2WH_2 discussed above. Other examples are $HCo(CO)_4$ 620 ppm to low frequency of $NaCo(CO)_4$, $HMn(CO)_5$ 630 ppm to low frequency of $Mn(CO)_6^+$, and Cp_2FeH^+ 1099 ppm to low frequency of Cp_2Fe. In the case of ^{59}Co, the $HCo(PF_3)_4$ signal is 300 ppm to high frequency of its $NaCo(PF_3)_4$ counterpart, although still 200 ppm to low frequency of $HCp(CO)_4$. This comparison adds weight to the second-order shielding effect hypothesis in which one ligand affects the shielding strength of neighbouring ligands, and in this case the hydrogen attenuates the strong shielding properties of PF_3.

F. Halogen substituents

Because halogen shielding patterns are common to both the high and low oxidation state metal complexes, they provide the largest body of data with which to compare shieldings in the two essentially different classes of compound. With the exception of ^{51}V, the halide ligands are included in Table XIV. All the metals show a NHD and normal (Cl–Br)/(Cl–I) ratios of *ca.* 0·3. The average per halogen (Cl–I) difference for each metal, arranged in order of increasing metal atom shielding sensitivity and with the average (Cl–Br)/(Cl–I) ratio value in brackets is: ^{55}Mn, 480 ppm (0·32); (145) ^{103}Rh, 510 ppm (0·32); (122) ^{183}W, 590 ppm (0·30); (140) ^{195}Pt, 770 ppm (0·31); (70) ^{59}Co, 815 ppm (0·28). (160) As in all other such comparisons, it is ^{59}Co

that comes out at the head of the pack. When the halogen is one atom removed from the metal centre, as in the SnX_3 and GeX_3 ligands, the ^{59}Co shieldings show (161) an IHD (Fig. 11) similar to the β,γ,δ alternation in shielding direction with methyl substitution undergone by ^{113}Cd-alkyls and ^{199}Hg-alkyls.

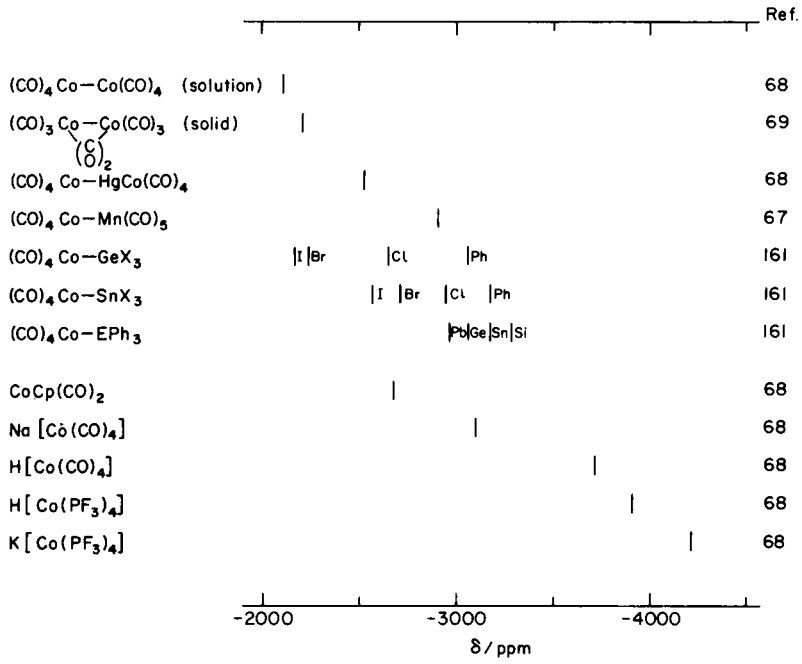

FIG. 11. ^{59}Co chemical shifts for some lower oxidation state cobalt compounds.

Those ligands that have a pronounced effect on metal shielding and which have been reported in combination with a sufficient number of metals to enable a generalization to be made have now been dealt with individually. For each metal, these ligands constitute the skeleton of a shielding pattern. The patterns can be filled out with those other ligands which have been studied in combination with particular metals but not generally. Table XIV contains these shielding patterns for those transition metals where more than two or three ligands have been studied. For ^{195}Pt, the ligand ordering has been obtained from the $PtCl_3L^{2-}$ Pt^{II} series of complexes. Where data for Pt^0 complexes are available, they are consistent with this ordering and there is no reason to expect any substantial difference between the Pt^{II} and Pt^0 ligand ordering. It *is* expected that the Pt^0 complexes will be uniformly shifted to higher shielding values.

TABLE XIV

Ligands listed in decreasing order of their ability to shield particular low oxidation state metals[a]

^{51}V	^{55}Mn	^{59}Co	^{183}W	^{103}Rh	^{195}Pt
CO	PF_3	PF_3	H	C_2H_4	PF_3
$SbPh_3$, $P(OMe)_3$	H	H	$SnMe_3$	CO	PR_3
$AsPh_3$, PPh_3, CN^-	$SnPh_3$	$SiPh_3$	CO	η^5-Cp	CO
$BiPh_3$	$SiPh_3$	$SnPh_3$	PR_3	PR_3	$AsMe_3$, $SbMe_3$
PMe_3	$GePh_3$	CO	η^5-Cp	I^-	$TeMe_2$, CNMe
NH_3	$PbPh_3$	$GePh_3$	I^-	Br^-	C_2H_4, $SeMe_2$, SMe_2
η^5-Cp	$MnCO_5$	$PbPh_3$, $SnCl_3$	Br^-	Cl^-	NCMe
	$SnBr_3$	$Mn(CO)_5$	Cl^-		NR_3
	$SnCl_3$	η^5-Cp			I^-
	CO, alkyl, acyl	$HgCo(CO)_4$			Br^-
	I^-	$Co(CO)_4$			Cl^-
	Br^-	I^-			
	Cl^-	Br^-			
		Cl^-			
		NO^+			

[a] Bracketed ligands are approximately equal in their shielding abilities.

XI. THE COPPER TRIAD

Only copper and silver have provided the NMR spectroscopist with a probe to investigate metal complexes in this grouping; gold, as befits its noble character and current price, has yet to yield its secrets to the blandishments of the magnet. The reason for this patrician status would appear to lie with its low receptivity coupled with a moderately large quadrupole moment likely to render inviolate all but the most symmetric gold compounds.

TABLE XV

Nuclear properties of the copper triad isotopes

Nucleus	Spin	Abundance (%)	Quadrupole moment . 10^{28} (m^2)	Usual shielding reference	Receptivity re ^{13}C
^{63}Cu	3/2	69	−0·16	$Cu(MeCN)_4^+$	365
^{65}Cu	3/2	31	−0·15	$Cu(MeCN)_4^+$	201
^{107}Ag	1/2	52	0	Ag^+(aq)	0·20
^{109}Ag	1/2	48	0	Ag^+(aq)	0·28
^{197}Au	3/2	100	0·59	—	0·14

With both copper and silver, the spectroscopist encounters a fundamental chemical difficulty shared equally by the compounds of the zinc triad. In keeping with their similarity to the alkali metals, the Cu^+ and Ag^+ ions form few complexes in solution, and those which do form are kinetically very labile such that the spectroscopist observes only a time-averaged resonance line characteristic of both the solvated cation and the complexed cation whose composition is subject to speculation. Given this circumstance, greater recourse is had to shielding data obtained from solid samples, and while care must be exercised in comparing these with solution shieldings, in many cases the results appear to be directly comparable.

A. Copper-63 and copper-65

The relative dearth of NMR information available on copper is striking when one looks at the properties of its two magnetic isotopes. Copper-63 ($I = 3/2$, 69% abundant, $Q = 0{\cdot}16 \times 10^{-28}$ m^2, receptivity = 365) is more readily detectable than ^{87}Rb and ^{133}Cs, while ^{65}Cu ($I = 3/2$, 31% abundant, $Q = 0{\cdot}15 \times 10^{-28}$ m^2, receptivity = 201) is only slightly less so. It is to the chemistry of copper rather than to the properties of the nuclei that we must look for the reason. The equilibrium constant for the disproportionation of Cu^I to Cu^{II} and Cu^0 is *ca.* 10^6 in water, and significant concentrations of cuprous complexes can only be maintained with ligands that stabilize copper(I) relative to copper(II) which with its d^9 electron configuration is

TABLE XVI

Some ^{63}Cu chemical shifts and related data

Assignment	Medium	$\delta(^{63}Cu)$ (ppm)	$W_{\frac{1}{2}}$ and ^1J(Cu–P) (Hz)	Ref.
$Cu(CN)_4^{3-}$		501		62, 63
$Cu(CN)_4^{3-} + Br^-$		501		63
$Cu(CN)_4^{3-} + I^-$		451		63
$Cu(py)_4^+$	pyridine (0·05m)	111	880	65
$Cu[P(OEt)_3]_4^+$	$P(OEt)_3$ (0·1 m)	92	$^1J(^{63}Cu–^{31}P) = 1224$	
			$^1J(^{65}Cu–^{31}P) = 1310$	65
$Cu[P(OMe)_3]_4^+$	$P(OMe)_3$ (0·04 m)	83	$^1J(^{63}Cu–^{31}P) = 1214$	
			$^1J(^{65}Cu–^{31}P) = 1302$	64, 65
$Cu(MeCN)_4(BF_4)$	MeCN (0·1 m)	0·0	540	66
$Cu(MeCN)_4^+$	MeCN (0·005 m)	−0·3	500	65
Cu_2HgI_4	powder	−270		63
CuCl	powder	−319(4)	2500	63, 66
CuI	powder	−321(4)	2600	63, 66
CuBr	powder	−381(5)	3400	63, 66
Cu	gas, free atom	−1820(8)		66

paramagnetic and unobservable by normal NMR methods. Indeed, the first copper NMR study to be reported was one in which McConnell and Weaver (61) measured the rate constant for Cu^I disproportionation.

By piecing together the fragmentary data from both solid and solution studies (63–66) it is possible to get a truncated picture of copper shieldings which span 900 ppm. The only successful solution studies to be carried out have utilized π-acceptor ligands to stabilize Cu^I; no information on CuO environments is yet available. The shielding of $CuClO_4$ and $CuBF_4$ in acetonitrile is insensitive to concentration, and the assumed $Cu(MeCN)_4^+$ complex has been chosen by Lutz and coworkers (65, 66) as the reference both for experimental and reporting purposes. This reference is adopted in Table XVI. Since data on the acetonitrile-coordinated metals are the only ones common to both ^{63}Cu and ^{109}Ag, the shift ranges for both plotted to the same scale have been aligned in Fig. 12 for comparative purposes. The solvation shift for Cu^+ in MeCN relative to the gaseous Cu atom is 1820 ppm (66) but this figure is not directly comparable with the hydration shifts available for other metal ions because of the different Cu^+ environment. If we assume the $\delta_{solvation}(^{109}Ag)/\delta_{solvation}(^{63}Cu)$ and $\delta_{hydration}(^{109}Ag)/\delta_{hydration}(^{63}Cu)$ ratios to be the same, then the hydration

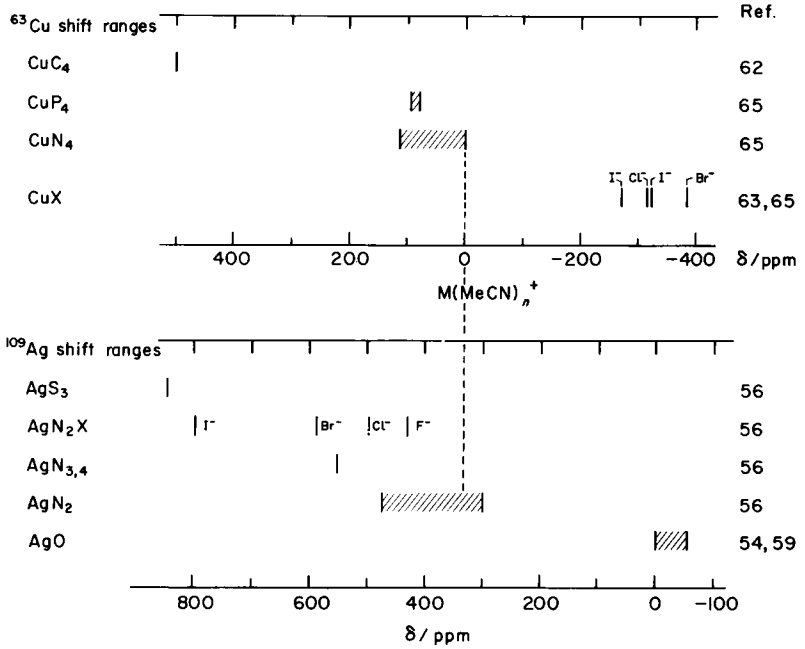

FIG. 12. ^{63}Cu and ^{109}Ag chemical shift ranges for some Cu^I and Ag^I compounds plotted to the same scale. The M^+ acetonitrile solvates are arbitrarily equated.

shift for the $Cu^+(aq)$ state relative to the free atom is estimated to be 1342 ppm.

The halogen dependence for copper shielding presents an intriguing picture. Two independent studies of the isostructural cuprous halide solids in which the Cu^+ ion occupies tetrahedral sites in the zinc blende structure confirm that the shielding increases in the order $CuCl \approx CuI > CuBr$. In order to decide whether copper shows a regular or IHD one must conclude that some feature of the solid causes the shielding of either CuCl or CuI to be anomalously low. The fact that the copper shielding in Cu_2HgI_4, where Cu^+ also sits in a 4-coordinate I^- environment, is even lower lends weight to the conclusion that it is the CuCl resonance position which is anomalous and that copper exhibits an IHD.

B. Silver-107 and silver-109

Both magnetically active isotopes of silver have spin $I = 1/2$. It is the less abundant ^{109}Ag (48·2% abundant, receptivity = 0·276) which is more sensitive than ^{107}Ag (51·8% abundant, receptivity = 0·195) because of a slightly larger magnetogyric ratio. In spite of its relatively high abundance, ^{109}Ag is difficult to observe experimentally because of the ease with which signal saturation occurs. Lacking a quadrupolar relaxation mechanism, it must rely for relaxation upon a magnetic dipolar mechanism made inefficient by the low magnetic moment of the nucleus. In practice the problem has been circumvented to some extent either by the introduction of a paramagnetic ion which facilitates relaxation but perturbs chemical shifts, or by use of a quadrature pulse detection method developed for the purpose. (58) Even so, the direct observation of ^{109}Ag is experimentally difficult, and this is reflected in the fact that only about half a dozen silver NMR studies have been reported, and activity has not increased in recent years.

While only a limited range of silver compounds has been studied, (54–57) the effects of S-, N-, and O-bonded ligands along with the halide ions generate shielding variations at the silver atom of roughly 1000 ppm. Comparison with shieldings observed for analogous cadmium compounds, where a richer variety of data is available, indicates that few examples of silver shieldings outside the present 900 ppm range are to be expected.

The reference that has been adopted for chemical shift reporting purposes is the $Ag^+(aq)$ state obtained by extrapolating the aqueous $AgClO_4$ or $AgNO_3$ shifts to infinite dilution. The Ξ values for this reference are ^{107}Ag, 4 047 897 Hz and ^{109}Ag, 4 653 623 Hz. (59) As a working reference with favourable relaxation characteristics Schwenk (54) and coworkers have used a 9·1 molal aqueous $AgNO_3$ solution containing 0·24 molal $Fe(NO_3)_3$ which is shifted to low frequency of $Ag^+(aq)$ to $\delta = -47$. By comparing the resonance frequency for $Ag^+(aq)$ with that for the free Ag atom obtained by

TABLE XVII

Some ^{109}Ag chemical shifts

Assignment	Medium	$\delta(^{109}Ag)$ (ppm)	Ref.
$Ag(S_2O_3)_3^{5-}$	3M aqueous $Na_2(S_2O_3)$	841(7)	56
$Ag(NH_2Et)_2I$	70% $EtNH_2$–H_2O (2 M)	790	56
$Ag(NH_2Et)_2Br$	70% $EtNH_2$–H_2O (2 M)	585	56
$Ag(NH_2Et)_2Cl$	70% $EtNH_2$–H_2O (2 M)	495	56
$Ag(en)_2^+$	ethylenediamine	554[a]	56
$Ag(NH_2Et)_2^+$	70% $EtNH_2$–H_2O (→ 0 M)	*ca.* 475	56
$Ag(py)_2^+$	pyridine (→ 0 M)	350[a]	56
$Ag(NCMe)_2^+$	acetonitrile (→ 0 M)	335[a]	56
$Ag(NCEt)_2^+$	propionitrile (→ 0 M)	303[a]	56
AgF	H_2O (5 M)	10	54
$Ag^+(aq)$	H_2O (→ 0 M)	0	54
$Ag(NO_3)$	H_2O (5 M)	−40	54
$Ag(ClO_4)$	H_2O (5 M)	−55	54
$AgNO_3$	H_2O (9·1 M); 0·24 M $Fe(NO_3)_3$	−47	54
Ag	gas, free atom	−940	54

[a] Evaluated from concentration dependence and formation constant data.

optical pumping, the hydration shift for Ag^+, which also provides a measure of σ_p for $Ag^+(aq)$, is 940 ppm.

The pattern of concentration and anion dependence in the chemical shifts of silver salts in aqueous solution (54) is similar to the now familiar pattern exhibited by the alkali metals, (60) with roughly linear concentration lines diverging away from the common $Ag^+(aq)$ point, oxyanions to low and halide ions to high frequency. The slopes for the linear portions are −11, −8, and +2 ppm m^{-1} for ClO_4^-, NO_3^-, and F^- respectively.

In N-coordinating solvents, formation constants for known silver complexes along with the observed concentration dependences of the ^{109}Ag chemical shift have been used to establish δ-values for the AgN_2 and AgN_3 or AgN_4 environments reported in Table XVII. One example of S-coordination, (56) $Ag(S_2O_3)_3^{5-}$, sets the present high frequency limit for silver shieldings with $\delta = 841$, while Maciel and coworkers report (55) high frequency shifts of up to 600 ppm for tetramethylthiourea and up to 900 ppm for thiourea complexes of Ag^+.

The most significant silver shielding data, because of the insight they provide during comparisons of metal shielding generally, are the δ-values for the four $Ag(NH_2Et)_2X$ (X = F, Cl, Br, I) complexes. Figure 12 reveals a typical (Cl–Br)/(Cl–I) ratio of 0·31, but an IHD with iodide to high frequency unlike the situation with ^{67}Zn, ^{113}Cd, and ^{199}Hg all of which exhibit regular halogen dependence with iodide to low frequency. The well

known insolubility of the silver halides prevents an aqueous solution study, but ^{109}Ag shifts for the AgX solids would be very useful for comparison purposes.

XII. THE ZINC TRIAD

Because there is no evidence of oxidation states higher than II for Zn, Cd, and Hg, the chemistries of these elements are not dominated by the partly filled d-subshell which characterizes the transition metals. Their chemical properties are sufficiently different from those of the alkaline earths, however, and similar to those of the late transition metals, to be usefully included in this review. All three form M^{2+} ions in aqueous solution which, in the cases of Zn and Cd, are similar in many respects to Mg^{2+} and can therefore be substituted in place of Mg^{2+} in biologically active molecules. In addition, mercury forms the unique series of mercurous compounds containing the metal–metal bonded grouping of mercury in the oxidation state of +I.

Unlike the alkaline earths, these metals have a pronounced tendency to form complexes with halide ions and other ligands, the Hg^{2+} complexes being orders of magnitude more stable than those of Zn^{2+} and Cd^{2+}. Typical stability constants for halide complexes in aqueous solution are 10^{-1} for Zn^{2+}, 10^{4} for Cd^{2+}, and 10^{20} for Hg^{2+}. From an NMR standpoint, however, these complexes are kinetically labile. Time-averaged signals, whose chemical shifts exhibit a marked concentration dependence, are more commonly encountered than multi-line spectra containing discrete lines assignable to specific complexes in solution.

The covalency of the bonding to these metals is greater than that in alkaline earth compounds (beryllium excepted) and increases in the order Zn < Cd < Hg. For this reason mercury forms a wide variety of stable organometallic compounds of the R_2Hg and RHgX varieties while zinc and

TABLE XVIII

Nuclear properties of the zinc triad isotopes

Nucleus	Spin	Abundance (%)	Quadrupole moment . 10^{28} (m^2)	Usual shielding reference	Receptivity re ^{13}C
^{67}Zn	5/2	4·1	0·15	Zn^{2+}(aq)	0·67
^{111}Cd	1/2	12·9	—	Me_2Cd	6·98
^{113}Cd	1/2	12·3	—	Me_2Cd	7·60
^{199}Hg	1/2	16·8	—	Me_2Hg, neat	5·42
^{201}Hg	3/2	13·2	0·50	Me_2Hg, neat	1·08

cadmium form similar organometallic compounds which are more sensitive to decomposition by air and water. The organometallic compounds of cadmium and mercury have received considerable study by NMR spectroscopy of the central metal, and the range of chemical shifts to be expected with typical organic R groups and typical X ligands is gradually emerging. Zinc has received less study and, while the halogen complexes have been investigated, the shielding parameters for organozinc compounds have yet to be determined.

A. Zinc-67

Zinc-67 is the only magnetically active isotope of this element to occur in Nature. It has a spin $I = 5/2$ and an abundance of 4·1% which offers the prospect of signal enhancement through isotopic enrichment where deemed advisable. The quadrupole moment of $0{\cdot}15 \times 10^{-28}$ m^2, intermediate between the small and the medium quadrupole nuclei, is comparable in magnitude to those of ^{27}Al and ^{71}Ga the complexes of which have been widely investigated, with those of ^{23}Na, ^{39}K, and ^{87}Rb whose shieldings and relaxation times have received considerable attention, and with ^{25}Mg, ^{43}Ca, ^{63}Cu, and ^{65}Cu which are only now beginning to receive attention from NMR spectroscopists. The receptivity of 0·67, which is lower than all these except ^{25}Mg and ^{43}Ca, along with its modest quadrupole moment producing reasonably broad signals in all except the more symmetrical environments, can account for the paucity of data on this nucleus. Once again it is the research laboratories of Lutz and Maciel that have laid the groundwork for what will undoubtedly, because of its biological significance, become a much studied metal.

In aqueous solution, the Zn^{2+} ion forms complexes with halide ions, but their characterization by NMR spectroscopy is made difficult by two factors. The formation constants for the ZnX^+, $ZnX_2(aq)$, ZnX_3^-, and ZnX_4^{2-} complexes are all less than 10, and in the case of $X = F^-$ there is no evidence of complex formation other than ZnF^+. Thus, the concentration of any specific complex which can be obtained in solution is limited. In addition, the lability of the complexes which do form is high, so only a single, time-averaged resonance for an equilibrium mixture of complexes is observed. The uncertainty in the formation constant for a particular complex under solution conditions suitable for NMR study is considerable, and the chemical shift assigned to that complex by fractionating the position of the time-averaged line is correspondingly uncertain. In spite of these difficulties, δ-values for $ZnCl_4^{2-}$, $ZnBr_4^{2-}$, and ZnI_4^{2-} have been obtained which show a NHD and appear reasonable when compared with those of other tetrahalogenometallates. Reliable values have also been obtained for $Zn(NH_3)_4^{2+}$ and $Zn(CN)_4^{2-}$ because of the large formation constants for

these complexes. The rather large high frequency shifts for $ZnCl_2$(aq) and $ZnBr_2$(aq) which emerge from a computerized solution of the simultaneous equilibria existing in these solutions should be taken *cum grano salis.* The shieldings of both 4-coordinate (^{27}Al, ^{73}Ge, ^{119}Sn) and 6-coordinate (^{93}Nb, ^{121}Sb) metals in chloride–iodide and chloride–bromide mixed tetrahalides and mixed hexahalides *all* undergo monotonic incremental shifts as iodide or bromide is successively replaced by chloride. It would be remarkable if the successive replacement of H_2O by Cl^- or Br^- in the first coordination sphere of Zn^{2+} were to give metal resonance shifts that are first to high frequency then to low frequency and then to high frequency again.

1. ^{67}Zn chemical shifts

The reference adopted for ^{67}Zn chemical shifts is Zn^{2+}(aq) present in either dilute aqueous solutions of $Zn(ClO_4)_2$ or $Zn(NO_3)_2$. For both salts, the position of the zinc resonance is insensitive to concentration up to and beyond 3 molal, and at low concentrations approaching infinite dilution the species present in solution is known from X-ray and Raman studies (1) to be $Zn(H_2O)_6^{2+}$. Lutz and coworkers (2) have established that this reference has a resonance position 690 ppm to high frequency of that of the free gaseous Zn atom in a $^1S_0$ state for which $\sigma_p = 0$. The resonance for the Zn^{2+}(aq) reference occurs near the low frequency end of the ^{67}Zn chemical shift range.

The relatively few zinc environments for which reliable shieldings are available are shown in Fig. 13. They span a range (3) of just over 300 ppm extending from ZnI_4^{2-} at $\delta = -36$ at low frequency to $Zn(CN)_4^{2-}$ at $\delta = 284$ and $Zn(NH_3)_4^{2+}$ at $\delta = 288$, both of which have cumulative stability constants (4) exceeding 10^9 making them the only zinc species present in solutions containing excess ligand. Fortunately sufficient data are available for the key tetrahalides of zinc to demonstrate that its chemical shift behaviour is consistent with the pattern established by neighbouring metals in the Periodic Table. The chloride–iodide difference of 292 ppm and the (Cl–Br)/(Cl–I) ratio of 0·30 shown in Table XIX place zinc among the metal atoms whose nuclear shielding follows a predictable pattern. It is the consistency of this pattern that supports the $\delta = 169$ value for $ZnBr_4^{2-}$ rather than the $\delta = 136$ obtained from the $[Br^-]$ dependence of the zinc shift which is subject to the significant uncertainties in the equilibrium constants used. As a result of the NHD exhibited by ^{67}Zn, the zinc resonance in aqueous solutions of $ZnCl_2$ and of $ZnBr_2$ undergoes a marked, concentration dependent, high frequency shift attributable to increasing complexation by halide ion. (2) The sulphate, nitrate, and perchlorate salts all give $\delta = 0$ signals showing no concentration dependence (2) which probably results, in the ClO_4^- and NO_3^- cases, from little tendency to associate, and in

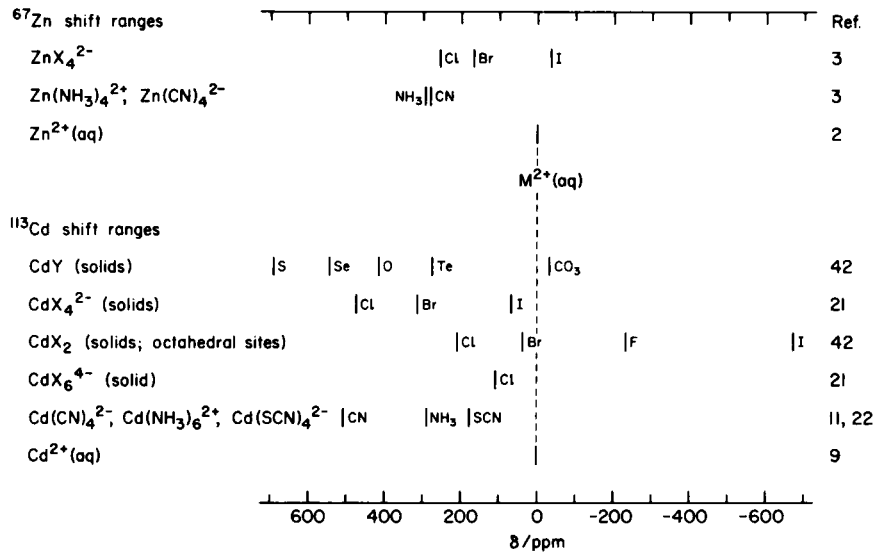

FIG. 13. ^{67}Zn and ^{113}Cd chemical shifts for the metal halides and chalcogenides plotted to the same scale. The shieldings for the M^{2+} hydrates have been arbitrarily equated.

TABLE XIX

Some ^{67}Zn, ^{71}Ga, and ^{73}Ge shielding patterns

	Metal atom δ			Range	Ratio	
	MCl_4	MBr_4	MI_4	Cl–I	$\frac{(Cl-Br)}{(Cl-I)}$	Ref.
^{67}Zn	257	169	−36	292	0·30	3
^{71}Ga	0	−211	−722	722	0·29	5
^{73}Ge	0	−343	−1117	1117	0·31	6

the SO_4^{2-} case, which has a complexation constant (4) of 500, from the Zn^{2+} ion retaining a coordination environment of six oxygen atoms magnetically similar to that in $Zn(H_2O)_6^{2+}$.

By extrapolating from the behaviour of mercury and cadmium compounds, we can predict that the resonances for organozinc compounds should be found in the region around $\delta = 360$, and those for S-coordinated zinc in the region around $\delta = 500$. The fact that no zinc spectrum for either type of compound has been reported may result from the combination of zinc quadrupole moment and ligand exchange rate broadening these signals beyond recognition. The fact that no ^{67}Zn signal could be detected (2) for ethanol, dimethyl ether, or acetone solutions of $ZnCl_2$ and $ZnBr_2$ suggests

that ion pair formation in these solvents is generating sizeable electric field gradients at the zinc nucleus.

B. Cadmium-111 and cadmium-113

Cadmium-111 (12·9% abundant) and cadmium-113 (12·3% abundant) together comprise 25% of naturally occurring cadmium, and both isotopes have spin $I = 1/2$. ^{113}Cd has a slightly higher receptivity and is the one commonly studied under direct observation, but the shieldings of the two isotopes exhibit no isotope effect (7) and chemical shifts evaluated for either can be used interchangeably. In ^{1}H or ^{13}C spectra which reveal coupling to ^{111}Cd and ^{113}Cd, double resonance techniques can and have been used to evaluate cadmium NMR parameters, but the kinetic lability of many organocadmium compounds destroys the couplings essential to this method and forces one to use direct observation with its requirement for specific frequency capabilities.

Some 25 cadmium NMR studies have been reported in the literature, with the majority appearing in the past 3 years. A recently reported shielding study of the cadmium halides provides the data necessary for positioning cadmium in the overall pattern of metal atom shielding sensitivity. Data for a full range of C-, N-, O-, and S-bonded ligands are available. Cadmium NMR is starting to be used to good advantage to investigate the nature of the metal binding sites in metalloenzymes and other metalloproteins. Several relaxation studies have been completed to determine the mechanisms making the major contributions to T_1. This knowledge, in turn, provides information about exchange phenomena, solvent coordination, and self-association at the cadmium centre. Because both of the cadmium isotopes observable are $I = 1/2$ nuclei, couplings to ^{1}H, ^{13}C, and ^{31}P have been observed and evaluated.

Because a considerable portion of cadmium NMR work is done by the INDOR method, a cadmium reference containing coupled protons is required for these studies and Me_2Cd as the neat liquid is the reference of choice. Its Ξ value (8) is 21 215 478 Hz for ^{111}Cd and 22 193 173 Hz for ^{113}Cd. Chemical shifts made by direct measurement using aqueous $Cd(ClO_4)_2$ as reference can be converted to the $\delta(Me_2Cd)$ scale using the following conversion factors:

$$\delta(Me_2Cd) = \delta(Cd(H_2O)_6^{2+}) - 643{\cdot}0$$

$$\delta(Me_2Cd) = \delta(0{\cdot}1\ \text{M}\ Cd(ClO_4)_2) - 643{\cdot}1 \qquad \text{(ref. 8)}$$

$$\delta(Me_2Cd) = \delta(1{\cdot}0\ \text{M}\ Cd(ClO_4)_2) - 644{\cdot}9 \qquad \text{(ref. 8, 10)}$$

A further reason for reporting cadmium shifts relative to Me_2Cd is the fact that ^{199}Hg shifts, with which it is frequently instructive to compare ^{111}Cd or ^{113}Cd shifts for analogous compounds, are normally reported relative to

Me_2Hg. To assist in making comparisons with ^{67}Zn shieldings, cadmium shifts referenced to $Cd^{2+}(aq)$ are included in Table XX. By comparing the resonance frequency for $Cd(H_2O)_6^{2+}$ extrapolated to infinite dilution with

TABLE XX

Some ^{113}Cd chemical shifts

Compound	Medium	$\delta(Cd^{2+}(aq))$	$\delta(Me_2Cd)$	Ref.
CdS_4				
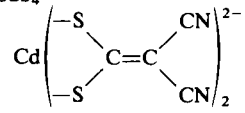	DMSO (0·5 M)	813	170	10
CdS (solid)		703	60	17
$Cd(SCH_2CH_2OH)_2$	DMSO (0·2 M)	655	12	10
$Cd_{10}(SCH_2CH_2OH)_{16}^{4+}$		515	−128	10
$\{Cd[-SP(=S)(OPr)_2]_2\}_2$	$PhCH_3$ (0·5 M)	401	−242	10
CdS_3				
$Cd_{10}(SCH_2CH_2OH)_{16}^{4+}$	H_2O (0·07 M)	382	−261	10
$Cd[-SC(=S)OEt]_3^-$	$CHCl_3$ (0·5 M)	277	−366	10
CdS_2				
Cd(glutathione)$_2$ (1 : 2)	H_2O (0·5 M), pH 9·5	315	−328	10
$Cd[-SC(=S)NEt_2]_2$	DMSO (0·08 M)	215	−428	10
CdS				
$Cd(glutathione)^+$	H_2O (2 M)	192[a]	−451[a]	14
$Cd(thiourea)^{2+}$	H_2O (2 M)	86[a]	−557[a]	14
$Cd(SCN)^+$	H_2O (2 M)	63[a]	−580[a]	14
CdN_6				
$Cd(NH_3)_6^{2+}$	1 : 1 NH_3–D_2O (1 M)	288	−355	11
$Cd(o\text{-phen})_3^{2+}$ (1 : 3)	H_2O (0·3 M)	266	−377	13
$Cd(MeHist)_3^{2+}$ (1 : 3)	H_2O (0·3 M)	254	−389	13
$Cd(MeHist)_2^{2-}$ (1 : 2)	H_2O (0·3 M)	224	−419	13
$Cd(Hist)_1^{2+}$	H_2O (2M)	80[a]	−563[a]	14
$Cd(Im)_6^{2+}$ (1 : 20)	H_2O (0·3 M), pH 12	201	−442	13
$Cd(Im)_n^{2+}$ (1 : 6)	H_2O (0·5 M), pH 8·3	133	−510	12
$Cd(Im)_n^{2+}$ (1 : 25)	H_2O (0·5 M), pH 5	74	−569	10
$Cd(Im)_1^{2+}$	H_2O (2 M)	43[a]	−600[a]	14
CdN_5				
Cd(TPP)–pyridine (1 : 10)	$CDCl_3$	430	−213	15
CdN_4				
$Cd(MeHist)_2^{2+}$ (1 : 2)	H_2O (0·3 M)	224	−419	13
CdN_3O_3				
$Cd(glycine)_3^{2+}$		177	−466	12
CdN_3O				
Cd(HCAB)		228	−415	13
CdN_2O_4				
$Cd(EDTA)^{2-}$	H_2O (0·5 M)	85	−558	10
$Cd(Hist)^{2+}$	H_2O (2 M)	80[a]	−563[a]	14
$Cd(glycine)_2^{2+}$	H_2O (*ca.* 1 M); pH 8·2	108	−535	12

TABLE XX—*cont.*

Some ^{113}Cd chemical shifts

Compound	Medium	$\delta(Cd^{2+}(aq))$	$\delta(Me_2Cd)$	Ref.
$CdNO_5$				
$Cd(Im)^{2+}$	H_2O (2 M)	43[a]	−600[a]	14
$Cd(glycine)^{2+}$	H_2O (2 M)	40[a]	−603[a]	14
$Cd(N_3)^+$	H_2O (2 M)	42[a]	−601[a]	14
$Cd(en)^{2+}$	H_2O (2 M)	35[a]	−608[a]	14
$Cd(pyridine)^{2+}$	H_2O (2 M)	20[a]	−623[a]	14
$Cd(NH_3)^{2+}$	H_2O (2 M)	12[a]	−631[a]	14
Cd halides				
$CdCl_6^{4-}$	solid	162	−481	21
$CdCl_5^{3-}$	solid	188, 172	−455, −471	21
$CdCl_4^{2-}$	solid	474	−169	21
$CdCl_4^{2-}$	H_2O ($[Cl^-]<0{\cdot}5$ M)	495	−148	21
$CdCl_4^{2-}$	DMSO (0·1–0·6 M)	442	−201	22
$CdCl_3^-$	H_2O ($[Cl^-]<0{\cdot}5$ M)	292	−351	21
$CdCl_3^-$	H_2O (0·1 M)	282	−361	22
$CdCl_2$	H_2O($[Cl^-]<0{\cdot}5$ M)	114	−529	21
$CdCl_2$	H_2O (0·1 M)	98	−545	22
$CdCl^+$	H_2O ($[Cl^-]<0{\cdot}5$ M)	89	−554	21
$CdCl^+$	H_2O (0·1 M)	63	−580	22
$CdCl^+$ (2:1)	H_2O (2 M)	32	−611	14
$CdBr_4^{2-}$	solid	365	−278	21
$CdBr_4^{2-}$	H_2O ($[Br^-]<0{\cdot}5$ M)	379	−264	21
$CdBr_4^{2-}$	H_2O (0·1 M)	399	−244	22
$CdBr_3^-$	H_2O ($[Br^-]<0{\cdot}5$ M)	365	−278	21
$CdBr_3^-$	H_2O (0·1 M)	186	−457	22
$CdBr_2$	H_2O ($[Br^-]<0{\cdot}5$ M)	75	−568	21
$CdBr_2$	H_2O (0·1 M)	83	−560	22
$CdBr^+$	H_2O ($[Br^-]<0{\cdot}5$ M)	72	−571	21
$CdBr^+$	H_2O (0·1 M)	62	−581	22
$CdBr^+$ (2:1)	H_2O (2 M)	27	−616	14
$Cd(SCN)_4^{2-}$	H_2O (0·1 M)	174	−469	22
$Cd(SCN)_3^-$	H_2O (0·1 M)	101	−542	22
$Cd(SCN)_2$	H_2O (0·1 M)	85	−558	22
$Cd(SCN)^+$	H_2O (0·1 M)	40	−603	22
$Cd(SCN)^+$(4:1)	H_2O (2 M)	63	−580	14
CdI_4^{2-}	solid	70	−573	21
CdI_4^{2-}	H_2O ($[I^-]<0{\cdot}5$ M)	71	−572	21
CdI_4^{2-}	H_2O (0·1 M)	71	−572	22
CdI_3^-	H_2O ($[I^-]<0{\cdot}5$ M)	140	−503	21
CdI_3^-	H_2O (0·1 M)	122	−521	22
CdI^+	H_2O ($[I^-]<0{\cdot}5$ M)	47	−596	21
CdI^+	H_2O (0·1 M)	46	−597	22
CdI^+ (2:1)	H_2O (2 M)	18	−625	14

[a] Extrapolated from the concentration dependence.

that for the free Cd atom, obtained by optical pumping techniques, the hydration shift of Cd^{2+} is found to be 1106 ppm to high frequency of that of the free atom. (9)

Spectroscopic work up to the present time has produced shielding data for a larger *variety* of cadmium environments than is the case for either zinc or mercury. Chemical shifts for diamagnetic cadmium compounds span a range of 825 ppm, with the shielding for the free Cd atom another 1100 ppm to low frequency of this range. The effect upon cadmium shielding of coordination by different ligand atoms is shown in Fig. 14. Beginning at the high frequency end of the range, it is ligands which bond through sulphur that give the most deshielded cadmium environments. Organocadmium compounds containing alkyl substituents are more highly shielded, followed by those with aryl substituents at higher shielding values. Oxygen and nitrogen bonding ligands cause greater shielding than do alkyl groups, and halide ions occur at the upper end of the shielding range, with I^- giving the most highly shielded environments. The aquated Cd^{2+} ion marks the present upper limit of the cadmium shielding range. While a Cd resonance for the metalloprotein Cd-concanavalin A has been observed (16) in the foreign region 130 ppm to low frequency of $Cd(H_2O)_6^{2+}$, speculation as to the cause

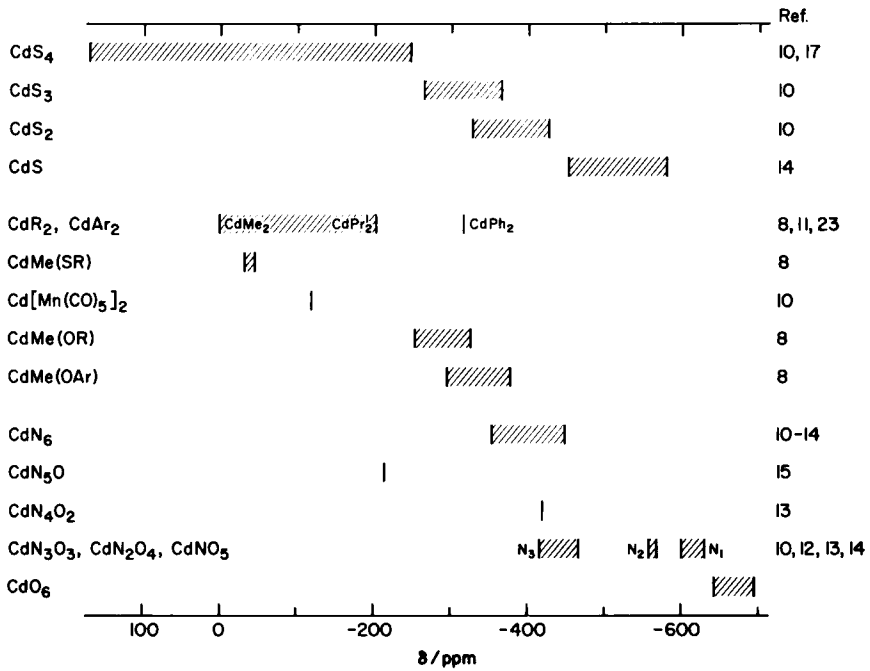

FIG. 14. ^{113}Cd chemical shift ranges for some organocadmium compounds and for chemical environments encountered in biological systems.

of this extremely high shielding must await an assignment of the structural environment of the cadmium.

1. Cd–S environments

The chemical shifts for cadmium bonded to sulphur span a range of 750 ppm, almost the total range for cadmium ligated by any atom. By investigating a series of model compounds, Holm and coworkers (10) have established the range of cadmium shifts occasioned by sulphur coordination, while at the same time showing that a sequential deshielding of cadmium occurs as the number of thiolate sulphurs increases along the series $Cd(SR)_2$, $Cd(SR)_3$, $Cd(SR)_4$. Examples of monodentate, bidentate chelating, and bridging ligands have been studied, as has the decanuclear cluster cation $Cd_{10}(SCH_2CH_2OH)_{16}^{4+}$ whose Cd–S framework in the solid state is known. Although this diversity of bonding action by sulphur renders uncertain the coordination numbers for some cadmium complexes in solution, Fig. 14 reveals a general high frequency shift in the cadmium resonance as the number of coordinated sulphur atoms increases. While the overlap between the CdS_2 and CdS_3 ranges precludes a structural assignment solely on the basis of a cadmium shift measurement, the separations are sufficient to indicate that $Cd(SCH_2CH_2OH)_2$ in DMSO achieves CdS_4 structural units through sulphur bridging, as it does in the solid state, rather than CdS_2O_2 bonding through chelation. In the case of the bis-dithiocarbamate, the $\delta = -428$ signal is inconsistent with CdS_4 coordination and indicates either CdS_2N_2 or $CdS_2O_2N_2$ through chelation or CdS_2O_2 through solvation by DMSO. It is useful to recognize the roughly incremental high frequency shifts that occur when water molecules are successively replaced by a sulphur-bonded ligand. One glutathione deshields cadmium by *ca.* 190 ppm (14, 19) while two deshield by *ca.* 400 ppm. (10, 19) More and better examples of this phenomenon are seen below with nitrogen-bonded ligands.

2. Cd–N environments

Coordination of cadmium by mono- and bi-dentate ligands containing nitrogen causes the metal chemical shift to vary over a range of 275 ppm to the high frequency side of $Cd(H_2O)_6^{2+}$. The macrocyclic tetraphenylporphyrin shifts the cadmium resonance a further 125 ppm to high frequency of this range. (15) While the CdN and CdN_2 types occupy ranges that are distinct from the others and from each other as shown in Fig. 14, the CdN_3, CdN_4, and CdN_6 types occupy ranges that overlap one another. In spite of the restricted range compared with sulphur ligands and the range overlap for higher nitrogen coordination, cadmium shifts still provide a diagnostic indication of local structure around cadmium. Reference to Table XXI where the data are grouped according to the structure type of the complex

TABLE XXI

Some incremented cadmium chemical shifts

	Deshielding (ppm)							
	$n=1$	$n=2$		$n=3$		$n=6$	
L	Increment	est.	obs.	est.	obs.	est.	obs.
Imidazole	43					258	201
Histidine	80	160	224	240	254		
Glycine	40	80	108	120	177		
NH_3	12					72	288

shows, on the basis of the cadmium δ-value only, that $Cd(en)^{2+}$ contains monodentate ethylenediamine while histidine is bidentate in $Cd(Hist)^{2+}$.

In spite of the kinetic lability of most of these complexes, it is possible to secure δ-values for a range of n in complexes CdL_n (L = imidazole, methylhistidine, glycine, NH_3). In all cases except NH_3, the shifts observed for higher values of n are consistent with a roughly (±50%) incremental high frequency shift with each substitution of L for H_2O coordinated to Cd^{2+}. While the top three ligands all give observed deshieldings that are within 50%* of the incremented value, NH_3 is off by a factor of 4. No obvious reason for this discrepancy presents itself.

3. Cd–halogen and Cd–chalcogen environments

Two closely related studies (21, 22) confirm that the shielding of cadmium coordinated by halide ions obeys a NHD. Limiting shift values for complexes containing a specific number of halides have proved difficult to obtain because of the lability of cadmium halides in solution and uncertainty about formation constants in the concentrated solutions required for NMR study. A further complication resides in the fact that at some stage in the preparation of tetrahedral CdX_4^{2-}, by addition of X^- to $Cd(H_2O)_6^{2+}$, the coordination number must change from 6 to 4. Against these difficulties rests the fact that cadmium shifts for the CdX_4^{2-} solids (21) have been measured and they compare favourably with solution values where halide concentrations are kept below 0·5 M. Above this concentration, perhaps due to the formation of higher order CdX_5^{3-} and CdX_6^{4-} halide complexes, the solution shift values deviate substantially from the results on solids. Two features of the halogen dependence pattern illustrated in Fig. 14 are worthy

* The best that can reasonably be expected, given the uncertainty in evaluating the increment for labile complexes plus the fact that shielding of metals is known to be a non-linear function of substitution.

of comment. In contradistinction to ^{67}Zn, and a number of other metals where the MI_4 resonance lies to low frequency of the $M(H_2O)_6$ signal, CdI_4^{2-} is to high frequency of the aquated cation by a significant amount. With a (Cl–Br)/(Cl–I) ratio of 0·27 for the CdX_4^{2-} complexes, the cadmium resonance in the bromide lies relatively closer to that for the chloride than is the case for the ZnX_4^{2-} compounds where the ratio is 0·30. The cadmium shifts, along with the shielding anisotropies, have recently been reported for the CdX_2 solids (X = F, Cl, Br, and I). The cadmium shieldings, while retaining normal halogen dependence, are shifted 270–600 ppm to low frequency of their CdX_4^{2-} counterparts. (42) Since Cd^{2+} occupies 6-coordinate octahedral sites in the chloride, bromide, and iodide dihalides, this data set provides a most striking example of the increase in σ_p which results when the coordination and symmetry are changed from octahedral to tetrahedral.

Cadmium is one of the few metals where, in addition to having data with which to assess the halogen dependence, we also have shielding values with which to evaluate the chalcogen dependence. Chemical shifts for the CdY solids (Y = S, Se, Te) in which cadmium occupies tetrahedral sites fit a pattern similar to that for the halogens, with shielding increasing with increasing size of the chalcogen along the series CdS < CdSe < CdTe. The (S–Se)/(S–Te) ratio is 0·34, remarkably similar to the analogous halogen ratio. (17, 42)

4. *Cd–C environments*

Three comprehensive investigations (8, 11, 23) have been made of the cadmium shieldings in organocadmium compounds. Because cadmium coupling to protons occurs in most of these compounds, much of the cadmium shielding data has been obtained indirectly by the ^1H–$\{^{113}Cd\}$ double resonance technique. A significant feature of cadmium NMR is the sizeable solvent shifts undergone by organocadmium compounds. These span a range of 100 ppm for Me_2Cd (11) and have their origin in the propensity of cadmium to achieve coordination numbers higher than 2, either through association involving bridging alkyl groups in the neat liquids or through solvation by O- and N-donor solvents. The latter cause low frequency shifts in 1 molar Me_2Cd solutions, relative to the neat liquid, of 5 ppm for diethyl ether, 28 ppm for pyridine, 41 ppm for acetone, and 66 ppm for THF. The directions of these shifts are consistent with those expected for O- and N-coordination on the basis of shift ranges for different cadmium environments outlined in Fig. 14. Non-coordinating solvents cause high frequency shifts of 2 ppm for benzene and for toluene, 3 ppm for methylene chloride, and 35 ppm for cyclohexane. These are presumably due to the break-up of the organized structure in neat Me_2Cd.

The pattern of shieldings in organocadmium compounds is illustrated in Fig. 14. Dialkylcadmium compounds span 200 ppm at the deshielded end of the cadmium spectrum. Turner and White (23) have shown that, within this 200 ppm span, shieldings relative to dimethylcadmium can be understood in terms of reasonably constant increments and decrements resulting from successive substitution of methyl groups for hydrogen atoms at positions β and γ to the cadmium atom. The constants which are additive for either or both alkyl groups are $\Delta\beta \approx -46$ ppm and $\Delta\gamma \approx +23$ ppm. Substitution of methyl for a hydrogen δ to cadmium has little effect on the shielding.

Methylcadmium alkoxide absorptions are shifted 200 ppm to low frequency, consistent with O- in place of C-bonding, and they span a range of 75 ppm. (8) Again a systematic pattern of substituent additivity constants is discernible, with $\Delta\gamma \approx +22$ ppm and $\Delta\delta \approx -7$ ppm for substitution of hydrogens by methyls in the alkoxide group. It is noteworthy that, as in the case of the alkyl group substitutions above, methyl substitution in the γ-position deshields and that alternate shielding, deshielding, shielding result from methyl substitution at the β, γ, and δ positions respectively.

The diphenylcadmium resonance occurs 314 ppm to low frequency of dimethylcadmium, (11) and methylcadmium aryloxides absorb to low frequency of their alkoxy counterparts. The $Cd(CN)_4^{2-}$ ion at $\delta = 510$ (11) is more usefully regarded as a pseudohalide and considered with the halide complexes.

5. Cd–O environments

In wrestling with the problem of ligand exchange in cadmium solutions, NMR spectroscopists have few limiting structures, the cadmium environment of which is known with certainty, to serve as a conceptual origin from which shielding differences can be visualized. The octahedral CdO_6 unit has been established for $Cd(H_2O)_6^{2+}$ at low concentrations, i.e. $Cd^{2+}(aq)$, by X-ray diffraction, (24) and its "absolute" shielding relative to the free Cd atom is represented by the high frequency hydration shift of -1106 ppm. (9) Oxyanions having little tendency to coordinate (ClO_4^-) and those which only coordinate through oxygen (SO_4^{2-}) have little or no effect (9, 14) on the position of the cadmium resonance, and cadmium shifts for aqueous solutions of these salts are essentially independent of concentration up to 2 molar.

The only solution cadmium environments with negative δ-values are those in which one or more solvating water molecules is replaced by an O-donor ligand. Thus counter-ion enhanced shielding of cadmium increases in the order formate < nitrite. The incorporation of DMF, acetone, DMSO, or dioxan into the solvent for $CdSO_4$ all shift the resonance to low frequency. The possibility of ligation by the nitrogen atom in an N-bonded nitrite

causing the large low frequency shift for $Cd(NO_2)^+$ cannot be entirely ruled out, but O-bonded nitrite is more likely to occur. The $Cd(DMSO)_6^{2+}$ ion has $\delta = -27$, (22) and the shift for solid $[Cd(H_2O)_6](ClO_4)_2$ is $\delta = -9$. (21) The $\delta = -15$ for the β-alanine complex indicates O-bonding only, whereas δ-values of 14 for alanine, 18 for phenylalanine, 20 for aspartic acid, and 18 for phosphoserine indicate a weighted average of N- plus O-bonding for these amino acids. (14) The $\delta = 40$ value for glycine (14) is consistent with N-bonding only. The cadmium resonance at $\delta = -130$ observed for the Cd(concanavalin A) complex (16) is so far above the normal shielding range for cadmium that speculation as to its origin must await a more precise structural assignment. It is interesting to note, however, that $Cd(AsF_6)_2$ dissolved in anhydrous SO_2 yields a signal at $\delta = -169$ which is probably assignable to SO_2-solvated Cd^{2+} although the influence of AsF_6^- on this low frequency shift cannot be ruled out. (27)

6. Biological macromolecule environments

Cadmium has no known biological function and is moderately toxic to all organisms, leading to renal failure in all mammals and linked to hypertension in man. Zinc, on the other hand, is essential to all organisms and constitutes the prosthetic group or active site in a number of enzymes. Because cadmium is a more sensitive NMR probe than zinc, recent investigators have substituted Cd as a surrogate for Zn in a number of biological systems with a view to obtaining structural information unobtainable for the zinc compound. In most of these studies, both the cadmium linewidth and chemical shift are strongly pH-dependent. Linewidth variations have been used to measure the rates of kinetic exchange processes occurring at the cadmium site, while chemical shifts have provided an indication of the number and nature of the atoms bound to the metal.

Cadmium substituted bovine and human carbonic anhydrase A and B have received the most attention. (12, 13, 25) The weight of evidence for the pH region 8·0–9·0 favours a tetrahedral CdN_3O structure in which added halide ion can be shown to replace the coordinated H_2O or OH^-. The pK_a for the activity-linked ionization of the enzyme is 9·1, and the 80 ppm low frequency shift of the Cd resonance at pH > 8·9 takes it out of the CdN_3O range (Table XX) and into the CdN_2O_2 region, suggesting the replacement of one of the imidazole nitrogens by oxygen at higher pH levels. Other enzymes studied are cadmium substituted alkaline phosphatase (25) with $\delta = 117$ at pH 6·0, suggesting CdN_2O_2 coordination, cadmium substituted carboxypeptidase plus β-phenylpropionate with $\delta = 133$ at pH 6·9, consistent with the expected CdN_2O_2 coordination, and cadmium substituted superoxide dismutase with $\delta = 170$ at pH 6·0, consistent with CdN_3O coordination.

TABLE XXII

^{113}Cd NMR data for some carbonic anhydrase enzymes

Metalloenzyme	pH	$\delta(Cd^{2+}(aq))$	$\Delta\nu$ (Hz)	Ref.
Cd^{II}(HCAB)	9·7	228	300	13
Cd^{II}(HCAB)	9·6	146	28	12
Cd^{II}(HCAB)	9·1	146		25
Cd^{II}(HCAB)+X^-	8·9	226–241		25
Cd^{II}(HCAC)	8·1	226		25
Cd^{II}(HCAC)+X^-	8·1	239		25
Cd^{II}(BCAB)	8·0	214		25

Seven different cadmium sites with δ-values ranging from 581 to 670 have been observed for the metallothionein complex, (26) all of which are consistent with CdS_4 coordination (Table XX) by the *ca.* 20 cysteine sulphur atoms in the protein. Cadmium–glutathione complexes (19) at pH 7·9 yield a resonance at $\delta = 610$ which is also consistent with CdS_4 coordination. The *meso*-tetraphenylporphyrin–pyridine complex (19) with CdN_5 coordination absorbs at $\delta = 430$ and provides the only unambiguous example of this particular geometry. Since the solvent in this case is $CDCl_3$, it is best regarded as a genuine case of 5-coordination.

Three separate resonances have been identified for the cadmium–concanavalin A complex (16) with $\delta = 43$ (S_1 sites), $\delta = 68$ (S_2 sites), and $\delta = -125$ (unassigned). The cadmium environment giving rise to this extremely high shielding is not readily apparent, the only comparable shift being Cd^{2+} in liquid SO_2 at $\delta = -300$. (27)

C. Mercury-199 and mercury-201

Mercury has both $I = 1/2$ and $I > 1/2$ isotopes, offering the prospect of narrow-line spectra with which to evaluate shieldings and quadrupolar-relaxed wide-line spectra with which to evaluate electric field gradients. In practice, only ^{199}Hg ($I = 1/2$, 16·8% abundant, receptivity 5·42) spectra have been measured. The reluctance of mercury to adopt the highly symmetric 4- and 6-coordinate environments means that all mercury compounds have large field gradients at the mercury centre which perhaps makes the quadrupolar relaxation sufficiently rapid to render the nuclear spin states unobservable by NMR. Some 25–30 ^{199}Hg studies have been reported in the literature, and a full range of chemical environments covering a chemical shift span of 3600 ppm has been investigated. The linear coordination present in most mercury compounds generates large anisotropies in mercury shielding, (33) the effects of which upon mercury relaxation are significant. (44)

In spite of its location near the high frequency end of the range, the resonance for neat Me_2Hg has been adopted as the $\delta = 0$ reference by most workers, and its Ξ value is 17 910 841 Hz. (48) In order to facilitate comparisons with zinc and cadmium shielding data, δ-values referenced to $Hg^{2+}(aq)$, using the conversion factor $\delta(Hg^{2+}(aq)) = \delta(Me_2Hg) + 2253$ (ref. 30, 32), are also provided in Table XXIII. The high frequency hydration

TABLE XXIII

Some ^{199}Hg chemical shifts

Assignment	Medium	$\delta(Hg^{2+}(aq))$	$\delta(Me_2Hg)$	Ref.
Hg-metal				
$Hg(SiMe_3)_2$		2734	481	31
$Hg(SiH_3)(SiMe_3)$		2580	327	31
$Hg(SiH_3)_2$		2449	196	31
$Hg(GeH_3)(SiMe_3)$		2412	159	31
$Hg(GeH_3)_2$		2106	−147	31
$Hg_2^{2+}(aq)$		800	−1453	30
HgC_2				
$HgMe_2$	neat	2253	0	—
$Hg(CH_2CMe_3)_2$	neat	2100	−153	33
$HgBu^n_2$	2 M, CCl_4	2045	−208	46
$HgPr^n_2$	neat	2013	−240	46
$HgEt_2$	neat	1964	−289	46
$Hg(CH_2CH_2Ph)_2$	neat	1948	−305	28
$HgPr^n_2$	neat	1613	−640	46
$Hg(CH_2Ph)_2$	1 M, CH_2Cl_2	1550	−703	46
$Hg(CH_2COOMe)_2$	2 M, CH_2Cl_2	1481	−772	46
$HgBu^t_2$	50%, toluene	1424	−829	33
$Hg(CH{=}CH_2)_2$	neat	1611	−642	46
$Hg(CH{=}CHCl)_2$		1413	−840	48
$Hg(CCl{=}CH_2)_2$	2 M,CH_2Cl_2	1108	−1145	46
$HgMe(C_5H_5)$	20%, $CDCl_3$	1546	−707	35
$HgPh_2$	1 M, CH_2Cl_2	1508	−745	46
$Hg(C_6F_5)_2$	satd., acetone	1333	−920	47
$HgMe(NH_3)^+$	0·1 M, CD_3OD	1310	−943	48
HgMe py$^+$	0·1 M, MeOH	1020	−1233	40
HgMe(2,6-dmpy)$^+$	0·1 M, MeOH	936	−1317	40
$HgMeN_2$				
HgMe(5,5′-dmbpy)$^+$	0·1 M, MeOH	878	−1375	40
HgMe(phen)$^+$	0·1 M, MeOH	756	−1497	40
HgP_2				
$Hg(PMe_3)_2^{2+}$	0·1 M, D_2O	1095	−1159	48
HgO_2				
$Hg(ClO_4)_2$	0 M, H_2O	0	−2253	30
$Hg(NO_3)_2$	2 M, 0·84 HNO_3	−108	−2361	28
$Hg(OCOMe)_2$	0·5 M, 1 M HOAc	−136	−2389	29

TABLE XXIII—*cont.*

Some ^{199}Hg chemical shifts

Assignment	Medium	$\delta(Hg^{2+}(aq))$	$\delta(Me_2Hg)$	Ref.
HgO				
HgMeOH	0·1 M, 0·1 M HNO_3, pH > 9	1225	−1028	39
$HgMe(OH_2)^+$	0·1 M, 0·1 M HNO_3, pH 1	1103	−1150	39
$HgMe(OCOCH_3)$	0·5 M, 3·5 M HOAc	1117	−1136	29
$HgMe(OD_2)^+$	1 M, D_2O	1107	−1146	48
$HgPh(OCOCH_3)$	1 M, DMSO	816	−1437	32
$HgPh(OCOC_6H_5)$	1 M, DMSO	825	−1428	32
HgS, HgS_2				
HgMe(glutathione)	0·1 M, H_2O, pH 3	1666	−587	39
HgMe(glutathione)	0·1 M, H_2O, pH 9	1668	−585	39
$Hg(glutathione)_2$	0·25 M, H_2O, pH 7	1260	−993	39
Halides				
$HgCl_2$	0 M, H_2O	1100	−1153	30
$HgCl_2$	0·5 M, H_2O	1050	−1203	45
$HgCl_2$	0·5 M, EtOH	756	−1497	32
$HgCl_3^-$	0·5 M, CH_2Cl_2	1070	−1183	48
$HgCl_3^-$	H_2O	1105	−1148	45
$HgCl_4^{2-}$	H_2O	1445	−808	45
$Hg(CN)_2$	2 M, pyridine	1183	−1070	28
$HgCl_2$	0·5 M, EtOH	756	−1497	48
$HgBr_2$	0·5 M, EtOH	101	−2152	48
HgI_2	1 M, DMSO	−853	−3106	48
$HgCl_3^-$	0·5 M, CH_2Cl_2	1070	−1183	48
$HgBr_3^-$	0·5 M, CH_2Cl_2	318	−1935	48
HgI_3^-	0·5 M, CH_2Cl_2	−569	−2822	48
HgMeCl	0·2 M, CH_2Cl_2	1439	−814	32
HgMeBr	0·2 M, CH_2Cl_2	1338	−915	32
HgMeI	0·2 M, CH_2Cl_2	1156	−1097	32
HgMe(SCN)	0·2 M, CH_2Cl_2	1548	−705	36
HgMe(CN)	0·1 M, C_6H_6	1538	−715	48
HgMeCl	0·2 M, CH_2Cl_2	1439	−814	36
HgMeBr	0·2 M, CH_2Cl_2	1338	−915	36
HgMeI	0·2 M, CH_2Cl_2	1156	−1097	36
$Hg\{CH_2C(OMe)Me_2\}(CN)$	40 mol%, $CHCl_3$	1326	−927	49
(SCN)	40 mol%, $CHCl_3$	1314	−939	49
Cl	40 mol%, $CHCl_3$	1108	−1145	49
Br	40 mol%, $CHCl_3$	1019	−1234	49
I	40 mol%, $CHCl_3$	867	−1386	49
$HgMe(SCN)_2^-$	CH_2Cl_2	1747	−506	36
Cl_2^-	CH_2Cl_2	1657	−596	36
Br_2^-	CH_2Cl_2	1565	−688	36
I_2^-	CH_2Cl_2	1364	−889	36

shift for Hg^{2+}, found by comparing the Hg^{2+}(aq) resonance position with that of the free Hg atom obtained by optical pumping, is 2432 ppm. (30)

Mercury resonances exhibit large solvent effects of up to 100 ppm. (32, 36) Whether these arise from solvent coordination or from general dilution, the effect is to vitiate detailed comparisons dependent upon small chemical shift differences except where uniformity of experimental conditions has been maintained throughout a series of compounds. Dimethylmercury dissolved in O- and N-donor solvents (1 M solution) is shifted to low frequency by 55–100 ppm, in aromatic hydrocarbons the shift is to low frequency by 45–55 ppm, in chlorinated hydrocarbons the shift is to low frequency by 10–45 ppm, and in saturated hydrocarbons the shift is to high frequency by 0–5 ppm. (32) A similar pattern of solvent dependence is seen with HgMeCl, except for pyridine which in this case causes a pronounced high frequency shift. (36)

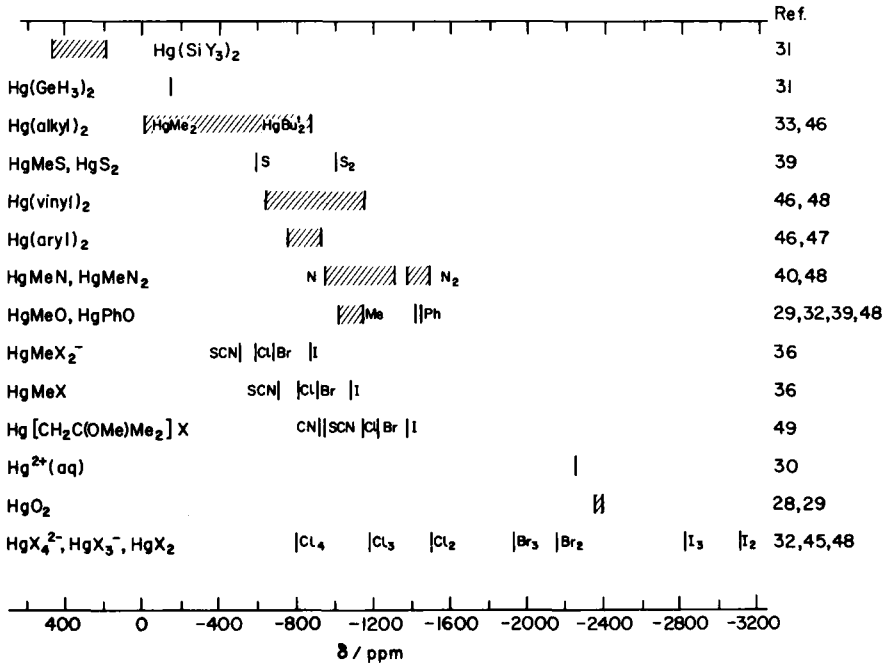

FIG. 15. ^{199}Hg chemical shift ranges for some different chemical environments.

1. Hg–metal environments

The compounds in which mercury is bonded to another metal contain the most deshielded mercury environments, (31) and $Hg(SiMe_3)_2$ with $\delta = 481$ establishes the high frequency end of the range at the present time. The data

in Table XXIII indicate that the substituent effects for GeH_3, SiH_3, and $SiMe_3$ are linearly additive, with the germanium ligand causing higher shielding than the silicon ligand, a pattern consistent with a NHD where the larger ligating atom within a group causes greater shielding. The mercurous ion is better viewed as a Hg-metal compound than as a lower oxidation state of mercury which might, by analogy with other metal resonances such as ^{51}V, ^{59}Co, and ^{205}Tl, be expected to adopt a range of shieldings considerably higher than that for mercury(II) compounds. The fact that it does not (30) supports its inclusion here. The narrow region for thermodynamic stability coupled with the insolubility of most mercurous compounds together account for the paucity of mercury(I) NMR data.

2. Hg–C environments

Organomercury compounds containing either one or two organic groups bonded to mercury have sufficient kinetic inertia to give well resolved limiting spectra and provide the large body of systematic data upon which rests our understanding of mercury NMR. The HgC_2 compounds (28, 33, 34, 35, 46, 47, 48, 50) cover the shielding range $\delta = 0$ for $HgMe_2$ to $\delta = -1187$ for $HgPh(CBr_2Cl)$, (32) with vinyl and aryl groups causing higher shielding than most of the alkyl groups. Among the dialkylmercury compounds it is $Hg(Bu^t)_2$ which is most highly shielded, (33) again implicating β-methyl substituents as shielding agents and establishing a pattern consistent with that of the cadmium alkyls. Successive substitution of methyl for hydrogen in one or both $HgMe_2$ alkyl groups gives additive and reasonably constant shielding increments of $\Delta\beta \approx -148$ (cf. -46 for cadmium), while methyl substitution into positions γ to Hg gives shielding decrements of $\Delta\gamma \approx +24$ (cf. $+23$ for cadmium). Constancy is maintained in these $\Delta\beta$ and $\Delta\gamma$ values when applied to the single alkyl group in RHgX halides, (34) but no theoretical understanding of the phenomenon, particularly the β,γ alternation (and β,γ,δ alternation in the case of cadmium alkoxides), has yet been provided.

3. Hg–N and Hg–P environments

In its propensity to form coordination complexes with typical N-, P-, O-, and S-bonding ligands, mercury is only a pale imitation of the typical transition metals, the reason being mercury's lack of vacant 5d-orbitals. Although no HgN_2 complexes have been reported, HgMeN complexes (40, 48) absorb in the region $\delta = -940$ to $\delta = -1317$, to low frequency of most HgC_2 environments. The chelating *o*-phenanthroline and bipyridine ligands yield 3-coordinate $HgMeN_2$ compounds with increased shielding values (40) around $\delta = -1450$. Data on phosphine complexes are even more scanty, with $Hg(PMe_3)_2^{2+}$ at $\delta = -1159$ being the only example reported. (48)

4. Hg–O and Hg–S environments

Both the HgO_2 (28, 29) and HgCO (29, 32, 39, 48) environments are well represented in the existing data, with HgO_2 coordination at $\delta = -2253$ to $\delta = -2389$ approaching the most highly shielded mercury environments obtaining in the iodide complexes, and including the $\delta = -2253$ value for $Hg^{2+}(aq)$ which is the analogue of the shielding references commonly adopted for zinc and cadmium shieldings. Alkyl and aryl mercury compounds with one Hg–O bond are shifted to high frequency, to the region intermediate between those for HgC_2 and HgO_2 environments, with carboxylate compounds having received the most attention. (29)

Sulphur ligands cause deshielding relative to oxygen ligands, and the shielding ranges for both HgS_2 and HgMeS environments are displaced about 400 ppm to higher δ-values of their oxygen counterparts. (39) The shifts for the glutathione complexes that have been investigated are particularly sensitive to pH changes which affect the number of sulphurs that bind to mercury.

5. Hg–halogen environments

Like their zinc and cadmium counterparts, the mercury halides are kinetically labile in solution and give rise to single resonances representing a weighted average of the HgX_4^{2-}, HgX_3^-, and HgX_2 environments. Only the chloride system has been analysed using equilibrium constants to obtain limiting shifts for the individual complexes, (45) and the usual caveat must be applied to shifts calculated from equilibrium constants obtained under concentrations and ionic strengths different from those for the NMR data. The shielding pattern for the halide complexes revealed in Fig. 15 is a very regular one in which a NHD is observed; the HgX_3^- resonance is shifted to high frequency of the HgX_2 resonance by 200–300 ppm for X = Cl, Br, and I. $HgCl_4^{2-}$ is another 340 ppm to high frequency of $HgCl_3^-$. The fact that the resonance positions for the bromide complexes lie almost half way between those for the chloride and iodide complexes, rather than closer to the chloride values as is the case with virtually all other metal halides, suggests that these shieldings be regarded with some caution, particularly when the (Cl–Br)/(Cl–I) ratios for the $HgMeX_2^-$, HgMeX, and $Hg\{CH_2C(OMe)Me_2\}X$ series all lie near the typical value of 0·3.

XIII. THE FUTURE

The past ten years have seen the transition from cw to FT NMR observation and with it a steady growth in the number of transition metals observed. We now have the situation where at least one element from each

triad has yielded chemical shift information. For the scandium, chromium, and zinc triads, all three elements in each triad have been studied.

The lowest receptivity element to provide spectral data of chemical interest is ^{57}Fe. Either isotopic enrichment or observation times of the order of days are required to achieve this objective. It seems unlikely that this effort will be repeated except in cases of particular structural significance. Those elements which have not yet been studied have either an extremely low receptivity or a large quadrupole moment, either of which will mitigate against the use of NMR spectroscopy as a method of characterization. We are unlikely to see much spectral data emerge from these elements over the next few years.

A number of the more receptive elements have received little attention, and in these cases we can look for increasing numbers of chemical shift studies to fill out the emerging shielding patterns. Titanium, niobium, and manganese fall into this category. Although blessed with lower receptivities, ^{183}W, ^{103}Rh, and ^{195}Pt can be studied indirectly by decoupling techniques, and the future should see considerable activity in this area.

The area of greatest current activity, which will undoubtedly continue into the near future, is the use of transition metals as surrogate atoms in biologically active molecules. Cadmium and mercury are at present seeing a lot of activity in this role, and lanthanum relaxation studies hold future promise for macromolecule characterization. Enough cadmium and mercury model systems have now been studied for chemical shift values to be used as indicators of coordination number and character of the primary coordination shell. In both cases, relaxation studies also hold potential for additional insight.

The transition metals are now firmly established on the nuclear magnetic resonance front. Their major value to the spectroscopist may ultimately lie with the impetus which they bring to the development of nuclear shielding theory.

Acknowledgements

I am indebted to Dr. P. A. W. Dean and to Dr. O. Lutz for their generosity in providing data prior to publication. Dr. B. H. Freeland provided valuable insights during our discussions about metal carbonyls. I also wish to thank Cel Foster who typed the manuscript.

REFERENCES

1. D. E. Irish, B. McCarroll and T. F. Young, *J. Chem. Phys.*, 1963, **39**, 3436.
2. B. W. Epperlein, H. Krüger, O. Lutz and A. Schwenk, *Z. Naturforsch.*, 1974, **29a**, 1553.
3. G. E. Maciel, L. Simeral and J. H. Ackerman, *J. Phys. Chem.*, 1977, **81**, 263.

4. L. G. Sillen and A. E. Martell, "Stability Constants of Metal Ion Complexes", Special Publication No. 17, The Chemical Society, London, 1964.
5. J. W. Akitt, N. N. Greenwood and A. Storr, *J. Chem. Soc.*, 1965, 4410.
6. R. G. Kidd and H. G. Spinney, *J. Amer. Chem. Soc.*, 1973, **95**, 88.
7. H. Krüger, O. Lutz, A. Nolle, A. Schwenk and G. Stricker, *Z. Naturforsch.*, 1973, **28a**, 484.
8. J. D. Kennedy and W. McFarlane, *J. Chem. Soc., Perkin*, 1977, 1187.
9. H. Krüger, O. Lutz, A. Schwenk and G. Stricker, *Z. Physik*, 1974, **266**, 233.
10. R. A. Haberkorn, L. Que, W. O. Gillum, R. H. Holm, C. S. Liu and R. C. Lord, *Inorg. Chem.*, 1976, **15**, 2408.
11. A. D. Cardin, P. D. Ellis, J. D. Odom and J. W. Howard, *J. Amer. Chem. Soc.*, 1975, **97**, 1672.
12. I. M. Armitage, R. T. Pajer, A. J. M. S. Uiterkamp, J. F. Chlebowski and J. E. Coleman, *J. Amer. Chem. Soc.*, 1976, **98**, 5710.
13. J. L. Sudmeier and S. J. Bell, *J. Amer. Chem. Soc.*, 1977, **99**, 4499.
14. R. J. Kostelnik and A. A. Bothner-By, *J. Magn. Resonance*, 1974, **14**, 141.
15. D. D. Dominguez, M. M. King and H. J. C. Yeh, *J. Magn. Resonance*, 1978, **32**, 161.
16. D. A. Bailey, P. D. Ellis, A. D. Cardin and W. D. Behnke, *J. Amer. Chem. Soc.*, 1978, **100**, 5236.
17. D. C. Look, *Phys. Stat. Sol.*, 1972, **50B**, K97.
18. H. B. Bürgi, *Helv. Chim. Acta*, 1974, **57**, 513.
19. B. Birgersson, R. E. Carter and T. Drakenberg, *J. Magn. Resonance*, 1977, **28**, 299.
20. I. M. Armitage, A. J. M. S. Uiterkamp, J. F. Chlebowski and J. E. Coleman, *J. Amer. Chem. Soc.*, 1978, **29**, 375.
21. J. J. H. Ackerman, T. V. Orr, V. J. Bartuska and G. E. Maciel, *J. Amer. Chem. Soc.*, 1979, **101**, 341.
22. T. Drakenberg, N. O. Bjork and R. Portanova, *J. Phys. Chem.*, 1978, **82**, 2423.
23. C. J. Turner and R. F. M. White, *J. Magn. Resonance*, 1977, **26**, 1.
24. H. Ohtaki, M. Maeda and S. Ito, *Bull. Chem. Soc. Japan*, 1974, **47**, 2217.
25. I. M. Armitage, A. J. M. S. Uiterkamp, J. F. Chlebowski and J. E. Coleman, *J. Magn. Resonance*, 1978, **29**, 375.
26. P. J. Sadler, A. Bakka and P. J. Beynon, *FEBS Lett.*, 1978, **94**, 315.
27. L. C. Damude and P. A. W. Dean, *J. Organometal. Chem.*, 1979, **168**, 123.
28. G. E. Maciel and M. Borzo, *J. Magn. Resonance*, 1973, **10**, 388.
29. M. Borzo and G. E. Maciel, *J. Magn. Resonance*, 1975, **19**, 279.
30. H. Krüger, O. Lutz, A. Nolle and A. Schwenk, *Z. Physik* (*A*), 1975, **273**, 325.
31. S. Cradock, E. A. V. Ebsworth, N. S. Hosmane and K. M. Mackey, *Angew. Chem. Internat. Edn.*, 1975, **14**, 167.
32. M. A. Sens, N. K. Wilson, P. D. Ellis and J. D. Odom, *J. Magn. Resonance*, 1975, **19**, 323.
33. J. D. Kennedy and W. McFarlane, *J. Chem. Soc., Faraday II*, 1976, **72**, 1653.
34. J. Browning, P. L. Goggin, R. J. Goodfellow, N. W. Hurst, L. G. Mallinson and M. Murray, *J. Chem. Soc., Dalton*, 1978, 872.
35. R. J. Goodfellow and S. R. Stobart, *J. Magn. Resonance*, 1977, **27**, 143.
36. P. L. Goggin, R. J. Goodfellow and N. W. Hurst, *J. Chem. Soc., Dalton*, 1978, 561.
37. P. F. Barron, D. Doddrell and W. Kitching, *J. Organometal. Chem.*, 1977, **139**, 361.
38. J. L. Sudmeier and T. G. Perkins, *J. Amer. Chem. Soc.*, 1977, **99**, 7732.
39. J. L. Sudmeier, R. R. Birge and T. G. Perkins, *J. Magn. Resonance*, 1978, **30**, 491.
40. A. J. Canty, A. Marker, P. Barron and P. C. Healey, *J. Organometal. Chem.*, 1978, **144**, 371.
41. T. R. Griffiths and R. A. Anderson, *J. Chem. Soc., Chem. Comm.*, 1979, 61.
42. A. Nolle, *Z. Naturforsch.*, 1978, **33a**, 666.

43. A. Fratiello, R. E. Lee and R. E. Schuster, *Inorg. Chem.*, 1970, **9**, 391.
44. C. R. Lassigne and E. J. Wells, *Canad. J. Chem.*, 1977, **55**, 1303.
45. P. D. Godfrey, M. L. Heffernan and D. F. Kerr, *Austral. J. Chem.*, 1964, **17**, 701.
46. A. P. Tupciauskas, N. M. Sergeyev, Yu. A. Ustynyuk and A. N. Kashin, *J. Magn. Resonance*, 1972, **7**, 124.
47. W. McFarlane, *J. Chem. Soc.* (*A*), 1968, 2280.
48. R. J. Goodfellow, in "NMR and the Periodic Table" (R. K. Harris and B. E. Mann, eds.), Ch. 8, Academic Press, London, 1978.
49. T. Ibusiki and Y. Saito, *Chem. Lett.*, 1974, 311.
50. R. B. Johannesen and R. W. Duerst, *J. Magn. Resonance*, 1971, **5**, 355.
51. R. A. Kovar and G. L. Morgan, *J. Amer. Chem. Soc.*, 1970, **92**, 5056; J. J. Delpuech, A. Peguy, P. Rubini and J. Steinmetz, *Nouv. J. Chim.*, 1976, **1**, 133.
52. O. Lutz, A. Schwenk and A. Uhl, *Z. Naturforsch.*, 1973, **28a**, 1534; 1975, **30a**, 1122; J. Banck and A. Schwenk, *Z. Physik*, 1973, **256**, 165.
53. B. N. Figgis, "Introduction to Ligand Fields", pp. 58, 59, Wiley-Interscience, New York, 1966.
54. C. W. Burges, R. Koschmieder, W. Sahm and A. Schwenk, *Z. Naturforsch.*, 1973, **28a**, 1753.
55. P. M. Hennrichs, J. J. H. Ackermann and G. E. Maciel, *J. Amer. Chem. Soc.*, 1977, **99**, 2544.
56. K. Jucker, W. Sahm and A. Schwenk, *Z. Naturforsch.*, 1976, **31a**, 1532.
57. A. K. Rahimi and A. I. Popov, *Inorg. Nucl. Chem. Lett.*, 1976, **12**, 703.
58. A. Schwenk, *J. Magn. Resonance*, 1971, **5**, 376.
59. A. Sahm and A. Schwenk, *Z. Naturforsch.*, 1974, **29a**, 1763.
60. C. Deverell and R. E. Richards, *Mol. Phys.*, 1966, **10**, 551.
61. H. M. McConnell and H. E. Weaver, *J. Chem. Phys.*, 1956, **25**, 307.
62. T. Yamamoto, H. Haraguchi and S. Fujiwara, *J. Phys. Chem.*, 1970, **74**, 4369.
63. R. W. Mebs, G. C. Carter, B. J. Evans and H. L. Bennet, *Solid State Comm.*, 1972, **10**, 769.
64. W. McFarlane and D. S. Rycroft, *J. Magn. Resonance*, 1976, **24**, 95.
65. O. Lutz, H. Oehler and P. Kroneck, *Z. Naturforsch.*, 1978, **33a**, 1021.
66. O. Lutz, H. Oehler and P. Kroneck, *Z. Physik* (*A*), 1978, **288**, 17.
67. E. S. Mooberry and R. K. Sheline, *J. Chem. Phys.*, 1972, **56**, 1852.
68. E. A. C. Lucken, K. Noack and D. F. Williams, *J. Chem. Soc.* (*A*), 1967, 148.
69. E. S. Mooberry, M. Pupp, J. L. Slater and R. K. Sheline, *J. Chem. Phys.*, 1971, **55**, 3655.
70. R. J. Goodfellow, in "NMR and the Periodic Table", pp. 250, 251 (R. K. Harris and B. E. Mann, eds.), Academic Press, London, 1978.
71. P. L. Goggin, R. J. Goodfellow, S. R. Haddock, B. F. Taylor and I. R. H. Marshall, *J. Chem. Soc., Dalton*, 1976, 459.
72. J. Brown, P. L. Goggin, R. J. Goodfellow, N. W. Hurst, L. G. Mallinson and M. Murray, *J. Chem. Soc., Dalton*, 1978, 872.
73. R. A. Dwek, Z. Luz and M. Shporer, *J. Phys. Chem.*, 1970, **74**, 2232.
74. S. J. S. Kerrison and P. J. Sadler, *J. Chem. Soc., Chem. Comm.*, 1977, 861.
75. S. J. S. Kerrison and P. J. Sadler, *J. Magn. Resonance*, 1978, **31**, 321.
76. C. Brown, B. T. Heaton, P. Chini, A. Fumagalli and G. Longoni, *J. Chem. Soc., Chem. Comm.*, 1977, 309.
77. A. Fumagalli, S. Martinengo, P. Chini, A. Albinati, S. Bruchner and B. T. Heaton, *J. Chem. Soc., Chem., Comm.*, 1978, 195.
78. I. M. Blacklaws, L. C. Brown, E. A. V. Ebsworth and F. J. S. Reed, *J. Chem. Soc., Dalton*, 1978, 877.
79. E. A. V. Ebsworth, J. M. Edward, F. J. S. Reed and J. D. Whitelock, *J. Chem. Soc., Dalton*, 1978, 1160.

80. N. N. Greenwood, J. D. Kennedy and J. Strauss, *J. Chem. Soc., Dalton*, 1978, 1146.
81. P. S. Pregosin, S. N. Sze, P. Salvadori and R. Lazzaroni, *Helv. Chim. Acta*, 1977, **60**, 2514.
82. A. von Zelewsky, *Helv. Chim. Acta*, 1968, **51**, 803.
83. J. J. Pesek and W. R. Mason, *J. Magn. Resonance*, 1977, **25**, 519.
84. W. G. Proctor and F. C. Yu, *Phys. Rev.*, 1951, **81**, 20.
85. H. C. E. McFarlane and W. McFarlane, *J. Chem. Soc., Dalton*, 1973, 2416.
86. J. S. Griffith and L. E. Orgel, *Trans. Faraday Soc.*, 1957, **53**, 601.
87. R. G. Kidd, in "NMR and the Periodic Table", Ch. 8 (R. K. Harris and B. E. Mann, eds.), Academic Press, London, 1978.
88. W. Hackbusch, H. H. Rupp and K. Wieghardt, *J. Chem. Soc., Dalton*, 1975, 1015.
89. A. Yamasaki, T. Aoyama, S. Fujiwara and K. Nakamura, *Bull. Chem. Soc. Japan*, 1978, **51**, 643.
90. N. Juranic, M. B. Celap, D. Vucelic, M. J. Malinar and P. N. Radivojsa, *Inorg. Chim. Acta*, 1977, **25**, 229.
91. M. R. Bendall and D. M. Dodrell, *Austral. J. Chem.*, 1978, **31**, 1141.
92. R. Weiss and J. G. Verkade, *Inorg. Chem.*, 1979, **18**, 529.
93. R. A. LaRossa and T. L. Brown, *J. Amer. Chem. Soc.*, 1974, **96**, 2072.
94. N. A. Matwiyoff and W. E. Wageman, *Inorg. Chim. Acta*, 1970, **4**, 460.
95. C. R. Kanekar and N. S. Biradar, *Current Sci.*, 1966, **35**, 37.
96. N. S. Biradar and M. A. Pujar, *Z. Anorg. Chem.*, 1972, **391**, 54.
97. F. Yajima, Y. Koike, A. Yamasaki and S. Fujiwara, *Bull. Chem. Soc. Japan*, 1974, **47**, 1442.
98. C. K. Jorgenson, "Absorption Spectra and Chemical Bonding in Complexes", Ch. 7, Pergamon Press, London, 1962.
99. J. S. Griffith and L. E. Orgel, *Trans. Faraday Soc.*, 1957, **53**, 601.
100. R. Freeman, G. R. Murray and R. E. Richards, *Proc. Roy. Soc.*, 1957, ***A*242**, 455.
101. S. S. Dharmatti and C. R. Kanekar, *J. Chem. Phys.*, 1959, **31**, 1436.
102. N. S. Biradar and M. A. Pujar, *Inorg. Nucl. Chem. Lett.*, 1971, **7**, 269.
103. C. R. Kanekar, M. M. Dhingra, V. R. Marathe and R. Nagarajan, *J. Chem. Phys.*, 1967, **46**, 2009.
104. S. Fujiwara, F. Yajima and A. Yamasaki, *J. Magn. Resonance*, 1969, **1**, 203.
105. R. L. Martin and A. H. White, *Nature*, 1969, **223**, 394.
106. C. K. Jorgenson, "Absorption Spectra and Chemical Bonding in Complexes", Ch. 8, Pergamon Press, London, 1962.
107. R. G. Kidd and D. R. Truax, *J. Amer. Chem. Soc.*, 1968, **90**, 6867.
108. E. R. Malinowski, *J. Amer. Chem. Soc.*, 1969, **91**, 4701.
109. R. G. Kidd and H. G. Spinney, *J. Amer. Chem. Soc.*, 1973, **95**, 88.
110. R. G. Kidd and H. G. Spinney, *Inorg. Chem.*, 1973, **12**, 1967.
111. N. F. Ramsey, *Phys. Rev.*, 1950, **78**, 699.
112. R. E. Walstedt, J. H. Wernick and V. Jaccarino, *Phys. Rev.*, 1967, **162**, 301.
113. S. Fujiwara, F. Yajima and A. Yamasaki, *J. Magn. Resonance*, 1969, **1**, 203.
114. R. L. Martin and A. H. White, *Nature*, 1969, **223**, 394.
115. H. W. Speiss, H. Hass and H. Hartmann, *J. Chem. Phys.*, 1969, **51**, 3057.
116. G. P. Betteridge and R. M. Golding, *J. Chem. Phys.*, 1969, **51**, 2497.
117. A. Johnson and G. W. Everett, Jr., *Inorg. Chem.*, 1973, **12**, 2801.
118. A. J. Freeman and R. E. Watson, in "Magnetism", Vol. IIA (G. Rado and H. Suhl, eds.), Academic Press, New York, 1965.
119. G. Malli and C. Froese, *Internat. J. Quant. Chem.*, 1967, **1**, 95.
120. P. B. Sogo and C. D. Jeffries, *Phys. Rev.*, 1955, **98**, 1316.
121. H. T. Weaver and R. K. Quinn, *Phys. Rev.* (*B*), 1974, **10**, 1816.

122. R. J. Goodfellow, in "NMR and the Periodic Table", pp. 244–8 (R. K. Harris and B. E. Mann, eds.), Academic Press, London, 1978.
123. T. H. Brown and P. J. Green, *J. Amer. Chem. Soc.*, 1970, **92**, 2359.
124. H. C. E. McFarlane, W. McFarlane and R. J. Wood, *Bull. Soc. Chim. Belg.*, 1976, **85**, 864.
125. E. M. Hyde, J. D. Kennedy, B. L. Shaw and W. McFarlane, *J. Chem. Soc., Dalton*, 1977 1571.
126. S. Martinengo, B. T. Heaton, R. J. Goodfellow and P. Chini, *J. Chem. Soc., Chem. Comm.*, 1977, **39**.
127. B. W. Epperlein, H. Krüger, O. Lutz, A. Nolle and W. Mayr, *Z. Naturforsch.*, 1975, **30a**, 1237.
128. O. Lutz, W. Nepple and A. Nolle, *Z. Naturforsch.*, 1976, **31a**, 1046.
129. Y. Egozy and A. Loewenstein, *J. Magn. Resonance*, 1969, **1**, 494.
130. B. N. Figgis, R. G. Kidd and R. S. Nyholm, *Canad. J. Chem.*, 1965, **43**, 145.
131. R. R. Vold and R. L. Vold, *J. Magn. Resonance*, 1975, **19**, 365.
132. O. Lutz, A. Nolle and P. Kroneck. *Z. Naturforsch.*, 1976, **31a**, 454.
133. O. Lutz, A. Nolle and P. Kroneck, *Z. Naturforsch.*, 1977, **32a**, 505.
134. W. D. Kautt, H. Krüger, O. Lutz, H. Maier and A. Nolle, *Z. Naturforsch.*, 1976, **31a**, 351.
135. K. V. Buckler, A. R. Haase, O. Lutz, M. Muller and A. Nolle, *Z. Naturforsch.*, 1977, **32a**, 126.
136. O. Lutz, A. Nolle and P. Kroneck, *Z. Physik* (*A*), 1977, **282**, 157.
137. P. C. Lauterbur, *J. Chem. Phys.*, 1965, **42**, 799.
138. P. J. Green and T. H. Brown, *Inorg. Chem.*, 1971, **10**, 206.
139. W. McFarlane, A. M. Noble and J. M. Winfield, *J. Chem. Soc.* (*A*), 1971, 948.
140. H. C. E. McFarlane, W. McFarlane and D. S. Rycroft, *J. Chem. Soc., Dalton*, 1976, 1616.
141. J. Banck and A. Schwenk, *Z. Physik* (*B*), 1975, **20**, 75.
142. A. Narath and D. C. Wallace, *Phys. Rev.*, 1962, **127**, 724.
143. O. Lutz and W. Steinkilberg, *Z. Naturforsch.*, 1974, **29a**, 1467.
144. A. R. Haase, O. Lutz, M. Muller and A. Nolle, *Z. Naturforsch.*, 1976, **31a**, 1427.
145. F. Calderazzo, E. A. C. Lucken and D. F. Williams, *J. Chem. Soc.* (*A*), 1967, 154.
146. S. Onaka, Y. Sasaki and H. Sano, *Bull. Chem. Soc. Japan*, 1971, **44**, 726.
147. G. M. Bancroft, H. C. Clark, R. G. Kidd, A. T. Rake and H. G. Spinney, *Inorg. Chem.*, 1973, **12**, 728.
148. R. J. Miles, Jr., B. B. Garrett and R. J. Clark, *Inorg. Chem.*, 1969, **8**, 2817.
149. T. Nakano, *Bull. Chem. Soc. Japan*, 1977, **50**, 661.
150. D. Gudlin and H. Schneider, *J. Magn. Resonance*, 1975, **17**, 268.
151. A. I. Popov, *Pure Appl. Chem.*, 1975, **41**, 275.
152. B. N. Figgis, R. G. Kidd and R. S. Nyholm, *Proc. Roy. Soc.*, 1962, *A***269**, 469.
153. R. G. Kidd, Ph.D. Thesis, University of London, 1962.
154. Y. Yamagata, *J. Phys. Soc. Japan*, 1964, **19**, 10.
155. A. Schwenk, *J. Magn. Resonance*, 1971, **5**, 376.
156. A. A. Koridze, P. V. Petrovskii, S. P. Gubin and E. I. Fedin, *J. Organometal. Chem.*, 1975, **93**, C26.
157. W. Sahm and A. Schwenk, *Z. Naturforsch.*, 1974, **29a**, 1763.
158. A. Schwenk, *Phys. Lett.* (*A*), 1970, **31**, 513.
159. J. P. Williams and A. Wojcicki, *Inorg. Chim. Acta*, 1975, **15**, L19.
160. D. Rehder and J. Schmidt, *Z. Naturforsch.*, 1972, **27b**, 625.
161. H. W. Speiss and R. K. Sheline, *J. Chem. Phys.*, 1970, **53**, 3036.
162. O. W. Howarth and R. E. Richards, *J. Chem. Soc.*, 1965, 864.
163. J. V. Hatton, Y. Saito and W. G. Schneider, *Canad. J. Chem.*, 1965, **43**, 47.
164. D. Rehder and J. Schmidt, *J. Inorg. Nucl. Chem.*, 1974, **36**, 333.
165. D. Rehder and W. L. Dorn, *Transition Metal Chem.*, 1976, **1**, 74.
166. D. Rehder and W. L. Dorn, *Transition Metal Chem.*, 1976, **1**, 233.

167. D. Rehder, L. Dahlenburg and I. Muller, *J. Organometal. Chem.*, 1976, **122**, 53.
168. D. Rehder, *Z. Naturforsch.*, 1976, **31b**, 273.
169. D. Rehder, *J. Magn. Resonance*, 1977, **25**, 177.
170. D. Rehder and J. Schmidt, *Transition Metal Chem.*, 1977, **2**, 41.
171. D. Rehder, *J. Organometal. Chem.*, 1977, **137**, C25.
172. I. Muller and D. Rehder, *J. Organometal. Chem.*, 1977, **139**, 293.
173. D. Rehder, *Z. Naturforsch.*, 1977, **32b**, 771.
174. R. Talay and D. Rehder, *Chem. Ber.*, 1978, **111**, 1978.
175. K. Paulsen, D. Rehder and D. Thoennes, *Z. Naturforsch.*, 1978, **33a**, 834.
176. D. Rehder, K. Paulsen and H. Lechert, *Z. Naturforsch.*, 1978, **33a**, 1597.
177. S. E. O'Donnell and M. T. Pope, *J. Chem. Soc., Dalton*, 1976, 2290.
178. O. W. Howarth and M. Jarrold, *J. Chem. Soc., Dalton*, 1978, 503.
179. Y. A. Buslaev, V. D. Kopanev and V. P. Tarasov, *Chem. Comm.*, 1971, 1175.
180. Y. A. Buslaev, V. D. Kopanev, S. M. Sinitsyna and V. G. Khlebodarov, *Russ. J. Inorg. Chem.*, 1973, **18**, 1362.
181. R. G. Kidd and H. G. Spinney, *Inorg. Chem.*, 1973, **12**, 1967.
182. V. P. Tarasov, V. I. Privalov and Y. A. Buslaev, *Mol. Phys.*, 1978, **35**, 1047.
183. J. A. S. Howell and K. C. Moss, *J. Chem. Soc. (A)*, 1971, 2483.
184. L. C. Erich, A. C. Gossard and R. L. Hartless, *J. Chem. Phys.*, 1973, **59**, 3911.
185. Y. A. Buslaev and E. G. Ilyin, *J. Fluorine Chem.*, 1974, **4**, 271.
186. R. G. Kidd, R. W. Matthews and H. G. Spinney, *J. Amer. Chem. Soc.*, 1973, **94**, 6686.
187. P. A. W. Dean and D. F. Evans, *J. Chem. Soc. (A)*, 1967, 698.
188. H. G. Spinney, Ph.D. Thesis, University of Western Ontario, 1972.
189. K. J. Packer and E. L. Muetterties, *J. Amer. Chem. Soc.*, 1963, **85**, 3035.
190. Y. A. Buslaev, S. P. Petrosyants, V. P. Tarasov and V. I. Chagin, *Zhur. Neorg. Khim.*, 1974, **19**, 1790.
191. G. A. Melson, D. J. Olszanski and E. T. Roach, *J. Chem. Soc., Chem. Comm.*, 1974, 229.
192. G. A. Melson, D. J. Olszanski and A. K. Rahimi, *Spectrochim. Acta*, 1977, **33A**, 301.
193. O. Lutz, *Phys. Lett. (A)*, 1969, **29**, 58.
194. C. Hassler, J. Kronenbitter and A. Schwenk, *Z. Physik (A)*, 1977, **280**, 117.
195. H. Krüger, O. Lutz and H. Oehler, *Phys. Lett. (A)*, 1977, **62**, 131.
196. J. Reuben, *J. Phys. Chem.*, 1975, **79**, 2154.
197. K. Nakamura and K. Kawamura, *Bull. Chem. Soc. Japan*, 1971, **44**, 330.
198. J. Reuben, *J. Amer. Chem. Soc.*, 1975, **97**, 3822.
199. J. Reuben and Z. Luz, *J. Phys. Chem.*, 1976, **80**, 1357.
200. L. S. Smith, Jr., D. C. McCain and D. L. Wertz, *J. Amer. Chem. Soc.*, 1976, **98**, 5125.
201. P. L. Rinaldi, S. A. Khan, G. R. Choppin and C. C. Levy, *J. Amer. Chem. Soc.*, 1979, **101**, 1350.
202. H. Spiesecke and W. G. Schneider, *J. Chem. Phys.*, 1961, **35**, 722.
203. J. H. Van Vleck, "The Theory of Electric and Magnetic Susceptibilities", Ch. VI, Oxford University Press, 1932.
204. C. J. Jameson and H. S. Gutowsky, *J. Chem. Phys.*, 1964, **40**, 1714.
205. G. A. Webb, in "NMR and the Periodic Table", pp. 52, 53 (R. K. Harris and B. E. Mann, eds.), Academic Press, London, 1978.
206. F. W. Wehrli, in "Annual Reports on NMR Spectroscopy", Vol. 9, p 125 (G. A. Webb, ed.), Academic Press, London, 1979.
207. R. K. Harris and B. E. Mann (eds.), "NMR and the Periodic Table", Academic Press, London, 1978.
208. J. A. Pople, *Mol. Phys.*, 1964, **7**, 301, and references therein.
209. W. H. Flygare and J. Goodisman, *J. Chem. Phys.*, 1968, **49**, 3122.
210. J. D. Kennedy, W. McFarlane and G. S. Pyne, *J. Chem. Soc., Dalton*, 1977, 2332.

This Page Intentionally Left Blank

NMR Chemical Shift Calculations and Stereochemical Structures of Synthetic Polymers

ISAO ANDO AND TETSUO ASAKURA

Department of Polymer Chemistry, Tokyo Institute of Technology, Ookayama, Tokyo, Japan

I. INTRODUCTION

Since the first observation (1) of the ^{1}H high-resolution NMR spectrum of polyisoprene in 1957 a number of papers have been published in the field of high-resolution NMR spectroscopy of polymers; also a number of excellent reviews and text-books have appeared. (2)

High-resolution NMR spectroscopy has given useful information about the stereochemical structures and conformations in polymer solutions through chemical shifts and spin couplings. Recently, the high-resolution NMR spectra of polymers in the solid state have been obtained by means of pulse Fourier transform (PFT) techniques. From these the chemical shift tensor, which cannot be obtained from measurements on liquids or solutions, is obtained. (3)

The chemical shifts of the nuclei in the polymers under consideration in this review depend upon their magnetic environment which depends upon the conformations of the neighbouring bonds and on the stereochemical structures of the polymer chains. Consequently the stereochemical structures and conformations of the polymers are obtained through the observation and calculation of the ^{1}H and ^{13}C chemical shifts.

In this review all chemical shifts are reported on the δ-scale. Chemical shifts that have been measured with respect to other reference standards have been converted to the δ-scale.

II. THEORETICAL DEVELOPMENTS

A polymer chain can assume an enormous number of conformers owing to the various possibilities of rotation around the chain bonds. Thus the factors governing the appearance of the NMR spectra include the stereochemical structures, the relative energies of the rotational isomers, the chemical shifts, and spin couplings. If the molecular motion in the polymer chain is slow the NMR spectrum represents the superposition of the spectra for the various conformers. However, if the rotation around the chain bonds is very fast the NMR spectrum is an average of the spectra for the conformers. The experimentally observed chemical shift for the nucleus A is given as

$$\langle \sigma_A \rangle = \sum_{i=1}^{n} P_i \sigma_i \tag{1}$$

The numerical indices refer to the preferred conformers, P_i and σ_i are the probability of occurrence and chemical shift of the preferred conformer i, respectively. Thus, we can interpret the behaviour of the observed chemical shift through an understanding of P_i and σ_i.

The chemical shift of an atom depends upon its electronic and molecular environments. The chemical shift for atom A may be estimated approximately by a sum of the following terms: (4)

$$\sigma_A = \sigma_A^{dia} + \sigma_A^{para} + \sigma_A^{aniso} + \sigma_A^{E} + \sigma_A^{ring} \tag{2}$$

where σ_A^{dia} is the diamagnetic term, σ_A^{para} the paramagnetic term, σ_A^{aniso} the neighbouring anisotropy effect arising from locally induced currents on the atoms other than the atom A in the molecule, σ_A^{E} the polar effect arising from the electric field due to any polar group in the molecule, (5) and σ_A^{ring} the ring current effect due to interatomic currents which flow around closed, conjugated loops. The relative chemical shifts for protons are estimated as the sum of σ_A^{dia}, σ_A^{aniso}, σ_A^{E}, and σ_A^{ring}, while σ_A^{para} is neglected. On the other hand, relative ^{13}C chemical shifts are predominantly governed by σ_A^{para}.

The contribution for the atom A from σ_A^{dia} is given (6) as

$$\sigma_A^{dia} = \frac{\mu_0}{4\pi}\frac{e^2}{3m}\sum_{\mu} P_{\mu\mu}\langle\mu|r_{\mu A}^{-1}|\mu\rangle \tag{3}$$

where $P_{\mu\mu}$ is the charge density in the atomic orbital μ at an average distance of $r_{\mu A}$ from the atom A. The matrix element is evaluated from

$$\langle\mu|r_{\mu A}^{-1}|\mu\rangle = Z_\mu/n^2a_0^2 \tag{4}$$

where n is the principal quantum number of orbital μ, a_0 is the Bohr radius, and Z_μ is the effective nuclear charge for electrons in this orbital which can be obtained from Slater's rules. Then, for protons, the following equation is used (in ppm):

$$\sigma_A^{dia}(H) = 17{\cdot}8q_H \tag{5}$$

where q_H is the electron density on the hydrogen atom under consideration. For the ^{13}C nucleus the following equation is used (in ppm):

$$\sigma_A^{dia}(^{13}C) = 4{\cdot}45[3{\cdot}25 - 0{\cdot}35(q_C - 4{\cdot}0)]q_C \tag{6}$$

where q_C is the electron density on the carbon atom. The paramagnetic contribution may be estimated according to the sum-over-states method (6) as follows:

$$\begin{aligned}\sigma_A^{para} = -\frac{\mu_0}{4\pi}\frac{2e^2\hbar^2}{3m^2}\langle r^{-3}\rangle_{2p}\sum_j^{occ}\sum_k^{unocc}(\Delta E_{k-j})^{-1}\\ \times\Big[(C_{yAj}C_{zAj} - C_{zAj}C_{yAk})\sum_B(C_{yBj}C_{zBk} - C_{zBj}C_{yBk})\\ +(C_{zAj}C_{xAk} - C_{xAj}C_{zAk})\sum_B(C_{zBj}C_{xBk} - C_{xBj}C_{zBk})\\ +(C_{xAj}C_{yAk} - C_{yAj}C_{xAk})\sum_B(C_{xBj}C_{yBk} - C_{yBj}C_{xBk})\Big]\end{aligned} \tag{7}$$

where C_{xAj} is the LCAO coefficient of the $2p_x$ orbital on the nucleus A in MO_j etc. The summations over atom B include A. ΔE_{k-j} is the singlet–singlet excitation energy of the jth occupied and the kth unoccupied orbitals. $\langle r^{-3}\rangle_{2p}$ is the mean inverse cube radius for the p-orbital on the atom A; this may be evaluated by means of the relationship

$$\langle r^{-3}\rangle_{2p} = \frac{1}{3}\left(\frac{Z_{2p}}{2a_0}\right)^3 \tag{8}$$

where Z_{2p} is the effective nuclear charge which is given (7) by

$$Z_{2p} = Z^0 + 0{\cdot}35q_A \tag{9}$$

in which Z^0 is the effective nuclear charge for the free atom and q_A is the net

charge on the atom A. With the average excitation energy (ΔE) approximation, equation (7) is simplified (8) to give

$$\sigma_A^{para} = -\frac{\mu_0}{4\pi}\frac{e^2\hbar^2}{2m^2}\frac{1}{\Delta E}\langle r^{-3}\rangle_{2p}\sum_B Q_{AB} \tag{10}$$

where the summation over B includes the atom A and all other atoms in the molecule. Q_{AB} is given by

$$\begin{aligned} Q_{AB} = {} & 4/3\delta_{AB}(P_{x_Ax_B}+P_{y_Ay_B}+P_{z_Az_B}) \\ & -2/3(P_{x_Ax_B}P_{y_Ay_B}+P_{x_Ax_B}P_{z_Az_B}+P_{y_Ay_B}P_{z_Az_B}) \\ & +2/3(P_{x_Ay_B}P_{x_By_A}+P_{x_Az_B}P_{x_Bz_A}+P_{y_Az_B}P_{y_Bz_A}) \end{aligned} \tag{11}$$

where $P_{x_Ax_B}$ is the element of the bond order matrix for the $2p_x$ atomic orbitals on the atoms A and B and δ is the Kronecker symbol.

The magnitude of σ_A^{aniso} depends solely on the nature of the other atoms or bonds B; if the atom or bond B is at a distance r_{AB} from A it is given (9) by

$$\sigma_A^{aniso} = (1/3r_{AB}^3)[(1-3\cos^2\theta_x)\chi_{xx}+(1-3\cos^2\theta_y)\chi_{yy}+(1-3\cos^2\theta_z)\chi_{zz}] \tag{12}$$

where χ_{xx}, χ_{yy}, and χ_{zz} are the three principal elements of the magnetic susceptibility tensor χ of the atom or bond B; θ_x, θ_y, and θ_z are the angles between the principal axes and the AB vector. If $\chi_{xx} \neq \chi_{yy} \neq \chi_{zz}$ and the y or x axis can be chosen such that r_{AB} lies in the zy (or zx) plane then equation (12) reduces to

$$\sigma_A^{aniso} = (1/3r_{AB}^3)(2\Delta\chi_1 - \Delta\chi_2 - \Delta\chi_1 3\cos^2\theta_z) \tag{13}$$

where $\Delta\chi_1 = \chi_{zz} - \chi_{yy}$ and $\Delta\chi_2 = \chi_{zz} - \chi_{xx}$. If the group B is axially symmetric, $\chi_{xx} = \chi_{yy} \neq \chi_{zz}$, equation (12) then becomes

$$\sigma_A^{aniso} = (1/3r_{AB}^3)\Delta\chi_B(1-3\cos^2\theta_z) \tag{14}$$

in which $\Delta\chi_B = \chi_B^{\parallel} - \chi_B^{\perp}$ and θ_z is the angle between the anisotropy axis and the internuclear vector r_{AB}.

The value of σ_A^E is estimated approximately by the Buckingham (5) expression

$$\sigma_A^E = -2\times10^{-12}E_z - 10^{-18}E^2 \tag{15}$$

where E_z is the component of a uniform electric field E in the bond direction of any specified proton.

According to the Johnson and Bovey scheme, the ring current effect σ_A^{ring} for a nucleus located at a point specified by the cylindrical coordinates ρ and z measured from the centre of the phenyl group and expressed in units of the

phenyl ring radius a, is given (10) by

$$\sigma_A^{ring} = \frac{\mu_0 n e^2 \times 10^6}{24\pi^2 m[(1+\rho)^2+z^2]}\left[K + \frac{1-\rho^2-z^2}{(1-\rho)^2+z^2}E\right] \tag{16}$$

where n is the number of π electrons, and K and E are the complete elliptic integrals whose modulus k is given by

$$k^2 = 4\rho/[(1+\rho)^2+z^2] \tag{17}$$

An interesting calculation of ^{13}C chemical shifts (11) relates to a series of saturated hydrocarbons, including the linear paraffins and several branched paraffins. The ^{13}C chemical shifts can be described by a linear equation of the form

$$\delta_C^i = B + \sum_j A_j \tag{18}$$

where δ_C^i is the shift of carbon i, A_j is an additive shift parameter for atoms in the jth position relative to carbon i, and B is a constant whose value is close to the methane carbon shift. This equation has been extended by Lindeman and Adams. (12) These empirical correlations provide the investigator with powerful analytical tools for the analysis of microstructures in hydrocarbon chains.

Let us consider the calculation of the probabilities of the preferred conformations in polymer chains. The skeletal bond is assumed to occur in any one of three discrete rotational states; these rotational states have the designations *trans* (T), *gauche* positive (G), and *gauche* negative (G'). G and G' are assumed to occur at rotational angles of 120° and −120° from T, respectively, with positive being in the clockwise direction. (13)

The statistical weight matrix **T** for the characterization of a polyethylene chain, which is handled in this work, is given (14) as

$$\mathbf{T} = \begin{array}{c} \\ \mathrm{T} \\ \mathrm{G} \\ \mathrm{G}' \end{array} \begin{array}{c} \begin{array}{ccc} \mathrm{T} & \mathrm{G} & \mathrm{G}' \end{array} \\ \begin{pmatrix} 1 & 1 & 1 \\ \sigma & \sigma & \sigma\omega \\ \sigma & \sigma\omega & \sigma \end{pmatrix} \end{array} \tag{19}$$

where σ is defined by $\exp(-E_\sigma/RT)$ and $\omega = \exp(-E_\omega/RT)$. E_σ is the energy difference between the *gauche* and *trans* states, and E_ω arises due to the four-bond interaction in the case of GG' or G'G. The probability of the *trans* state (P_T) or the *gauche* state (P_G) is calculated as follows:

$$P_T = 1 - (1/2)(\partial \ln \lambda_{max}/\partial \ln \sigma) \tag{20}$$

$$P_G = 1 - P_T \tag{21}$$

where λ_{max} is the largest eigenvalue of the matrix **T**.

Next, we consider the calculation of the probabilities of the preferred conformations in various configurations in vinyl polymers as a function of the racemic units, f_r. For convenience, the planar conformation in any specified configuration of a vinyl polymer is shown in Fig. 1. Newman

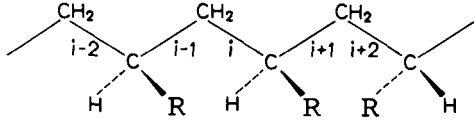

FIG. 1. The planar conformation of any specified configuration of a vinyl polymer.

projections of the rotational isomeric states about the $(i-1)$th bond are given in Fig. 2. The statistical weight matrices for the characterization of the array of chain conformations of vinyl polymers are given by Flory *et al.* (15,

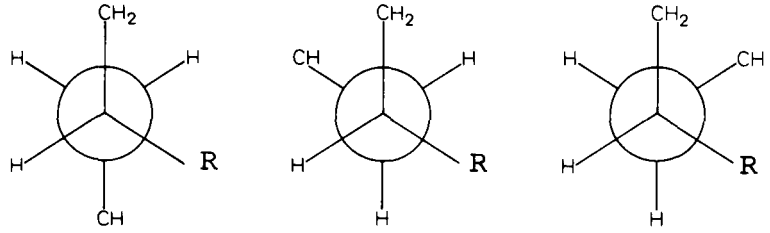

FIG. 2. Newman projections of the rotational isomeric states about the $(i-1)$th bond in Fig. 1; T depicts *trans*, G and G′ the two *gauche* conformations; η, 1, and τ are statistical weight factors.

16) The purpose of calculating the probability that the pairs of skeletal bonds within the kth dyad, the kth triad, and so on in a chain are in particular rotational states is that such statistical weights are used to construct statistical weight matrices $\mathbf{U} = \mathbf{U}'\mathbf{U}''$. In such matrices rows are associated with rotational states about bond $i-1$ and columns with rotational states about bond i. The complete statistical weight matrix for bond pairs meeting at a CHR group in a chain is $\mathbf{U}'$. The statistical weight matrices in the case of pairs of bonds adjoining CHR groups are designated $\mathbf{U}''$. These matrices are expressed as

$$\mathbf{U}' = \begin{pmatrix} \eta & 1 & \tau \\ \eta & \omega & \tau \\ \eta & 1 & \tau\omega \end{pmatrix} \tag{22}$$

for the first skeletal bond of a dyad and

$$\mathbf{U}''_{\mathrm{m}} = \begin{pmatrix} \eta\omega & 1 & \tau\omega \\ \eta & \omega & \tau\omega \\ \eta\omega & \omega & \tau\omega^2 \end{pmatrix} \tag{23}$$

$$\mathbf{U}''_{\mathrm{r}} = \begin{pmatrix} \eta & \omega & \tau\omega \\ \eta\omega & 1 & \tau\omega \\ \eta\omega & \omega & \tau\omega^2 \end{pmatrix} \tag{24}$$

for the second; the former matrix, equation (23), is for a *meso* dyad and the latter for a racemic one. The statistical weight factors 1, η, and τ are defined in Fig. 2. The configuration partition function Z for the entire chain is the sum of the statistical weights for all molecular conformations of the chain consisting of n bonds, or $x = (1/2)n$ repeating units,

$$Z = \mathbf{J}^* \left(\prod_{i/2=1}^{n/2-1} \mathbf{U}'_i \mathbf{U}''_{i+1} \right) \mathbf{J} \tag{25}$$

where $\mathbf{J}^* = (1\ 0\ 0)$ and $\mathbf{J}$ is the transpose of $(1\ 1\ 1)$. Let β and γ denote indices from the set T, G, G'. The probability $P_{\beta\gamma:k''}$ that the pair of skeletal bonds within the kth dyad are in rotational states β and γ respectively is the ratio of the sum of the statistical weights for any conformation meeting this condition to the sum Z of the statistical weights for all conformations. It is given by

$$P_{\beta\gamma:k''} = Z^{-1} \mathbf{J}^* \left(\prod_{h=1}^{k-1} \mathbf{U}'_h \mathbf{U}''_{h+1} \right) (\mathbf{U}'_k \mathbf{U}''_{(\beta\gamma)k}) \left(\prod_{i=k+1}^{x-1} \mathbf{U}'_i \mathbf{U}''_{i+1} \right) \mathbf{J} \tag{26}$$

in which $\mathbf{U}''_{(\beta\gamma)k}$ is the matrix representing the second bond of the kth dyad with all of the elements, except $U''_{\beta\gamma}$, replaced by zero. $P_{\beta\gamma:k''}$ is usually estimated by generating Monte Carlo chains. Then, an averaged chemical shift is obtained for the Monte Carlo chains according to the block diagram shown in Fig. 3.

III. EXPERIMENTAL ASPECTS

In general, the NMR spectra of polymers in solution consist of a number of closely spaced, often partially overlapping, signals. The appearance of microtacticity along the chain together with the time-averaged occurrence of various conformations in solution are characteristics of polymers and become causes of complexity in polymer spectra.

Several kinds of experimental techniques have been applied to simplify polymer spectra and to increase sensitivity. An example is that of polypropylene (PP) which is a typical vinyl polymer. With increasing magnetic

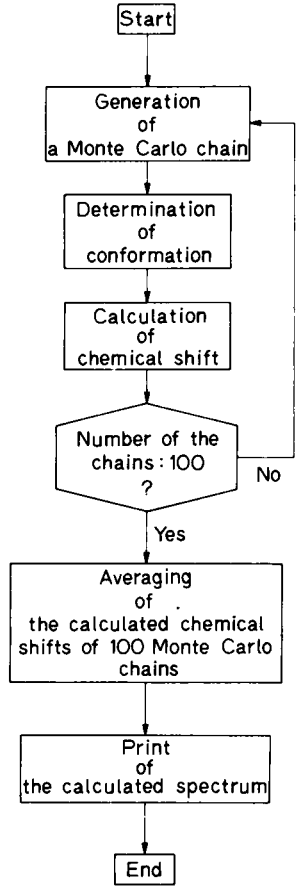

FIG. 3. Block diagram for the calculation of chemical shifts by generating 100 Monte Carlo chains.

field, the chemical shift difference between various nuclei increases while the magnitude of the spin–spin coupling does not change. Therefore spectral simplicity is attained at high magnetic fields. This is made clear by comparing the 60 MHz ^{1}H NMR spectra (17) (Fig. 4) with the 220 MHz ^{1}H NMR spectra (Fig. 5) (18) of isotactic and syndiotactic PP samples. The methine, methylene, and methyl resonances are clearly separated in the 220 MHz spectra, and the difference between these polymers in the resonance positions of each proton corresponds to the microtacticity of these chains. However, when the racemic contents increase in an isotactic sample of PP the spectrum seems to be complex even when using 300 MHz NMR apparatus as shown in Fig. 6. (19)

In deuterated polymers the proton resonances appear as singlets at the chemical shifts corresponding to the various microtacticities since all proton–proton spin coupling is effectively removed by deuteration. Figure 7 shows the 220 MHz ^{1}H NMR spectra of atactic PP-*trans*-1,2,3,3,3-d_5 (a) and atactic PP-*cis*-1,2,3,3,3-d_5 (b). (20) Thus very simple spectra are obtained compared with those from samples without deuteration. The peaks are assigned to the tetrad configurational sequences in the polymer chain.

The advent of PFT techniques with proton decoupling has resulted in a major breakthrough in the feasibility of obtaining ^{13}C natural-abundance NMR spectra on polymers due to a large gain in sensitivity in a given time compared with the continuous-wave (CW) method. The sensitivity of the PFT technique has recently been augmented by the use of high magnetic fields and larger sample tubes. Such a combination of experimental improvements has led to usable ^{13}C natural-abundance spectra from a number of synthetic polymers and biopolymers. As an example, the methyl region of a 25 MHz ^{13}C NMR spectrum of an amorphous PP is shown in Fig. 8. (21) Pentad assignments are made for these peaks by consideration of an additivity relationship among the methyl resonances.

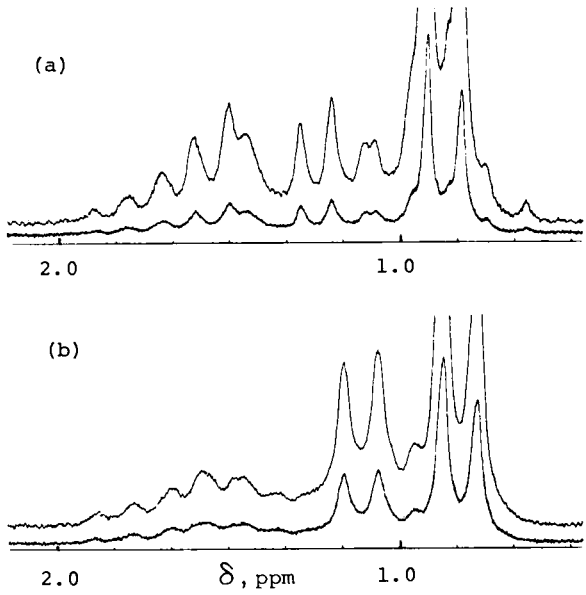

FIG. 4. 60 MHz ^{1}H NMR spectra of (a) isotactic polypropylene (boiling-n-octane-insoluble, boiling-xylene-soluble portion of a $TiCl_3$–$Al(C_2H_5)_3$-catalysed polymer), and (b) highly syndiotactic polypropylene. 8% w/v solutions in *o*-dichlorobenzene at 150 °C. The original chemical shifts were in ppm to high frequency of hexamethyldisiloxane. (17) The ones reported here are converted to the δ scale by adding 0·04 ppm.

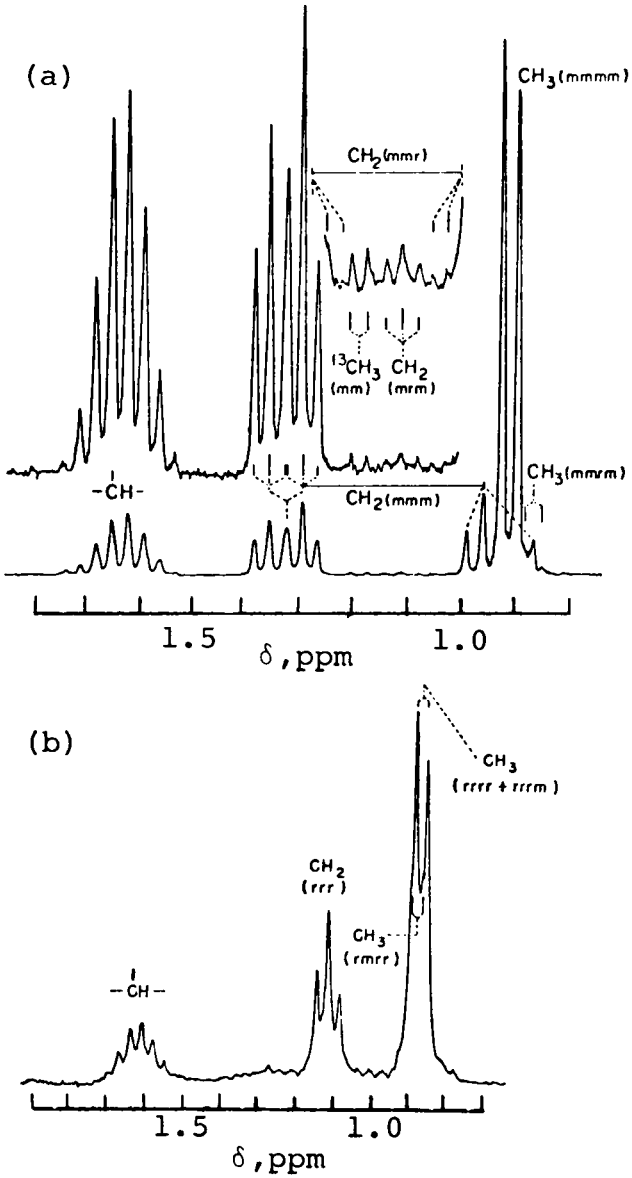

FIG. 5. 220 MHz ^{1}H NMR spectra of (a) isotactic polypropylene (benzene-insoluble residue from exhaustively extracted Hercules Profax polypropylene), and (b) highly syndiotactic polypropylene (sample polymerized at −78 °C in n-hexane, using a 1 : 15 molar ratio of VCl_4 and $Al(C_2H_5)_2Cl$ as catalyst). 10% w/v solutions in *o*-dichlorobenzene at 145 °C. The original chemical shifts were in ppm to high frequency of hexamethyldisiloxane. (18) The ones reported here are converted to the δ scale by adding 0·04 ppm.

A recently developed nuclear double resonance technique which permits sensitive detection, together with high resolution, of rare spins in solids has been applied to the study of natural abundance ^{13}C NMR in synthetic polymers. (22) The spectra of dilute spins (^{13}C) are obtained with enhanced intensity and higher resolution by transferring polarization from abundant spins (^{1}H). This is called the proton-enhancement technique. The experimental data often give the chemical shift anisotropy which provides a rich source of new information on solids. The powder patterns arising from non-equivalent rare spin overlap prevent resolution and interpretation of the individual resonances. It has recently been shown that the powder patterns can be collapsed to sharp lines by spinning the sample about the "magic axis" (54°44′) at a frequency ω which exceeds the anisotropy width. The appearance of the resulting spectrum of the solid, with linewidths generally of the order of 50 Hz, is then comparable to that of the same

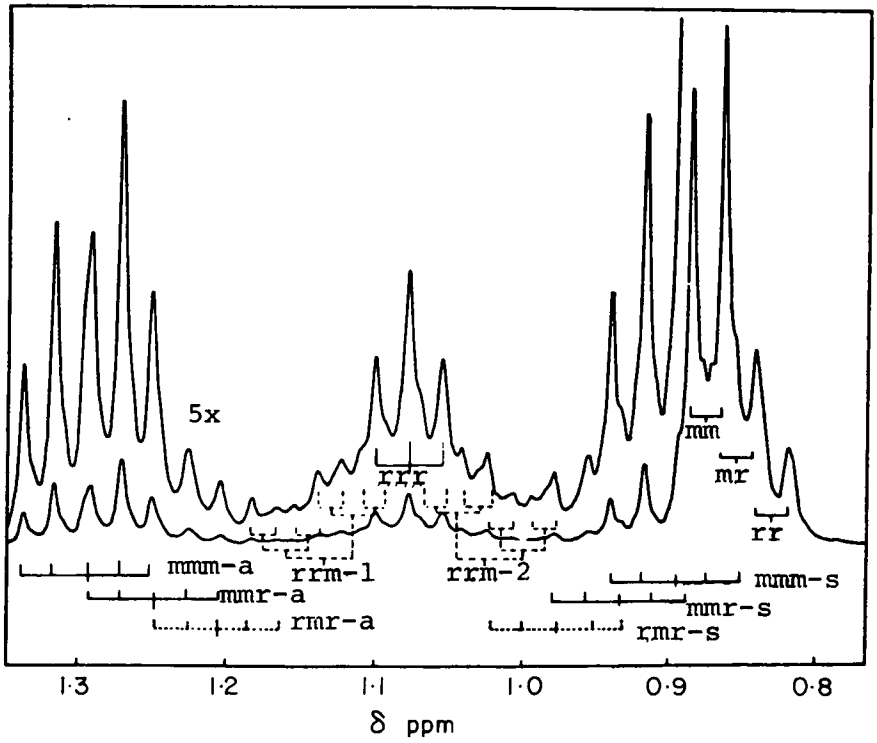

FIG. 6. 300 MHz ^{1}H NMR spectrum of a hexane-insoluble, heptane-soluble fraction from a commercial polypropylene. 5% w/v solution in *o*-dichlorobenzene at 150 °C. The original chemical shifts were in ppm to high frequency of hexamethyldisiloxane. (19) The ones reported here are converted to the δ scale by adding 0·04 ppm.

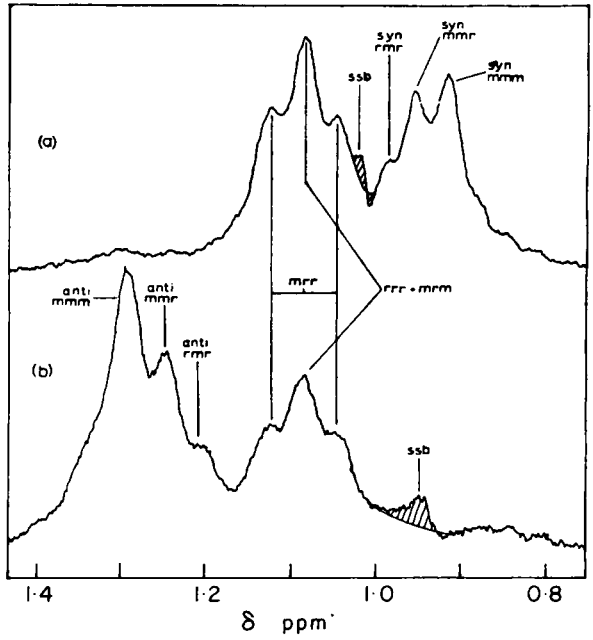

FIG. 7. 220 MHz ^{1}H NMR spectra of (a) atactic polypropylene-*trans*-1,2,3,3,3-d_5, and (b) atactic polypropylene-*cis*-1,2,3,3,3-d_5. 10% w/v solutions in *o*-dichlorobenzene at 145 °C. The original chemical shifts were in ppm to high frequency of hexamethyldisiloxane. (20) The ones reported here are converted to the δ scale by adding 0·04 ppm.

material in some suitable solvent. This is called the magic-angle spinning proton-enhancement technique. (23)

IV. OBSERVATIONS AND CALCULATIONS OF CHEMICAL SHIFTS IN SYNTHETIC POLYMERS

A. Polyethylene and paraffins

Polyethylene (PE) is the most simple and fundamental molecule in polymer chemistry. The unperturbed dimension which gives us information about conformation has been obtained as a function of such fundamental factors as bond length, bond angle, and hindered rotational potential characterizing the molecular chain. The estimation of the energy differences among various rotational isomeric states has been rigorously performed by comparing the experimental results with those calculated in the unperturbed dimension. (15)

The ^{1}H and ^{13}C NMR spectra of PE have a single signal. Thus it is not easy to obtain information about the conformation from these spectra because of

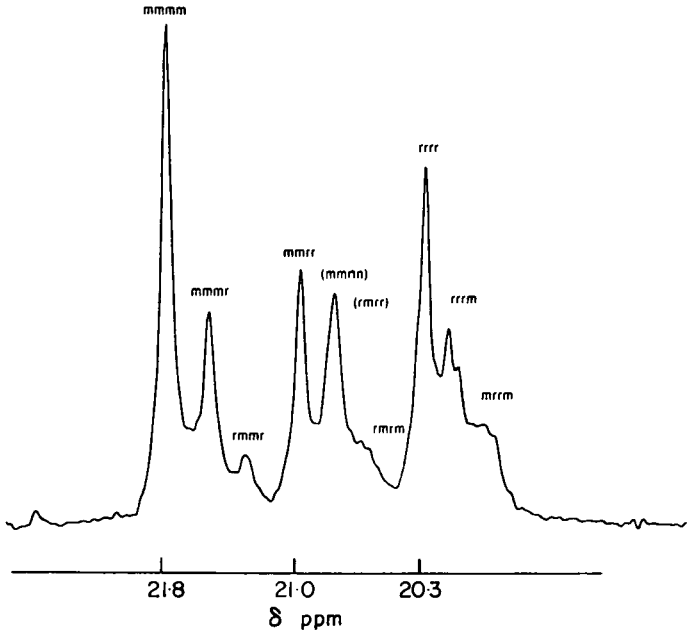

FIG. 8. Methyl region of a 25·2 MHz ^{13}C NMR spectrum of an amorphous polypropylene. (21)

their extreme simplicity. As one approach to this problem Zatta *et al.* (24) have synthesized an isotopically substituted PE by copolymerizing per-deuteroethylene and 1-^{13}C-enriched ethane and have obtained information about the conformation of the C–C bond using the interproton vicinal coupling constants of the CH_2–CH_2 fragment. They have obtained 2900 ± 650 J mol^{-1} as the value of the energy difference E_σ between the *trans* and *gauche* forms.

On the other hand, the temperature dependence of the chemical shift provides in principle sufficient information about the conformation of polymers. According to this suggestion comparison of the experimental and calculated ^1H chemical shifts and shapes of the signals has been carried out for the unbranched paraffin $C_{44}H_{90}$, which is one kind of PE, using equation (1) and 100 Monte Carlo chains. (25) The chemical shift difference between the CH_2 and terminal CH_3 protons, calculated as functions of σ and ω, is shown in Fig. 9, where the value used for $\Delta\chi$ of the C–C bond is $9{\cdot}1 \times 10^{-30}$ cm^3, (26) and σ^{dia} is calculated by the CNDO/2 method. (27)

The theoretical temperature dependence of $\Delta\delta(CH_3$–$CH_2)$ as a function of ω for several values of E_σ is shown in Fig. 10, together with the observed data in CCl_4 solution. It is found that the calculated values of $\Delta\delta(CH_3$–$CH_2)$

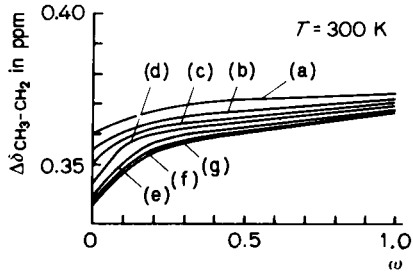

FIG. 9. Calculated values of $\Delta\delta(CH_3–CH_2)$ against ω at 300 K; E_σ(J mol^{-1}) = (a) 836, (b) 1254, (c) 1672, (d) 2090, (e) 2508, (f) 2926, (g) 3344. (25)

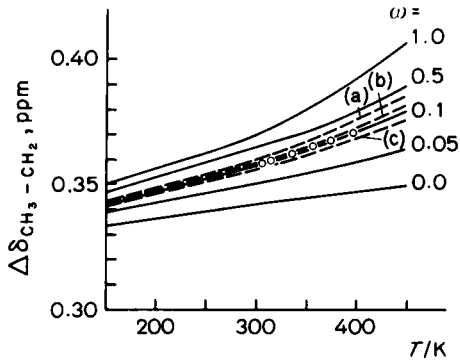

FIG. 10. Temperature dependence of the calculated chemical shift difference $\Delta\delta(CH_3–CH_2)$ as a function of the four-bond interaction ω; solid lines, E_σ = 2090 J mol^{-1}; dashed lines, ω = 0·1; E_σ(J mol^{-1}) = (a) 1672, (b) 1880, (c) 2300; symbols ○ denote experimental data. (25)

increase with increasing temperature for all values of ω; this tendency is consistent with the observed one. The values of E_σ and E_ω required to fit the observed data are found to be 1880–2300 J mol^{-1} and 5270–6275 J mol^{-1} respectively. In these results, the value of E_σ agrees with the spectroscopic value ($E_\sigma = 2100 \pm 420$ J mol^{-1}), (28) and the values predicted from a comparison of the experimental and calculated results on the average dimension and the temperature coefficient (E_σ = 1800–2470 J mol^{-1}; E_ω = 7100–8370 J mol^{-1}). (29) The relationship between $\Delta\delta(CH_3–CH_2)$ and the end-to-end distance of the chain has provided information about the dimension of the chain in solution.

Liu (30) has found that the signal of the CH_2 protons of linear paraffins in α-chloronaphthalene (α-ClNap) begins to split into two peaks if the number of carbon atoms present is more than 18. He has suggested the possibility of a chain-folding mechanism in relation to such splitting. This suggestion may be a working hypothesis at present but it is reasonable to consider that the

phenomenon may not be interpreted by a completely random conformation of the molecule, and may be related to some peculiar conformations of the chains in solution.

Calculations of the proton chemical shifts of the CH_2 and terminal CH_3 protons comprising the chain of some paraffins have been performed by a similar method in the case of n-$C_{44}H_{90}$. (31) Contrary to the single peak obtained by averaging the chemical shifts of specified CH_2 protons for 100 Monte Carlo chains, double peaks are interpreted by plotting the distribution of the chemical shifts of the CH_2 protons without averaging them. A comparison of the observed and calculated chemical shift differences $\Delta\delta(CH_3–CH_2)$ between the CH_3 and CH_2 protons in some unbranched paraffins is given in Table I.

TABLE I

Comparison of the observed and calculated chemical shift differences $\Delta\delta(CH_3–CH_2)$ between CH_3 and CH_2 protons in some unbranched hydrocarbons

	$\Delta\delta(CH_3–CH_2)$ (ppm)											
	C_9H_{20}		$C_{16}H_{34}$		$C_{22}H_{46}$				$C_{30}H_{62}$			
					I[a]		II[b]		I[a]		II[b]	
T (°C)	obs.	calc.	obs.	calc.	obs.	calc.	obs.	calc.	obs.	calc.	obs.	calc.
22	0·26	0·30	0·28	0·32	0·29	0·28	0·34	0·36	0·30	0·30	0·37	0·38
80	—	—	—	—	0·34	0·28	0·38	0·36	—	—	—	—
120	0·33	0·34	0·36	0·34	—	—	0·41	0·38	—	—	0·42	0·50

[a] I, low frequency peak. [b] II, high frequency peak.

Campa *et al.* (32) have synthesized some n-paraffins with a terminal *N*-maleimide ring in order to hinder the internal motions of the n-paraffin chain and to decrease the rate of exchange amongst various conformations. They have obtained double peaks for the CH_2 signal when $n \geq 10$, even in benzene. These phenomena are explained by the above-mentioned consideration. (31)

More recently, Matsumoto *et al.* (33) have indicated that the collapse of the doublet CH_2 signal, with increasing temperature, can be explained by considering the exchange of CH_2 protons which appear at different chemical shift positions.

A recently developed proton-enhanced NMR technique has been applied to the study of natural abundance ^{13}C in amorphous linear PE at room temperature. (22) The spectrum has a non-axially symmetrical pattern with the following eigenvalues: $\sigma_{11} = 78{\cdot}3$, $\sigma_{22} = 92{\cdot}0$, and $\sigma_{33} = 115{\cdot}9$ ppm to low frequency of external $^{13}C_6H_6$. From these values the chemical shift

anisotropy, $\Delta\sigma = \sigma_{33} - (\sigma_{11} + \sigma_{22})/2$, is obtained to be 30·75 ppm. VanderHart (34) has measured the CH_2 carbon chemical shift tensors in a single crystal of n-$C_{20}H_{42}$ using the same technique. He reports the following data: $\sigma_{11} = 142{\cdot}6 \pm 2{\cdot}0$, $\sigma_{22} = 154{\cdot}6 \pm 2{\cdot}0$, and $\sigma_{33} = 175{\cdot}6 \pm 2{\cdot}0$ ppm to low frequency of external $^{13}CS_2$. Thus $\Delta\sigma = 27{\cdot}3 \pm 2{\cdot}0$ ppm. This value is near to that in amorphous PE.

The calculated principal values (35) of the paramagnetic contribution to the screening of the central CH_2 carbon of the *trans* zigzag n-$C_{15}H_{32}$ chain, using the sum-over-states theory with the MINDO/2 method, (36) have been reported to be $\sigma^P_{xx} = -179$, $\sigma^P_{yy} = -157$, and $\sigma^P_{zz} = -195$ ppm, where the x-axis is along the long molecular axis, the y-axis is along the bisector of the C–C–C angle, and the z-axis is perpendicular to the plane containing C–C–C. The value $\Delta\sigma$ is about 30 ppm and agrees with the observed values for amorphous PE and n-$C_{20}H_{42}$.

The observation of ^{13}C–^{13}C dipolar satellites at natural abundance in highly oriented PE has been shown to be useful for assigning the chemical shift tensor orientation. (34)

A given PE sample may have short or long branches in its chain. The ^{13}C NMR spectrum of PE can be used to identify the short branches using the Grant and Paul relationship. (11) From a comparison of the observed spectrum and the calculated stick spectrum of PE with short branches using the Grant and Paul relationship or that of Lindeman and Adams (12) the assignment of peaks due to short branches may be carried out and their amount in a given PE sample has been estimated by many research groups. Randall has improved on the Grant and Paul parameters, as applied to polymers, and has noted that the correction term is temperature-sensitive. (37)

B. Poly(vinyl chloride)

^1H and ^{13}C NMR spectroscopies have been widely applied to the study of the distribution of stereochemical configurations in vinyl polymers. Poly(vinyl chloride) (PVC) is one of the typical vinyl polymers in which monomer-placement assignments (dyad, triad, tetrad, etc.) are generally made.

1. ^1H NMR studies

The ^1H spectrum of PVC consists of two regions which correspond to the CH_2 and CH signals. The former appears to low frequency of the latter. Splitting due to spin coupling and various stereochemical configurations appears in each of the signals. The analysis of the stereochemical configurations has been carried out by means of high-field NMR, the decoupling technique, the use of deuterated samples, and computer-calculated spectra.

(2d, 38, 39, 96) The spectrum is interpreted in terms of pentads for the CH proton and tetrads for the CH_2 protons. The observed stick spectra of dyads and triads in chlorobenzene and in pentachloroethane are shown in Fig. 11.

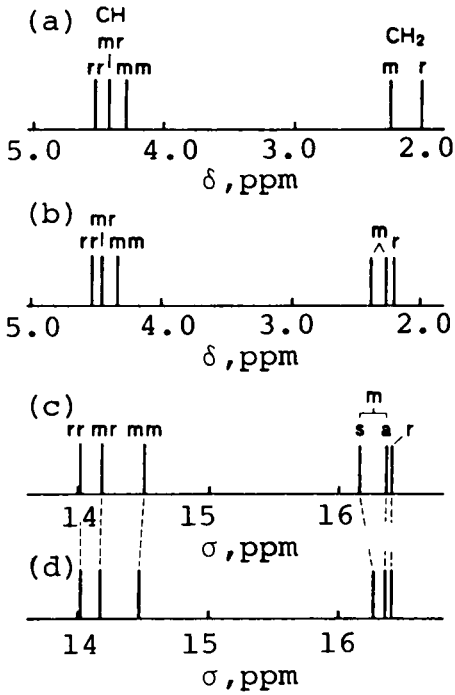

FIG. 11. Calculated and observed stick spectra of dyads and triads in poly(vinyl chloride). (a) Observed in 15% w/v solution in chlorobenzene at 150 °C and 60 MHz. (39) (b) Derived from the chemical shifts of tetrads and pentads respectively, observed in 5% w/v solution in pentachloroethane at 140 °C and 220 MHz. (38) (c) Calculated screening for fraction of racemic unit $f_r = 0{\cdot}5$ and statistical weight factors $\omega = \omega' = \omega'' = 0$. (d) Calculated screening for $f_r = 0{\cdot}5$ and statistical weight factors $\omega = \omega'' = 0{\cdot}032$ and $\omega' = 0{\cdot}071$. (40)

The observed stick spectra of tetrads in *o*-dichlorobenzene and pentachloroethane at 220 MHz are shown in Fig. 12. In the case of tetrads the order of the chemical shifts is different.

Calculation of the chemical shifts of dyads, triads, and tetrads provides an explanation of the observed spectrum and information about the sample's conformation. (40) As the first procedure, the chemical shifts for the preferred conformations are calculated for 2,4-dichloropentane, 2,4,6-trichloroheptane, and 2,4,6,8-tetrachlorononane, as models for the dyad, triad, and tetrad configurations respectively, as a sum of σ_A^{dia}, σ_A^{aniso}, and σ_A^{E},

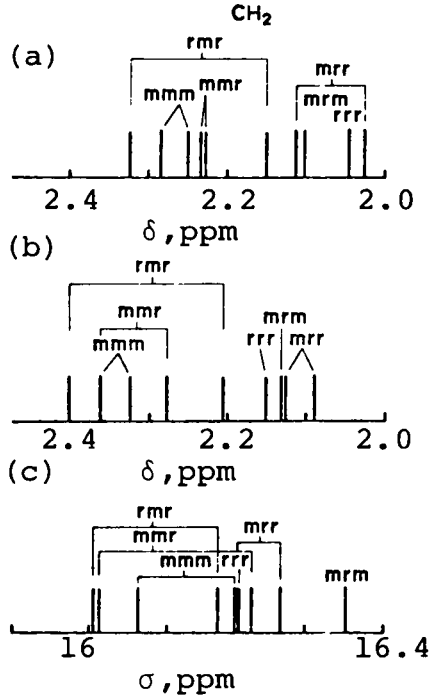

FIG. 12. Calculated and observed stick spectra of tetrads in poly(vinyl chloride). (a) Observed in 5% w/v solution in *o*-dichlorobenzene at 140 °C and 220 MHz. (38) (b) Observed in 5% w/v solution in pentachloroethane at 140 °C and 220 MHz. (38) (c) Calculated screening for $f_r = 0{\cdot}5$ and statistical weight factors $\omega = \omega' = \omega'' = 0$. (40)

where σ_A^{dia} is calculated using equation (5) with the CNDO/2 method. In the calculation of σ_A^{aniso}, the values $9{\cdot}1 \times 10^{-30}$ cm^3 and $5{\cdot}0 \times 10^{-30}$ cm^3 are used for $\Delta\chi$(C–C) and $\Delta\chi$(C–Cl) respectively. (41) The electric field necessary for the estimation of σ_A^E is evaluated using the distribution of electron density calculated by the CNDO/2 method. The probabilities of the preferred conformations are estimated as a function of the fraction of racemic units, f_r, using Monte Carlo chains. The statistical weight factors for this polymer have been reported from the analysis of the stereochemical equilibrium composition of 2,4-dichloropentane by Flory and Williams (42) using $\eta = 4{\cdot}2$, $\tau = 0{\cdot}5$, $\omega = \omega'' = 0{\cdot}032$, and $\omega' = 0{\cdot}071$. Here, the factor ω is introduced for conformations engendering interactions between a pair of CH_2 or CH groups, the factor ω' is associated with second-order interactions between a CH_2 group and a Cl atom, and the factor ω'' accounts for the interaction between Cl atoms. As for the four-bond interaction, two cases are considered: Case A, $\omega = \omega' = \omega'' = 0{\cdot}0$; Case B, $\omega = \omega'' = 0{\cdot}032$ and $\omega' = 0{\cdot}071$. In this way the averaged chemical shifts of dyads, triads, and

tetrads are calculated as shown in Figs. 11 and 12. The calculated order of chemical shifts for the CH_2 protons in the m and r dyads agrees with that observed. The two peaks of the CH_2 protons in the m dyad are assigned to the *anti* and *syn* protons respectively when moving to higher frequencies, which is consistent with the observed results. As for the triads, the calculated chemical shifts appear in the order mm, mr, and rr, corresponding to a decrease in nuclear screening in agreement with the experimental results. As for tetrads, there are some discrepancies between the calculated and experimentally assigned results, especially for mrm tetrads. This may be due to solvent effects. The calculated chemical shifts depend upon f_r; the dependence for tetrads is larger than that for dyads and triads. The chemical shift difference between the m and r dyads is found to decrease with increasing temperature. (43) The calculation of chemical shifts for Case A indicates no temperature dependence but for Case B a temperature dependence is implied. In the latter calculation the chemical shift difference decreases linearly with increasing temperature which agrees with the observed temperature dependence. It is suggested that the statistical weight for the four-bond interaction is very small but significant in understanding the behaviour of the temperature dependence of the chemical shifts.

2. ^{13}C *NMR studies*

The ^{13}C NMR spectrum of PVC allows peak area measurement of its stereochemical configurations with better resolution. (44) The three distinct CH carbon resonances are assigned to triad configurations for which the line order from high to low frequency is rr, mr, mm. The CH_2 carbon resonances are assigned to tetrad configurations. Carman *et al.* (45) have reported well resolved FT NMR spectra of the CH_2 groups which can be assigned to tetrad configurations. These are slightly different from those suggested by Inoue *et al.* (46) as shown in Fig. 13. The partial discrepancy between them may be ascribed to solvent effects since the CH_2 tetrad signal becomes three peaks in a mixture of *o*-dichlorobenzene and DMSO. The tetrad signal may be interpreted as shown in Fig. 14. (47) The averaged ^{13}C chemical shifts of triad and tetrad configurations have been calculated with CNDO/2 parameters as a function of f_r. The calculations of the preferred conformations were performed using 2,4,6-trichloroheptane and 2,4,6,8-tetrachlorononane as model compounds for the triad and tetrad configurations respectively. The nuclear screening is given as the sum of σ_A^{dia} and σ_A^{para} estimated within the ΔE approximation. The probabilities of the preferred conformations were obtained by generating 100 Monte Carlo chains. The calculated ^{13}C spectrum of the CH and CH_2 carbons is shown in Fig. 15.

The CH_2 carbon is predicted to appear to low frequency of the CH carbon, which agrees with the observed results. Quantitatively the calculated

chemical shift difference between the CH_2 and CH carbons is smaller than that observed. For the CH carbon, the calculated results for the triads are in the order mm, mr, rr with increasing frequency, which agrees with the Inoue and the Carman assignments. However, the calculated results for tetrads are in the order mmm, mmr, mrm, rmr, mrr, rrr with increasing frequency. This ordering suggests a low frequency movement of the mean tetrad chemical shift when neighbouring r dyads are replaced by m. This order agrees with the Inoue assignment, but the order of mrr and rmr is opposite to the Carman assignment. In this calculation solvent effects are not taken into account, thus the assignment is not conclusive. However, both assignments can be understood by assuming that the chemical shift difference between the m- and r-centres depends upon the nature of the solvent, the difference in the case of DMSO being somewhat larger than that for *o*-dichlorobenzene as shown in Fig. 15. When a mixture of *o*-dichlorobenzene and DMSO (volume ratio 2 : 1) is used as solvent the CH_2 signal pattern is considerably different from the above two cases as shown by Chatani. (48) This may be also interpreted by assuming that the shifts for the m- and r-centred tetrads

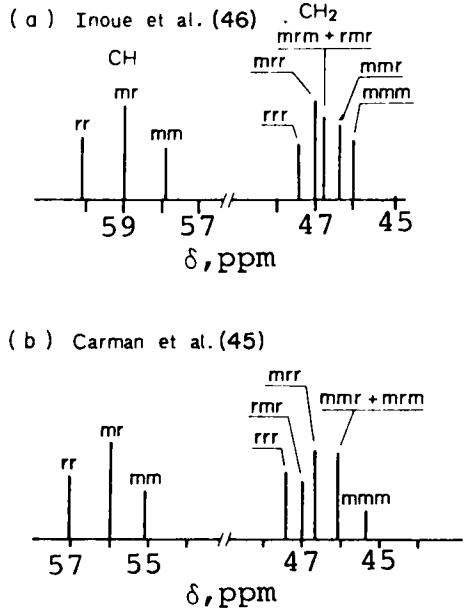

FIG. 13. Inoue's (46) (a) and Carman's (45) (b) assignments for the CH_2 and $CH^{13}C$ NMR signals in poly(vinyl chloride). (c) Observed at 25 MHz in 20% w/v solution in DMSO at 70 °C. The original chemical shifts were measured relative to methanol and are converted to the δ scale by adding 49·3 ppm. (b) Observed at 25 MHz in 10% w/v solution in *o*-dichlorobenzene at 100 °C.

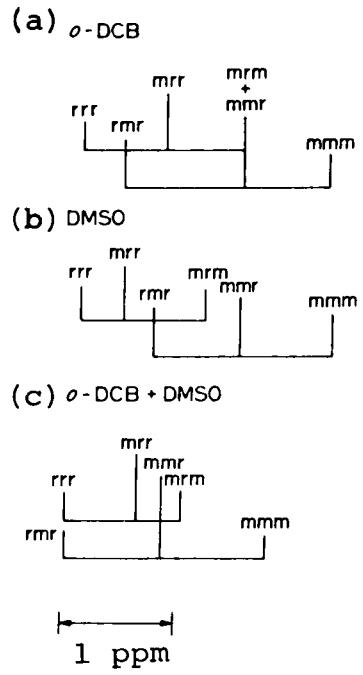

FIG. 14. Overlapping of the tetrads in the ^{13}C NMR spectra of poly(vinyl chloride) in various solvents: (a) *o*-dichlorobenzene; (b) DMSO; (c) mixture of *o*-dichlorobenzene and DMSO (volume ratio 2 : 1). (40)

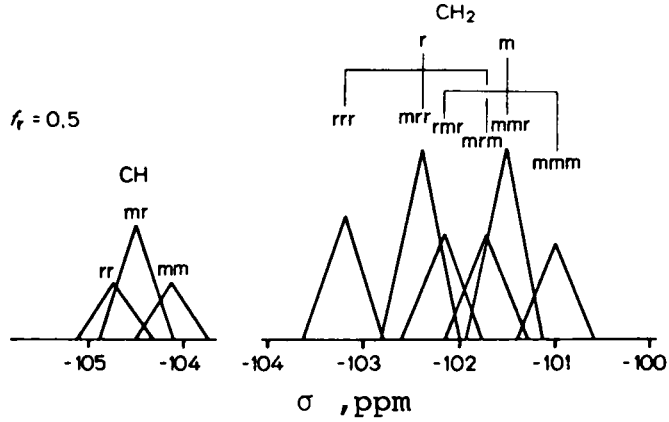

FIG. 15. Calculated ^{13}C screenings of the CH and CH_2 carbons in poly(vinyl chloride). The half-height width for all the configurations is assumed to be equal (10 Hz at 25 MHz); each peak is taken to be a triangle and the distribution of stereoregularity in a chain is considered to obey Bernoullian statistics ($f_r = 0{\cdot}5$). (40)

overlap with each other. Therefore, the behaviour of the chemical shifts in the three solvent systems may be reasonably interpreted using this scheme.

As described above, the solvent dependence for the triad splitting of the CH carbon is negligible while that for the tetrad CH_2 carbon is large. In order to complete the interpretation of the chemical shift in various solvents the nature of the solvent effect must be understood. For this purpose the chemical shifts of *meso* and racemic 2,4-dichloropentanes (DCP) were measured in various types of solvents covering a wide range of dielectric constants. (49) The observed chemical shifts in various solvents are plotted as a function of $(\varepsilon-1)/2\varepsilon$ in Fig. 16 (ε = dielectric constant). The CH carbons in *meso* and racemic DCP shift to high frequency with a constant separation, with increasing $(\varepsilon-1)/2\varepsilon$. On the other hand, the CH_3 carbons shift slightly to low frequency and the separation increases slightly with increasing $(\varepsilon-1)/2\varepsilon$. For the *meso* and racemic CH_2 carbons the order is reversed in DMSO solution, being different from the order in other solvents.

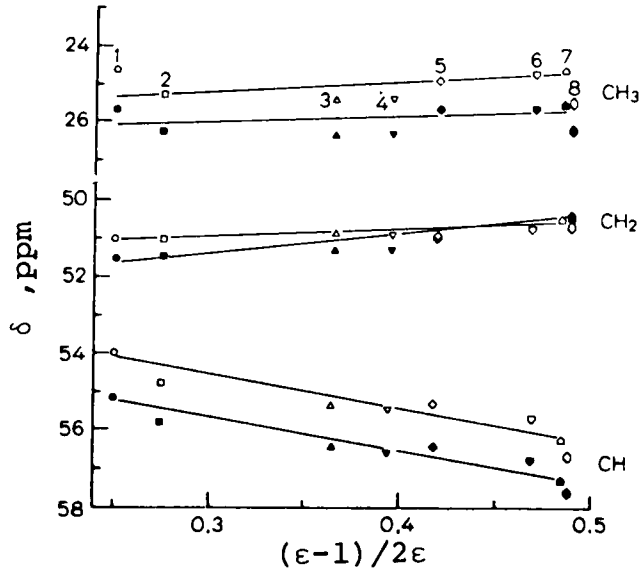

FIG. 16. Dependence on dielectric constant, ε, of the observed ^{13}C NMR chemical shifts, δ, of the CH_3, CH_2, and CH carbons in *meso* (open symbols) and racemic 2,4-dichloropentanes (filled symbols). Solvents: 1, cyclohexane; 2, CCl_4; 3, $CHCl_2CCl_3$; 4, $CDCl_3$; 5, acetic acid; 6, acetone; 7, nitromethane; 8, DMSO (external reference, TMS). The *meso* and racemic CH_2 carbon signals in solvents 6 and 7 overlap each other. (49)

This observation corresponds to that in PVC where the position of the CH_2 carbon signals depends considerably upon the solvent, while that of the CH carbon signals does not.

It is interesting to handle solvent effects theoretically. For this purpose the solvaton theory can be applied. (50–52) In this theory, it is assumed that (i) upon addition of a solute at infinite dilution to an aprotic solvent of dielectric constant ε, a number of charges (called the solvatons) are induced in the solvent, (ii) one solvaton is associated with each atom of the solute and its charge is equal in magnitude but opposite in sign to the net charge on the atom.

The averaged chemical shifts of *meso* and racemic DCP have been calculated as a function of ε by using a sum of σ_A^{dia} and σ_A^{para} obtained by incorporating the solvaton theory with CNDO/2 calculations as shown in Fig. 17. The value of σ_A^{para} is obtained from equation (10). As for the CH_2 carbon, the plotted lines of the chemical shifts of the *meso* and racemic DCP are found to cross in the proximity of $(\varepsilon - 1)/2\varepsilon = 0{\cdot}45$, and therefore in

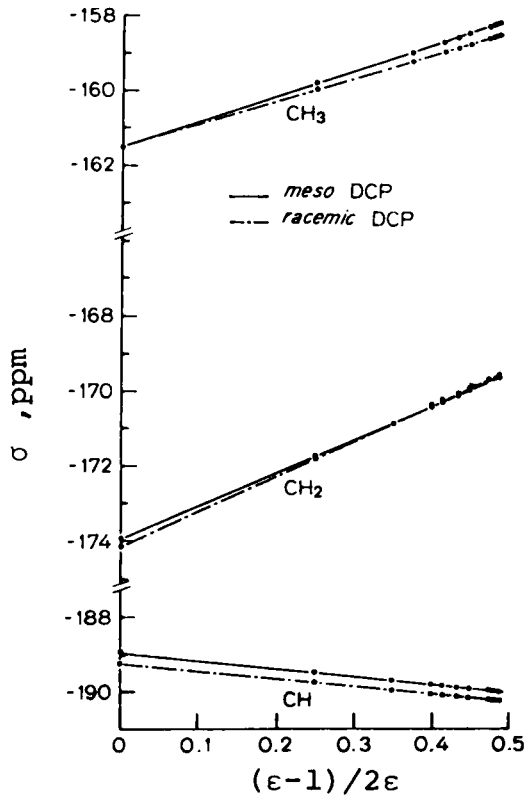

FIG. 17. Dependence on dielectric constant, ε, of the calculated chemical shieldings, σ, for *meso* (—) and racemic 2,4-dichloropentanes (– · – ·) averaged over the preferred conformations. (49)

DMSO solution the reversal of the observed chemical shifts in *meso* and racemic DCP may be understood. As for the CH carbon, both plotted lines are found to be parallel, but as in the case of the CH_3 carbon the separation between the lines seems to decrease slightly with increasing magnitude of $(\varepsilon - 1)/2\varepsilon$. These results agree with those observed, although not quantitatively.

The temperature dependence of the chemical shifts in both model compounds is discussed on the basis of the solvaton theory using the following relationship: (53)

$$(\varepsilon + 1)T \propto \text{constant} \tag{27}$$

where T is the temperature. The calculated values of the CH_3 and CH_2 carbon signals shift to high frequency with increasing temperature, and the position of the CH carbon signal becomes independent of temperature. The temperature dependence of the CH_2 carbon is larger than that of the other carbons and the separation between the *meso* and racemic CH_2 signals decreases with increasing temperature. These tendencies agree with those observed. The trend described above demonstrates the potential application of the solvaton theory to aprotic solvent effects.

C. Polypropylene

Numerous studies of the stereochemical structures of polypropylene (PP) have been made using ^1H NMR (18–20, 54–65) and, more recently, ^{13}C NMR. (2i, 21, 66–77)

The ^1H NMR spectra of PP are complicated because the CH_3 protons couple strongly to the CH protons and the chemical shift differences among the CH, CH_2, and CH_3 protons are relatively small. Therefore, the use of deuterated PP samples is very effective since all proton–proton spin coupling is removed by deuteration. Heatley and Zambelli (20) have reported a tetrad assignment for the CH_2 peak of the 220 MHz ^1H NMR spectra of atactic PP prepared from *cis*- and *trans*-1,2,3,3,3-d_5 monomers as shown in Fig. 7. Although these spectra are relatively simple the assignment of the mrm tetrad peak is the subject of some controversy. This assignment is closely connected with the estimation of the amounts of the isolated racemic units contained in a highly isotactic PP. Heatley and Zambelli (20) assumed the mrm tetrad to have the same chemical shift as the rrr tetrad on the basis of intensity measurements and statistical relationships among sequence probabilities. (63) Moreover, they have reported the 220 MHz ^1H spectrum for a highly isotactic PP prepared with a $TiCl_3$–$Al(C_2H_5)_2Cl$ catalyst. In the spectrum the triplet centred on $\delta = 1{\cdot}16$ ppm is assigned to the mrm tetrad because it appears at the same position as the line assigned to this tetrad in the atactic polymers-d_5 and there should not be any observable syndiotactic

sequences of three or more dyads in length in such highly isotactic polymers. Consequently, Heatley *et al.* concluded that the racemic dyad content of this polymer is only about 2% from the measurement of the peak intensities of the tetrads.

Flory *et al.* (29, 78–81) have claimed that the typical isotactic polymer chains are stereoirregular to an appreciable degree. Namely, the observed characteristic ratio (end-to-end distance of the chain) for the so-called isotactic polymer is considerably smaller than the theoretical value estimated for a perfect stereoregular structure. Therefore the presence of 5–10% of stereoirregular units is required to obtain good agreement between the calculated and observed results.

Since the average incidences of various conformations for an mrm tetrad sequence must depart markedly from those for the rrr tetrad sequence these tetrad peaks are expected to resonate at considerably different positions from each other. Nevertheless the mrm tetrad is assigned to the same chemical shift as that of rrr by Heatley and Zambelli.

The recent conclusion, obtained following a ^{13}C NMR study (19, 70, 71) of the mechanism for the generation of racemic placements in a highly isotactic PP, is inconsistent with the conclusion obtained using ^{1}H NMR by Heatley *et al.* (63)

In order to examine these problems in detail, Flory and Fujiwara (82) have calculated the expected chemical shifts of the tetrad CH_2 protons of PP and compared these with the experimental data. Although their calculation is semi-empirical, quantitative agreement between the tetrad assignment by Heatley and Zambelli (20, 62) and that calculated by Flory and Fujiwara is obtained with the exception of the mrm tetrad. In this calculation, the probabilities of the occurrence of the preferred conformation are calculated by the statistical weight matrix method. (15, 16) It is assumed that the magnetic shielding effect of *o*-dichlorobenzene, which is usually used as a NMR solvent for PP, is much larger than the intramolecular shielding effect of the polymer chain. Attention is concentrated on the occurrence of the specified conformations that preclude magnetic shielding by solvent molecules through juxtaposition of the CHR group of an adjoining dyad to the proton of the CH_2 group. The chemical shifts of the CH_2 protons in the *meso* and racemic dyads are calculated as follows.

For the respective CH_2 protons of a *meso* dyad,

$$\Delta\nu_{m:a} = \nu_0 + (P'_{gt} + P'''_{tg})\delta\nu_a \tag{28}$$

$$\Delta\nu_{m:b} = \nu_0 + (P'_{gt} + P'''_{tg})\delta\nu_b \tag{29}$$

and for the protons of a racemic dyad,

$$\Delta\nu_{r:1} = \nu_0 + P'_{gt}\delta\nu_a + P'''_{tg}\delta\nu_b \tag{30}$$

$$\Delta\nu_{r:2} = \nu_0 + P'_{gt}\delta\nu_b + P'''_{tg}\delta\nu_a \tag{31}$$

The subscripts 1 and 2 distinguish the two protons of the racemic dyad.

As for the equivalent protons of a racemic dyad, $P'_{gt} = P'''_{tg}$

$$\Delta\nu_r = \nu_0 + P'_{gt}(\delta\nu_a + \delta\nu_b) \tag{32}$$

where ν_0 is the chemical shift for a proton which occurs in situations where it is not subject to consequences arising from the proximity of a CHR group. $\delta\nu_a$ is the chemical shift relative to ν_0 for an *anti* proton in the *meso* dyad and $\delta\nu_b$ is the chemical shift relative to ν_0 for a *syn* proton of the specified conformation that precludes magnetic shielding effects by solvents through the juxtaposition of the CHR group of an adjoining dyad to the proton of the CH_2 group in question. On the basis of the Zambelli and Segre experiment (62) for the stereoregular PP, Flory and Fujiwara have determined that $\nu_0 = 95{\cdot}6$ Hz, $\delta\nu_a = 37{\cdot}1$ Hz, and $\delta\nu_b = -14{\cdot}9$ Hz. The probabilities of the gt conformation, P'_{gt}, for the pair of main-chain bonds preceding the CH_2 group, and similarly, of the tg conformation, P'''_{tg}, for the following bond pair are calculated by generating the Monte Carlo chains according to the statistical weight matrix method, where $\eta = 1{\cdot}0$, $\tau = 0{\cdot}5$, $\omega = 0{\cdot}04$, and $f_r = 0{\cdot}5$. The calculated chemical shifts for the atactic PP are shown in Table II (82) together with the observed results. (62) On the basis of the calculation, Flory and Fujiwara (82) pointed out that the mrm tetrad resonance

TABLE II

Comparison of the calculated (82) line positions and abundances of the tetrad methylene protons of atactic polypropylene with the experimental results (62)

Tetrad; proton	δ(calc.)[a]	δ(obs.)[a]	Relative abundance Calc.	Obs.
mmm; a	119·8	123·3	0·29	0·24
mmr; a	115·3	118·4	0·22	0·21
rmr; a	108·4	113·6	0·04	0·10
rrm; 1	109·9	106·3	0·15	0·14
mrm	109·4			
rrr	101·8	101·7	0·20	0·19
rrm; 2	98·1	97·6	0·10	0·12
rmr; b	90·5	91·5	0·04	0·11
mmr; b	87·7	88·6	0·22	0·21
mmm; b	85·9	84·4	0·29	0·23

[a] NMR frequency shifts at 100 MHz in Hz.

is expected to occur in the vicinity of those for the rmr *anti-meso* CH_2 proton and the high frequency heterosteric protons of the mrr tetrads. In particular, the two peaks attributable exclusively to the heterosteric protons of mrr tetrads are expected to be of equal intensity. However, the high frequency peak is more intense in the observed spectrum. (20) Therefore, the unequal intensities of the peaks offer direct evidence as to which mrm resonance differs markedly from the rrr resonance and shifts to high frequency. Thus the assignment for the mrm tetrad by Flory and Fujiwara is different from the Heatley and Zambelli assignment. (20, 62–64)

Asakura *et al.* (83) have calculated the ^1H chemical shifts of dyad, triad, and tetrad protons in an isolated PP chain by combining the statistical weight matrix method (16) and equation (1). The chemical shift of the preferred conformation is calculated as a sum of σ_A^{dia} and σ_A^{aniso}, where σ_A^{dia} is estimated by using equation (5) with the CNDO/2 method and σ_A^{aniso} is estimated by using equation (14) together with the magnetic anisotropies of the CH–CH_2 and CH–CH_3 bonds. The probabilities of the preferred conformations are calculated by generating the Monte Carlo chain by the statistical weight matrix method ($\eta = 1{\cdot}0$, $\tau = 0{\cdot}5$, and $\omega = 0{\cdot}0$ or $0{\cdot}1$). The stick spectra calculated for several sets of appropriate values of $\Delta\psi$, a, and $\Delta\chi$(C–C) are shown in Fig. 18 together with the observed spectrum by Stehling. (57) The parameter $\Delta\psi$ is the deviation for the rotational angle from T (0°), G (120°) and G′ (−120°), and the parameter a is the ratio of the magnetic anisotropies of the CH–CH_3 and the CH–CH_2 bonds. The calculation reproduces the observed order for each peak of dyad and triad qualitatively. However, the agreement between the calculated and observed tetrad spectra is poor. This may come from the crudeness of some of the approximations used in the chemical shift calculations, especially the neglect of conformations that contain E_ω interactions even if the individual probability of these conformations is relatively very small. About 0·1 has been reported for the magnitude of ω by many investigators (84–88) and the chemical shift difference between the *syn* and *anti* protons in the PP chain is very large for such conformations.

Recently, ^{13}C NMR has been successfully applied to estimates of the stereoregularity of various kinds of PP samples and to discussions of the mechanism for the generation of racemic placements in a highly isotactic PP. (2i, 21, 66, 67)

It is expected that useful information on the polymerization mechanism can be drawn from a comparison of the observed ^{13}C NMR peaks, due to the chemical inversion in the PP chain, with the corresponding peak position predicted using the Grant and Paul (11) relationship or the Lindeman and Adams relationship. (12) Asakura *et al.* (75) have observed several new peaks in the ^{13}C NMR spectrum of PP prepared with a VCl_4–$Al(C_2H_5)_2Cl$ catalyst as shown in Fig. 19. These peaks do not appear in the ^{13}C NMR

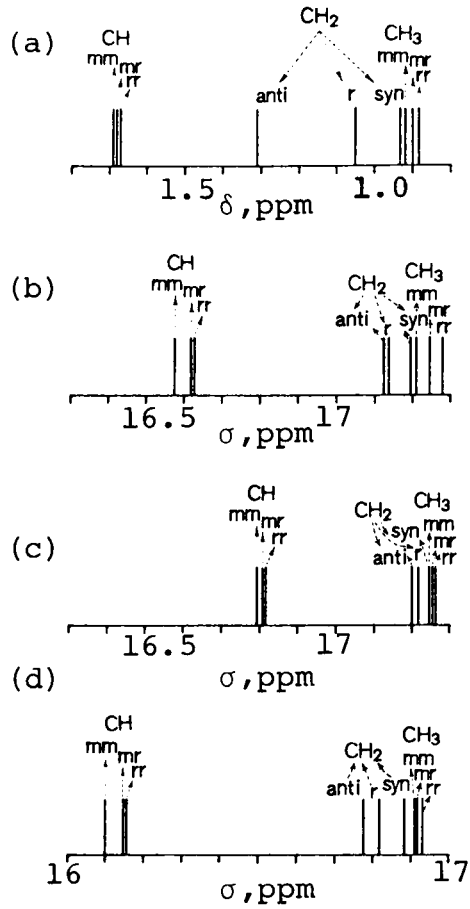

FIG. 18. Observed and calculated stick spectra of dyad and triad protons in polypropylene (σ^T is the sum of the chemical shifts arising from the anisotropic and diamagnetic terms: $\sigma^T = \sigma_A^{dia} + \sigma_A^{aniso}$). (a) Observed in 10% w/v solution in *p*-dichlorobenzene at 175 °C (60 MHz). (57) (b) Calculated screening for $f_r = 0{\cdot}5$; 4-bond interaction parameter $\omega = 0$; deviation of rotational angle $\Delta\psi = 0°$; $a = 1{\cdot}25$; magnetic anisotropy of C–C bond, $\Delta\chi(\text{C–C}) = 9{\cdot}1 \times 10^{-30}\,\text{cm}^3$. (c) Calculated screening for $f_r = 0{\cdot}5$; $\omega = 0$; $\Delta\psi = 20°$; $a = 1{\cdot}10$; $\Delta\psi(\text{C–C}) = 9{\cdot}1 \times 10^{-30}\,\text{cm}^3$. (d) Calculated screening for $f_r = 0{\cdot}5$; $\omega = 0$; $\Delta\psi = 20°$; $a = 1{\cdot}14$; $\Delta\chi(\text{C–C}) = 14 \times 10^{-30}\,\text{cm}^3$. (83)

spectra of PP reported previously (2i, 21, 66–74) and are assigned to the ^{13}C NMR nuclei located near the chemical inversion units such as an isolated head-to-head or tail-to-tail unit on the basis of the predicted peak positions of the ^{13}C nuclei in the possible sequences which contain the chemical inversion using the Lindeman and Adams relationship. From this result it is

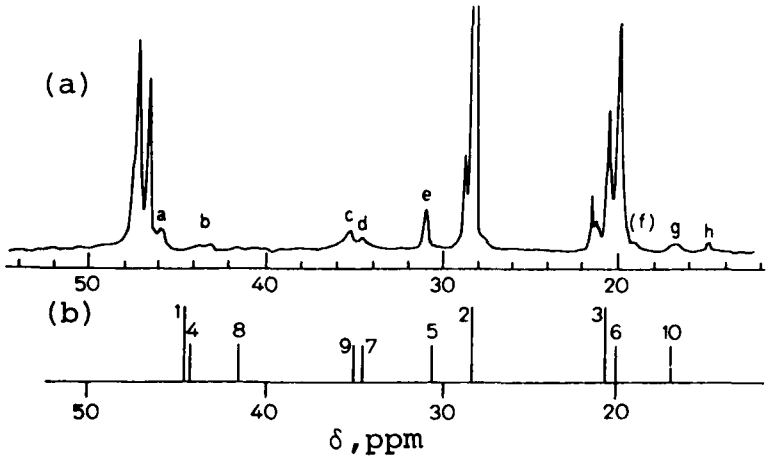

FIG. 19. (a) Observed ^{13}C NMR spectrum of a polypropylene sample polymerized with a VCl_4–$Al(C_2H_5)_2Cl$ catalyst. The new peaks other than those resulting from stereoregularity in the chain are numbered a, b, . . . , h with decreasing frequency; f is put in parentheses because of the uncertainty of its assignment. (b) Calculated stick spectrum of polypropylene using the Lindeman and Adams relationship for the ^{13}C NMR nuclei located near the chemical inversion units such as isolated tail-to-tail [1] and head-to-head [2] units. (75)

[1] The sequence contains an isolated tail-to-tail (tt), i.e. · · · (th)(th)(tt)(ht)(ht) · · · unit.

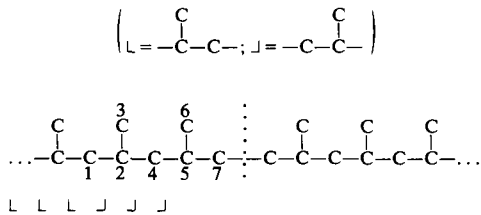

[2] The sequence contains an isolated head-to-head (hh), i.e. · · · (ht)(ht)(hh)(th)(th) · · · , unit.

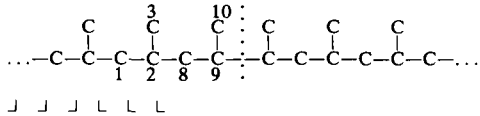

concluded that the control of monomer orientations with the syndiospecific catalyst VCl_4–$Al(C_2H_5)_2Cl$ and with the aspecific catalyst VCl_4–$Al(C_2H_5)_3$ depends on the terminal unit of the growing chain end.

It has been suggested that the observed ^{13}C chemical shifts may be attributed to the conformational differences existing among the various stereosequences. (89, 90) It is well known that the *gauche* arrangement of a carbon atom with respect to a non-hydrogen substituent in the γ-position produces a low frequency shift relative to that of the same carbon atom in the

trans-planar arrangement. The magnitude of the γ-effect experienced by a given carbon atom in a vinyl polymer chain should depend on the proportion or probability of those bond conformations that produce a *gauche* arrangement between the carbon atom of interest and those carbon atoms attached in the γ-position. Thus the ^{13}C chemical shift pattern observed for a vinyl polymer is expected to be directly related to its conformational characteristics. On the basis of these considerations, Provasoli and Ferro (91) have calculated the ^{13}C chemical shifts of the central 9-CH_3 carbon in the various stereoisomers of 3,5,7,9,11,13,15-heptamethylheptadecane which is a model compound for PP using the Boyd–Breitling (85) rotational isomeric state model. Tonelli (92) has calculated the ^{13}C chemical shifts of the 9-C^{α} and 9-CH_3 carbons and the 8- and 10-CH_2 carbons in the various stereoisomers of the same model compound as used by Provasoli and Ferro using the Suter–Flory (88) rotational isomeric state model. The agreement between the observed (72) and calculated ^{13}C chemical shifts is very good. Thus they clarify that the ^{13}C NMR chemical shift differences among the various stereosequences in PP are predominantly due to the γ-effect which in turn depends directly upon the conformational characteristics of a given stereosequence.

D. Polystyrene

Since Bovey's observation (93) of the ^1H NMR spectra of polystyrene (PSt) and its oligomers at 60 MHz many research groups have observed the ^1H and ^{13}C NMR spectra of PSt and deuterated PSt and have studied their stereochemical configurations and conformations in solution. (2d, 2i, 94, 95)

The ^1H NMR spectra of isotactic and atactic PSt-d_7, which have the proton in the α-position, are spread over a much wider range of frequencies than those for the main dyad in a predominantly stereoregular chain. These observations are related to the greater magnetic field produced by the phenyl ring. Fujiwara and Flory (97) have tried to explain the observed six pentad peaks by the ring current effect of the phenyl group and the conformational probabilities within various pentads in vinyl polymer chains with particular reference to the conformations affecting the CH proton in PSt. In order to estimate ^1H chemical shifts they have considered the conformations in which the CH protons are shielded by a phenyl group. In the preferred conformations, the phenyl group is constrained by the steric interactions of its *ortho* protons and carbons to assume an orientation about the C–Ph bond with its plane perpendicular to that defined by the adjoining skeletal bonds. Consequently the CH proton is perpendicular to the plane of the phenyl group and at a distance of 2·5 Å from it. According to the calculation of Johnson and Bovey for the ring current effect, (10) the chemical shift of the proton is about 0·5 ppm when account is taken of the

possible rotary fluctuations of the benzene ring. They defined a quantity ϵ representing the expected number of appositions of neighbouring phenyl groups with respect to the CH proton. Therefore, the chemical shift for the proton under consideration is estimated as

$$\tau = \tau_0 + 0{\cdot}5\epsilon \tag{33}$$

in ppm, or

$$\nu = \nu_0 - 50\epsilon \tag{34}$$

in Hz at 100 MHz. τ_0 and ν_0 can be arbitrarily chosen to optimize agreement with the observation. The quantity ϵ, which affords a measure of the chemical shielding of the proton, is calculated as follows. If the kth and $(k-1)$th dyads, i.e. the dyads preceding and following $(\mathrm{CHR})_k$ respectively, are both *meso*, then

$$\epsilon_{\mathrm{mm}:k} = P''_{\mathrm{tg}:k} + P''_{\mathrm{gt}:k+1} + P''_{\mathrm{g't}:k} + P''_{\mathrm{tg}':k+1} \tag{35}$$

For a syndiotactic triad,

$$\epsilon_{\mathrm{rr}:k} = P''_{\mathrm{tt}:k} + P''_{\mathrm{tt}:k+1} + P''_{\mathrm{g'g}:k} + P''_{\mathrm{gg}':k+1} \tag{36}$$

For a heterotactic triad,

$$\epsilon_{\mathrm{mr}:k} = P''_{\mathrm{tg}:k} + P''_{\mathrm{tt}:k+1} + P''_{\mathrm{g\bar{t}}:k} + P''_{\mathrm{g\bar{g}}:k+1} \tag{37}$$

The various conformation probabilities P'' are estimated by using equation (26) with the Monte Carlo method. From these approaches, the ^{1}H chemical shifts for the CH protons in atactic PSt-d_7 are estimated with $f_r = 0{\cdot}5$, $\omega = \omega'\omega'' = 0{\cdot}01$, $\eta = 1{\cdot}5$, and $\tau = 0{\cdot}5$, and are shown in Fig. 20 together with the observed ^{1}H NMR spectra of isotactic (inset) and atactic PSt-d_7 in *o*-dichlorobenzene at 160 °C, (98) where τ_0 and ν_0 are taken to be 7·33 and 267 respectively. By comparing the calculated and observed results it appears that the resonances reported by Segre *et al.* at 226 Hz and 216 Hz are due to pentads whose central triads are isotactic. Those at 206 Hz and 199 Hz are probably due to heterotactic triads, and the more intense peaks observed at 195 Hz and 193 Hz represent combinations of syndiotactic and heterotactic triads.

Izu *et al.* (99) have calculated the chemical shifts of the CH and phenyl protons due to the ring current effect and to Flory's conformational probability in order to understand the ^{1}H NMR of atactic PSt. In this calculation the ring current effect is estimated more exactly than in the Fujiwara–Flory method. The calculation satisfactorily accounts for the observed splitting of the phenyl signal due to the stereochemical configurations.

Ikuta *et al.* (100) have calculated the ^{1}H chemical shifts of the CH_2, CH, and phenyl protons of isotactic PSt, assuming a 3_1 helix with 11 monomer units and taking into account the ring current and bond anisotropy [$\Delta\chi$(C–C)

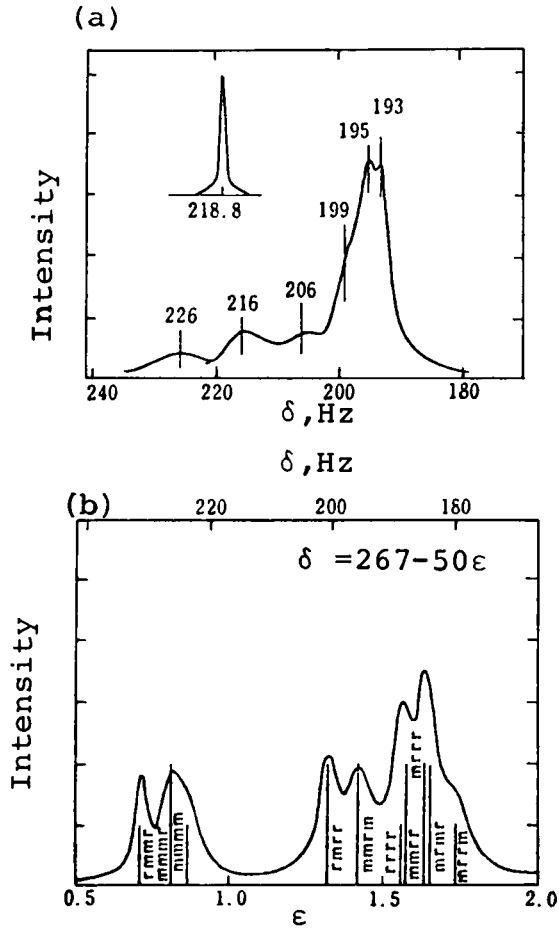

FIG. 20. (a) ^{1}H NMR spectrum of isotactic (inset) and atactic polystyrene-d_7 as observed in *o*-dichlorobenzene at 160 °C. (98) (b) ^{1}H NMR spectrum calculated for the methine protons in atactic polystyrene-d_7 with $f_r = 0{\cdot}5$, $\omega = 0{\cdot}01$, $\eta = 1{\cdot}5$, and $\tau = 0{\cdot}5$. The vertical lines represent mean frequencies calculated for the indicated pentads. The curve represents the sum of the intensities calculated assuming each to be Lorentzian in shape. (97)

and $\Delta\chi$(C–Ph)] contributions. The CH_2 protons are assigned such that the *syn* proton appears at lower frequency than the *anti* proton. The angular dependence of the chemical shifts around the main chain shows that the ideal 3_1 helix is the most probable case. Rotation of the phenyl group does not appreciably affect the chemical shifts and a perpendicular orientation for the skeletal bonds is probable.

The chemical shifts, τ_{ph}, have been calculated (101) for the CH and aromatic protons of the central $>CHC_6H_5$ group in the all-*meso* nonad m_8

and in the nonads rrm_6, $mrrm_5$, m_2rrm_4, and m_3rrm_3 containing a single racemic triad each nonad being situated within an isotactic PSt chain using the following equation: (19)

$$\delta_{ph} = \delta^0_{ph} + \sum_{\alpha} \delta_\alpha P_\alpha + \sum_{\alpha\beta} \delta_{\alpha\beta} P_{\alpha\beta} \tag{38}$$

where δ^0_{ph} is a constant for the protons of a given class and δ_α is the shift parameter due to the phenyl group attached to the adjoining C^α atom when the intervening dyad is in the conformation specified by α whose probability of occurrence is P_α; the shift parameter due to the phenyl group separated from the resonant proton by two dyads, when the two intervening dyads are in the conformations specified by α and β respectively, is $\delta_{\alpha\beta}$; the probability of this conformation is $P_{\alpha\beta}$. P_α and $P_{\alpha\beta}$ are calculated by the Fujiwara–Flory method. δ_α and $\delta_{\alpha\beta}$ are estimated using equation (38) and are found to be sensitive to changes in the torsional angles. In recognition of the correlations of the averaged departures of two angles from their symmetrical locations, $\phi_t = \Delta\phi$ and $\phi_g = 120° - \Delta\phi$. The value of $\Delta\phi$ was varied from 0° to 20°. The calculated chemical shifts of the CH and phenyl protons as a function of $\Delta\phi$ are shown in Fig. 21 together with the observed stick spectra. For the CH proton, in the range $\sim 8° < \Delta\phi < \sim 15°$, the relative locations of the theoretical spectra are in reasonable agreement with the experimental results. For the phenyl protons qualitative agreement with experiment is obtained for $\Delta\phi \approx 0°$ except for the additional peaks observed at $\tau_{ph} < 0$.

Randall has calculated the ^{13}C chemical shifts of atactic PSt in conjunction with the Grant and Paul paramaters to obtain information about the distribution of stereochemical configurations. (37)

E. Polyamino acids

NMR spectroscopy has become one of the principal experimental methods employed to study the conformations of amino acids and their derivatives, small peptides, cyclic peptides, polyamino acids, and biopolymers. The progress made in the conformational analysis of these molecules using NMR as the major tool has been reviewed frequently by several authors. (2e–h, 102–104)

In order to understand more exactly the conformations it is undoubtedly very important to study theoretically the chemical shifts of these compounds. However, there are only a few studies involving ^1H chemical shift calculations. To discover the origin of the magnetic shielding effect caused by an amino group is a basic requirement encountered in estimating the ^1H chemical shifts of polyamino acids. Since Narashimhan and Rogers' work, (105) there have been some studies on the estimation of the

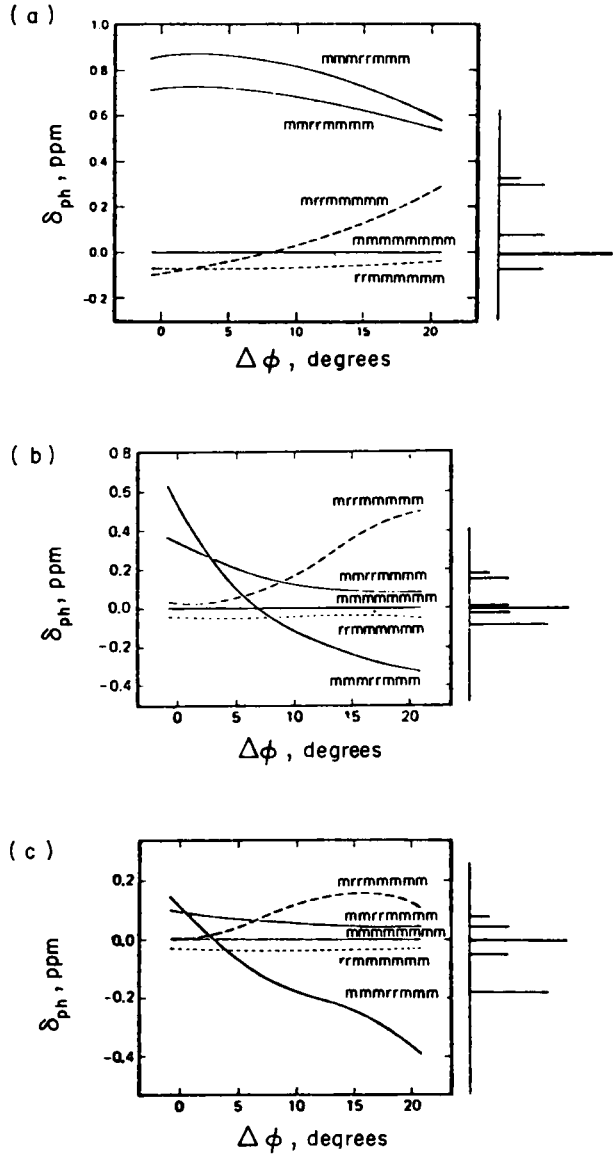

FIG. 21. (a) Chemical shifts of the central methine proton of the indicated nonads due to the first- and second-neighbour phenyls, plotted against $\Delta\phi$. The experimental results are shown by the stick diagram on the right-hand ordinate. (b) Chemical shifts of the central *o*-aromatic protons of the indicated nonads, situated in an otherwise isotactic chain, due to the first- and second-neighbour phenyls, plotted against $\Delta\phi$. (c) Chemical shifts of the central *m*-aromatic protons of the indicated nonads, situated in an otherwise isotactic chain, due to the first- and second-neighbour phenyls, plotted against $\Delta\phi$.

magnitude of the magnetic dipolar field and the electric field from a dipole located on the carbonyl bond. These make use of the observed chemical shift difference between the *cis* and *trans* protons in simple amide molecules. (106–108) A report by Raynes and Raza (109) provides a warning about such estimations on the basis of the observation that the chemical shift difference between the *cis* and *trans* N–CH_3 protons, $\Delta\sigma$(N–CH_3), of dimethylformamide (DMF) is very small at the infinite dilution in non-polar solvents. This is due to the absence of specific interactions between solute and solvent and tends to nearly zero by extrapolating $(\varepsilon - 1)/(2\varepsilon + n^2) \rightarrow 0$, where n is the refractive index of the solute. This means that $\Delta\sigma$(N–CH_3) in DMF is solvent-induced and there is no chemical shift difference between the non-equivalent protons in an isolated DMF molecule not only at high temperatures but at low temperatures also. Thus carefully performed experiments and thoughtful considerations are required to clarify the origin of the magnetic shielding effect from the amide group.

A calculation of the ^1H chemical shifts of a polyamino acid has been carried out by Sternlicht and Wilson. (110) They have considered the α-CH protons of polyglycine with a helical conformation taking into account the electric field effect from the large permanent dipoles of the peptide residues. The difference in the magnetic shielding environment of the two kinds of α-CH proton in the helical polyglycine corresponds to the α-CH chemical shift difference between right-handed and left-handed helical polyamino acids. A set of uniquely determinable monopoles, i.e. charges at the amide atoms which at large distances reproduce the calculated dipole moment, is used in order to calculate the electric field. The resonance from the α-CH protons in an infinite right-handed helix is predicted to appear about 0·5 ppm to high frequency of the corresponding resonance for an infinite left-handed polyamino acid.

A particularly significant feature of the conformational behaviour of linear polyamino acids is the helix–random coil transition. High resolution NMR spectroscopy has been extensively applied to the study of this transition. (2e, 2g) Of special interest is the observation of changes in the chemical shift of the backbone α-CH proton during the transition in a mixed solvent system consisting of the helix-supporting solvent ($CHCl_3$) and the coil-supporting solvent (TFA). For example, Goodman *et al.* (112) have reported that the α-CH peak of poly(L-alanine) (PLA) moves continually to higher frequency as the proportion of TFA in the $CDCl_3$–TFA solvent increases. Finally the α-CH peak position obtained by extrapolating to 100% $CDCl_3$ solution is observed at about 0·4 ppm to low frequency of that in 100% TFA solution. For the causes of the high frequency shift of the α-CH proton in TFA the following two factors are considered: (i) an intramolecular shielding effect which is intrinsic to the conformation of polyamino acids (111) and, (ii) a solvation effect (2e, 113, 114) and/or

protonation (115–117) of the amide group by the acetic acid. However, it would be difficult to discriminate between the contributions experimentally.

Asakura *et al.* (118, 119) have tried to calculate the ^{1}H chemical shifts of PLA with both helical and coil conformations in order to clarify to what extent the intramolecular shielding contribution plays a role in the coil state α-CH proton chemical shift observed in TFA solution. Since PLA is the simplest optically active polyamino acid known to form a right-handed α-helix in solution, it possesses much intrinsic interest as an object of conformational study. PLA is present in a non-polar solvent such as $CHCl_3$ as a helical form, and therefore the intramolecular shielding contribution to the ^{1}H chemical shifts of α-helical PLA seems to be dominant.

The chemical shifts of the NH, α-CH, and CH_3 protons in the PLA chain with an α-helical conformation have been calculated by taking into account only intramolecular shielding effects and compared with the observed results. (118) Since the carbonyl group of any residue forms a hydrogen bond to the NH proton of the fourth residue ahead in the α-helical chain as shown in Fig. 22, the magnetic anisotropy and electric fields due to the N–C=O group may produce secondary fields which may add in the helical formation to produce significant shifts. This provides a characteristic shielding effect for a proton in α-helical PLA compared with that in the vinyl polymers described above.

The ^{1}H chemical shift of PLA has been estimated as a sum of σ_A^{dia}, σ_A^E, and σ_A^{aniso}. In the estimation of these terms the electron density distribution was calculated for *N*-acetyl-L-alanine methylamide in the α-helical form hydrogen-bonded with two formamide molecules which is used as a model of the α-helical form of PLA. σ_A^{aniso} is estimated using the modified McConnell equation due to ApSimon *et al.* (121, 122) It is expected that the shielding effect from magnetically anisotropic C–N bonds may make a significant contribution to ^{1}H chemical shifts. The magnitude of the magnetically anisotropic (O=)C–N and (H)C$^\alpha$–N bonds is estimated semi-empirically by taking into account (i) the observed chemical shift data of all the protons in six amides, i.e. formamide, acetamide, *N*-methylformamide, *N*-methylacetamide, *N,N*-dimethylformamide, and *N,N*-dimethylacetamide, (118) (ii) a shielding effect due to the peptide group from the ^{1}H spectra of quinolizidone and derivatives as suggested by Bohlmann and Schumann, (123) and (iii) the value of the magnetic anisotropy of the formamide molecule as obtained from a measurement of the magnetic molecular Zeeman effect in formamide-^{15}N by Tigelaar and Flygare. (124) Although the method of estimation is rough, the large values of C–N bond anisotropies obtained imply that the shielding contributions of these bonds are significant in considering the polyamino acid ^{1}H chemical shifts.

The calculated spectrum which consists of the NH, α-CH, and CH_3 protons in the central peptide residue, number 8 of the 15-residue helix, is

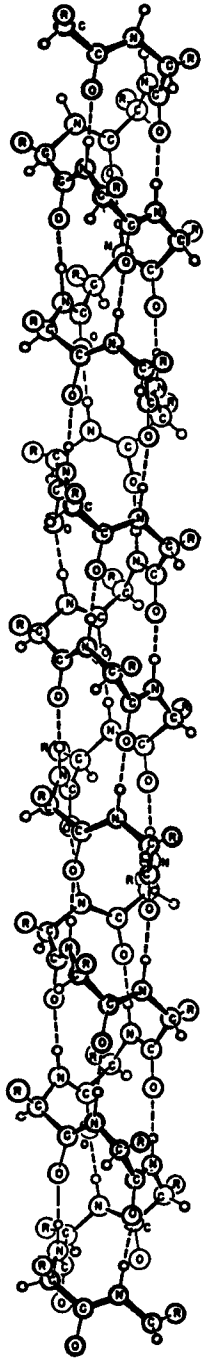

FIG. 22. The α-helix. (120)

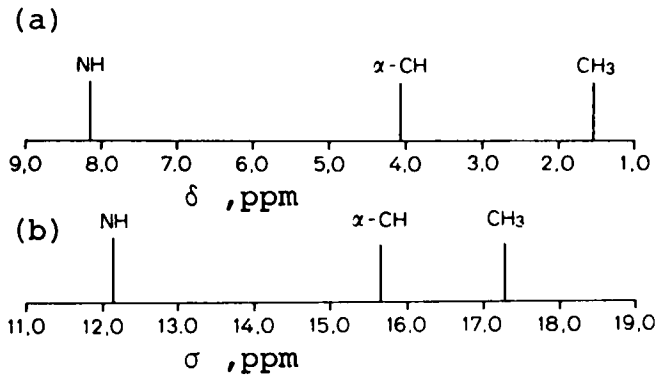

FIG. 23. (a) The observed ^{1}H chemical shifts of poly-(L-alanine) obtained by extrapolating to zero concentration of TFA in a TFA–$CDCl_3$ solvent system. (b) The calculated ^{1}H screenings of poly-(L-alanine). (118)

represented in Fig. 23 as a stick spectrum together with the observed spectrum of PLA (DP = 16) obtained by extrapolating to zero concentration of TFA in $CDCl_3$. (118) Additionally each shielding contribution is shown separately in Table III. The agreement between the experimental and theoretical spectra appears to be reasonable.

TABLE III

Some shielding contributions to the ^{1}H chemical shifts of α-helical poly-(L-alanine) (ppm)

	NH	α-CH	CH_3
σ^{dia}	$15{\cdot}27_8$	$17{\cdot}75_4$	$17{\cdot}65_6$
σ^{E}	$0{\cdot}60_4$	$-0{\cdot}75_9$	$-0{\cdot}09_2$
σ^{aniso}, C=O	$-1{\cdot}28_0$	$-0{\cdot}30_3$	$-0{\cdot}23_5$
σ^{aniso}, (O=)C–N	$-1{\cdot}79_8$	$-0{\cdot}40_7$	$-0{\cdot}05_7$
σ^{aniso}, (H)C^{α}–N	$-0{\cdot}66_7$	$-0{\cdot}61_4$	$0{\cdot}00_5$
σ^{T}	$12{\cdot}13_8$	$15{\cdot}67_1$	$17{\cdot}27_8$

The α-CH chemical shift of PLA in the coil form (119) has been calculated by a procedure similar to that used in calculating the ^{1}H chemical shifts of α-helical PLA. It appears that the internal α-CH proton chemical shift of random-coil PLA is mainly affected by the shielding effect due to the two peptide units directly connected with the specified C^{α} carbon as shown in Fig. 24. This arises from careful examination of the α-CH regions of the ^{1}H NMR spectra of the alanine oligopeptides observed by Goodman *et al.* (125,

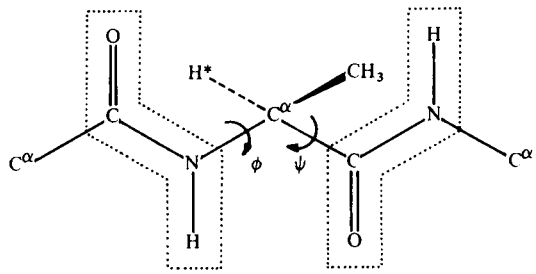

FIG. 24. Schematic representation of a coil model of poly-(L-alanine).

126) and by Shoji *et al.* (127) In this fragment of a PLA chain it is possible for rotation to occur around the skeletal N–C^{α} and C^{α}–C bonds, the internal rotational angles being represented by ϕ and ψ respectively. Two kinds of conformational energy map of the alanine dimer have been reported by Ramachandran *et al.* (128, 129) (Model I) and by Momany *et al.* (130) (Model II). These are used to calculate the probability of the coil conformation.

The charge distribution for *N*-acetyl-L-alanine methylamide, which is a model compound for PLA, is calculated using the CNDO/2 method for 60° increments in the angles ϕ and ψ. As an example, the results for the α-CH proton in this molecule are represented in Fig. 25. It is noteworthy that the electron density of the proton changes considerably on varying ϕ and ψ, especially in the region of $\phi = 0$–120°. Similarly, the charges on the other atoms in the molecule are found to undergo noticeable changes for various values of ϕ and ψ. Thus it is important to pay attention to the

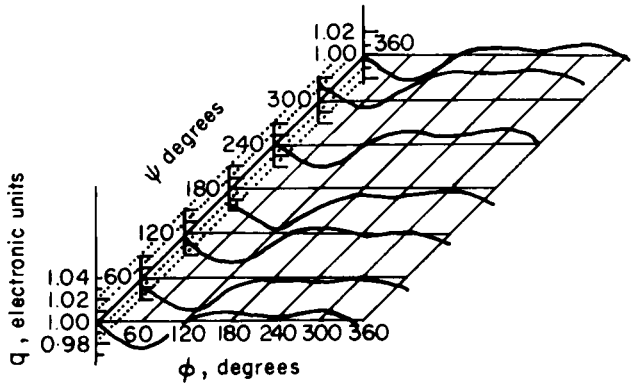

FIG. 25. Electron densities, q, of the α-CH protons in *N*-acetyl-L-alanine methylamide, calculated using the CNDO/2 method, represented as a function of the rotational angles ϕ and ψ. (119)

significant changes in the charge distributions that arise from conformational changes.

In the case of Model I, 39 conformations are chosen by Ramachandran *et al.* (128) representing 30° increments of ϕ and ψ, in the allowed regions of the ϕ–ψ map. The sum of the shielding effects, σ^{T}, changes considerably from 14·99 ppm to 16·29 ppm (Table IV) and the α-CH chemical shift in the coil state is estimated as 15·75 ppm by averaging over the 39 conformations. Thus the coil α-CH peak is expected to resonate at 0·08 ppm to low frequency of that in the helical state (15·67 ppm). (118)

TABLE IV

α-CH proton chemical shifts (ppm) calculated for 39 conformations chosen from the allowed regions in Ramachandran's map (128)

ψ (degrees) \ ϕ (degrees)	0	30	60	90	120	150	180	210	240	270	300	330
330	16·13	15·87	15·67	15·84	16·13							
300	16·29	16·00	15·84	15·94	16·26							
270	16·23	15·94	15·78	16·01	16·18				15·83			
240	16·01	15·71	15·57	15·81					15·68			
210	15·82	15·66	15·38	15·55					15·54			
180												
150	15·56			15·28	15·53							
120	15·52	15·26	14·99	15·26	15·50							
90												
60												
30												
0	16·00	15·62	15·55	15·68	15·93							

In the case of Model II the four low-energy minima in the ϕ–ψ map, computed by the CNDO/2 method for *N*-acetyl-L-alanine methylamide by Momany *et al.*, (130) are taken into account for the chemical shift calculation and 15·80 ppm is obtained for the α-CH chemical shift by averaging over these conformations and by taking into account their conformational energy differences. Thus, although Models I and II differ considerably, the coil peak position is expected to appear about 0·1 ppm to low frequency of the helical peak position, regardless of the model chosen. This contrasts with the experimental high frequency shift of *ca.* 0·4 ppm.

On the basis of these results it is suggested that the high frequency shift of the α-CH proton in PLA observed in TFA solution comes mainly from the solvent effect of TFA including the rearrangement of the charge distribution along the PLA chain in the strong acid.

The α-CH proton chemical shifts in the helical and random-coil forms of PLA have also been calculated by using only the measured magnetic

susceptibility anisotropy of the amide group. (124) The calculation predicts a low frequency shift of 0·1 ppm when PLA undergoes the helix to coil transition in agreement with prediction. (118)

Finally chemical shift calculations for the protons in some nucleosides have been reported by Giessner-Prettre and Pullman. (131, 132) They have calculated the chemical shift of the non-exchangeable proton of the ribose ring of some pyrimidine nucleosides as a function of the torsional angle, χ_{CN}, about the glycosyl bond by taking into account the ring current, the magnetic anisotropy, and the electric field effects. Figure 26 shows the sum of the contributions from these three shielding effects on the proton in uridine nucleoside as a function of χ_{CN}. (131) The observed difference between the chemical shift of the non-exchangeable protons of the ribose of 5-methyl- and 6-methyl-uridine corresponds to a modification in the value of the torsional angle about the glycosyl bond from a value of $0° < \chi_{CN} < 60°$ in the 5-methyluridine nucleoside to a value of $250° < \chi_{CN} < 300°$ in the 6-methyl derivative. This predicted variation is reasonable since most pyrimidine nucleosides unsubstituted at C_6 have a value of χ_{CN} between 0° and 60°, and a value of $\chi_{CN} = 250°$ has been observed for a crystal of 6-methyluridine. (133) Similar ^1H chemical shift calculations were carried out successively for some cytidine and purine nucleosides. (132)

F. Copolymers

A number of ^1H and ^{13}C NMR studies on the stereochemical structures of copolymers have been reported. Some theoretical studies of the chemical shifts of copolymers provide information about the stereochemical configurations and conformations; in addition the analysis of their configurations has been carried out by using the empirical Grant and Paul relationship. (37, 134–147)

Let us introduce the calculation of ^1H and ^{13}C chemical shifts of acrylate–styrene copolymers. Koinuma *et al.* (148) have studied the characteristic splittings observed in the ^1H NMR due to cotacticity in the methoxy proton region of the alternate copolymers of methyl methacrylate (MMA) and methyl acrylate (MA) with styrene (St) and α-methylstyrene (MSt). The separation of these splittings, $\Delta\delta$, between the *meso* and racemic configurations has been calculated by generating the Monte Carlo chains with Flory's matrix method. The contribution to the chemical shift from the ring current of the phenyl group in the adjacent St or MSt units is also included. The results are in Table V. The good agreement between the $\Delta\delta$ values thus clearly indicates the use of calculations in explaining the ^1H chemical shift behaviour of alternating copolymers. Matsuo and Chujo (149) have estimated the ^1H chemical shifts of a random MMA–St copolymer by a similar method.

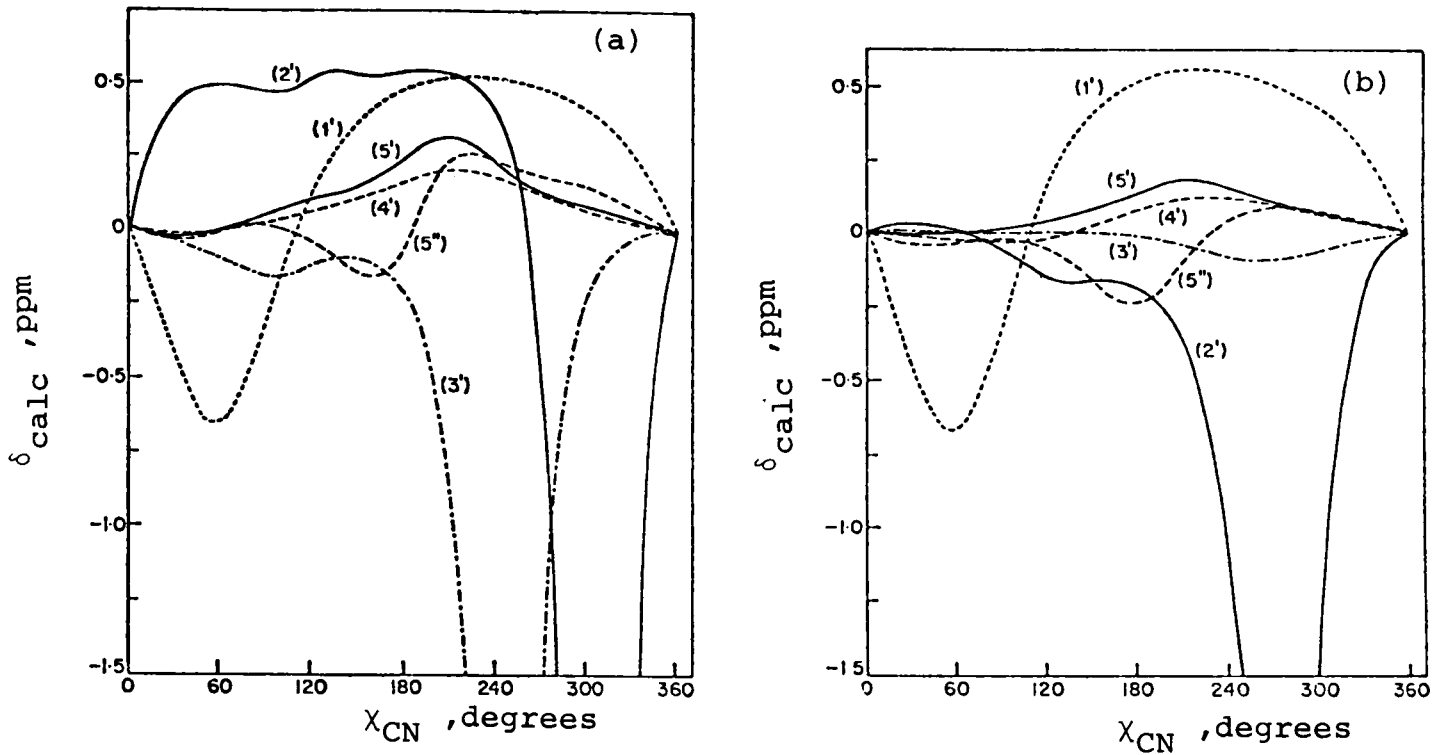

For legend see facing page

TABLE V

Some calculated and observed ^{1}H chemical shift differences, $\Delta\delta$, of acrylate–styrene copolymers (ppm)

	MA–St	MA–MSt	MMA–St	MMA–MSt
$\Delta\delta$(calc.)	0·09	0·60	0·49	0·20
$\Delta\delta$(obs.)	0·11	0·55	0·50	0·25

Koinuma *et al.* (150) have calculated the ^{13}C chemical shifts of alternate copolymers of MMA and MA with St and MSt as a sum of σ_A^{dia}, σ_A^{para}, and σ_A^{aniso} where σ_A^{para} is estimated by using the CNDO/2 and ΔE approximations. The calculated results are in Table VI. Both the magnitude and sign of the calculated $\Delta\delta$ values agree with the observed results. For example, the

TABLE VI

Some calculated and observed ^{13}C chemical shift differences, $\Delta\delta$, of acrylate–styrene copolymers (ppm)

	$\Delta\delta$(C=O)		$\Delta\delta$(C_1)		$\Delta\delta$(OCH_3)		$\Delta\delta$(OCH_3)		$\Delta\delta$(α–CH_3)	
MMA–St	0·82	0·98	0·44	1·88	0·35	0·56	0·36	0·45	−0·45	−0·25
MA–αMeSt	0·86	1·30	0·99	1·05	0·40	0·45	0·39	0·50	0·0	0
MA–St	0·10	0·00	0·00	0·01	0·10	0·00	0·10	0·11	—	—
MMA–αMeSt	0·45	1·20	0·12	1·20	0·35	0·30	0·19	0·25	−0·60[a]	−0·50[a]

[a] α-Methyl of MMA.

FIG. 26. Variation of the sum of the contributions of the ring current effect, the magnetic anisotropy effect, and the electric field effect to the chemical shift of the non-exchangeable protons of the ribose in uridine nucleoside [3] as a function of the torsional angle χ_{CN} about the glycosyl bond. (a) 3′-*endo,gauche-gauche*; (b) 2′-*endo,gauche-gauche*. (131)

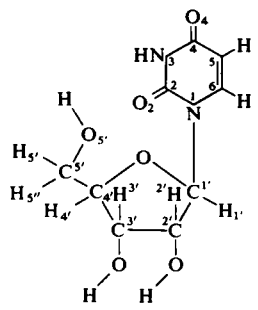

[3]

observed three peaks for the C_1 carbon in the alternate MMA–St copolymer, which have been assigned to rr, mr, and mm in passing from high to low frequency, are accounted for by this calculation.

The Grant and Paul relationship has been used successfully to assign the ^{13}C NMR spectra of ethylene–propylene (E–P) copolymers. (134–146) The ^{13}C NMR spectrum of a typical E–P copolymer is in Fig. 27 together with the assignment of each peak. From the ^{13}C NMR analysis the copolymer composition and the monomer sequence distribution in the E–P copolymer are determined and the E–P reactivity ratio product discussed.

Some of these studies have been directed toward the elucidation of the mechanisms of steric control exerted by Ziegler–Natta catalysts in the stereospecific polymerization of propene. (75–77, 135–137, 140, 144, 146) In these investigations E–P copolymers of low ethylene content, (144) some with ^{13}C enriched ethylene carbons, (136, 137, 146) are polymerized in the presence of isospecific or syndiospecific catalysts. The resulting spectra are shown in Fig. 28. (146) The resonances marked by one or two stars arise from the insertion of isolated ^{13}C enriched ethylene units. Only one narrow resonance for each ^{13}C-enriched CH_2 carbon is observed in the spectrum of the E–P sample prepared by an isospecific catalyst as shown in Fig. 28(a), This suggests that the ethylene units are in the same stereochemical environment.

The resonances of the isolated ethylene units detected in the spectrum of the E–P sample prepared by a syndiospecific catalyst [Fig. 28(b)] are split and broader. This suggests that the ethylene units are in different stereochemical environments. From these observations Zambelli *et al.* (136, 137, 146) concluded that the isotactic regulation arises from the asymmetric spatial arrangement of the ligands in the catalytic centres, whereas the syndiotactic regulation arises from the asymmetry of the last unit of the growing chain end.

Recently the chemical shifts of the peaks arising from the insertion of isolated ethylene units in the low ethylene content E–P copolymers have been calculated by a quantitative analysis of the γ-effects experienced by the CH_2 carbons in question. (151) The chemical shift calculation was carried out for the CH_2 carbons, $-^{d}CH_2-$, $-^{l}CH_2-$, and $-^{d*}CH_2-$, in an isolated ethylene unit [14] appropriate to various E–P copolymers

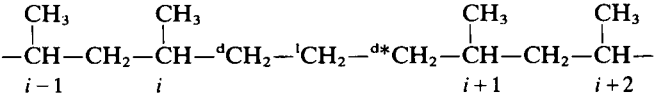

[14]

The rotational isomeric state model for the E–P copolymer, developed by Mark, (152) was used to calculate the average number of three-bond

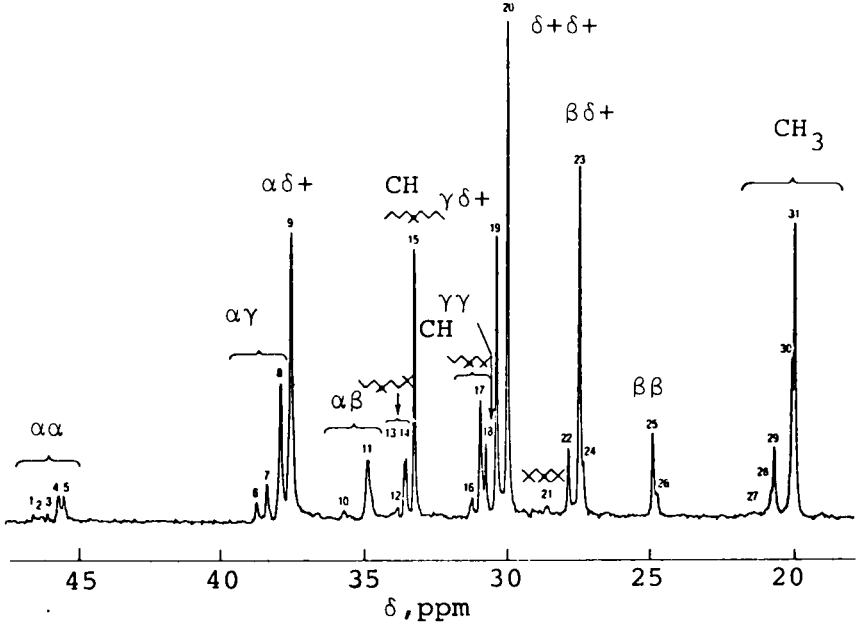

FIG. 27. 25·2 MHz ^{13}C NMR spectrum of a 50/50 ethylene–propylene copolymer at 125 °C in 1,2,4-trichlorobenzene. Chemical shifts are in ppm to high frequency of TMS. The methylene carbon resonances are identified according to the structural entity [4]–[11] from which they originated. The Greek notations are those suggested (134) by Carman. (145)

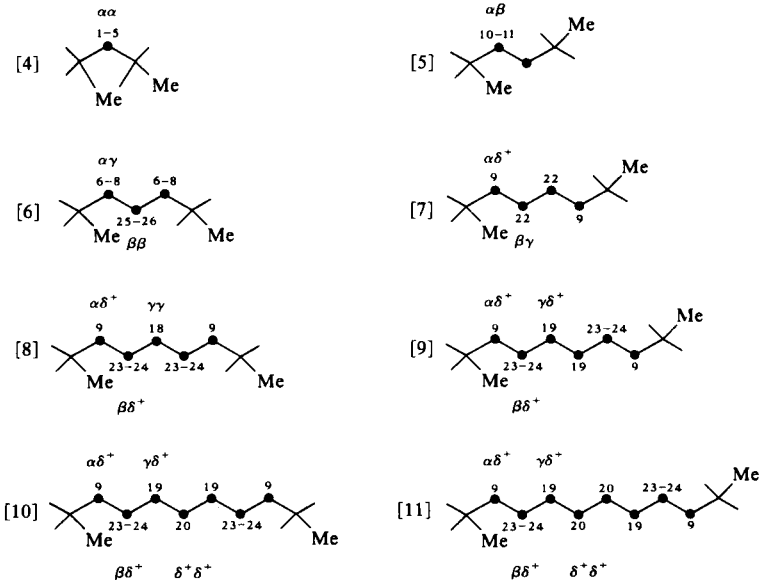

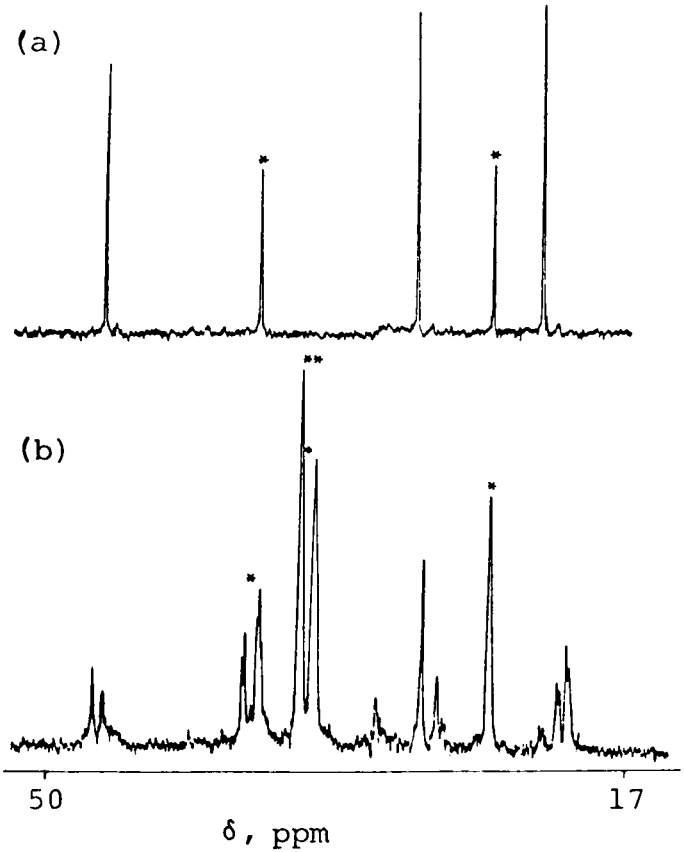

FIG. 28. 22·6 MHz ^{13}C NMR spectra of two 1-^{13}C-enriched ethylene–propylene copolymers polymerized in the presence of (a) isospecific and (b) syndiospecific catalysts at 140 °C in 1,2,4-trichlorobenzene. Chemical shifts are in ppm to high frequency of hexamethyldisiloxane, with a correction of +2·0 ppm. Peaks marked by a star are due to ethylene in location 1 [12], the peak marked by two stars is due to ethylene in location 2. [13] (146)

Location 1:

[12] ··· ⊢—• ⊢—⊣ ⊢—• ···

⊢—•: $-CH_2-\underset{\displaystyle CH_3}{CH}-$ ⊢—⊣ : $-CH_2CH_2-$ •—⊣ : $-\underset{\displaystyle CH_3}{CH}-CH_2-$

Location 2:

[13] ··· ⊢—• ⊢—⊣ •—⊣ ···

carbon–carbon *gauche* or γ interactions involving the d, l, d* CH_2 groups as a function of the surrounding PP stereoregularity. The chemical shift calculated for $-^{l}CH_2-$ is virtually independent of the stereosequence of the surrounding PP units, which is consistent with the observed results. (146)

The chemical shifts calculated for $-^{d}CH_2-$ and $-^{d^*}CH_2-$ are independent of the m or r arrangement of the propylene units $i,i+1$ across the ethylene fragment. A chemical shift difference of *ca.* 1 ppm is expected for the $-^{d}CH_2-$ and $-^{d^*}CH_2-$ carbons adjoining an m propylene dyad $i-1,i$ or $i+1,i+2$ relative to those next to an r propylene dyad. On the basis of the calculation Tonelli (151) concludes that the calculated and observed chemical shifts of the d and d* CH_2 carbons in low ethylene content E–P copolymers are compatible only if the stereosequence of the propylene units adjoining, and not spanning, the isolated ethylene unit influence their chemical shifts. Therefore ^{13}C NMR studies of E–P copolymers do not aid in the elucidation of the mechanism of stereospecific catalysis in α-olefin polymerization.

G. Other polymers

Poly(methyl methacrylate) (PMMA) is one of the vinyl polymers which can be obtained with a wide range of tacticities. Historically the first observation of stereochemical configurations in vinyl polymers was carried out on this polymer by means of ^1H NMR. (153–155) Since this observation a number of ^1H and ^{13}C NMR studies on its stereochemical structure have been reported. However, there are few studies of the calculation of the chemical shift of PMMA except for the calculation of the ^1H chemical shifts of isotactic PMMA. The ^1H spectrum of a predominantly isotactic PMMA in nitromethane at 120 °C consists of the α-CH_3 protons which give a strong isotactic peak, the two *meso* CH_2 protons which are non-equivalent with a relative shift of about 0·5 ppm, and a single OCH_3 signal. Ando and Nishioka (156) have calculated the ^1H chemical shifts of the α-CH_3 and CH_2 protons. These include the polar and magnetic anisotropy effects of the carbonyl group with the 5_1 and 5_2 helical conformations which have been suggested by X ray diffraction and infrared data. (157) The calculated contribution from the dyad monomer units to the CH_2 proton shifts gives a larger magnetic shielding to the *threo* proton than to the *erythro* proton, and that from the triad monomeric units to the α-CH_3 protons shifts the position of the α-CH_3 protons to slightly lower frequency than the *threo* proton. This order of chemical shifts agrees with the experimentally determined one. (158–160) The chemical shifts calculated for the 5_1 helical conformation explain the observed values better than those on the 5_2 conformation.

Schaefer *et al.* (161) have measured the natural abundance dipolar-decoupled ^{13}C NMR spectrum of solid PMMA at room temperature. The carbonyl carbon resonance, with its pronounced chemical shift anisotropy, appears at high frequency and the quaternary carbon resonance is at 30 ppm from the α-CH_3 carbon line; 30 ppm is approximately equal to the known chemical shift between the quaternary and α-CH_3 carbons in solution. The

chemical shift anisotropy of the carbonyl carbon appears to be about 130 ppm. This value is near that observed for the carbonyl carbon in some small molecules. (162)

Other polymers for which we can find some theoretical calculations of ^{13}C chemical shifts include the *meso* and racemic 2,4-dimethoxypentanes, (163) 2,4-dicyanopentanes, (164) and 2,4-dicyano-2,4-dimethylpentanes, (165) which are model compounds of poly(vinyl methyl ether), polyacrylonitrile, and polymethacrylonitrile. These include the CNDO/2 and ΔE approximations and take into account the preferred conformations in order to explain the observed chemical shifts of the polymers. Some relevant papers (166) appeared too late to be discussed in this review.

Acknowledgements

The authors would like to thank Dr. G. A. Webb of the University of Surrey for his encouragement and helpful comments on this review, and Dr. H. Koinuma of the University of Tokyo for kindly furnishing reprints of his studies during the course of this work.

REFERENCES

1. H. S. Gutowsky, A. Saika, M. Takeda and D. E. Woessner, *J. Chem. Phys.*, 1957, **27**, 537.
2. For examples: (a) P. R. Sewell, *Ann. Rev. NMR Spectroscopy*, 1968, **1**, 210. (b) I. Ya. Slonim and A. N. Lynbinov, "The NMR of Polymers", Plenum, New York, 1970. (c) F. A. Bovey, "Polymer Conformation and Configuration", Academic Press, New York, 1969. (d) F. A. Bovey, "High Resolution NMR of Macromolecules", Academic Press, New York, 1972. (e) E. M. Bradbury, P. D. Cary, C. Crane-Robinson and P. G. Hartman, *Pure Appl. Chem.*, 1973, **36**, 53. (f) G. C. Levy, "Topics in Carbon-13 NMR Spectroscopy", Interscience, New York, 1974. (g) F. A. Bovey, *J. Polymer Sci., Macromol. Rev.*, 1974, **9**, 1. (h) W. A. Thomas, *Ann. Reports NMR Spectroscopy*, 1974, **6**, 1. (i) J. C. Randall, "Polymer Sequence Determination. Carbon-13 NMR Method", Academic Press, New York, 1977.
3. M. Mehring, in "NMR, Basic Principles and Progress (1976)", Vol. 11, Springer-Verlag, Berlin.
4. J. A. Pople, *Proc. Roy. Soc.*, 1957, *A***239**, 541, 550.
5. A. D. Buckingham, *Canad. J. Chem.*, 1960, **38**, 300.
6. J. A. Pople, *J. Chem. Phys.*, 1962, **37**, 53, 60.
7. J. C. Slater, *Phys. Rev.*, 1930, **36**, 57.
8. J. A. Pople, *Mol. Phys.*, 1964, **7**, 301.
9. H. M. McConnell, *J. Chem. Phys.*, 1957, **27**, 226.
10. C. E. Johnson and F. A. Bovey, *J. Chem. Phys.*, 1958, **29**, 1021.
11. D. M. Grant and E. G. Paul, *J. Amer. Chem. Soc.*, 1964, **86**, 2984.
12. L. P. Lindeman and J. Q. Adams, *Analyt. Chem.*, 1971, **43**, 1245.
13. S. Mizushima, "Structure of Molecules and Internal Rotation", Academic Press, New York, 1954.
14. (a) C. A. Hoeve, *J. Chem. Phys.*, 1961, **35**, 1266. (b) K. Nagai and T. Ishikawa, *J. Chem. Phys.*, 1962, **37**, 496.
15. P. J. Flory, "Statistical Mechanics of Chain Molecules", Interscience, New York, 1969.

16. P. J. Flory and Y. Fujiwara, *Macromolecules*, 1969, **2**, 315.
17. J. C. Woodbrey, *J. Polymer Sci.* (*B*), 1964, **2**, 315.
18. R. C. Ferguson, *Macromolecules*, 1971, **4**, 324.
19. F. C. Stehling and J. R. Knox, *Macromolecules*, 1975, **8**, 595.
20. F. Heatley and A. Zambelli, *Macromolecules*, 1969, **2**, 618.
21. J. C. Randall, *J. Polymer Sci., Phys. Edn.*, 1974, **12**, 703.
22. J. Urbino and J. S. Waugh, *Proc. Nat. Acad. Sci. USA*, 1974, **71**, 5062.
23. E. O. Stejskal, J. Schaefer and R. A. McKay, *J. Magn. Resonance*, 1977, **25**, 569.
24. L. Zatta and G. Gatti, *Macromolecules*, 1972, **5**, 535.
25. I. Ando and A. Nishioka, *Makromol. Chem.*, 1975, **176**, 3089.
26. I. Ando and A. Nishioka, *Bull. Chem. Soc. Japan*, 1973, **46**, 1040.
27. J. A. Pople and G. A. Segal, *J. Chem. Phys.*, 1966, **44**, 3289.
28. N. J. Sheppard and G. J. Szasz, *J. Chem. Phys.*, 1962, **17**, 496.
29. A. Abe, R. L. Jernigan and P. J. Flory, *J. Amer. Chem. Soc.*, 1966, **88**, 631.
30. K. J. Liu, *J. Polymer Sci.* (*A*-2), 1967, **5**, 1209; 1968, **6**, 947.
31. I. Ando and A. Nishioka, *Makromol. Chem.*, 1972, **152**, 7; 1972, **160**, 145; 1973, **171**, 195.
32. J. I. González de la Campa, J. M. Barrales-Rienda and J. González Ramos, *Macromolecules*, 1977, **10**, 989.
33. J. Matsumoto, I. Ando and A. Nishioka, *Rept. Progr. Polymer Phys.* (Japan), 1978, **21**, 429.
34. D. L. VanderHart, *J. Chem. Phys.*, 1976, **64**, 830; *J. Magn. Resonance*, 1976, **24**, 467.
35. I. Ando and A. Nishioka, *Rept. Progr. Polymer. Phys.* (Japan), 1976, **19**, 451.
36. M. J. S. Dewar and E. Haselbach, *J. Amer. Chem. Soc.*, 1970, **92**, 590.
37. J. C. Randall, *J. Polymer Sci., Phys. Edn.*, 1975, **13**, 889.
38. F. Heatley and F. A. Bovey, *Macromolecules*, 1969, **2**, 241.
39. F. A. Bovey, E. W. Anderson and D. C. Douglass, *J. Chem. Phys.*, 1963, **39**, 1199.
40. I. Ando, A. Nishioka and T. Asakura, *Makromol. Chem.*, 1975, **176**, 411.
41. T. Schaefer and T. Yonemoto, *Canad. J. Chem.*, 1964, **42**, 2318.
42. P. J. Flory and A. D. Williams, *J. Amer. Chem. Soc.*, 1969, **91**, 3118.
43. I. Ando, *Makromol. Chem.*, 1978, **179**, 2663.
44. J. Schaefer, *Macromolecules*, 1969, **2**, 210.
45. C. J. Carman, A. R. Tarpley, Jr., and J. H. Goldstein, *J. Amer. Chem. Soc.*, 1971, **93**, 2864.
46. Y. Inoue, I. Ando and A. Nishioka, *Polymer J.*, 1972, **3**, 246.
47. I. Ando, Y. Kato and A. Nishioka, *Makromol. Chem.*, 1976, **177**, 2759.
48. Y. Chatani, private communication.
49. I. Ando, Y. Kato, M. Kondo and A. Nishioka, *Makromol. Chem.*, 1977, **178**, 803.
50. G. Klopman, *Chem. Phys. Lett.*, 1967, **1**, 200.
51. H. A. Germer, Jr., *Theor. Chim. Acta*, 1974, **34**, 145.
52. I. Ando, A. Nishioka and M. Kondo, *J. Magn. Resonance*, 1976, **21**, 429.
53. J. Wyman, *J. Amer. Chem. Soc.*, 1936, **58**, 1482.
54. S. Satoh, R. Chujo, T. Ozeki and E. Nagai, *J. Polymer. Sci.*, 1962, **62**, S101.
55. Y. Kato and A. Nishioka, *Bull. Chem. Soc. Japan*, 1964, **37**, 1622.
56. S. Ohnishi and K. Nukada, *J. Polymer. Sci.* (*B*), 1965, **3**, 179.
57. F. C. Stehling, *J. Polymer Sci.* (*A*), 1964, **2**, 1815.
58. W. C. Tincher, *Makromol. Chem.*, 1965, **85**, 34.
59. E. Lombardi, A. Segre, A. Zambelli, A. Marinangeli and G. Natta, *J. Polymer Sci.* (*C*), 1967, **16**, 2539.
60. A. Zambelli, A. Segre, M. Farina and G. Natta, *Makromol. Chem.*, 1967, **110**, 1.
61. A. Zambelli, M. G. Giongo and G. Natta, *Makromol. Chem.*, 1969, **112**, 183.
62. A. Zambelli and A. L. Segre, *J. Polymer Sci.* (*B*), 1968, **6**, 473.

63. F. Heatley, R. Salovey and F. A. Bovey, *Macromolecules*, 1969, **2**, 619.
64. A. Zambelli, L. Zatta, C. Sacchi and C. Wolfsgruber, *Macromolecules*, 1972, **5**, 440.
65. K. Mitani, *J. Macromol. Chem.*, 1974, ***A8***, 1033.
66. L. F. Johnson, F. Heatley and F. A. Bovey, *Macromolecules*, 1970, **3**, 175.
67. Y. Inoue, A. Nishioka and R. Chujo, *Makromol. Chem.*, 1972, **152**, 15; 1973, **168**, 163.
68. A. Zambelli, D. E. Dorman, A. I. Richard Brewster and F. A. Bovey, *Macromolecules*, 1973, **6**, 925.
69. A. Zambelli, C. Wolfsgruber, G. Zannoni and F. A. Bovey, *Macromolecules*, 1974, **7**, 750.
70. C. Wolfsbruber, G. Zannoni, E. Rigamonti and A. Zambelli, *Makromol. Chem.*, 1975, **176**, 2765.
71. Y. Doi and T. Asakura, *Makromol. Chem.*, 1975, **176**, 507.
72. A. Zambelli, P. Locatelli, G. Bajo and F. A. Bovey, *Macromolecules*, 1975, **8**, 687.
73. J. C. Randall, *J. Polymer Sci., Phys. Edn.*, 1976, **14**, 1693.
74. J. C. Randall, *J. Polymer Sci., Phys. Edn.*, 1976, **14**, 2083.
75. T. Asakura, I. Ando, A. Nishioka, Y. Doi and T. Keii, *Makromol. Chem.*, 1977, **178**, 791.
76. A. Zambelli and G. Gatti, *Macromolecules*, 1978, **11**, 485.
77. Y. Doi, *Macromolecules*, 1979, in press.
78. P. J. Flory, J. E. Mark and A. Abe, *J. Amer. Chem. Soc.*, 1966, **88**, 639.
79. P. J. Flory and J. D. Baldeschwieler, *J. Amer. Chem. Soc.*, 1966, **88**, 2873.
80. P. J. Flory, *Macromolecules*, 1970, **3**, 613.
81. P. J. Flory, *J. Polymer Sci., Phys. Edn.*, 1973, **11**, 621.
82. P. J. Flory and Y. Fujiwara, *Macromolecules*, 1969, **2**, 1327.
83. T. Asakura, I. Ando and A. Nishioka, *Makromol. Chem.*, 1976, **177**, 523.
84. F. Heatley, *Polymer*, 1972, **13**, 218.
85. R. H. Boyd and S. M. Breitling, *Macromolecules*, 1972, **5**, 279.
86. V. BisKup and H. J. Cantow, *Macromolecules*, 1972, **5**, 546.
87. T. Asakura, I. Ando and A. Nishioka, *Makromol. Chem.*, 1975, **176**, 1151; 1976, **177**, 1493.
88. V. W. Suter and P. J. Flory, *Macromolecules*, 1975, **8**, 765.
89. C. J. Carman, *Macromolecules*, 1973, **6**, 725.
90. F. S. Bovey, Proc. Internat. Symposium on Macromolecules, Rio de Janeiro, 1974, July 26–31, (E. B. Mano, ed.), Elsevier, Amsterdam, 1975, p. 168.
91. A. Provasoli and D. R. Ferro, *Macromolecules*, 1977, **10**, 874.
92. A. E. Tonelli, *Macromolecules*, 1978, **11**, 565.
93. F. A. Bovey, G. V. Tiers and G. Filipovich, *J. Polymer Sci.*, 1959, **38**, 73.
94. F. A. Bovey, F. P. Hood III, E. W. Anderson and L. C. Snyder, *J. Chem. Phys.*, 1965, **42**, 3900.
95. F. Heatley and F. A. Bovey, *Macromolecules*, 1969, **1**, 301.
96. A. M. Hassan, *J. Polymer Sci., Phys. Edn.*, 1974, **12**, 655.
97. Y. Fujiwara and P. J. Flory, *Macromolecules*, 1970, **3**, 43.
98. A. L. Segre, P. Ferruti, E. Toja and F. Danusso, *Macromolecules*, 1969, **2**, 35.
99. M. Izu, N. Yamamoto and T. Kagiya, Reprint of 19th Polymer Symposium (1970), Kyoto, p. 807.
100. T. Ikuta, I. Ando and A. Nishioka, *Rept. Progr. Polymer Phys.* (Japan), 1972, **15**, 461.
101. D. Y. Yoon and P. J. Flory, *Macromolecules*, 1977, **10**, 562.
102. T. L. James, 'Nuclear Magnetic Resonance in Biochemistry', Academic Press, New York, 1975.
103. K. Wüthrich, "NMR in Biological Research: Peptides and Proteins", North-Holland, Amsterdam, 1976.
104. P. F. Knowles, D. Marsh and H. W. E. Rattle, "Magnetic Resonance of Biomolecules", Interscience, New York, 1976.

105. P. T. Narashimhan and M. T. Rogers, *J. Phys. Chem.*, 1959, **63**, 1388.
106. H. Paulsen and K. Todt, *Angew. Chem.*, 1966, **78**, 943.
107. D. L. Hooper and R. Kaiser, *Canad. J. Chem.*, 1965, **43**, 2363.
108. R. Barlet, J. L. Pierre and P. Arnaud, *Compt. Rend.*, 1966, **262**, 855.
109. W. T. Raynes and M. A. Raza, *Mol. Phys.*, 1969, **17**, 157; 1971, **20**, 339.
110. H. Sternlicht and D. Wilson, *Biochemistry*, 1969, **6**, 2881.
111. W. E. Stewart, L. Mandelkern and R. E. Glick, *Biochemistry*, 1967, **6**, 143.
112. M. Goodman, F. Toda and N. Ueyama, *Proc. Nat. Acad. Sci. USA* 1973, **70**, 331.
113. E. M. Bradbury, B. G. Carpenter, C. Crane-Robinson and H. W. E. Rattle, *Nature*, 1968 **220**, 69.
114. F. J. Joubert, N. Loton and H. A. Scheraga, *Biochemistry*, 1970, **9**, 2197.
115. J. H. Bradbury and M. D. Fenn, *Austral. J. Chem.*, 1969, **22**, 357.
116. J. W. O. Tam and I. M. Klotz, *J. Amer. Chem. Soc.*, 1971, **93**, 1313.
117. J. W. O. Tam and I. M. Klotz, *Biopolymers*, 1973, **12**, 2435.
118. T. Asakura, I. Ando and A. Nishioka, *Makromol. Chem.*, 1977, **178**, 1111.
119. T. Asakura, I. Ando and A. Nishioka, *Makromol. Chem.*, 1977, **178**, 1521.
120. L. Pauling and R. B. Corey, *Proc. Nat. Acad. Sci. USA*, 1951, **37**, 205, 235.
121. J. W. ApSimon, W. G. Craig, P. V. Demarco, D. W. Mathieson and L. Saunders, *Tetrahedron*, 1967, **23**, 2357.
122. R. F. Zürcher, *Prog. NMR Spectroscopy*, 1967, **2**, 205.
123. F. Bohlmann and D. Schumann, *Tetrahedron Lett.*, 1965, **28**, 2435.
124. H. L. Tigelaar and W. H. Flygare, *J. Amer. Chem. Soc.*, 1972, **94**, 343.
125. M. Goodman, N. Ueyama and F. Naider, *Biopolymers*, 1975, **14**, 901.
126. M. Goodman, N. Ueyama, F. Naider and C. Gilson, *Biopolymers*, 1975, **14**, 915.
127. A. Shoji, T. Kawai and A. Nishioka, *Rept. Progr. Polymer Phys.* (Japan), 1975, **18**, 555, 559, 563.
128. G. N. Ramachandran, C. Ramakrishnan and V. Sasisekharan, *J. Mol. Biol.*, 1963, **7**, 95.
129. G. N. Ramachandran and V. Sasisekharan, *Adv. Protein Chem.*, 1968, **23**, 283.
130. F. A. Momany, R. F. McGuire, J. F. Yan and H. A. Scheraga, *J. Phys. Chem.*, 1971, **75**, 2286.
131. C. Giessner-Prettre and B. Pullman, *J. Theor. Biol.*, 1977, **65**, 171.
132. C. Geissner-Prettre and B. Pullman, *J. Theor. Biol.*, 1977, **65**, 189.
133. E. A. Green, R. D. Rosenstein, R. Shiono, D. J. Abraham, B. L. Trus and R. E. Marsh, *Acta Cryst.*, 1975, **B31**, 102, 1221.
134. C. J. Carman and C. E. Wilkes, *Rubber Chem. Technol.*, 1971, **44**, 781.
135. W. O. Crain, Jr., A. Zambelli and J. D. Roberts, *Macromolecules*, 1971, **4**, 330.
136. A. Zambelli, G. Gatti, C. Sacchi, W. O. Crain, Jr., and J. D. Roberts, *Macromolecules*, 1971, **4**, 475.
137. A. Zambelli, in "NMR, Basic Principles and Progress (1971)", Vol. 4, Springer-Verlag, Berlin.
138. Y. Tanaka and K. Hatada, *J. Polymer Sci., Chem. Edn.*, 1973, **11**, 2057.
139. C. E. Wilkes, C. J. Carman and R. A. Harrington, *J. Polymer Sci., Polymer Symp. No 43*, 1973, 237.
140. F. A. Bovey, M. C. Sacchi and A. Zambelli, *Macromolecules*, 1974, **7**, 752.
141. K. F. Elgert and W. Ritter, *Makromol. Chem.*, 1976, **177**, 2781.
142. C. J. Carman, R. A. Harrington and C. E. Wilkes, *Macromolecules*, 1977, **10**, 536.
143. G. J. Ray, P. E. Johnson and J. R. Knox, *Macromolecules*, 1977, **10**, 773.
144. J. M. Sanders and R. A. Komoriski, *Macromolecules*, 1977, **10**, 1214.
145. J. C. Randall, *Macromolecules*, 1978, **11**, 33.
146. A. Zambelli, G. Bajo and E. Rigamonti, *Makromol. Chem.*, 1978, **179**, 1249.
147. J. C. Randall, *Macromolecules*, 1978, **11**, 592.

148. H. Koinuma, T. Tanabe and H. Hirai, Reprint 26th IUPAC Congress, Tokyo, 1977, p. 1173.
149. H. Matsuo and R. Chujo, Reprint 25th Polymer Symposium, Tokyo, 1976, p. 333.
150. T. Tanabe, H. Koinuma and H. Hirai, Reprint 26th Polymer Symposium, Nagoya, 1977, p. 1294.
151. A. E. Tonelli, *Macromolecules*, 1978, **11**, 634.
152. J. E. Mark, *J. Chem. Phys.*, 1972, **57**, 2541.
153. F. A. Bovey and G. V. D. Tiers, *J. Polymer Sci.*, 1960, **44**, 173.
154. A. Nishioka, H. Watanabe, I. Yamaguchi and H. Shimizu, *J. Polymer Sci.*, 1960, **45**, 232.
155. U. Johnson and T. Kessmer, *Kolloid-Z.*, 1960, **168**, 160.
156. I. Ando and A. Nishioka, *Polymer J.*, 1970, **1**, 288.
157. (a) J. D. Stroupe and R. E. Hughes, *J. Amer. Chem. Soc.*, 1958, **80**, 2341. (b) H. Tadokoro, Y. Chatani, H. Kusanagi and M. Yokoyama, *Rept. Progr. Polymer Phys.* (Japan), 1969, **12**, 173.
158. F. A. Bovey, "Macromolecular Chemistry", Vol. 3 (IUPAC), Butterworths, London, 1967.
159. C. Schuerch. W. Fowells, A. Yamada, F. A. Bovey, F. P. Hood and E. W. Anderson, *J. Amer. Chem. Soc.*, 1964, **86**, 4482.
160. T. Yoshino, J. Komiyama and M. Shinomiya, *J. Amer. Chem. Soc.*, 1964, **86**, 4482.
161. J. Schaefer, E. O. Stejskal and R. Buchdahl, *Macromolecules*, 1975, **8**, 291.
162. (a) I. Ando and A. Nishioka, *Bull. Chem. Soc. Japan*, 1975, **48**. 841. (b) K. A. K. Ebraheem and G. A. Webb, *Progr. NMR Spectroscopy*, 1977, **11**, 149.
163. I. Ando, M. Kondo, T. Ikuta and A. Nishioka, *Makromol. Chem.*, 1973, **169**, 285.
164. A. Nishioka, I. Ando and Y. Inoue, *Kobunshi Kagaku*, 1973, **30**, 139.
165. I. Ando and A. Nishioka, *Kobunshi Kagaku*, 1973, **30**, 604.
166. A. E. Tonelli, F. C. Schilling, W. H. Starnes, L. Sheppard and I. M. Plitz, *Macromolecules*, 1979, **12**, 78; A. E. Tonelli, *Macromolecules*, 1979, **12**, 225, 252.

Biological ^{31}P NMR Spectroscopy

I. K. O'NEILL* AND C. P. RICHARDS

Laboratory of the Government Chemist, Cornwall House, Stamford Street, London, SE1 9NQ, U.K.

* At present on secondment to RTZ Services Ltd., York House, Bond Street, Bristol, BS1 3PE, U.K.

I. INTRODUCTION

A. General remarks

In common with all areas of NMR investigation, the advent of FT NMR spectrometers has revolutionized the study of biological materials and biochemical systems. This revolution applies to both ^{13}C and ^{31}P NMR studies since the former was limited by its low natural abundance and the latter by its low concentration in tissue. As a consequence, the use of ^{31}P NMR spectroscopy has spread now to many areas of biological interest at all organizational levels, from pure chemicals up to viable organs and living small creatures. Thus, this review has been prepared at a time when the ever-increasing pace of ^{31}P NMR publications has necessitated the use of a fairly exclusive definition of biochemical systems. Therefore work concerned with the general organic chemistry of biologically important molecules has been excluded and many papers detailing conformational and interaction studies are only briefly reported.

The aim of this review is to survey the literature on ^{31}P NMR of biochemical systems over the period 1970–1978, and to present an account of the methods employed, the results obtained, and the likely future developments and applications. We have omitted detailed discussions of separate NMR and biological phenomena, but have provided a necessary minimum of biochemical background for understanding the significance of the ^{31}P NMR information. We have written this review with the non NMR specialist in mind too, and have attempted to be as descriptive as possible.

Phosphorus is a constituent of almost all biological substances except enzymes, and even many of these can be studied by ^{31}P NMR because of their action on phosphorus-containing substrates. Unlike most other methods of biochemical investigation, NMR is inherently non-invasive and non-destructive and does not perturb the chemical species or reaction under observation. While ^{31}P NMR shares the same basic spectroscopic parameters of chemical shift, relaxation times, etc. with ^{1}H, ^{13}C, and other nuclei, there are important differences arising from the chemical nature of biological molecules containing phosphorus. Usually there are only one, two, or three phosphorus atoms per biomolecule, thereby permitting simultaneous observation of many different molecular species in biological samples. The phosphorus species are usually present as polar, complexable, and titrable phosphate groups (which means that ^{31}P NMR spectrum reproducibility is sensitive to factors often irrelevant in ^{1}H and ^{13}C NMR examinations); consequently the biologically important phenomena of ionic strength, complexation, pH, and phosphate pK are directly accessible.

The ^{31}P NMR study of phosphorus compounds was last reviewed in Annual Reports on NMR by Mavel who covered the literature from 1965 to 1969. (1) Although he presented an extensive compilation of NMR data, he considered the field of biological applications to lie outside the scope of his review. Previously, the single most comprehensive review of the ^{31}P NMR literature was by Van Wazer and coworkers who surveyed the whole of high resolution ^{31}P NMR to 1967. (2) Although sections of both the Chemical Society's Specialist Periodical Reports concerning nuclear magnetic resonance (3) and organophosphorus chemistry (4) regularly include results obtained by ^{31}P NMR, this is not the subject of a specific chapter. For background work, one should consult a chapter by Van Wazer on the experimental and some theoretical aspects of ^{31}P NMR in the Determination of Organic Structures by Physical Methods series. (5)

The NMR properties of the biologically relevant nuclei ^{13}C, ^{15}N, and ^{31}P have been recently compared. (6) Illustrative examples of the types of information to be obtained from these nuclei are given but a comparison based on nuclear properties does not give a full impression of the biochemical importance that ^{31}P NMR studies have achieved. As shown in this

review, ^{31}P NMR of biological substances has progressed to the point where ^{31}P NMR as a technique is directly producing medically significant information and is being considered as a medical tool.

Most organic phosphate esters display ^{31}P–^{1}H spin–spin coupling, which can complicate ^{31}P spectra, and so most of the ^{31}P NMR work reviewed has utilized broad-band ^{1}H-decoupling. The reader should assume that, unless otherwise specified, ^{1}H broad-band decoupling was used in the reviewed literature. Except where stated to the contrary ^{31}P shifts are quoted with respect to 85% orthophosphoric acid; high frequency values are taken to be positive.

B. List of biological phosphorus-containing substances that have been observed by ^{31}P NMR

Almost any biological material will show detectable ^{31}P NMR signals, but the following list includes only common substances that have been positively identified as chemical entities within biological materials. The aim of presenting this list is two-fold: to demonstrate the substantial range of common biochemical substances that can be detected and distinguished, and to provide a key for the abbreviations appearing in this review. The names generally conform with those of the IUPAC-IUB Commission on Biochemical Nomenclature and are those found in the literature reviewed. The list does not include phospholipids or DNA/RNA bases (Figs. 13 and 25 respectively).

Name used	Abbreviation
Inorganic phosphates	
1. Orthophosphate ion	P_i
2. Calcium hydroxyapatite	
3. Pyrophosphate ion	
4. Polyphosphate ions	
Phosphoric monoesters; one phosphorus per biomolecule	
5. Adenosine-5′-phosphate	AMP
6. Creatine phosphate	P-Cr
7. Dihydroxyacetone phosphate	DHAP
8. Glucose-1-phosphate	Glucose-1-P
9. Glucose-6-phosphate	Glucose-6-P
10. Glyceraldehyde phosphate	GAP
11. Phosphoenolpyruvate	PEP
12. Phosphorylcholine	
13. Phosphoserine	
14. Phosphorylarginine	

Name used	Abbreviation
Phosphoric oligoesters; more than one phosphoric monoester per molecule	
15. 1,3-Diphosphoglycerate	
16. 2,3-Diphosphoglycerate	DPG
17. Fructose-1,6-biphosphate	FBP
18. Glucose-1,6-biphosphate	
19. Inositol pentaphosphate	
20. Inositol hexaphosphate	Phytic acid
Diesters of phosphoric acid	
21. Glycerol-3-phosphorylcholine	GPC
22. Glycerol-3-phosphorylethanolamine	
23. L-Serine ethanolamine phosphodiester	
24. Transfer RNA	t-RNA
Higher phosphates	
25. Adenosine 5'-diphosphate	ADP
26. Adenosine 5'-triphosphate	ATP
27. Cytidine 5'-triphosphate	CTP
28. Guanosine 5'-triphosphate	GTP
29. Thymidine 5'-triphosphate	TTP
30. Uridine 5'-diphosphate	UDP
31. Uridine 5'-triphosphate	UTP
32. Uridine 5'-diphosphoglucose	UDPG

II. ^{31}P NMR OF ORTHOPHOSPHATE SPECIES

Most phosphorus in biological systems is present in the form of orthophosphate esters or salts (bone), and an understanding of those factors which influence their ^{31}P NMR spectra is fundamental to the interpretation of results from biochemical systems. A variety of factors affect the ^{31}P chemical shift of monoesters, but diesters are relatively unaffected and this has been used to distinguish them in the presence of each other. Gorenstein (7) investigated the effects of changes in the oxygen–phosphorus–oxygen bond angle (Fig. 1) and torsion angle (8) on the ^{31}P chemical shift of orthophosphate diesters. This work has been used in the study of phosphodiesters in DNA etc.

The effects in aqueous solution of ionic strength and various counter-ions on phosphate ester chemical shifts have been studied (Fig. 2). (9) The change in chemical shift as the pH is changed (generally shown by a high frequency shift as the pH is increased) has long been known, but the demonstration that this effect could be used as a non-invasive method for determining the pH within tissue compartments was first made by Moon and Richards in 1973. (10) What is probably the second most biologically useful chemical shift

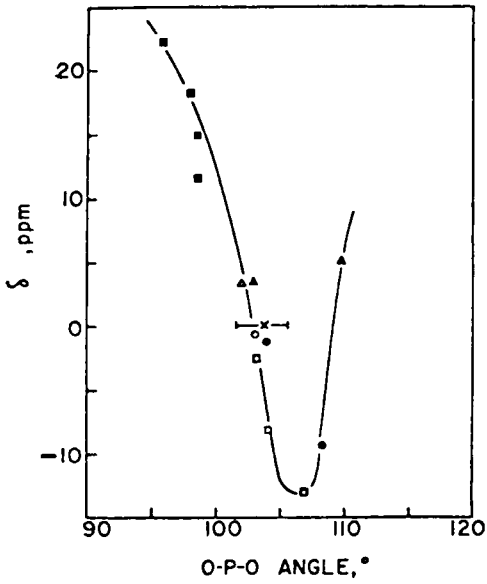

FIG. 1. ^{31}P NMR chemical shift of phosphate esters as a function of O–P–O bond angle (■ five-membered cyclic esters; △ monoester dianions; × monoester monoanions; ● acyclic diester free acids; □ six-membered cyclic esters; ▲ Li_3PO_4); the curve has no theoretical significance. (7)

effect, that arising from $^{18}O/^{16}O$ isotope effects, has been discovered only recently and is now being applied to biological (enzyme) problems. This shift dependence upon the oxygen isotopic composition of the phosphate group (Fig. 3) allows ^{18}O labelling and thus determination of phosphate bond-breaking mechanisms. (11–13)

The effects of solvent, cation, and pH on orthophosphate spin–lattice relaxation times (T_1) (14, 15) and on nuclear Overhauser effects (NOE) (16, 17) have been described, although these have not yet been widely used in biochemical investigations. Several detailed accounts of the chemical shift assignments, ^2J(P–O–P) spin-coupling constants, cation effects, and Mg(II) complexation of condensed orthophosphates (chain polyphosphates and cyclic metaphosphates) have appeared. (18–20) These reports on inorganic compounds might appear to be out of place in a biochemical review, but ^{31}P NMR has been used to confirm the presence of naturally occurring inorganic polyphosphates with chain lengths of from 10 to >5000 condensed orthophosphate units in fractions isolated from bacteria, (21) mammalian brain, liver and other tissues. (22) Although it has been postulated that these polyphosphates are the vestigial remains of "metabolic fossils", no universally accepted explanation of their function has been proposed as yet.

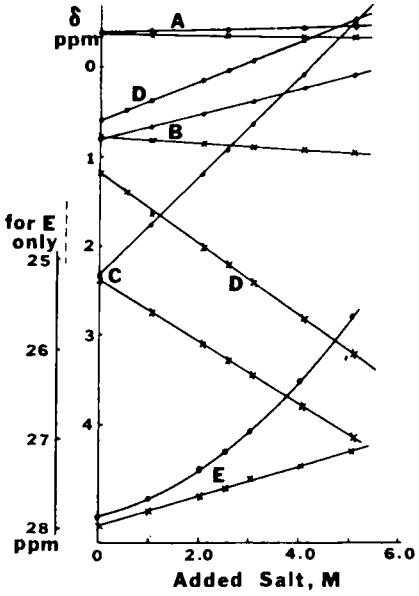

FIG. 2. ^{31}P NMR chemical shifts of 0·01 M aqueous solutions at pH 7·00 as a function of added salt concentration for (A) triethyl orthophosphate, (B) the diethyl orthophosphate anion, (C) the monoethyl orthophosphate anion, (D) the inorganic orthophosphate anion, and (E) the ethylphosphonate anion (● added salt is tetramethylammonium chloride and tetramethylammonium is the phosphate counterion; × added salt is sodium chloride and phosphate counterion is sodium ion). (9)

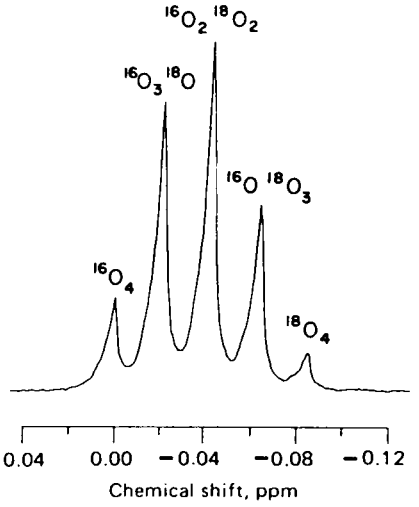

FIG. 3. 145·7 MHz ^{31}P NMR spectrum of a randomized sample of P_i(^{16}O, ^{18}O). (11)

An unusual class of naturally occurring orthophosphate analogue compounds are the phosphonates, in which there is a direct C–P bond [1].

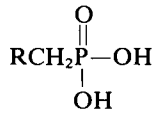

[1]

Although their presence in ruminant protozoa had been reported, no direct method for the determination of phosphonates existed until the development of ^{31}P NMR. (23) Their occurrence in lipid extracts obtained from various marine invertebrates was shown by ^{31}P NMR spectroscopy. (24, 25) Phosphonates have a substantially different chemical shift from the orthophosphate ^{31}P NMR region.

Much of the basic work of establishing the stereosensitivity of phosphorus–proton couplings in P–O–C–H and P–O–C–C–H systems had been performed before 1970. Further reports of theoretical studies and of more accurate quantitative correlations continue to appear. (26, 27) However, since most experimentally determined values are usually obtained from ^{1}H NMR spectra [e.g. (28)], the subject will not be further considered here.

Most studies of the association of biological phosphates with metal ions are concerned with nucleoside phosphates, which are considered in the next section of this review. Nevertheless, occasional reports have appeared of the interaction between magnesium ions and simpler organic phosphates of biochemical significance. These include acetyl phosphate (29) and 2,3-diphosphoglycerate (DPG). (30) DPG is a human red blood cell metabolite, which exercises a control function on haemoglobin oxygen exchange and is found to have two independent divalent metal ion binding sites of similar affinity ($K_D = 3{\cdot}0 \pm 0{\cdot}5$ mM), one on each phosphoryl group.

Phosphate esters of carbohydrates form a major class of biological substances that are detected by ^{31}P NMR. These are important both in the cell metabolism and as structural components. The multiplicity of carbohydrate forms that can affect the ^{31}P NMR spectrum has been discussed. (31) Likewise, Costello *et al.* (31) have discussed the variety of ^{31}P NMR signals that arise from carbohydrate cell-wall components.

III. MONO- AND DI-NUCLEOTIDES

Nucleoside monophosphates are the primary structural units of nucleic acids (Section VII), and nucleoside di- and tri-phosphates are fundamental in biological energy transfer. Nucleoside phosphates are known as nucleotides. As a consequence of their importance in biochemistry, they have been extensively investigated, with much of the work being performed before the

period covered by this review. Nevertheless, further studies continue to be reported in the literature, many of which are not detailed here. This section presents a representative selection of publications of particular importance for biological ^{31}P NMR, rather than an exhaustive compilation of the latest work.

A. Introduction

Cozzone and Jardetzky (32) reported the ^{31}P NMR spectra of adenine, uracil, and thymine mononucleotides, their cyclic analogues, and corresponding dinucleotides. From the pH dependence of the chemical shift (Fig. 4), pK_a values of the second ionization of the phosphate group were found. These lie between 6·25 and 6·30 for all the 5′-mononucleotides examined, being unaffected by the nature of the base or by the presence or absence of a 2′-hydroxyl group. The comparable pK_a values for the 3′-mononucleotides are between 5·71 and 5·85 in the presence of the 2′-hydroxyl group (i.e. ribonucleotides) and are about 6·25 in its absence (i.e. deoxyribonucleotides).

In both 3′,5′-cyclic mononucleotides and the dinucloetides ApA, dApdA, UpU, UpA, and ApU, the phosphorus resonance was unaffected by pH change over the range 3–12. An exception is TpT, of which the chemical shift change with titration showed an inflection at a pH value corresponding to ionization of the thymine base (pK_a = 9·9).

In a further publication (33) these authors extol the advantages of using ^{31}P NMR spectra in the determination of J(P–H) coupling constants, thereby avoiding any problems associated with complex ^{1}H NMR spectra and their complete assignment which may require extensive computer simulation. They reported that the ^{31}P signal from 5′-mononucleotides consists of a triplet, due to ^{3}J(P–H) coupling to the pair of 5′-protons, each component of which is split into a close doublet due to ^{4}J(P–H) coupling to the 4′-proton. The value of ^{3}J(P–H$_{5'}$) is 4·9 Hz and is virtually independent of pH over the range tested (1–12), temperature, nature of the base, and presence or absence of the 2′-hydroxyl group. This indicates that the orientation about the O$_{5'}$–C$_{5'}$ bond remains constant under these perturbations and the value of the coupling is consistent with a *gauche–gauche* conformation [2]. However, the ^{4}J(P–H$_{4'}$) coupling is found to be sensitive

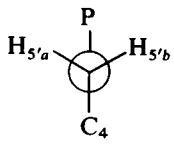

[2]

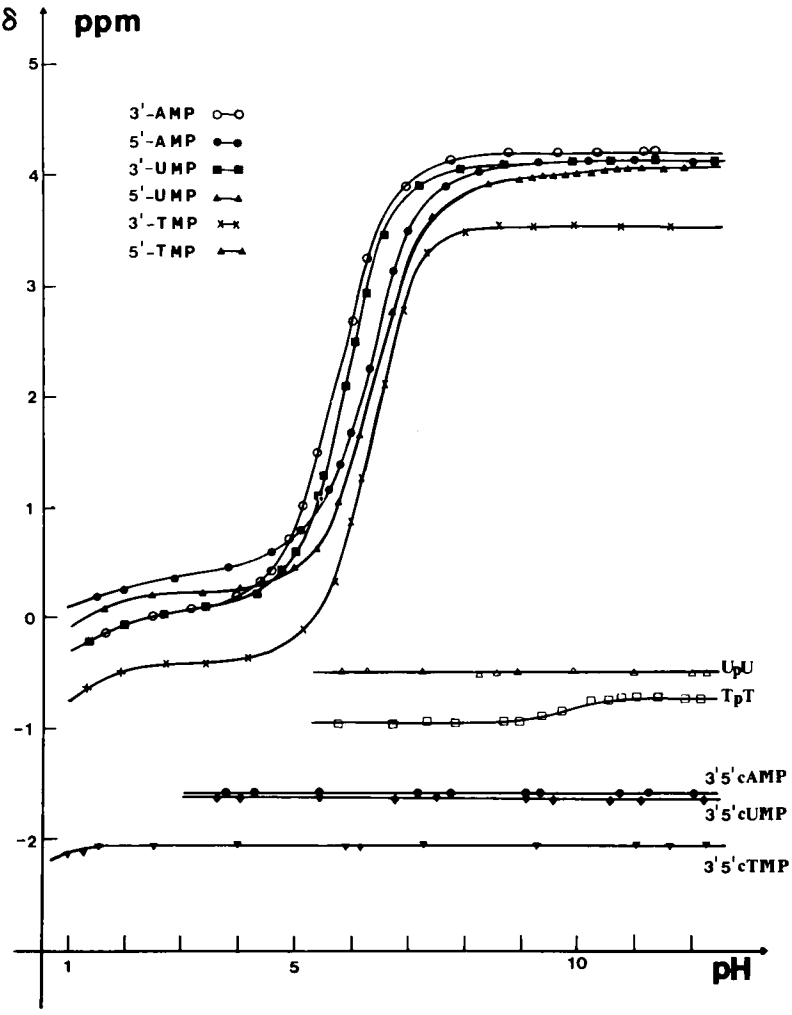

FIG. 4. ^{31}P NMR chemical shifts of various nucleotides as a function of pH from 5mM nucleotide solutions (○ 3'-AMP; ● 5'-AMP, 5'-dAMP; ■ 3'-UMP; ▲ 5'-UMP, 5'-dUMP, 5'-TMP; ×3'-TMP, 3'-dAMP). (32)

to pH changes (being a maximum of ~2·5 Hz in acid and a minimum of ~0·5 Hz in alkaline conditions), and also sensitive to the structure of both ribose and base groups. The maximum value corresponds to a coplanar W arrangement of the P–$O_{5'}$–$C_{5'}$–$C_{4'}$–H linkage. This all-*trans* structure, which becomes destabilized in the 5'-mononucleotides on deprotonation of the phosphate, is also found in dinucleotides but is not affected by pH in this case.

Labotka *et al.* (34) examined the conformations of nucleoside diphosphates and triphosphates in aqueous solution and in anhydrous tetramethylurea. The latter is, they claimed, a more appropriate environment since the surfaces of enzyme proteins and biomembranes, where many biochemical reactions occur, are best considered as non-aqueous. The chemical shifts and coupling constants (Table I) are inferred as supporting a structure folded about the ribose ring with the phosphate side-chain overlying the base. In ATP there is evidence that this conformation is stabilized by the formation of a hydrogen bond between the β-phosphoryl group and the 6-amino nitrogen of the base. The self-association of ATP in D_2O solution was studied by ^{1}H and ^{31}P NMR and the results, while indicating association, failed to distinguish between the alternative situations of limited monomer–dimer–trimer base stacking or unlimited polymeric linear models. (35)

TABLE I

Nucleotide ^{31}P NMR chemical shifts and coupling constants in water and in anhydrous tetramethylurea at H^+ ion concentrations corresponding to pH 7·40. (34)

Compound	Solvent	Chemical shifts[a]			Coupling constants (Hz)	
		α	β	γ	$J(\alpha-\beta)$	$J(\beta-\gamma)$
ADP	H_2O	−11·13	−6·96		23·1	
	TMU	−10·84	−8·54		22·6	
ATP	H_2O	−11·45	−22·66	−7·33	19·75	19·75
	TMU	−12·25	−23·17	−10·64	25·6	23·6
dATP	H_2O	−11·43	−22·83	−7·71	20·50	20·50
	TMU	−13·47	−23·46	−10·46	28·3	24·6
TDP	H_2O	−11·26	−7·02		23·6	
	TMU	−13·61	−13·61		—[b]	
UDP	H_2O	−11·18	−6·85		23·6	
	TMU	−9·40	−8·80		20·8	
UTP	H_2O	−11·50	−22·92	−7·52	20·53	20·53
	TMU	−12·36	−22·70	−10·45	25·1	23·8
IDP	H_2O	−11·03	−7·11		22·1	
	TMU	−9·40	−9·40		—[b]	
ITP	H_2O	−11·49	−22·84	−7·63	20·75	20·75
	TMU	−12·34	−23·03	−10·87	25·1	23·6
CDP	H_2O	−11·13	−6·94		22·6	
	TMU	−9·66	−8·98		23·3	
CTP	H_2O	−11·51	−22·77	−7·25	20·25	20·25
	TMU	−12·28	−22·74	−10·45	25·1	23·1
GDP	H_2O	−11·10	−6·69		23·1	
	TMU	−9·45	−9·45		—[b]	
GTP	H_2O	−11·49	−22·85	−7·70	19·25	19·25
	TMU	−12·04	−23·12	−10·97	25·6	25·0

[a] In ppm relative to 85% H_3PO_4.

[b] Not measurable because of equivalence of α and β groups.

B. Interaction of nucleotides with metal ions

The topic of this sub-section is the interaction of nucleoside diphosphates and triphosphates with metal ions; it has been known for a long time that these interactions have great biological significance. The conclusions of the early workers in this area using ^{1}H and ^{31}P NMR on ATP were that Mn(II), Co(II), and Ni (II) bind to all three phosphate groups whereas Mg(II), Ca(II), and Zn(II) bind to the P_β and P_γ groups only. (2)

Subsequent T_1 studies on ATP at various temperatures using Mn(II) were thought to show that P_α is more distant from the metal than P_β or P_γ, consistent with binding via the latter pair of phosphoryl moieties. (36) A more extensive investigation, using lanthanide(III) ions (Pr, Nd, Eu, or Yb) and measuring their perturbing effect on the eight ^{1}H and three ^{31}P resonances, allowed the calculation of a number of possible conformations. One of these, which closely agrees with one of the known solid-state ATP conformations (X-ray diffraction), has the lanthanide ion binding predominantly to P_β and P_γ phosphoryl groups. (37) Further work on the binding of Cu(II) to ATP at pH values between 8 and 12 was thought to show binding to P_β, P_γ, and to N(7) of the base at neutral and slightly alkaline pH. However, at pH 11·5, no binding to the phosphate chain or base could be detected and it was suggested that binding occurs via the ribose group. (38)

The interaction between ATP and Mg(II) is of particular interest since the latter is an essential *in vivo* cofactor in many enzymatic reactions in which ATP is a substrate. Since the published conclusion that Mg(II) binds both P_β and P_γ phosphoryl groups, subsequent results have been interpreted in the same way. (39) However, an alternative explanation (40) has been given for the chemical shift changes of the P_β and P_γ resonances observed on Mg(II) binding to a whole range of nucleoside triphosphates, including ATP, GTP, and UTP, at neutral and acid pH values. This is that only P_β binds the metal ion and that the shift of the P_γ resonance arises from a consequent change in the pK_a of the P_γ-phosphoryl group. A similar explanation for the Mg(II)–nucleoside diphosphate interaction has been put forward by the same group, (41) in that metal binding only occurs via the P_β group and that the P_γ resonance shift is a pK effect.

C. Interaction of nucleotides with biogenic amines

The interactions of various physiologically active amines with ATP have been investigated to determine if there could be a simple molecular basis for the hypothesis that ATP is involved in the uptake, storage, and action of these compounds.

Granot (42) measured the changes in phosphorus chemical shifts, coupling constants, and T_1 values for adenine nucleotides when dopa (3,4-

dihydroxyphenylalanine, a catecholamine) or norepinephrine (a hormone of the adrenal medulla) were added at constant (acid) pH. (42) He concluded that association occurs between the phosphate and amine, probably by electrostatic interaction with the protonated ammonium group. The interaction is primarily via the α-phosphate, with the terminal phosphoryl group (P_β of ADP and P_γ of ATP) participating to a lesser extent. He also examined the interactions between the same amines and ATP–divalent metal ion (Mg, Co, Ni, Mn) chelates. (43) The induced chemical shifts indicated a 1 : 1 : 1 stoichiometry of catecholamine–ATP–M(II) complex. He found that the catecholamine associates only via the ATP molecule, with no direct interaction with the metal ion, and that the stability of these ternary complexes is lower than that of the binary ATP–catecholamine complex. Association of epinephrine (adrenalin) with Mg(II)–ATP at acid pH has also been reported; (39) again bonding via the P_α phosphoryl group and the protonated amino group is suggested, and again the interaction is reported to be weak.

The effect of Cu(II) on the spectra of AMP and spermine was observed by ^{13}C and ^{31}P NMR. (44) No chemical shift change in the AMP ^{31}P resonance was noted although the signal was ultimately nulled when sufficient Cu(II) was added. ^{13}C NMR showed the nucleotide purine ring to be affected and not the amine. Although these NMR results suggested no interaction with the spermine, it is concluded from circular dichroism measurements that ternary complex formation actually occurs.

IV. ^{31}P NMR OF LIVING TISSUE AND SINGLE-CELL SPECIES AND THEIR COMPONENTS

Living tissue is fundamentally different from defined mixtures of chemicals in that the life process requires a series of phosphate-containing substances which are interdependent and heterogeneously organized. Gradients of concentration, pH, and complexants have long been known to exist, so from first principles it was clear that ^{31}P NMR of tissue would have broad spectral features. Nevertheless, remarkable and fascinating results have been obtained. Such work has required the conjunction of a range of skills and disciplines, as well as expensive instrumentation, so the results reviewed in this section arise from the efforts of a few groups in the UK and USA.

A. Direct ^{31}P NMR observation of intact resting muscle

The first ^{31}P NMR observations of living tissue were made at 129 MHz in a specially constructed NMR spectrometer (45) by the Oxford group. (46) Observation of an intact muscle from a rat hind leg showed several

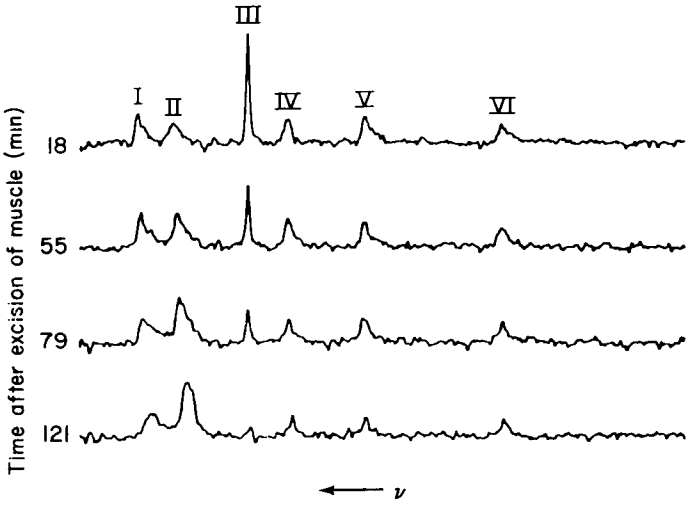

FIG. 5. First published ^{31}P NMR spectra of an intact muscle, from a rat hind leg, recorded at 129 MHz. Peak assignments are: I, sugar phosphate and phospholipid; II, P_i; III, P-Cr; IV, γ-ATP; V, α-ATP; VI, β-ATP. The times are the midpoints of the 50 scan spectral accumulations. The muscle was bathed in a minimum volume of calcium-free Locke ringer. (46)

phosphorus-containing substances (Fig. 5) known to be important in muscle activity. These included creatine phosphate (P-Cr) and ATP together with inorganic phosphate (P_i) and sugar phosphates. The internal pH of the muscle was measured by calibration of P_i chemical shift and found to decrease as the muscle aged. This and other aspects of the muscle behaviour could be correlated with established biological processes. Thus, the ratio P-Cr/P_i observed depended on the degree of stimulation of the rat muscle before the animal's death. As the muscle aged, [P-Cr] declined but [ATP] was initially unaffected. The P_i line-width suggested that a range of pH values were present in the muscle sample. The Chicago group observed the same general phenomena in intact frog muscles. (47) ^{31}P NMR spectra of perchloric acid extracts showed the same general features as the muscle but with greater resolution (Fig. 6). The line-widths in the extract were greatly reduced by the addition of ethylenediaminetetraacetic acid (EDTA).

Comparison of intact excised muscles (48) by ^{31}P NMR showed significant differences between normal and diseased states, vertebrates and invertebrates, and even in the same muscle of different species (Fig. 7). [ATP] remained unchanged until the P-Cr had almost disappeared, and the ATP chemical shifts indicated it to be complexed with Mg(II) and not Ca(II). The pH of frog muscle as shown by P_i chemical shift (10) is 7·2. Measurement of T_1 for P-Cr (49) in muscle and model solutions at 4 °C shows dipole–dipole interactions with Mg(II) to be the dominant relaxation pathway in both

circumstances. Measurement of T_2 for P-Cr thereby indicates a concentration of 4·4 mM for intracellular free Mg(II). The temperature of 4 °C was used to maintain the physiological condition of the muscle for sufficient time to permit ^{31}P NMR observation; however, other workers (50) have developed a system in which excised muscles can be maintained at physiologically ambient conditions for many hours (Fig. 8). Taking into account the need to preserve magnetic and RF homogeneity, muscles are supplied with oxygen, nutrients, and electrical impulses and the muscle tone is monitored. Under these conditions [P-Cr] approximates to that measured chemically but, most significantly, [P_i] is less than half that found chemically. This work indicates that ^{31}P NMR observation is capable of non-invasive, dynamic muscle investigations that probe the muscle energy processes more effectively than any chemical analysis.

The first *in vivo* observations of P_i chemical shifts (46) indicated that some distribution of pH is likely. Apparent line-widths for P_i are much broader than for P-Cr, (51) and as excised rabbit white muscle ages the broad P_i signal develops two peaks. The T_2 value measured by the CPMG method is ~100 msec corresponding to a line-width of only ~3 Hz, and thus the broad P_i signals arise from many partially overlapping components presumably caused by pH compartmentation. By contrast, P_i signals of rabbit red muscle do not broaden in this manner and show a lower [P-Cr] consistent with the known lower requirement for this substance in slow red muscles compared with fast twitch white muscles. These apparent compartmentation effects are

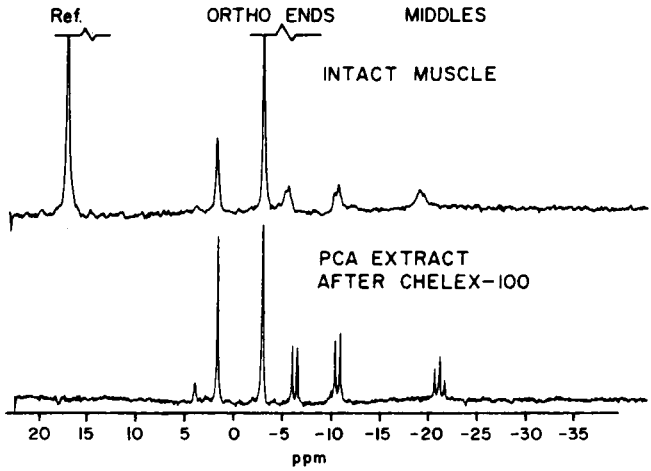

FIG. 6. 36·4 MHz ^{31}P NMR spectra of a Southern frog leg muscle (top) and perchloric acid (PCA) extract of this muscle (bottom) taken from the other leg of the same frog. Peak assignments are the same as in Fig. 5, except that an external chemical shift reference appears at the far left in the top spectrum. (48)

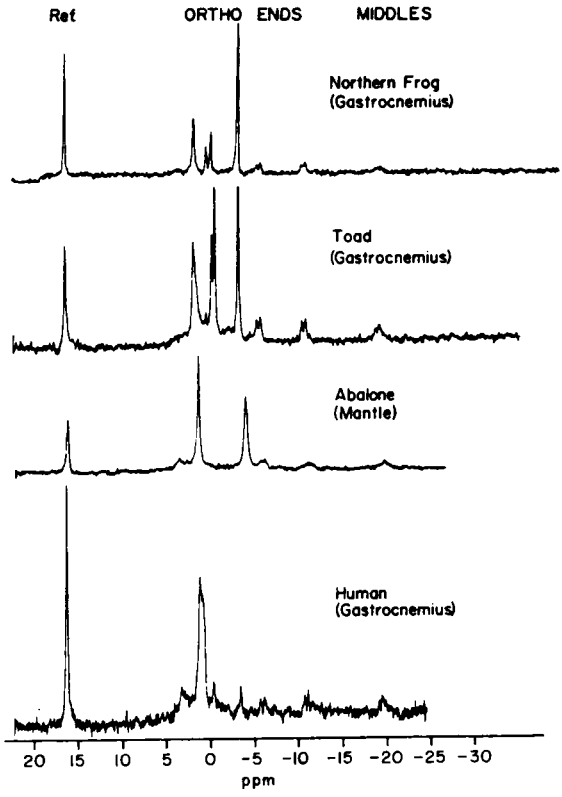

FIG. 7. Comparison of the 36·4 MHz ^{31}P NMR spectra of various muscles. (48)

not observed with P-Cr or ATP even when the muscles are placed in solutions of low pH. (52) However, P_i signals of intact muscles in aqueous sodium acetate at pH 5·2 simulate the same type of broadening and splitting, but are unaffected by the presence of Mn(II) (known not to penetrate cell walls unlike acetate) and thus the compartmentation is intracellular. While these experiments do not define the compartments or show that the metabolites are distributed in the same way in undisturbed muscle, these ^{31}P NMR results infer detection of P_i in the sarcoplasm and sarcoplasmic reticulum.

Unexpected ^{31}P NMR resonances were detected (53) in the phosphodiester region in all cardiac and red muscles examined by the Chicago group, but not at significant levels in undiseased white muscles. Extraction into perchloric acid yielded a substance identified as glycerol-3-phosphorylcholine. This was detected at relatively high concentration in dystrophic chicken pectoralis muscles. Further ^{31}P NMR investigation (54)

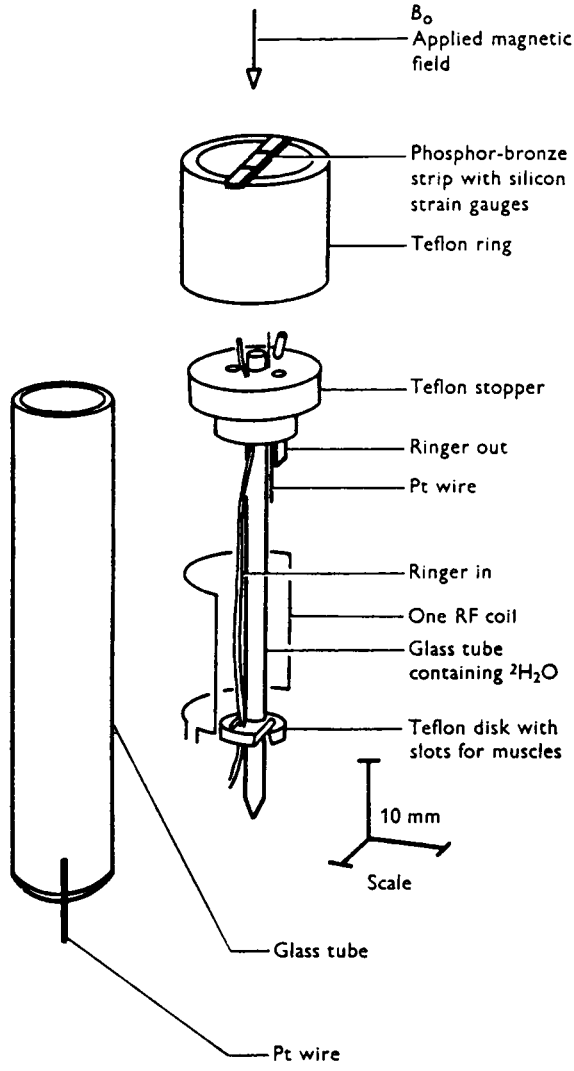

FIG. 8. Design of experimental chamber for maintaining muscles within the NMR tube. The volume in which the NMR measurement is made is defined by the two single-turn radio-frequency (RF) coils, only one of which is shown in the diagram. The arrangement allows for stimulating, recording tension, and perfusing oxygenated Ringer solution. (56)

of chickens with this hereditary condition revealed other phosphodiesters, one identified as L-serine ethanolamine phosphodiester being characteristic of this condition but not found in other parts of the bird. Examination (55) of $HClO_4$ extracts of biopsies from human dystrophic muscles showed no P-Cr,

almost no ATP, and [NADH] almost five times normal. Glycerol-3-phosphorylcholine normally present was absent, but other resonances were observed in the phosphodiester region. ^{31}P NMR examination of an ageing human muscle from a patient with a neuromuscular disease showed approximately half the normal phosphorus, with [P-Cr] decreasing, [P_i] increasing, and ATP declining earlier than normal.

B. Direct ^{31}P NMR observation of contracting and recovering muscle

The Oxford group have developed a technique for the maintenance of excised muscles and their electrical stimulation. Muscles are mounted on a device to measure forces developed by stimulation in the NMR tube. Initial results (50) for resting muscle show that good muscle condition is maintained. After contraction, recovery in [P-Cr] can be followed and a second P_i, that formed on contraction, disappears. Contraction itself is difficult to study, but in a later publication (56) these workers have presented the accumulated results of many contractions. The concentrations of ATP, P-Cr, P_i, and sugar phosphates are all in reasonable agreement with those found chemically.

Similar observations were made (57) with muscles chemically treated to inhibit selectively stages in the energy process. Contracted muscles with glycolysis poisoned by iodoacetate and cyanide in oxygen-free conditions show neither subsequent P-Cr hydrolysis nor replenishment of P-Cr. Thus, the contraction process is shown to have used approximately half the original P-Cr. In pseudo-recovery of the muscle, [P_i] decreases and [sugar phosphates] increase concomitantly. These and other ^{31}P NMR experiments confirm directly and independently the validity of methods of quick freezing, extraction, and chemical analysis devised over many years. In other work, (55) sustained isometric contraction caused by caffeine is shown to exhaust completely P-Cr while in a control muscle much of the P-Cr was metabolized to ATP. In muscles treated with 2,4-dinitrofluorobenzene and iodoacetate, (58) the ATP disappears quickly thereby showing that anaerobic glycolysis is insufficient even for the resting energy consumption, but that oxidative phosphorylation is sufficient for this purpose.

Following these experiments, it is possible (59) to relate muscular fatigue (i.e. decline in force development measured by the device in Fig. 8) to changes in the concentrations of phosphorus metabolites, the decrease in rate of phosphorus utilization, and the rate at which ATP is hydrolysed. [H^+] increased in fatigue, and in severe fatigue the γ and β ATP peaks shift as if H^+ displaces some Mg(II) from $MgATP^{2-}$.

C. Direct ^{31}P NMR observation of intact hearts

Following the successful observation of intact muscle metabolism, (46) the Oxford group (60) described ^{31}P NMR observation at 129 MHz of intact

rat hearts. After excision and rapid cooling to 0 °C to induce cardiac arrest, hearts were observed at 4 °C in Ringer's solution. The characteristic spectrum of sugar phosphates, P_i, P-Cr, and $MgATP^{2-}$ was obtained as with resting muscle. By warming to 30 °C in order to impose an energy requirement, the decline of [P-Cr] and [ATP] is seen at the same time as a pH drop from 7·0 to 6·0. Later work (61) with a perfusion technique showed that hearts can be kept alive at 37 °C for at least 5 hours and without appearance of ischaemic patches, i.e. patches appearing to suffer from loss of blood-flow. The ^{31}P NMR results for perfused hearts compare favourably with those from extracts of freeze-clamped hearts and demonstrate the feasibility of studying cardiac metabolism by this NMR method.

Hearts cooled to 0 °C were mounted on a glass tube and perfused with warm buffer gassed with 95% O_2–5% CO_2. ATP was shown to be present as MgATP, P_i indicated a pH of 7·4, and the anomalous ratio of ATP resonances suggested the presence of NAD^+/NADH. After the perfusion was stopped temporarily so as to induce global ischaemia, recovery of the phosphorus metabolites was followed after its resumption. A group at Baltimore described similar work (62) with ^{31}P NMR at 40·5 MHz but with added refinement of simultaneous measurement of the left ventricular pressure to monitor the heart's performance during NMR spectroscopy. Partial ischaemia was induced by decreasing the pressure of circulating fluid and led to reduced [P-Cr] and [ATP] and reduction in the heart's performance. Global ischaemia caused a pH drop from 7·4 to 5·7 as measured by the chemical shift of P_i, which was eventually the only species observed. Some P_i appeared to be washed out into the perfusing fluid during ischaemia.

Later work by this same group was performed in a wide-bore superconducting NMR spectrometer with ^{31}P observation at 72·9 MHz. Beating rabbit hearts weighing approximately 6 g were perfused at 36 °C (Fig 9) and afforded a greatly improved signal/noise ratio. (63) By tying off an artery, regional ischaemia is induced, and then detected by the appearance of a P_i signal (corresponding to pH 6·6) additional to the P_i of the rest of the heart (pH 7·4). In order to confirm that the additional signal is for the ischaemic zone, total ischaemia was induced and the pH 7·4 P_i signal disappeared. The authors suggested that the ^{31}P NMR capability of distinguishing normal from ischaemic tissue could one day allow medical diagnosis of heart damage with NMR spatial resolution techniques. (64) Using the same equipment, these workers (65) described rapid ^{31}P NMR observations from which usable spectra can be obtained in 30 seconds total observation. Together with the simultaneous monitoring of the heart's muscular performance, relatively rapid kinetic analyses of ischaemic effects are made. After inducing total ischaemia, 60–90 s elapse before a pH change can be observed by ^{31}P NMR although the muscular performance has declined by

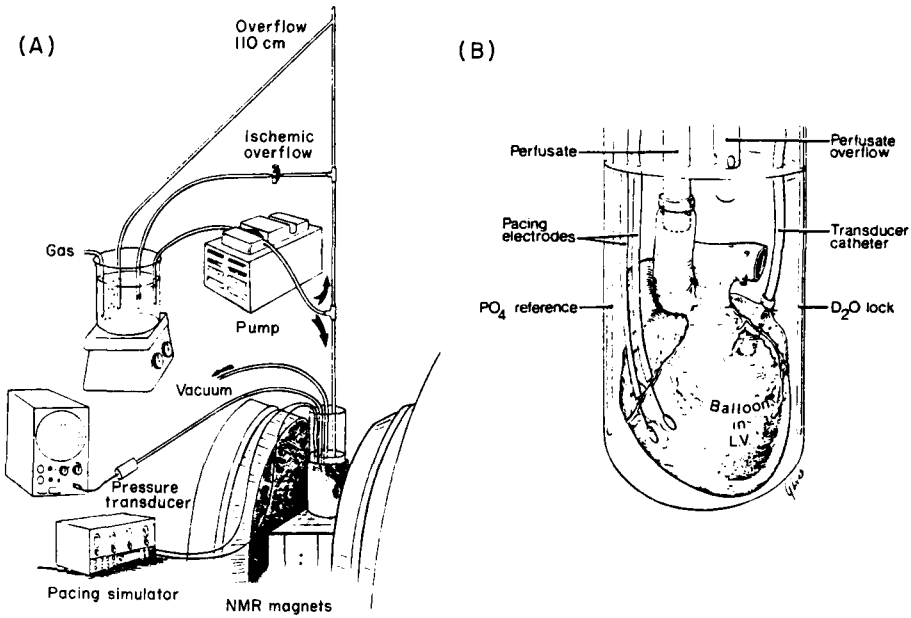

FIG. 9. Diagram of a perfused heart in the NMR spectrometer with accessory instrumentation as used by Hollis and coworkers. (63) (A) Arrangement of perfusate bath, peristaltic pump, perfusate flow lines with normal (110 cm) and ischaemic overflows, pressure transducer with oscilloscope, and pacing simulator. The vacuum line is for perfusate removal. (B) Exploded view of the perfused heart in the NMR sample tube. The perfusate cannula is positioned in the aorta above the aortic valve. Isovolumic left ventricular pressure was measured with a fluid-filled balloon and the hearts were paced with electrodes sewn on the surface of the right ventricle.

60% in 20 seconds. Following total ischaemia for 40 minutes, reperfusion led to a pH of 7·35 and P-Cr was restored but only 50% of the heart function was recovered. Physiological experiments had previously suggested that the low-oxygen-induced pH decrease was responsible for the loss of heart performance. These rapid ^{31}P NMR experiments show this not to be so but instead that other unobserved changes cause loss of performance and then the pH changes. This was checked by perfusing hearts with fluid saturated with N_2 instead of O_2–CO_2. (66) After 20 min, the pH declined only to 7·21, [P-Cr] and [ATP] were only slightly reduced, and heart muscular performance declined only by 26%. Thus ^{31}P NMR in these experiments revealed that lack of oxygen caused relatively minor changes compared to those of ischaemia.

The same group examined the effect of KCl arrest, (67) a commonly used method to arrest heart beat and prevent irreversible damage to cardiac tissue. Hearts subjected to ischaemia for 40 min in the presence of KCl

showed a pH decrease to 7·0, and the retention of most ATP and some P-Cr, unlike control ischaemic hearts which declined to pH 6·1. Re-perfusion of KCl-arrested hearts showed full recovery of performance after 6 min and virtually complete recovery of [ATP] and [P-Cr]. Non-arrested hearts at 40 min after re-perfusion commenced showed only 70% recovery of performance and an abnormal P-Cr/ATP ratio although the pH is restored to the previous value of 7·4. The observed effect of KCl arrest is as predicted from physiological experiments. These perfusion fluids contain physiological amounts of Ca(II) as it has been established previously that perfusion without Ca(II) causes marked cell damage on re-exposure to Ca(II). A study (68) of this "calcium paradox" was performed at various temperatures since it is known that low temperatures alter the calcium flux across cell membranes. First, ^{31}P NMR showed retention of ATP and P-Cr in Ca(II)-free perfusion, and morphological examination shows a limited amount of cell damage. With re-exposure to Ca(II) at 37 °C there is complete and rapid disappearance of all organic ^{31}P resonances and corresponding severe cell damage. At lower temperatures, this damage is reduced such that at 30 °C almost complete protection is found. Thus the value of ^{31}P NMR is demonstrated for a rapid non-invasive evaluation of living and working hearts which can be directly correlated with morphological studies.

D. Direct ^{31}P NMR observation of other organs and whole creatures

Human kidney transplants are subject to a substantial failure rate. ^{31}P NMR spectroscopy has been used to study (69) a rat kidney situation as close as possible to human transplantation. Initially, excised rat kidneys were examined at 129 MHz at 4 °C, and P-Cr, ATP, P_i, sugar phosphates, and a phosphodiester were found. The energy pool was gradually depleted during this cold ischaemia corresponding to the period when a human kidney is stored prior to transplantation. This depletion is relatively rapid, possibly due to low [P-Cr] but, unlike heart and muscle, there is no significant pH decrease. Re-perfusion by blood connections to an "assist" rat (Fig. 10) led to the re-synthesis of ATP, which seems to occur via intermediate ADP.

Using a wide-bore superconducting NMR spectrometer, other workers (70) were able to place an anaesthetized rat in the NMR tube so that its brain was within the active volume. Relatively broad signals were obtained for ATP, P-Cr, P_i, and sugar phosphate; the resolution was insufficient to detect much effect of low oxygen supply except the usual reduction of P-Cr and ATP seen in damaged tissue. Better resolution was obtained by rapid freezing of brain tissue to −196 °C followed by a ^{31}P NMR examination at −12 °C, a temperature at which sufficient molecular mobility exists. The usual pattern of phosphorus metabolites is observed, together with the usual changes as the sample ages. This fast freezing technique is calculated to trap

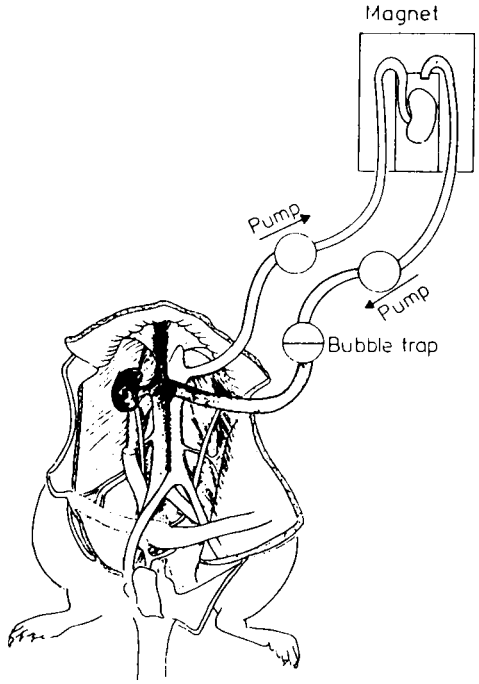

FIG. 10. Perfusion of a small rat kidney using the blood circulation of a large "assist" rat. The right kidney of the large rat has been removed and its aorta and vena cava connected to the external blood circuit. (99)

the metabolites in a normal metabolic state, and the authors suggest it to be a valuable innovation in this field.

Perfused rat liver was studied by Salhany *et al.* (71) with ^{31}P NMR at 60·7 MHz and showed the expected array of phosphorus metabolite peaks including ATP and NAD^+, but pH was not determined. While maintaining oxygen flow, 2 mM KCN was introduced into the perfusing fluid and caused an immediate change as shown by apparent loss of ATP and substantial enhancement of external [P_i]. However, no ADP was visible and the authors suggested that it was bound within the liver mitochondria to paramagnetic species. As cyanide is known to bind reversibly to cytochromes, cyanide-free re-perfusion was performed and some restoration (~40%) of ATP occurred. The authors suggest that the advantage of being able to follow high energy phosphate metabolism during a liver toxic event should prove useful in characterizing the effects of other toxic substances such as ethanol and drugs.

Perfused ventral nerve cords from crayfish were examined by Nishikawa *et al.* (72) It was found that excitability of the cords remained with oxygen

gassing of the perfusate, but was reduced by nitrogen gassing of the perfusate and lost altogether with no perfusion during ^{31}P NMR spectroscopy. The spectra (of poor signal/noise ratio) show the presence of several sugar phosphates and ATP but are dominated by phosphorylarginine; all these disappear in the absence of perfusion. For these

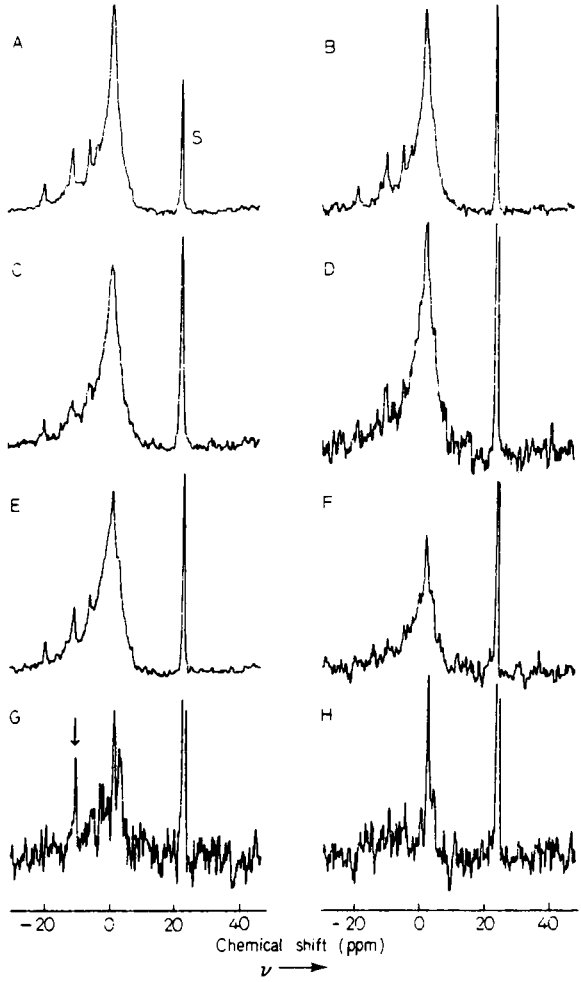

FIG. 11. 129 MHz ^{31}P NMR spectra of developing tadpoles (*Xenopus laevis*). Spectra were obtained from: (A) unfertilized eggs (600); (B) mid-blastula, stage 8 (349); (C) late gastrula, stage 11 (285); (D) post-neurala, stage 23 (160); (E) spontaneous movement, stage 26 (384); (F) heart-beat, stage 33/34 (218); (G) swimming tadpole, stage 41 (106); (H) feeding tadpole, stage 46 (83). Numbers in brackets above refer to the number of embryos contributing to spectra. Indicated peak in spectrum G was not reproducible. (73)

experiments, twenty freshly isolated nerve cords were suspended in a 10 mm NMR tube; the excitability could be maintained for 10 hours.

^{31}P NMR spectroscopy has been used to follow the development of *Xenopus laevis* (frog) eggs into tadpoles. (73) Despite poor resolution, nucleoside triphosphate, P-Cr, and P_i can be distinguished in the developing eggs until the stage of spontaneous movement (Fig. 11). Although the creatures are subjected to intense magnetic and RF fields, there is no apparent abnormality; this may be significant for the postulated human medical uses of NMR spectroscopy.

The ^{31}P NMR spectroscopy of living tissue is the subject of a recent review. (74)

E. Possible use of ^{31}P NMR for discrimination of malignant tissue

Considerable controversy exists as to the utility of NMR for distinguishing normal and malignant tissues. There has developed a substantial literature on the possible use of ^{1}H NMR since the original suggestion of Damadian, (75) and recently ^{31}P NMR has been similarly investigated. T_1 values were measured for several rat tumours and the corresponding normal tissues. (76) The ^{31}P values in tumours are found to be substantially longer and in no case to overlap the T_1 range of normal tissue. Spectral differences were sought (but not found) in order to distinguish tumour from normal tissue (77) and for the far-fetched proposed application of NMR for cancer therapy. However, later work (78) by this group with improved equipment detected small chemical shift differences for P_i and sugar phosphate in malignant mice tissues, and apparently no P-Cr or ATP in a mouse sarcoma. These preliminary results are alleged to show a significant pH shift and a metabolic difference from normal tissue.

Work by others has aimed at explaining the apparently successful discrimination of malignant tissue by T_1 of the metabolic phosphates. One cause proposed (79) is that the major nuclear relaxation pathway for phosphorus is by way of its interaction with cell water. This is believed to be much more tightly bound in normal tissue and it is suggested that ^{31}P amplifies such differences relative to ^{1}H NMR because of the smaller ^{31}P gyromagnetic ratio. Another cause advanced (80) is the increased level of K^+ in malignant tissue and the much reduced relaxing effect this has on metabolic phosphates compared with Na^+.

F. ^{31}P NMR of muscle and bone components

The molecular basis of muscle action is known to involve networks of interpenetrating proteins known as actin and myosin which are caused to slide past each other with the involvement of ATP. ^{31}P NMR has been used in a few studies of muscle protein, isolated chemically as distinct from the

intact muscle work. Cozzone *et al.* (81) studied the binding of ATP to rabbit muscle actin in the pH range 6·5–10·5 and found by T_1 and T_2 measurements that the β and γ phosphate portions of ATP bind to actin via a calcium bridge. Bagshaw and Reed (82) investigated the equilibria in complexation of ADP with a myosin sub-fragment, with Mn(II) substituting for the biologically essential Mg(II). Mak *et al.* (83) used ^{31}P NMR and other techniques to study phosphorylation of one myosin fragment; the result suggested a covalently bound phosphate in α-tropomyosin and its absence in the β component of rabbit skeletal muscle.

Bone and tooth are formed by mineralization of protein, and ^{31}P NMR has been used (84) to investigate chelation-extracted bovine dentine. The residual protein was found to be particularly rich in phosphoserine which readily bound calcium as shown by broadening of the ^{31}P signal. IR data show the presence of calcium–carboxylate interactions, so that carboxylate and orthophosphate are involved in regions of high-affinity binding. Circular dichroism data suggest the presence of sheet-like arrays that may present faces for initiation of crystal growth. ^{31}P NMR observation of the solid calcium hydroxyapatite present in bone and tooth gives very broad lines. Yesinowski (85) has obtained a line-width of about 100 Hz by preparing very finely divided material as a colloidal suspension. Griffin (86) obtained high resolution spectra by magic-angle spinning and was able to distinguish the final calcium hydroxyapatite from an intermediate mineral calcium phosphate species in incompletely mineralized, forming teeth.

G. *In vivo* ^{31}P NMR studies of bacterial and mammalian cells

In vivo NMR studies of single cell species present far fewer technical problems than differentiated tissue. In principle, intact single cells can be maintained almost indefinitely in NMR conditions. The first report (87) of this kind concerned ^{31}P NMR studies of yeasts at 145·7 MHz. Several metabolic phosphates were observed, but of particular significance was the detection of long-chain polyphosphates. The results are consistent with polyphosphate acting as a phosphate store in the yeast cell, and the molecular weight is determined by ratioing the end to middle peaks. The cells appear to maintain their cytoplasmic pH around 6·3 which is much higher than the acidic extracellular pH at which they normally live. A later report on yeasts (88) describes the use of both ^{31}P and ^{13}C NMR to analyse the fermentation process, and the production of extracellular ATP from adenosine. While ^{31}P NMR can detect only those species containing phosphorus, ^{13}C NMR detects many more substances and this demonstrates a limitation of the ^{31}P technique.

Escherichia coli is a much studied species that similarly is amenable to *in vivo* NMR observation. Suspensions of *E. coli* were observed at 145·7 MHz

(89) and phosphomonoesters, P_i, nucleotide triphosphate, NAD^+, UDPG, polyphosphate, and phosphoenolpyruvate were found. The chemical shift of P_i has been used to determine both intracellular and extracellular pH and thus the ΔpH across the cell wall. In cell respiration, the cells maintain an internal pH of 7·55 despite the external pH being varied in the range 6·0–8·0. The results are consistent with a ΔpH being created by reversal of the ATPase reaction and with protons being pumped outward during respiration. Several carbon sources and an ATPase inhibitor were used in experiments that led to these conclusions. In order to maintain oxygen levels, oxygen was bubbled through in synchronization with the lock system. (90) In this way the pH is measured with a time resolution of a few seconds, and it is shown (91) that while the internal pH is maintained by the cells at $7{\cdot}5 \pm 0{\cdot}1$ for >15 s after oxygen bubbling ceases the internal pH decays in several minutes.

Further work was conducted by these authors on *E. coli* in anaerobic conditions. (92) The previously listed range of metabolic phosphates was observed, but dihydroxyacetone phosphate was also found. With glucose as a carbon source, *E. coli* produces acids anaerobically and develops a transmembrane ΔpH. Glycolysis can be determined from the change in external pH, and the rate found to be strongly dependent on external pH. By use of ATPase inhibitor and other reagents, it is postulated that ATP produced by glycolysis is hydrolysed by membrane ATPase to generate a ΔpH.

Mammalian tumour cells have been cultured to produce stable single cell growths that may relate to human cancer conditions. Ehrlich ascites tumour cells were examined (93) by ^{31}P NMR at 145·7 MHz both as intact cells and $HClO_4$ extracts. As extracts, the substances detected are fructose-1,6-biphosphates (FBP), dihydroxyacetone phosphate (DHAP), ATP, ADP, AMP, P_i, NAD^+, phosphorylcholine, glycero-3-phosphorylcholine, glycero-3-phosphorylethanolamine, and glyceraldehyde-3-phosphate (GAP). Higher resolution is obtained with the extracts than with the cells, but all these substances except the last can be detected *in vivo*. From the known pH dependence of P_i, it is shown that the ΔpH value is $<0{\cdot}2$ pH unit. It is possible to show that the hydrolysis of FBP $\rightleftarrows$ DHAP + GAP is in equilibrium but that the DHAP $\rightarrow$ GAP reaction is not. In the presence of oxygen, [ATP] increases as [ADP] decreases. Thus an extraordinary amount of dynamic metabolic detail is determined.

Similar ^{31}P NMR work (94) on HeLa cells grown from human tissue culture gives comparable detail. However, it is found possible to resolve the four nucleoside triphosphates (ATP, GTP, UTP, and CTP) in model admixture at pH 7·4, and thereby to determine that UTP is one-fifth of the total HeLa cell nucleoside triphosphate. The authors were able to detect the effect of enzyme inhibitors and concluded that ^{31}P NMR may allow direct

observation of the effects of anti-cancer drugs. Other human cell lines were examined (95) and found to display no appreciable ΔpH across the cell membrane, unlike the large ΔpH detected in micro-organisms. Many phosphorus metabolites are distinguished, but there is no common metabolic pattern among the various mammalian tumour cell lines except possibly in that phospholipid metabolites seem to occur at high concentration.

Isolated rat liver cells were examined (96) at 4 °C at 145·7 MHz; phosphorus metabolites were detected, and ΔpH was measured between the mitochondria and cytosol in the intact cell. Valinomycin, a substance known to enhance ΔpH, was added and ΔpH followed with time. External pH was changed and, whereas the cytosolic pH responded, the mitochondrial pH remained constant. From these experiments it is concluded that mitochondrial P_i is present in a higher pH environment. In a separate study (97) by the same workers, mitochondrial pH was measured as being 7·4. Many phosphorus metabolites were observed, and it was possible to follow oxidative phosphorylation by separate resonances of P_i and adenine nucleotides both internal and external to the mitochondria. There is an apparent increase in total internal [ATP + ADP], but it has not been ascertained whether this is from phosphorylation of AMP or due to freeing of tightly bound ATP/ADP in the energization of mitochondria.

H. ^{31}P NMR studies of chromaffin granules

Chromaffin granules are the catecholamine storage vesicles of the adrenal medulla that accumulate adrenalin by a mechanism apparently coupled to a proton-translocating ATPase. ^{31}P NMR observations were made at 129 MHz of the intragranular ATP in order to measure the internal pH. (98, 99) A pH value of 5·6 ± 0·1 was determined from the γ-phosphorus chemical shift, and then found to decrease by 0·2–0·5 unit on addition of external ATP in the presence of ions such as chloride that can penetrate the granules. This is a significant change as the granules have substantial buffering capacity; however, the method of pH measurement relies upon chemical shift calibrations of ATP in a simulated environment.

Other workers (100) have subsequently sought to obtain a more representative pH calibration and have demonstrated that the titration curve for the P_γ of ATP is quite different from that of *in vitro* sodium, calcium, or magnesium salts of ATP, or of ATP in the physiologically stoichiometric mixture. After using nigericin/K^+ to collapse ΔpH across the granule membrane, direct intragranular titration becomes straightforward and leads to an *in vivo* pH value of 5·7. Subsequently it is calculated that this pH value has ~95% of the adenosine ring nitrogens unprotonated and ~95% of ATP P_γ protonated, thereby leaving ATP with a minimum net charge. This is reckoned to be consistent with the high packing density of

ATP in the granules and with the consequent pH dependence of the granule function.

From the measurable buffering capacity of a reconstituted intragranular solution pH changes may be converted into an absolute number of protons translocated. (101) This appears to be 1·0 per molecule of ATP hydrolysed, which agrees with those from a chemical method and with H^+/ATP stoichiometries calculated from the pH observed in the external medium. The ^{31}P NMR of excised adrenal glands is nearly identical to that of the isolated granules and so the ^{31}P NMR technique is believed not to perturb significantly the characteristics of the granule matrix.

V. ^{31}P NMR STUDIES OF PHOSPHOLIPIDS AND RELATED COMPONENTS OF MEMBRANES

A. Introduction

Biological membranes were regarded for many years merely as permeability barriers, but more recently they have come to be considered as dynamic multifunctional structures. Development of isolation techniques for the membrane components, and application of investigational tools to membranes have led to a realization of the importance of the membrane in cell biology. Relatively recent reviews on the application of NMR spectroscopy (102–104) contain little or no reference to the use of ^{31}P NMR in this field. A review prepared in 1976 (105) contains a few references to ^{31}P NMR, and it is since then that so much ^{31}P NMR work on membrane systems has appeared. However, NMR is only one of many tools used in the study of membranes; a recent review (106) compares and contrasts all the physicochemical techniques for probing membrane structure. In the majority of recent ^{31}P NMR publications concerning membranes, the work described has also employed other techniques such as differential scanning calorimetry, scattering methods, or electron spin resonance.

Membranes are assemblies (Fig. 12) of a variety of materials only some of which are amenable to ^{31}P NMR observations. ^{13}C and ^{1}H NMR observations appear separately or in conjunction with ^{31}P NMR work in order to probe other membrane components or other parts of phospholipids. Most of the work concerning ^{31}P NMR of membranes involves the observation of phospholipids (Fig. 13) which form a characteristic bilayer. Apart from the fact that there are several types of phospholipid found in greatly varying proportions according to the source of the membrane, the nature of the substituent fatty acids shows great variation and therefore many combinations and permutations of these discrete phospholipid components are found even within one membrane. Consequently, there are believed to be hundreds of phospholipids in the human red blood cell membrane. (107)

In addition to the phospholipids, sterols, especially cholesterol, are found as a major constituent of membranes. Their role is uncertain, and a number of the reviewed ^{31}P NMR publications examine the effects of cholesterol. However, the rigid cholesterol molecules may be imagined as stiffening inserts within a semi-fluid matrix of flexible phospholipids. Substances of high molecular weight that are found within the membrane include glycoproteins, glycolipids, and lipoproteins. The structural and functional effects that these large molecules have upon the membrane are not well understood. However, membranes also have molecules of which the function is well understood such as enzymes and photoreceptors. Some of the large molecules are believed to penetrate right through the membrane, while others are associated with only one side of it. Part of the ^{31}P NMR work reviewed here deals with the effect of such molecules.

Of profound importance for the ^{31}P NMR observation is the size of the membrane unit, its internal organization, and the thermal phase phenomena of the phospholipid matrix. For large units, the only motional narrowing in the NMR spectra is determined by local molecular motions. These local motions are restricted in the gel phase and yield broad NMR lines while better resolved spectral features are available from the liquid crystalline phase. Thus the phase transition temperature is a critical factor for this work. The best resolved ^{31}P NMR spectra for such materials have been achieved through the use of magic-angle spinning and intense proton decoupling.

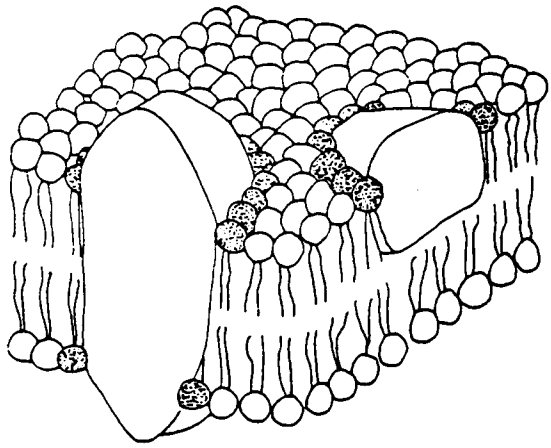

FIG. 12. A current "simplified" model for the organization of lipids and proteins in biological membranes. The spheres represent the polar head-groups of the phospholipid molecules and the wavy lines represent the fatty-acid chains. The larger globular structures represent protein molecules, and the shaded polar head-groups represent lipids interacting with the proteins. (151)

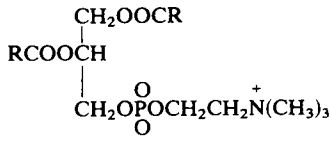

Phosphatidylcholine
(PC)

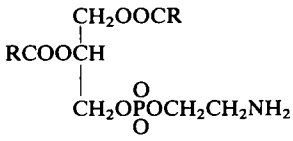

Phosphatidylethanolamine
(PE)

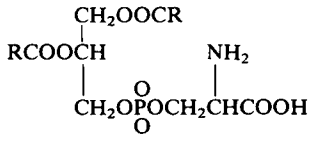

Phosphatidylserine
(PS)

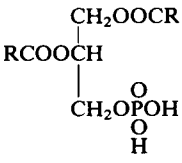

Phosphatidic acid

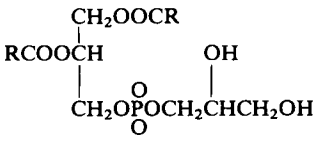

Phosphatidylglycerol
(PG)

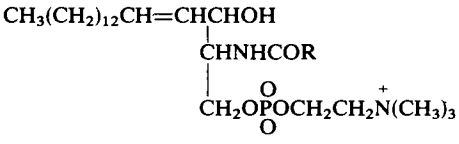

Sphingomyelin

FIG. 13. Major lipid components of membranes of which effects have been observed by ^{31}P NMR. Nomenclature follows that of the IUPAC-IUB Commission on Biochemical Nomenclature (*Biochem. J.*, 1978, **171**, 21–35). Extracts of natural membrane systems have widely varying mixtures of long-chain fatty-acid substituents, and the generic abbreviations above are used in this review unless synthetic, chemically defined phospholipids were the subject of the investigation. Lysophospholipids have one less fatty-acid substituent so that e.g. the glyceride backbone has a free hydroxyl group.

(108) Nevertheless, there is a large body of work concerned with analysis of the ^{31}P chemical screening anisotropy to obtain details of phospholipid head-group motion and orientation. By subjecting membranes and liposomes to intense ultrasonic irradiation, closed single bilayer vesicles are produced which have a quite different type of ^{31}P NMR spectrum (Fig. 14). Such vesicles yield highly resolved lines more akin to those from molecules in isotropic solution, presumably because the overall vesicle rotation is sufficiently rapid. (109) Vesicles are only a metastable aggregation of the phospholipid molecules, but provide useful working models for many purposes. Thus, the ^{31}P NMR phospholipid literature tends to fall into two categories depending upon whether the species under examination has been sonicated or not.

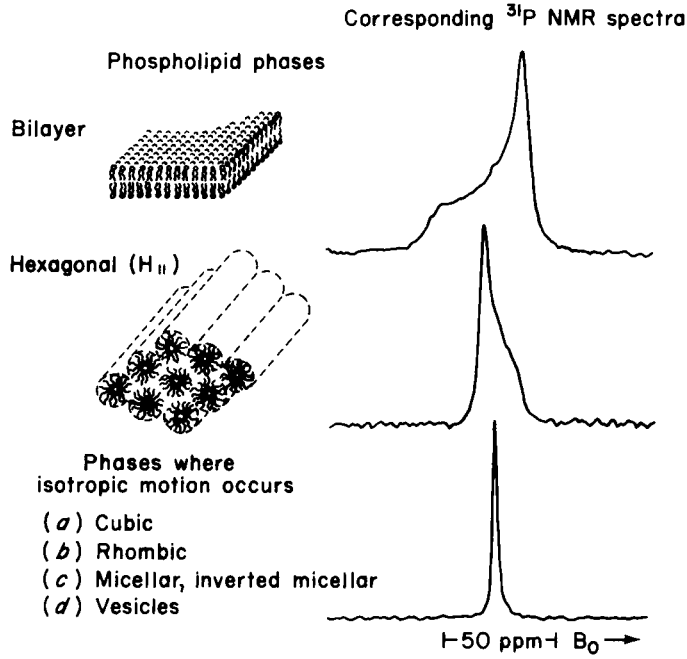

FIG. 14. Phospholipid phases and 36·4 MHz ^{31}P NMR spectra observed. The spectra were obtained from unsonicated aqueous dispersions of egg yolk PC at 30 °C (bilayer), soya PE at 30 °C (hexagonal H_{11}), and a mixture of the two (cubic, rhombic, or inverted micellar phase). (149)

B. Development of ^{31}P NMR spectroscopy of membranes and model membranes

The first ^{31}P NMR observations of aqueous phospholipid dispersions were made in the 1971–2 period in the UK, (110) USA, (111) and USSR. (112) The first group measured T_1 and T_2 for several sonicated lipid–water dispersions, and for dipalmitoyl-phosphatidylcholine at several temperatures. They concluded that the ^{31}P relaxation times reflect the mobility of the lipid head-group. The second group compared relaxation times and linewidths for unsonicated and sonicated phosphatidylcholines and found that sonication produced well defined ^{31}P resonances that are unchanged after further sonication. They also showed a spectrum of unsonicated membranes from *E. coli*. The third group were able to discriminate the inner and outer surfaces of phosphatidylcholine vesicles by addition of Pr(III) ions, a technique that they had previously developed in ^{1}H NMR work. Thus these basic observations and techniques were described almost as soon as FT NMR equipment became available.

Sheetz and Chan (113) examined the effect of sonication on a phosphatidylcholine bilayer system by ^{31}P and ^{1}H NMR and demonstrated a progressive narrowing of spectral lines as the vesicle size was reduced by sonication. They also attributed the spectral effects to variations in the molecular packing of phospholipid molecules in the bilayer phase. At about the same time, Davis (114) showed that there is a linear relationship between the line half-width in egg yolk phosphatidylcholine and the strength of the external magnetic field. Chemical screening anisotropy (CSA) of the lipid phosphate group was proposed to account for this phenomenon. Berden *et al.* (115) agreed with this explanation after examination of sonicated phosphatidylcholine and sphingomyelin vesicles and found it possible to distinguish outside and inside resonances at low external field and with the vesicles above the phase transition temperature. These authors concluded that, taking into consideration sensitivity and CSA line-broadening, the optimum frequency for ^{31}P NMR observation would be 50 MHz.

The gel–liquid crystalline phase transition occurs in many biologically important membranes, and several groups of workers have studied the effects upon ^{31}P NMR spectra using variable-temperature techniques. Göldner *et al.* (116) studied sonicated dipalmitoyl-PC dispersions in water and found a marked alteration in T_2 at 38 °C, but no significant effect upon T_1. The sharpness in alteration of T_2 with temperature increases with the time that the dispersion is allowed to stand after sonication. Uhing (117) confirmed the marked effect upon T_2 of temperature for this system. Further variable-temperature work (118) with dipalmitoyl-PC–water employing Pr(III) ions suggests that the rate of penetration of the bilayer by these ions is temperature dependent and sharply increases at the phase transition temperature.

The first publication by Bystrov *et al.* (112) demonstrated that ^{31}P NMR has a much greater usefulness for outside/inside ratio determination using paramagnetics than ^{1}H observation. A ratio of approximately 1·9 to 1 was obtained for sonicated egg lecithin vesicles in this first publication. The validity of this approach was confirmed by Hutton *et al.* (119) who found a value of $2{\cdot}1 \pm 0{\cdot}1$ regardless of the nucleus studied, position of the nucleus relative to the metal binding site, molar ratio of metal to phospholipid over three orders of magnitude, or location of the metal ion inside or outside the vesicle. They found that the metal ion apparently interacts with all of the phospholipid on the exposed bilayer surface in the NMR time-scale. With the bilayer remaining intact, only the outside surface is exposed to paramagnetic ions as with Pr(III) used by Bystrov *et al.* or Co(III) used by Berden *et al.* (115)

In considering the somewhat fluid nature of the lipid bilayer, it is of fundamental importance to be able to investigate the exchange of phos-

pholipid between vesicles, or between the inner and outer surface, or the fusion of two vesicles. By mixing dispersions of two types of vesicles, Bergelson and Bystrov (120) were able to observe the effect of proteins capable of catalysing such exchange between vesicles. Barsukov *et al.* (121, 122) have shown that the new phospholipid molecules are incorporated into the outer layer, thus creating asymmetric bilayers. This observation has permitted the study of exchange between the outer and inner surfaces.

A number of these publications utilise the interaction of metal ions with phospholipid bilayers; this technique has been widely used since by many authors. Of significance is the fact that metal ions are known to have important interactions with membranes in the natural state, with concentration gradients of Na^+, K^+, and Ca^{2+} being maintained by membranes. Hutton *et al.* (119) have thoroughly investigated the use of chemically-shifting paramagnetic ions for measuring inside/outside ratios; they also found that Ca(II) weakly interacts with egg PC vesicles and that the lanthanides are adequate substitutes for Ca(II) since neither metal is found to perturb measurably the average polar head-group conformation. Grasdalen *et al.* (123) examined the same interactions and found that the binding efficiency is controlled by the electrostatic potential produced by the cations bound to the membranes surface. Recent work by Barsukov *et al.* (124) has shown that anion binding has a fundamental influence on the effects of cations in ^{1}H, ^{13}C, and ^{31}P NMR spectroscopy. Nolden and Ackermann (125) have studied the interactions of egg PC and other phospholipid vesicles with several paramagnetic ions by ^{1}H, ^{13}C, and ^{31}P NMR spectroscopy, and found that Pr(III) ions reside close to the phosphate and methylenes of the PC head-group but relatively far from the $N(CH_3)_3$ end. McLaughlin *et al.* (126, 127) studied the interaction of Co(III) with glycerophosphoryl and PC membranes and found that Co(II) is useful as a model divalent cation for phospholipid bilayer membrane work. By use of electrophoresis, the binding is found to decrease in the order Mn(II), Mg(II), Ca(II), Co(II), Ni(II), Sr(II), Ba(II).

Workers at Oxford, UK, have devised a phosphonium analogue for choline (128) in order to provide a distinct ^{31}P NMR signal. Investigation of the gel–liquid crystalline transition temperature, the variable-temperature ^{31}P NMR behaviour, and distribution in vesicles (129) shows that the phosphonium analogue simulates choline well. Unsonicated liposomes containing the analogue give ^{31}P NMR spectra (Fig. 15) with the phosphonium ^{31}P resonance much sharper than the phospholipid resonances, i.e. without substantial broadening by CSA. The metabolism of this analogue in cultured cells is found to be similar in nearly all respects to that of choline. (130) Rats have been maintained on a diet in which choline was fully replaced by the analogue, (131) and using radio-labelling it is found that the analogue enters all tissues but with an adverse discrimination factor of

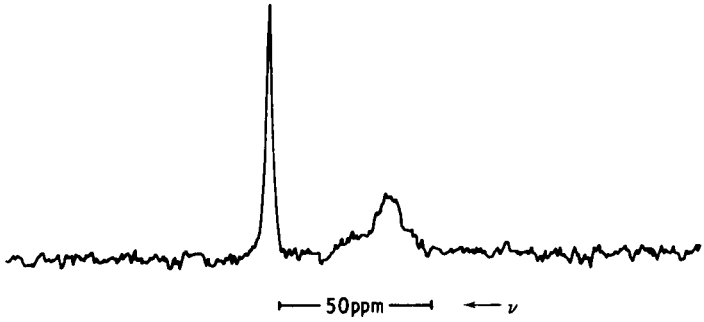

FIG. 15. 129 MHz ^{31}P NMR spectrum of unsonicated liposomes of the phosphonium analogue of distearoyl PC. The sharper resonance arises from the phosphonium signal. (129)

1·3–3·2. The ^{31}P NMR chemical shift of the phosphonium resonance is reported to be 28·2 ppm relative to external 85% phosphoric acid. The use of the analogue in labelling a range of cell membranes (132) is shown, and it appears that this technique has considerable promise for the application of ^{31}P NMR to membrane studies.

C. Use of ^{31}P NMR to distinguish the outer and inner layers of vesicles

When membranes or aqueous dispersions of phospholipids are subjected to ultrasonic irradiation, small vesicles are formed with a highly curved surface. Some biological membranes are known to have regions of high curvature, so results from the experimental vesicles may have direct application, as well as extrapolation to natural membranes enclosing larger systems. The generally used method of distinguishing the outer and inner layers of vesicles is by addition of paramagnetic ions, i.e. Eu(III), that chemically shift (Fig. 16) the resonances of the outer layer with respect to those of the inner layer. (112) Another technique (115) used initially is the addition of Co(II) to obliterate only the outer resonances by extreme broadening.

The main interest in distinguishing the outer and inner layers is to determine if there are chemical or physical differences between them. In one natural membrane system, it has been demonstrated (133) that PC and sphingomyelin are mainly in the outer layer but PE and PS are mostly in the inner layer. Several groups have examined the effects of sonicating together two phospholipids; the results are in Table II. It is apparent that the state of charge of the head-groups is of particular importance, but there are disagreements between publications for PC–PE mixtures, and PC–PA mixtures. It is likely that experimental error was significant in earlier publications in this field, especially in not sufficiently allowing for NOE and relaxation differences between the outer and inner head-groups.

^{31}P NMR and hydrodynamic data have been used by two groups of workers to calculate the packing geometry of egg yolk PC molecules in vesicles. Chrzeszczyk *et al.* (134) found that, although the total bilayer thickness is virtually identical to that of planar bilayers, the outer monolayer is thicker than the inner monolayer (Fig. 17). The average surface area for the head-group is found to be larger at the outer than at the inner surface, and the converse applies to the cross-sectional area of the hydrocarbon tails at the interface of the two monolayers. These figures imply that the hydrocarbon tails are more extended in the outer monolayer and that larger head-groups are more readily accommodated at the outer surface. Huang

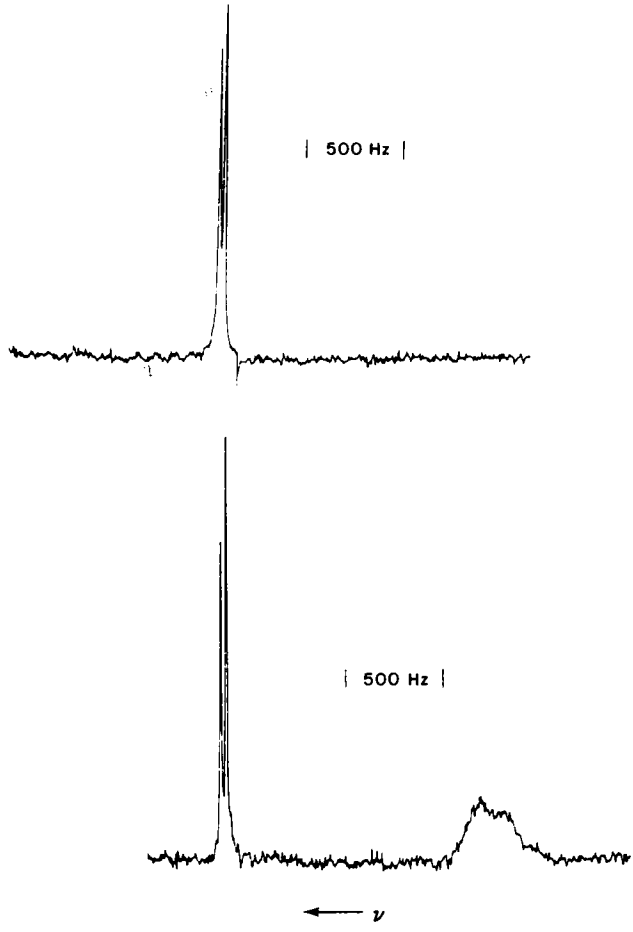

FIG. 16. 40·5 MHz ^{31}P NMR spectra of cosonicated PC–sphingomyelin at 50 °C (top), and in the presence of approximately 10 mole % Eu(III) (bottom). (141)

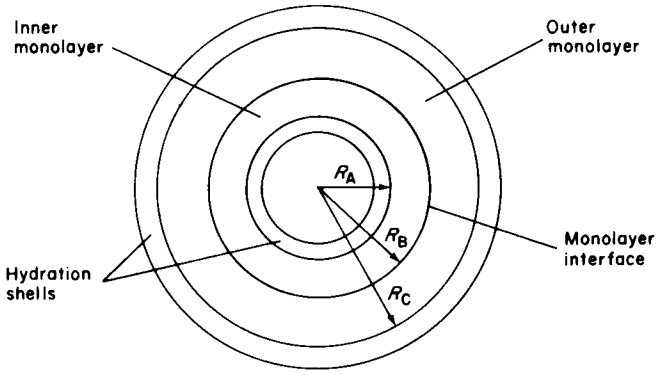

FIG. 17. Geometric packing parameters for egg PC vesicles.

	Ref. 134	Ref. 135
R_C (Å)	105–113	99
Outer thickness ($R_C - R_B$) (Å)	18–21·6	21
Inner thickness ($R_B - R_A$) (Å)	13·5–16·9	16
Head-group surface area: outer (Å^2)	70·8–80·4	74
inner (Å^2)	58·2–77·5	61
Acyl chain cross-section area at R_B: outer (Å^2)	45·0–56·5	46
inner (Å^2)	89·6–105·7	97

and Mason (135) have made a similar study, after fractionation of their material so as to have a homogeneous vesicle size. The data of the two groups are in agreement with each other and with data obtained by completely different methods.

In the light of these geometric considerations, it is interesting to re-examine earlier work on outside/inside asymmetry induced by the fatty acid components of the phospholipids. De Kruijff *et al.* (136) have found that the outside/inside ratio and the vesicle size are both affected by the lengths of the hydrocarbon chains. Increasing chain length gives lower outside/inside ratios and the introduction of *cis* or *trans* double bonds also has a slight effect. Yeagle *et al.* (137) using ^{31}P and ^{13}C NMR found that in mixtures of phosphatidylcholine derivatives the unsaturated chains preferred the outer monolayer. Incorporation of cholesterol into aqueous dispersions of either 1,2-dimyristoyl- or 1,2-dioleoyl-phosphatidylcholine produces larger vesicles (136) but, whereas cholesterol is symmetrically distributed with the saturated acyl derivative, it prefers the inside monolayer with the unsaturated derivative. Several detailed explanations of these phenomena have been advanced but it appears basically that unsaturated acyl chains prefer the longer and narrower environment of the outer monolayer.

Much of the above work made use of paramagnetic ions to distinguish the outer and inner monolayers by creating a difference between the aqueous

TABLE II

^{31}P/^{1}H determinations of asymmetric concentrations in cosonicated phospholipids

Phospholipid mixture	Conclusion	Aqueous conditions	Ref.
PC and sphingomyelin	o/i for lecithin = 1·53; o/i for sphingomyelin = 1·97	pH 7	115
Egg PC and phosphatidylglycerol (PG) equimolar	No segregated patches; outer layer has PG/PC = 2	pD 8·0	138
Egg PC and PE equimolar	No asymmetry detected	pD 11·0	139
Egg PE and PC total PE/PC = 1·08	Outside PE/PC = 0·92; inside PE/PC = 1·38; thus PE favours inner layer	pD 7·2	140
Egg PC and PA	PA prefers inside, but vesicle is not really formed	pD 6	140
Egg PC and PS	PS prefers inside at lower pH values, but outside with pD > 9	pD > 9	140
Egg PC and Pinositol	Pinositol prefers inside		140
PC and PS	PS/PC outside *ca.* 3	pD 8·3	125
Egg PC and beef brain sphingomyelin	Slight sphingomyelin preference for outer surface; may be experimental error	pD 7·7	141
Various acyl derivatives of PC with cholesterol	Cholesterol strongly prefers inside layer with one acyl derivative but not another	pD 7·0	136
Egg PC and PA	No asymmetry detected	pD 7·0	142

solutions adjacent to the monolayers. When vesicles are prepared by sonication of aqueous dispersions, the aqueous volume enclosed within the vesicle contains species present in the original aqueous phase thereby allowing the use of marker molecules. Chrzeszczyk *et al.* (143) have labelled the vesicular inner cavity with dimethyl phosphate in order to supplement the information available with just Pr(III) ion effects alone. It has been shown that, when such labelled vesicles are broken by resonication, the label is lost on a one-shot basis rather than gradually. Palatini *et al.* (144) have included 0·3 M Na_2HPO_4 at pH 7 in order to determine the effects of external media in altering the internal pH. Acetate is able to penetrate the membrane rapidly, chloride less rapidly, and sulphate not at all. Other workers (145) entrapped glucose-6-phosphate in order to follow pH changes.

D. Use of ^{31}P NMR to study phospholipid translocation and cell fusion

The normal biological processes of cell division, cell fusion, etc., and the fluid mosaic concept of membrane structure, together imply that phospholipid molecules have substantial mobility within the biological

membrane. The demonstration that paramagnetic shift reagents allow the outer and inner surfaces of bilayer membranes to be distinguished by ^{31}P NMR (112) led to a study of phospholipid exchange between vesicles formed separately of phosphatidylinositol and phosphatidylcholine. (121) It was shown that there is a slow spontaneous exchange of phospholipid which is greatly accelerated in the presence of a protein fraction from rat liver. However, it was also shown that the vesicles maintained their integrity during the exchange. This work has led to an examination of the mechanism of the protein's action (120, 122) and it is concluded that the protein is adsorbed on to the outer monolayer prior to detachment of P_i and transport as a lipoprotein to the PC vesicle. This thereby produces asymmetric vesicles with P_i only in the outer monolayer. P_i is found to be transported one-way only from P_i vesicles to PC vesicles, but in contrast to this specific action of the protein, added lyso-PC (Fig. 13 caption) causes an indiscriminate exchange.

Stable asymmetric vesicles have been produced by several workers by co-sonication of phospholipid mixtures (reviewed elsewhere), and asymmetric membranes have been found in Nature. (146) De Kruijff and Baken (147) have treated egg PC vesicles with phospholipase D in order to convert some outer monolayer PC into phosphatidic acid and thereby to study its translocation to the inner monolayer. They found that phosphatidic acid thus formed is translocated with a half time of 30–40 min or less and that part of the inner layer PC moves to the outer layer. By ^{31}P NMR observation of P_i trapped inside the vesicles it was established that the vesicles preserve their structural integrity during this process. The Ca(II)-induced aggregation and fusion of mixed PC–phosphatidic acid vesicles has been studied (142). It is reported that a reversible vesicle aggregation precedes the Ca(II)-induced fusion and that the Ca(II) concentration required to cause vesicle fusion is related to the surface concentration of the phosphatidic acid in the outer monolayer. In the mixed phospholipid vesicle, Ca(II) ions significantly increase permeability to glucose-6-phosphate. However, no attempt has been made to determine whether the presence of Ca(II) increases the outside/inside ratio of phosphatidic acid by translocation to the outer monolayer.

The same general conclusions have been reached by Liaq and Prestegard (148) who examined the same phospholipid system. These authors used ^{14}C-labelled sucrose and tetraethylammonium bromide to show that vesicle contents were retained in the final structure after fusion. Use of Cd(II) successfully as a Ca(II) substitute allowed ^{113}Cd NMR which showed Cd(II) to be internalized during the fusion process. The ^{113}Cd chemical shift suggested a phosphate interaction. This is consistent with Ca(II) internalization and it was suggested that progressive internalization of Ca(II) as fusions occur would eventually limit the extent of Ca(II)-induced fusion in these and other systems.

Cullis and Hope (149) observed unsonicated aqueous dispersions of erythrocyte ghosts (i.e. the empty membranes) incubated with reagents known to induce fusion of erythrocytes. The ^{31}P NMR spectra show the progressive conversion from the bilayer to the hexagonal (H_{11}) phase as more "fusogenic" agent is added. These agents, namely oleic acid and glycerol mono-oleate, allow well-defined spectra of the phospholipids only in the presence of Ca(II) ions. However, these substances were added at concentrations approximately equimolar with the phospholipids present. A mechanism of cell fusion was proposed wherein protein-free areas of bilayer make contact and the two outer monolayers combine to form a zone of intermediate hexagonal (H_{11}) phase which is subsequently restabilized to bilayer structure for completion of the fusion process (Fig. 18).

E. ^{31}P NMR studies of phospholipid head-group behaviour

Most of the lipids in biological membranes are phospholipids for which ^{31}P NMR provides a tool to study the motion and average orientation of the phosphate group in relatively unperturbed samples. The effects of other membrane components, of ions and change of temperature or pH, can be determined indirectly through ^{31}P NMR spectroscopy. Relatively intact membranes which have been separated physically from cellular materials giving ^{31}P interferences, but not subjected to ultrasonic irradiation, yield broad (30–50 ppm wide) ^{31}P spectra. Purified phospholipids give somewhat similar spectra, and this whole area of work is characterized by broad asymmetric resonances (Fig. 14) that require fundamentally different treatment from high resolution ^{31}P NMR spectroscopy. The difference may arise in part from the effects of curvature on molecular packing (113), although some workers (150) have concluded that sonication does not disrupt significantly the structure around the phosphate group. This section deals with ^{31}P NMR investigations that do not exploit high resolution spectral information, such as chemical shift, but which derive information from the line-shape and intensity variations.

The broadness and asymmetry found with unsonicated PC bilayers, which is not so marked in their ^{13}C and ^{1}H spectra, (151) arises from the relative immobility of the phosphate group. The physical size of unsonicated membranes precludes the rapid rotational narrowing for the head-group phosphate found with sonicated preparations. (109) By comparison, the phosphonium ^{31}P signal in the phosphonium analogue of PC is much sharper than the corresponding phosphate resonance (129) presumably because the phosphonium motion is much less restricted. The asymmetry of the phosphate resonances arising from this aspect is fairly well understood and has been the subject of recent reviews. (152, 153) These provide an account of the mathematical interpretations of chemical shift anisotropy including the ^{31}P NMR examination of single crystals, powders, oriented bilayers, and

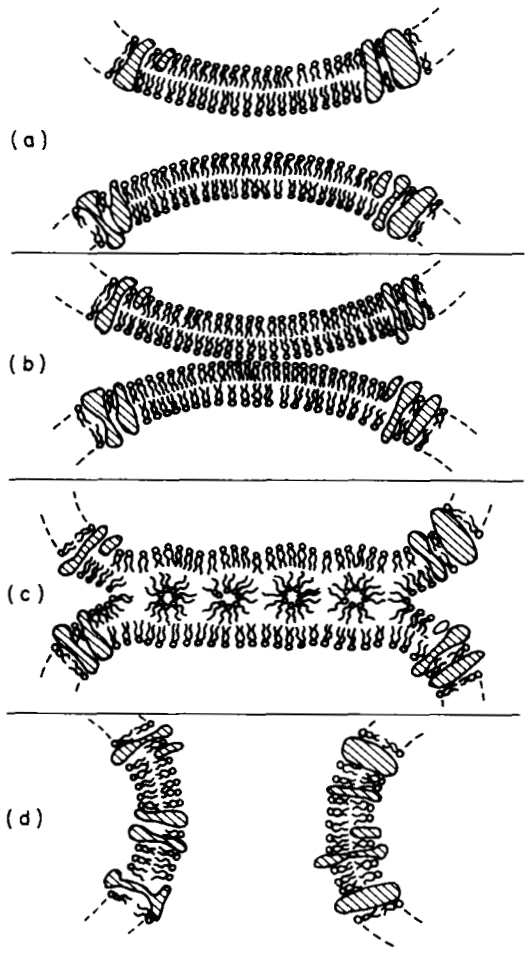

FIG. 18. Mechanism of membrane fusion proposed by Cullis and Hope. (149) The slashed areas traversing the membrane indicate integral membrane protein. Note that the diameter of the aqueous channels of the hexagonal phase component of part *c* are drawn approximately to scale with respect to the bilayer thickness.

biological membranes. Yeagle (154) has given a non-mathematical explanation of the same phenomena. In the present chapter the salient features of these reviews are presented together with more recent results and a compilation of biological systems examined by ^{31}P NMR.

Membrane lipids have often been assumed to be wholly ordered in a lamellar fashion of which the bilayer is the simplest case. However, various workers have shown that aqueous dispersions of phospholipids can adopt cylindrical structures (Fig. 14). Phospholipids have quite different motional

possibilities in the cylindrical (known as hexagonal H_{11}) phase or lamellar phase, resulting in a pronounced difference in the CSA. It has been shown (155) that ^{31}P NMR spectroscopy can be used to distinguish these two structures. Depending upon the relative interactions of the lipids with each other and the aqueous environment, one phase may be favoured over another. Forrest *et al.* (156) have concluded from the CSA that human aorta from an atherosclerotic patient is not in the hexagonal (H_{11}) phase. Other workers (149) have shown that cell fusion may occur via an intermediate hexagonal (H_{11}) phase. The CSA also has been used in various other publications to diagnose this profound change in phospholipid packing for lipid mixtures or where phospholipids have been treated with various reagents in the aqueous phase. Precise measurement of the CSA, (153) combined with data from other techniques, can give head-group conformations in phospholipids.

NOE data have been used extensively (154) to obtain head-group conformations. Observation of the ^{31}P NMR intensity as a function of the ^{1}H decoupling frequency has been used to show which protons are closest to the phosphate group because the NOE is critically dependent upon the ^{31}P–^{1}H internuclear distance. Selective deuteration of the head-group has helped to refine the information in this work, both by eliminating specific ^{1}H contributions and by permitting ^{2}H NMR observation.

1. Phosphatidylcholine

Phosphatidylcholine (PC) systems have been the subject of several types of investigation, all of which show that the choline head-group is aligned essentially parallel to the membrane surface. These include the ^{31}P NMR observation of oriented bilayers, (157–159) ^{31}P–(^{1}H) NOE in vesicles, (160, 161) combined ^{31}P CSA/^{2}H NMR data, (162, 153) and neutron diffraction. (163) Through combination of differential scanning calorimetry and ^{31}P NMR it has been shown that $\Delta\sigma$ (the difference in nuclear shielding for the various orientations of head-group with respect to the magnetic field) is insensitive to temperature above the gel–liquid crystalline transition temperature (164, 165) but that below the transition temperature $\Delta\sigma$ increases continuously with decreasing temperature. The transition temperature is taken to be a cooperative melting of the hydrocarbon chains, and variations in the hydrocarbon moieties have pronounced effects upon the transition temperature. Shorter fatty acid derivatives are found to lower the transition temperature as does unsaturation in the fatty acids. Cholesterol has the effect of abolishing the transition altogether.

The DSC of fully hydrated synthetic PC shows a pre-transition not evident from changes in the CSA (166) but coincident with line narrowing which is believed to be associated with the onset of rapid axial rotation of the

phosphocholine residue. (167) The effect of hydration on phospholipid ^{31}P NMR spectra is significant: Griffin (159) has observed PC powders in the presence of low water concentration and concluded that small amounts of water have a substantial influence. After 4–5 waters of hydration, the phosphate conformation appears to be unaffected by additional water. It has been shown (168) that, whereas binding of La(III) or $Fe(CN)_6^{3-}$ has no effect on the CSA, Eu(III) produces an apparent reversal of the CSA sign as well as chemical shift.

2. Phosphatidylethanolamine

Similar studies have been made with phosphatidylethanolamine (PE) systems, and it has been shown by both X-ray crystallography (169) and $^{31}P/^{2}H$ NMR (170) that the ethanolamine head-group is parallel to the membrane surface with the positively charged ammonio group interacting with a neighbouring phosphate. Thermal NMR studies (167) confirm previous calorimetric results wherein PE systems have higher (by 20–30 °C) transition temperatures than the corresponding PC systems. However, anomalous behaviour is found with unsaturated PE derivatives, in that both dioleoylphosphatidylethanolamine (167) and PE isolates [from human erythrocytes, hen egg yolk, and *E. coli* (171)] show well defined, reversible bilayer to hexagonal (H_{11}) phase transitions. However, addition of cholesterol to the natural unsaturated PE systems has no dramatic effect upon the transition. These effects with natural unsaturated PE derivatives are modified by a change of pH, and it is suggested that the phase transition may be related to important properties of biological membranes.

In the light of these findings, one should view critically the earlier works on PE systems wherein the PE was derived from natural sources, or mixed with PC in cosonicated vesicles. It has been found (139) that pH has a marked effect upon molecular motion; at physiological pH values, *E. coli* PE is found to be more restricted than PC. These alterations may well have reflected the bilayer–hexagonal (H_{11}) transition. Yeagle and coworkers (172, 161) observed ^{31}P–(^{1}H) NOE of mixed egg PE–PC vesicles, and concluded that the PC *N*-methyl groups interact with the phosphates of neighbouring PE molecules, but the PE amino groups do not. However, given the above-mentioned combined effects of pH and temperature on phase with egg PE systems (amongst others), these conclusions must be re-examined.

3. Sphingomyelin

As with PC and PE, ^{31}P NMR has shown that the sphingomyelin head-group is oriented parallel to the surface. (161) ^{31}P and ^{1}H data (173) on pure sphingomyelin and sphingomyelin–PC vesicles indicate the presence of both

inter- and intra-molecular hydrogen bonding in sphingomyelin bilayers. Yeagle *et al.* (174) have demonstrated, using both ^{13}C and ^{31}P NMR that at physiological temperatures the lamellar phase of beef-brain sphingomyelin is unstable. Only at low temperatures does sphingomyelin form a lamellar phase, and the higher temperature form is best described as a hexagonal phase. Both egg PC and cholesterol are shown to stabilize sphingomyelin bilayers; this is suggested to have important physiological consequences for sphingomyelin-rich membranes.

4. Other phospholipids

$\Delta\sigma$ has been studied as a function of temperature for phosphatidylserine (PS), (175) phosphatidic acid, (175, 115) and phosphatidylglycerol (PG). (115) These three lipids all have a negative charge on the polar head-group under physiological conditions, which is different from the zwitterionic character of PC and PE. The CSA of phosphatidic acid (115) is strongly affected by pH, which also influences the gel–liquid crystal phase transition temperature. Change in pH has a rather different effect upon PG, and addition of Ca(II) leads to the appearance of a broad, powder-like ^{31}P resonance. Clearly there are many parameters that could be studied but Ca(II) effects are important in that Ca(II)–membrane interactions have been implicated previously in a number of ways. The interaction of PS with Ca(II) was also studied. (175)

5. Natural membranes

The natural membrane systems examined to date by ^{31}P NMR spectroscopy are listed in Table III. Generally the spectra (Fig. 19) are similar to those of the constituent lipids, arising in the main from the phospholipid phosphates. McLaughlin *et al.* (176) have reported that the biological membranes consistently show higher amplitude in the high frequency shoulders. Given that no more than 3% of the membrane phospholipid is shown to be bound to protein in human erythrocyte ghosts, (177) perhaps there is no substantial reason why the intact membranes should give different ^{31}P NMR spectra from the mixed constituent lipids. However, the relaxation time of the phosphate group in intact vesicular stomatitis virus membrane (178) is much shorter than that of the constituent lipids, and this is attributed to lipid–protein interactions. Other workers (179) have found no apparent evidence of lipid–protein interactions in *Acholeplasma laidlawii* bacteria cells, although relaxation times were not measured. Substantial differences between the ^{31}P NMR spectrum of liver microsomal membranes and that of the constituent lipids are reported. (180) The data are interpreted as showing isotropic motion for a part of the phospholipids in the natural membrane, possibly arising from transitory formation of

TABLE III

Spectra of natural membranes (in order of publication)

Membrane	Ref.
E.coli	111
Sarcoplasmic reticulum	182, 183
Human erythrocyte ghosts	176, 177, 149, 151
Chromaffin granule	176
Bovine spleen nerve	176
Rat liver microsomes P^+	131, 180
Rat brain P^+	131
Acholeplasma laidlawii cells	179
Chick embryo fibroblasts	175
Sheep erythrocyte	177
Vesicular stomatitis virus	178
Rat erythrocyte P^+	132
Rat liver P^+	132
Nil cells P^+	132
Bovine liver microsomes	180
Rabbit liver microsomes	181
Human atherosclerotic aorta	156

P^+ designates natural membranes containing phosphonium-labelled phosphatidylcholine analogues.

intramembrane non-bilayer lipid configurations with which the bulk (bilayer) phospholipids are in rapid exchange. In rabbit liver microsomal membranes, other workers (181) found ^{31}P NMR evidence for non-lamellar intramembrane structures accommodating cytochrome P-450. Thus it would appear that in some natural membrane systems, but not in others, one may expect to observe ^{31}P NMR phenomena that arise from interactions of the constituent phospholipids with other membrane components.

F. ^{31}P NMR investigations of the effects of cholesterol

Cholesterol is found in membranes usually at concentrations at least as great as that of some of the phospholipid components, but its function remains largely unknown. From thermal analysis, it has been found that cholesterol depresses or abolishes the gel–liquid crystalline transition at biological temperatures. NMR work in this field was reviewed in 1976 by Wennerström and Lindblom (105) and in 1977 by Seelig. (153) In the latter review, Seelig collated various NMR and non-NMR work and concluded that the evidence available at that time showed cholesterol to have essentially a bulk packing effect on the hydrocarbon chain portions and no significant hydrogen-bonding to the phosphate groups. Work cited included

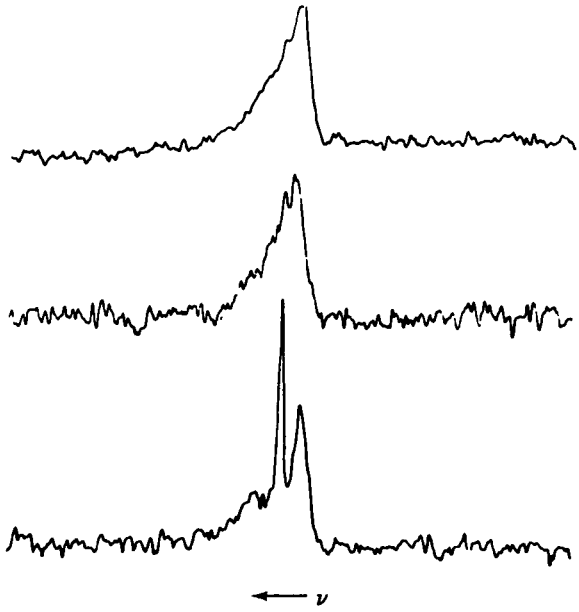

FIG. 19. 129 MHz ^{31}P NMR spectra of some unsonicated natural membranes; top, chromaffin granule membranes; middle, sarcoplasmic reticulum; bottom, bovine spleen nerve. The spectra arise from the phospholipids except the narrow peak in the centre of the bottom spectrum. Total spectral width is approximately 400 ppm. (176)

^{31}P NMR examination of erythrocyte ghosts (194) and pure lipid–water dispersions. (164, 185) ^{31}P–(^{1}H) NOE influences of cholesterol upon the phospholipid phosphate group have been shown to be small (186) but significant, (161) indicating a disruption of phospholipid intermolecular interaction in PC bilayers.

More recent publications have tended to confirm the above conclusions that cholesterol acts upon the hydrocarbon chains of the phospholipid fatty acids to inhibit phase transition phenomena. Thus the phase transition in ether-extracted erythrocyte ghosts could be reversibly removed by re-addition of cholesterol. (177) The ether-extracted ghosts consist largely of sphingomyelin, and it is significant that cholesterol is shown by other workers (174) to stabilize the lamellar phase in aqueous dispersions of bovine brain sphingomyelin. However, ^{31}P NMR observation of a simulated phospholipid mixture from vesicular stomatitis virus membrane (178) shows no apparent effect on the phospholipid spectrum.

Several recent papers have demonstrated that significant effects of cholesterol upon the fatty acid portions of the phospholipids relate to the nature of the fatty acids. Whereas incorporation of cholesterol (136)

decreases the outside/inside ratio and increases the size of 1,2-dimyristoylphosphatidylcholine vesicles, the cholesterol concentration in the outside and inside monolayers is approximately the same. By comparison, the 1,2-dioleoyl analogue shows an increase in vesicle size but the outside/inside ratio is increased with the incorporation of cholesterol. Of particular significance with the unsaturated analogue, cholesterol is found to be asymmetrically distributed and to prefer the inside monolayer of the vesicles.

^{31}P NMR investigation of the effects of cholesterol upon membrane systems containing phosphatidylethanolamine (187) shows that bilayers may be destabilized by cholesterol for this phospholipid. This result is discussed in the light of previous observations that biological membranes containing high concentrations of phosphatidylethanolamine also contain little or no cholesterol. It is suggested that the bilayer structure of lipids in biomembranes may be in dynamic equilibrium with other available phases. The relative shapes of the associations between phospholipid and cholesterol were discussed (187) in terms of their effects on relative stabilities of the bilayer or alternate phases. Further work with equimolar mixtures of synthetic phosphatidylethanolamine and phosphatidylcholine (188) confirms the preferential interaction of cholesterol with the phosphatidylcholine component. Cholesterol is found to stabilize the bilayer phase with a mixture of unsaturated PE and saturated PC, but to destabilize the bilayer phase when both phospholipids have unsaturated fatty acid components. The temperature dependent polymorphic phase behaviour of the latter mixture is found to show a pronounced hysteresis which is progressively reduced by addition of cholesterol.

Thus ^{31}P NMR spectroscopy has been used to show cholesterol to have substantial bulk effects upon the phospholipids in membranes, depending upon the nature of both the phospholipid head-group and fatty-acid moieties. As the degree of unsaturation depends upon the natural origin of the phospholipids, the source of phospholipids for these investigations will need to be delineated and a fatty acid analysis taken into account in future work involving cholesterol in membrane systems.

G. Structure and effect of other membrane components

Cross-linked lipopolysaccharides are structural components of cell walls and ^{31}P NMR has shown (189) that pyrophosphate diesters are present in one example, i.e. a variant of Lipid A from *Salmonella*. However, no evidence was found for phosphodiester or pyrophosphodiesters cross-linking the lipopolysaccharide sub-units. ^{31}P NMR has also been used to study (190, 191) precursors in the biosynthesis of Lipid A. Structural analysis was similarly performed (192) upon another membrane

component, lysocardiolipin, which has been implicated in mammalian phospholipid exchange reactions via a diacyl–monoacyl cycle. It is found to consist of three glyceryl units linked by two phosphodiester bonds.

Several publications have appeared concerning glycophorin A, the major sialoglycoprotein of the human red blood cell membrane. It was previously known that glycophorin A enhances permeability, that it contains a non-polar portion in its protein chain, and that it has a phospholipid part. Use of ^{31}P NMR and enzyme digestion (193) showed this to be diphosphoinositide and that it is closely associated with the non-polar intramembranous protein section. Other workers (194) have demonstrated by ^{31}P NMR that glycophorin immobilizes very strongly in their phosphate regions nine lipid molecules when incorporated into sonicated vesicles of dioleoyl-phosphatidic acid, most likely via electrostatic interactions. Altogether 80–100 lipid molecules are found to be perturbed by each glycophorin molecule, and the authors concluded that this leads to several effects including increased permeability. (195) Other workers (181) observed reconstituted liver microsomal membranes containing cytochrome P-450 and found non-lamellar structures. The ^{31}P NMR data are consistent with inverted micelles consisting predominantly of PE within the bilayer at the PC/PE ratio found naturally, and with the aggregation of these inverted micelles being affected by the oxidative state of the P-450.

Natural substances that affect membrane stability and permeability have potentially important consequences on biological function. By methods including ^{31}P NMR, two groups have examined the effect of rhodopsin which is a light sensitive protein found both in vertebrate receptor cells and light-sensitive bacteria. Incorporation of rhodopsin (193) into egg yolk PC membranes is found to restrict the motion of the phospholipid phosphate, methylene, and methyl groups. In the dark, the membrane stays sealed to paramagnetic ions but exposure to light allows rapid equilibration of Mn(II) and Co(II), and more slowly Eu(III), across the membrane. The authors concluded that the data support the idea of the protein penetrating the membrane. Other workers (145) incorporated a bacterial rhodopsin into egg yolk PC vesicles containing entrapped glucose-6-phosphate as a pH indicator. Illumination of the vesicles by a laser beam caused, in about one-quarter of the vesicles, a chemical shift which corresponds to an acidic pH change of approximately three units. This occurs reversibly at several extravesicular pH values; the heterogeneity of the vesicle preparations could not be explained readily.

Cullis and Grathwohl (177) examined the interactions between lipid and protein in erythrocyte ghost membranes. By use of ^{31}P NMR and other techniques, it was concluded that all detectable phospholipids are in bilayer structures and that various types of protein have differing effects on the phospholipid motion. The erythrocyte protein spectrin-actin was combined

with synthetic PS and PS–PC vesicles by other workers. (196) It is found that dimyristoyl-PS vesicles collapse and fuse into multilamellar structures in the presence of spectrin-actin, and that the protein prevents phase separations of mixed PS–PC bilayers. The protein also reduces the crystallizing effect of Ca(II) on mixed PS–PC mixtures. From the work described above, it thus seems that ^{31}P NMR is able to provide information on protein–phospholipid interactions.

Fung *et al.* (197) observed by ^{31}P NMR and other techniques the interaction between *E. coli* phospholipids and *E. coli* D-lactate dehydrogenase. The results suggest that the lipid–protein interactions are essential for optimal enzymatic activity but ^{31}P NMR is unable to contribute much beyond showing a spectral alteration. Other workers (178) were able to resolve the ^{31}P NMR spectrum of intact and unperturbed membrane-enclosed vesicular stomatitis virus into two distinct lines. A short ^{31}P relaxation time found in the intact virus is believed to arise from lipid–protein interactions.

An undesirable change in membrane stability is found in the widespread human condition of atherosclerosis; Cushley *et al.* have used ^{31}P NMR and other techniques to study the effect of natural components on membrane stability. They showed that there are two effects of incorporation of cholesterol esters (as found in atherosclerosis) into vesicles. (370) Firstly incorporation of 5 mole % cholesterol palmitate increases the permeability to Pr(III) ions ten-fold but, secondly, the same incorporation of cholesterol linoleate does not affect permeability. Since the effect of the saturated acid ester of cholesterol is opposite to that of cholesterol itself, the authors concluded that ^{31}P NMR has shown an effect related to the increased permeability of glucose etc. in atherosclerosis, which in turn is characterized by a marked increase in the ratio of cholesterol ester/free cholesterol. Other work (198) with incorporation of vitamin E and phytanic acid into lecithin vesicles showed that these two substances greatly increase the permeability of Pr(III) ions (the latter substance having a 2900-fold effect). ^{13}C NMR relaxation measurements show the lecithin bilayer to be greatly destabilized, especially by the phytanic acid.

Thus it can be seen that ^{31}P NMR can provide biological information on the effects of substances that do not themselves contain a phosphorus nucleus. For membrane studies, ^{31}P NMR gives detail that is difficult or impossible to obtain in other ways.

H. Interaction of membranes with therapeutic and other agents

It is believed that many pharmaceuticals have their site of action at membrane surfaces. The effects of the anaesthetic phenothiazine derivatives

Chlorpromazine [2-chloro-10-(3-dimethylaminopropyl)phenothiazine hydrochloride] and Diethazine [10-(2-diethylaminoethyl)phenothiazine hydrochloride] were investigated with ^{31}P and ^{13}C NMR of unsonicated dipalmitoyl-PC liposomes. (199) The drugs appear to reduce the mobility of the head-group by strong surface complexation and to increase mobility of the fatty-acid region and thereby lower the phase transition temperature. Other workers (200) interpreted the effect of Chlorpromazine on cardiolipin as an induction of the hexagonal (H_{11}) phase and found a similar effect for dibucaine and for Ca(II) ions. From these results it was suggested that these anaesthetics function by neutralizing the surface charge of negatively charged lipids, and this was related to previous hypotheses of anaesthetic action based on alteration of membrane fluidity.

^{31}P NMR was used to measure the permeability changes in egg yolk lecithin vesicles caused by the polyene macrolide antibiotic nystatin. (201) The prior incorporation of sterols into the vesicle has an effect which is dependent upon the sterol structure (related to differences between fungal and mammalian sterols and possibly therefore to selective action against fungi). However, the technique shows that nystatin causes a substantial permeability increase in the absence of the sterols. The interaction of the plant hormone 3-indoleacetic acid with membrane phospholipids in $CDCl_3$ solution was studied; (202) the results support previous work wherein specific interactions had been found.

Fluorescent probes have been used widely in other physico-chemical techniques, and an investigation (203) was made of the interaction with lipids by one such probe, 1-anilino-8-naphthalenesulphonate. While egg yolk PC vesicles show a relatively simple interaction, that with a total lipid extract reveals a more complicated effect involving the cholesterol present. In another study, the effect of an amine oxide detergent upon lecithin vesicles was studied. (204) The detergent is incorporated rapidly into some vesicles and then appears to be distributed by vesicle–vesicle collision.

VI. ^{31}P NMR OF BIOLOGICAL FLUIDS AND THEIR COMPONENTS

Fluid samples are clearly ideal for simple NMR observations but there are few biological fluids of which the phosphorus-containing components can be usefully observed. Nearly all the papers that have appeared concern blood components, of which erythrocytes (red blood cells) and lipoproteins have engaged most interest. From the papers reviewed in this section, it appears that ^{31}P NMR has a considerable contribution to make to advances in the phosphate biochemistry of biological fluids.

A. ^{31}P NMR observation of erythrocytes (red blood cells), erythrocyte components, and other blood cells

The main function of erythrocytes is to transport oxygen and carbon dioxide via their association with haemoglobin. The complexation of oxygen is sensitive to partial pressure and can be precluded by various poisons such as carbon monoxide. The main use of ^{31}P NMR is in the observation of intact erythrocytes or *in vitro* models of important biochemical processes within the erythrocytes.

The first publication (205) utilizing ^{31}P NMR for observation of haemoglobin action concerned an *in vitro* study of the binding of 2,3-diphosphoglycerate to human haemoglobin at various stages of ligand binding. The information derived from ^{31}P NMR chemical shifts is consistent with that from visible spectroscopy at various degrees of carbon monoxide binding. The authors concluded that release of diphosphoglycerate lagged behind CO binding, this being consistent with previous investigations. The first observation of intact erythrocytes by ^{31}P NMR was by Moon and Richards (10) who monitored the intracellular pH by measuring the difference in chemical shifts of the two phosphorus nuclei in DPG. They used rabbit erythrocytes with haemoglobin bonded to CO but cautioned that the DPG resonance positions could be complicated by interaction with the deoxyhaemoglobin.

Henderson *et al.* (206) examined fresh whole human blood and found the DPG to decrease with time, and that addition of inosine and pyruvate to aged blood led to an increase of [DPG]. ATP, P_i, and serum phospholipids were also observed in the fresh whole blood samples. Labotka *et al.* (207) observed the ^{31}P NMR of separated blood components including rabbit erythrocytes and reticulocytes and human platelets (Fig. 20). The ^{31}P NMR assays of ATP, DPG, and P_i give values in agreement with established techniques and are used to assay the phosphorus-containing metabolites in these blood components in a variety of conditions. The use of inosine and pyruvate produces a profile of intermediates which is quantitatively different from that of fresh erythrocytes. One pronounced difference between erythrocytes and platelets is the lack of DPG in the latter, but a relatively large amount of unidentified phosphates are found both in platelets and reticulocytes. Platelets stored at 4 °C are found to be depleted of their high energy phosphate reserves to a greater extent than when stored at room temperature; this observation is in accord with their known survival characteristics.

Costello *et al.* (208) examined separately the interactions between haemoglobin and DPG or ATP by observation of changes in the ^{31}P NMR chemical shifts ($\Delta\delta$) of these compounds on the addition of haemoglobin. A direct relationship was observed between $\Delta\delta$ of DPG and the proportion of

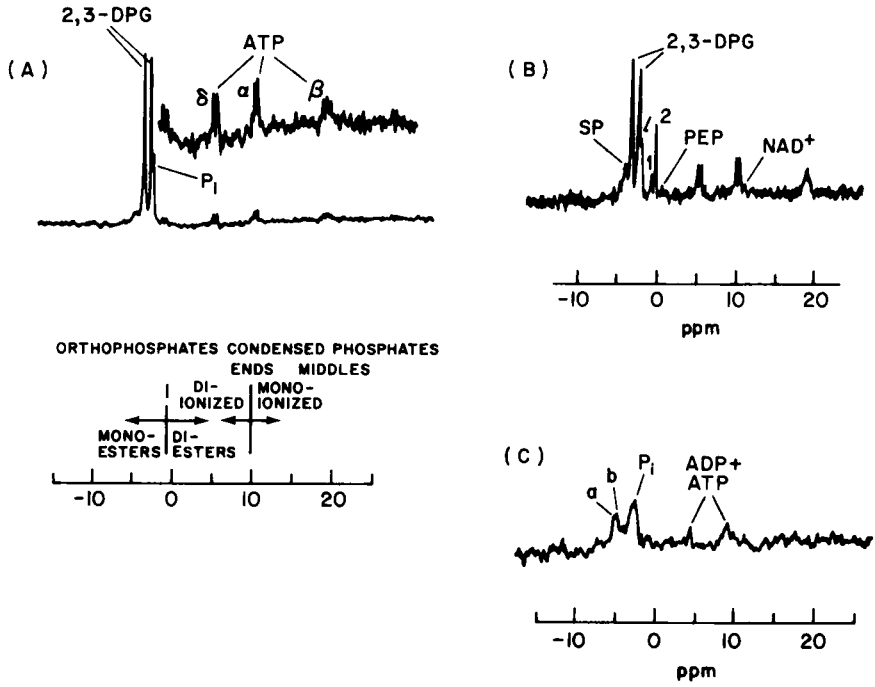

FIG. 20. 36·4 MHz ^{31}P NMR spectra of blood components. (A) Fresh intact rabbit erythrocytes treated with inosine and pyruvate. (B) Intact rabbit reticulocytes treated with inosine, pyruvate, and ferricyanide. (C) Fresh intact human platelets. Labelled compounds include 2,3-diphosphoglycerate (DPG), phosphoenolpyruvate (PEP), and sugar phosphates (SP). (207)

DPG bound to haemoglobin. This relationship was used by Huestis and Raftery (209) to examine haemoglobin cooperativity. This proportion was varied by altering pH, oxygenation state, or [DPG]. Later work by the same group (210) (Fig. 21) examined DPG in intact human erythrocytes at 37 °C, by comparison of chemical shifts with the model solutions. More DPG appeared to be bound in erythrocytes than in the model solutions, but less than would have been expected from the analogous binding to haemoglobin of other ligands. Fossel and Solomon (211) found that the ^{31}P NMR chemical shifts of DPG *cannot* be attributed to interaction with haemoglobin, cell pH, ionic strength, or Mg(II)/DPG ratio, but instead that in dog erythrocytes the cell membrane shape is of greatest importance. From the use of reagents that alter erythrocyte membrane area, these authors concluded that DPG interacts with a binding site in the cell that is dependent upon the physical condition of the cell membrane. ^{31}P relaxation times have been used (212) to obtain a mean distance of 24 ± 1 Å between the DPG

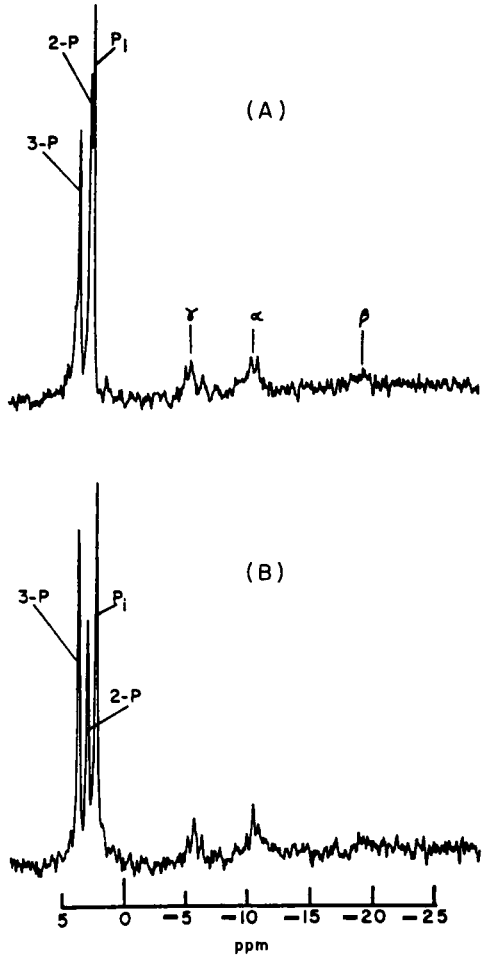

FIG. 21. 36·4 MHz ^{31}P NMR spectra of DPG and ATP in intact human erythrocytes incubated without substrate, (A) in air and (B) in nitrogen. Spectra A and B represent cells in which 33% and 67% of the total DPG were bound, respectively, and the chemical shifts of the DPG 2-phosphate and 3-phosphate were used for this determination. (210)

phosphorus nuclei and the four haeme iron atoms, this figure being in agreement with X-ray crystallographic results.

Initial work performed with ATP showed no linear $\Delta\delta$ relationship with haemoglobin concentration (208) or significant binding to haemoglobin in erythrocytes. (210) However, in later work (213) the same group has reported a linear relationship between $\Delta\delta$ of ATP γ-phosphate and the proportion of ATP bound to both oxyhaemoglobin and deoxyhaemoglobin.

In the presence of Mg(II), the $\Delta\delta$ changes differently for the two haemoglobin states and it is suggested that extra ATP binds to deoxyhaemoglobin through groups other than phosphate. The significance of Mg(II) was confirmed by Gupta *et al.* (214) who showed that there is a competition for binding ATP between deoxyhaemoglobin and Mg(II), although oxyhaemoglobin has relatively little effect (Fig. 22). Deoxyhaemoglobin also has a greater broadening effect on the ATP resonances. The affinities of ATP and MgATP for deoxyhaemoglobin are found to differ by more than an order of magnitude but to be comparable for oxyhaemoglobin. ESR data show little binding of Mg(II) to haemoglobin. The same authors (215) used ^{31}P NMR and prior knowledge of *in vitro* Mg(II) complexing to determine intracellular free [Mg] in erythrocytes. In accord with the previous work, much more DPG and ATP are shown to be complexed to haemoglobin in anaerobic cells.

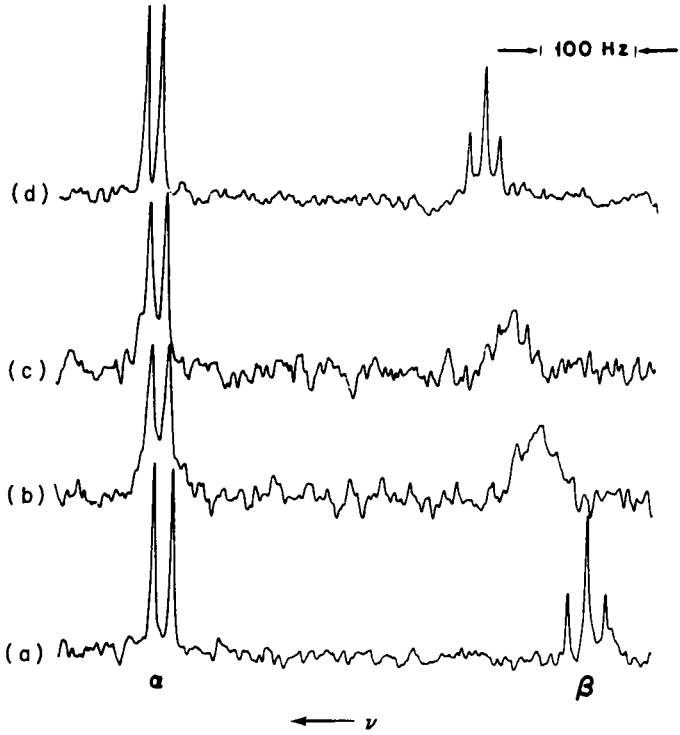

FIG. 22. Effect of haemoglobin state on the ^{31}P resonances of an equilibrium mixture containing ATP and MgATP at 40·5 MHz. Present in the samples were: (a) ATP (4·33 mM); (b) ATP (2·47 mM), magnesium (1·86 mM), and deoxyhaemoglobin (3·53 mM); (c) ATP (2·47 mM), magnesium (1·86 mM), and oxyhaemoglobin (3·53 mM); (d) ATP (2·47 mM) and magnesium (8·18 mM). (214)

^{31}P NMR has been used to study the binding of other phosphorus-containing species to haemoglobin and a related respiratory protein. The displacement of DPG by phytic acid (inositol hexaphosphate) was examined by alteration of the DPG T_1 values as the DPG phosphorus nuclei became less influenced by the haeme iron nuclei. (212) ^{1}H T_1 determinations show the phytic acid to alter the haemoglobin conformation. The ^{31}P NMR of phytic acid and the related inositol pentaphosphate (a component of bird's blood presumably from eating seeds rich in phytic acid) were examined by line-width and chemical shift as a function of pH. (216) This latter work was performed in apparent ignorance of an earlier publication. (217) The electrostatic intramolecular interaction between the phosphate groups was advanced as a reason for the extended titration range of these highly phosphorylated molecules, which influence the binding of oxygen to haemoglobin. ^{31}P NMR and ESR have been employed (218) to examine the binding of ATP to haemocyanin, a copper-containing respiratory pigment in molluscs. The ATP β and γ phosphoryl oxygens appear to be bound to the copper nuclei as indicated by selective broadening of the ^{31}P signals.

^{31}P NMR has been used to differentiate between erythrocytes in disease conditions from normal cells. The above-mentioned work with phytic acid (212) was part of a study on the reversible gelation of sickle cell oxy-haemoglobin in the presence of phytic acid. It was suggested that this gelation (shown by simple visual inspection) could be used as a simpler routine screening test for sickling disorders than conventional methods. This gelation could not be induced by DPG under any conditions, and phytic acid readily displaced DPG as shown by ^{31}P NMR. Kagimoto *et al.* (219) compared phosphorus metabolite levels and intracellular pH as a function of time in hereditary spherocytes and normal erythrocytes (Fig. 23). Approx-

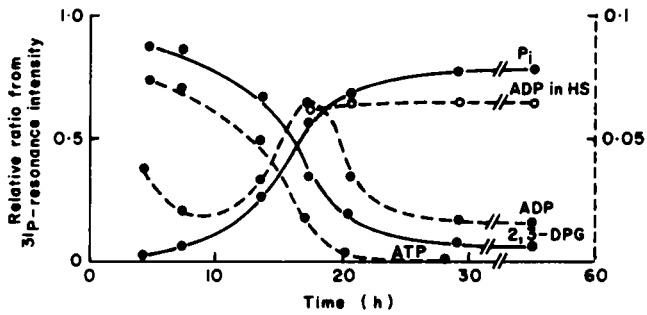

FIG. 23. Time course of the variation in levels of nucleotides and phosphate metabolites in normal erythrocytes and hereditary spherocytes (HS). The ordinate represents relative ratios of individual phosphoryl compounds as determined from the ^{1}H-decoupled ^{31}P NMR intensities at 40·5 MHz. Data for ADP and ATP were plotted on a scale one-tenth that for DPG and P_i. (219)

imately 20 hours after NMR observation was started, both [ADP] and intracellular pH deviated markedly between the two cell types and it was suggested that there is a causal link between the two observations based on the cell metabolism of ADP being related to pH.

B. ^{31}P NMR studies of lipoproteins

Lipoproteins are macromolecular lipid–protein complexes found in blood plasma which have the function of transporting lipids in a water-soluble form. Lipoprotein particles consist of a neutral lipid core surrounded by a surface layer of protein components and polar lipids, and have characteristic sizes, compositions, and densities. The density has usually been used to characterize them and there are several categories including very low density lipoproteins (VLDL, for liver triglyceride transport), low density lipoprotein (LDL, implicated in formation of atherosclerotic plaques), and high density lipoprotein (HDL, containing most of the plasma cholesterol). The lipoproteins have a relatively low energy of stabilization, and may be fragmented into lipid and protein components, and then recombined. These materials are the subject of a recent review. (220)

Assmann *et al.* (221) published the first ^{31}P NMR spectra of human lipoproteins, and were able to assign the main ^{31}P resonances to phosphatidylcholine and sphingomyelin. They found the PC/sphingomyelin phosphorus ratio to be approximately 1·5 and 4·4 respectively in LDL and HDL samples. HDL protein–phospholipid interactions in recombined lipoproteins cause no significant chemical shift change compared with aqueous dispersions of the lipids but produce line-narrowing. This is believed to be due to the protein having a preference for vesicles of a specific diameter. Addition of Eu(III) causes broadening and shifting of the phospholipid resonances; earlier work (112) has shown that outer and inner phospholipid resonances of vesicles can be distinguished, and thus the authors conclude that essentially all of the phospholipid phosphorus is located at the outer surface of the HDL particles.

Similar spectra of the native human lipoproteins were obtained by Glonek *et al.* (222) who found a substantial effect of the counter-cations upon the phosphate head-group chemical shifts. The same workers (223) have developed a paramagnetic quenching agent (Mn^{2+}–EDTA ratio 1:2·2) to broaden selectively the outer phospholipid resonances of bilayer systems present in the lipoprotein particles (as suggested previously by X-ray diffraction work with LDL). Only ~50% of the phospholipid phosphorus signal of LDL is quenched upon addition of the reagent, consistent with the bilayer structure, and ~80% of HDL phospholipid signal is also quenched. Nevertheless, ~20% of the HDL signal remains and the authors suggest that this arises from head-groups interacting with the protein in the particles.

Significant differences are reported for the behaviour of the HDL subclasses, HDL_2 and HDL_3. However, recent work (224) in which the action of α-phospholipase A_2 on human HDL is followed by ^{31}P NMR leads to the conclusion that essentially all of the PC is located at, or in rapid equilibrium with, the surface of the lipoprotein particle.

Yeagle *et al.* (225) have found human LDL to have two phospholipid environments. One, occupied by four-fifths of the phospholipid, shows high resolution resonances with similar properties to phospholipids in vesicles. The second, occupied by one-fifth, shows broad lines indicative of immobilization. Treatment of the LDL particles cleaves the protein into smaller peptides without fragmenting the particles and has a ^{31}P NMR spectrum showing little or no immobilized phospholipid. It was concluded that immobilization in the native LDL particle can be attributed to lipid–protein interactions. This group of workers (226) also probed human LDL with low concentrations of Pr(III) and obtained results concerning the phospholipids that conflict with those obtained (222) using a Mn–EDTA complex. They found that the head-groups of *all* mobile phospholipids are likely to be on the surface of the LDL particles. The results also suggest that cholesterol is not associated with the surface phospholipids. With HDL, it is found that phospholipid immobilization does not occur, consistent with the known occurrence of smaller peptides in these particles.

C. ^{31}P NMR examination of semen

Human and chicken semen samples have been studied (227, 228) by ^{31}P NMR, and phosphorus-containing species are found in the plasma that are significant for fertility. The spectrum shows the presence of P_i, phosphorylcholine, and glycerol-3-phosphorylcholine (GPC) in ejaculates but the phosphorylcholine hydrolyses rapidly on storage. The GPC level is stable and unaffected by frozen storage. The GPC level, as determined by ^{31}P NMR, is shown to correlate significantly with sperm motility and also to be eliminated from ejaculates by vasectomy operations. Previously GPC has been found to associate with the spermatozoa, and the authors concluded that GPC is a protective agent for spermatozoa during maturation.

Examination of whole chicken semen (228) showed GPC to be absent. However, there is a substantial concentration of serine ethanolamine phosphodiester and it has been suggested that this material plays an analogous role.

VII. ^{31}P NMR OF REPRODUCTIVE AND DEFENCE SYSTEMS

A great effort has been made in the past 20 years to tackle the problems of cancer and immunologically related diseases. As part of this effort, the roles

of DNA and various RNA's have emerged, and recently several groups have applied ^{31}P NMR (amongst many other techniques) to determine the configurations of these polynucleotides. The work reviewed here does not include a large number of publications on the ^{31}P NMR of mono- and di-nucleotides which, although of biological origin, have been studied *in vitro* in conditions very different from those found in tissue.

A. DNA and chromatin

Since Watson and Crick showed that DNA forms a double-helix structure a central question for molecular biology has been the manner in which the enormously long DNA molecules are gathered up in the cell. DNA is known to form a complex with proteins (histones) and this complex has recently been found to resemble beads on a string. (229) The DNA–protein complex, known as chromatin, has been investigated by several groups with ^{31}P NMR (amongst many techniques) in order to ascertain the nature of the DNA–histone interactions. ^{31}P NMR and circular dichroism have been used (230) to compare calf thymus DNA and chromatin. The ^{31}P signal half-width and chemical shift are not significantly different in the two cases but the intensities of the chromatin signals are reduced by an amount corresponding to the proportion of nucleotide residues in the "bead" portions. This could arise from immobilization of the nucleotide residues by complexation with histones in the "beads". The half-width of the DNA signal, with molecular weight of 2×10^6 to 9×10^6, is approximately 50 Hz. This is reduced to approximately 20 Hz on sonication to give a molecular weight of 140 000.

Cotter and Lilley (231) have used ^{31}P NMR, IR, and thermal techniques to compare the conformations of DNA and protein within chromatin with those of extracted DNA and bare protein particles. Unfortunately, ^{31}P NMR at 36·4 MHz is poorly discriminating for such complex determinations and the only conclusions that can be drawn are that (a) the environment and strain in the DNA phosphate groups and (b) the histone core secondary structures are not significantly different. Kallenbach *et al.* (232) have examined similar systems at 145·7 MHz for clarification of the previously established fact that one nucleotide in ten is highly susceptible to nuclease attack. This possibly arises from the sharp kinking necessary in the DNA chains in order to pack 140 base-pairs around each histone complex. Reasoning that one way to kink the DNA chain is by torsion in the phosphate linkage (Fig. 1), and that such torsion should show in the ^{31}P NMR spectrum, the authors sought asymmetry in the apparently symmetrical ^{31}P signal and a second component in T_1 measurements. By careful phasing of the spectra and subtraction of the reversed spectrum (Fig. 24), it was established that the maximum asymmetry corresponds to one base pair in twenty and more likely to no more than one in thirty. There is no second

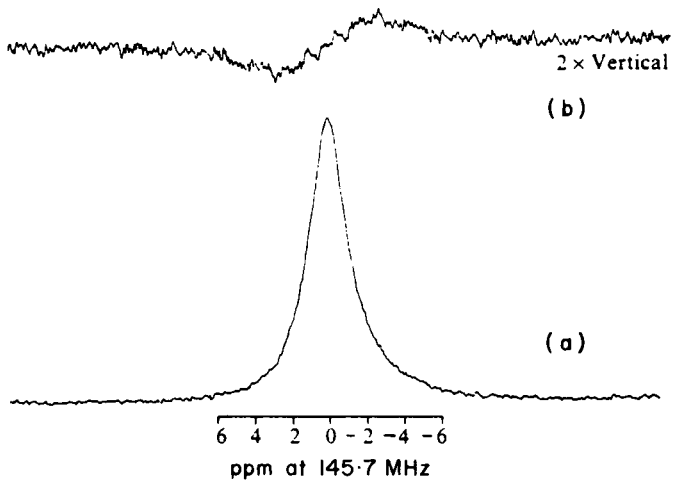

FIG. 24. 145·7 MHz ^{31}P NMR spectrum of (a) DNA nucleotides complexed to histones to form the "bead" portions of chromatin, and (b) the result of subtracting the right to left reversed spectrum from spectrum (a). (232)

T_1 component and so the authors concluded that kinking in DNA leaves the phosphodiester linkage unperturbed or that chain kinking is less frequent than previously thought.

Yamada *et al.* (233) have examined single-stranded DNA at 145·7 MHz at two different pH values in order to determine if there is a ^{31}P NMR spectral change on transition from helix (P–O configuration locked into *gauche,gauche* position) to the coil conformation (where various P–O configurations can be assumed). Such a change has been detected previously with model polynucleotide systems. (234, 235, 236) The helix–coil transition is indeed evidenced by ^{31}P NMR chemical shift changes and the authors use this to show that there is substantial heterogeneity in the DNA backbone structure in the single-stranded form. From a ^{31}P NMR spectrum of DNA with purine residues removed and which shows several distinct resonances, the authors conclude that heterogeneity in the DNA backbone conformation is related to the nucleotide sequence. The resolution achieved in this work with single-stranded DNA is much greater than with the double-stranded version.

B. Polynucleotides as DNA/RNA models

Akasaka *et al.*, (237) noting that their own previous unpublished ^{31}P NMR work with DNA showed mainly one broad resonance line, set out to examine the factors that determine ^{31}P chemical shifts of nucleic acids using simpler systems. pH is found to have a great influence on line-width and this

is ascribed to the rate of protonation/deprotonation of the base residue. The ^{31}P chemical shifts of polyriboguanylic acid (poly G) and polyriboadenylic acid (poly A) are found to alter only slightly on a pH change, unlike those of polyribocytidylic acid (poly C) and polyribouridylic acid (poly U). The same group (238) used ^{31}P and ^{1}H NMR to study the interaction of poly A with Mn(II) ions and found every Mn(II) ion to be bound directly to two phosphate groups and also to the adenine ring. Results with poly G (239) in solution are consistent with this existing in a relatively rigid multi-stranded form and with some heterogeneity in backbone conformations giving rise to a range of overlapping chemically-shifted ^{31}P resonances. Examination of the other polynucleotides (240) shows the molecular motion of the phosphorus moieties to be faster in the order poly A < poly C < poly U.

DNA/RNA nucleotides are generally

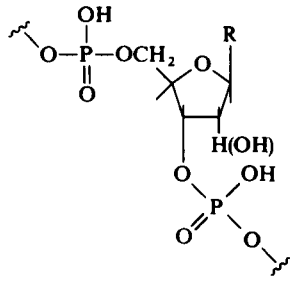

where R is one of

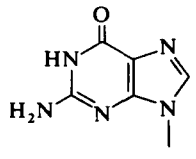

(G)

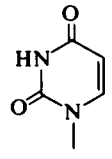

(C)

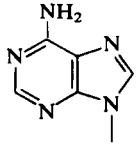

(A)

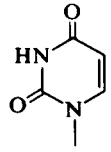

(U)

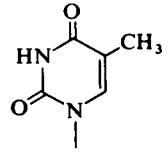

(T)

FIG. 25. The five most abundant nucleotides found in RNA and DNA.

As the helix–coil transition is of particular importance for the conformation of polynucleotides, the ^{31}P NMR spectral changes between 5 °C and 82 °C for the homopolyribonucleotides and various homo- and heterodinucleotides have been studied. (234) Without exception, the temperature change causes a 0·2–0·6 ppm low frequency shift that is consistent with removal of the *gauche,gauche* interactions and not found with simple phosphate diesters. Thus ^{31}P NMR is shown to be capable of providing some detail of the phosphate ester geometry in polynucleotides. Patel (235) found similar temperature-induced ^{31}P chemical shift alterations with tetra- and hexa-nucleotide duplexes. The use of ^{1}H NMR on these systems shows that there is "fraying" at the terminal base-pairs in these short duplexes. Complex formation with the antibiotic actinomycin D by the tetranucleotide PcGpCpG duplex produces marked chemical shifts for the nearby phosphate diesters, and removes the two-fold symmetry of the duplex. As actinomycin D is known to bind to double-helix conformations of DNA, it was suggested that the ^{31}P NMR results show the duplexes to have a similar conformation. Further work on the helix–coil transition has been carried out (236) from which it is concluded that ^{31}P NMR and ^{1}H NMR spectra monitor rather different effects in the duplex structure.

C. RNA in ribosomes

Ribosomes are the site of protein synthesis and contain a large proportion of RNA as this acts as the template for the protein amino-acid sequences. ^{31}P chemical shifts, T_1, and NOE values for *E. coli* ribosomes, their subunits, and RNA have been reported. (241) As well as the predominant resonance expected for phosphodiester linkages, the ribosomes show one or two narrower resonances that have pH-dependent chemical shifts and are assigned to phosphate monoesters. These are believed to be short oligomers of RNA derived from degradation of the RNA. The line-width of the RNA narrows by about a factor of 4 when the ribosomal protein is removed, indicating substantial immobilization of the RNA in the ribosomes, analogous to the DNA/histone situation. The ^{31}P spectra of the subunits are essentially the same as that of the ribosomes. The phosphorus relaxation is found to be largely dipolar in origin.

D. Transfer RNA

Transfer RNA molecules function by transferring amino-acids to the sites of protein synthesis. Many individual t-RNA systems have been isolated as pure chemicals and their nucleotide sequences determined. Generally, they contain less than 100 nucleotide units, which makes them very large compared to other purified chemical systems but not so large that ^{31}P NMR

does not have the possibility of showing resolvable features. Prior to the first ^{31}P NMR work, it had been shown that the t-RNA tertiary structures were generally of a "clover-leaf" form with three loops emanating from double-helix regions (Fig. 26).

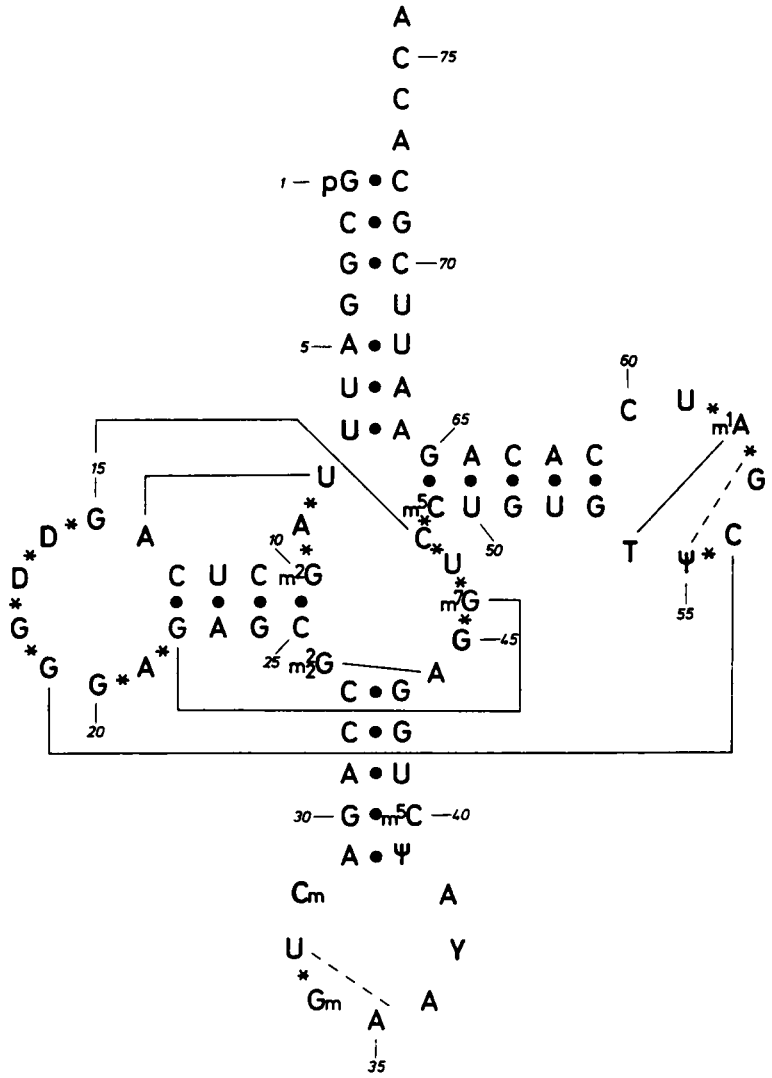

FIG. 26. Cloverleaf structure of yeast tRNA^{phe} as determined by Raj Bhandary and Chang (*J. Biol. Chem.*, 1968, **243**, 598). Asterisks indicate phosphodiesters with a deviating geometry. The dashed lines represent two base–phosphate interactions. Solid lines represent tertiary H-bond interactions. (246)

E. coli t-RNA^{glu} and yeast t-RNA^{phe} were examined (242) by continuous wave ^{31}P NMR at 40 MHz. Both give highly resolved spectra which are unfortunately confused by limited signal/noise facilities. Both systems show a predominant, sharply limited region corresponding to the phosphodiester chemical shifts observed later in DNA/RNA publications. Of particular significance is the fact that several spectral features appear on either side of the main group of resonances and that some line-widths are as small as 2 Hz. The main central features are attributed to phosphodiesters present in helical regions and in unkinked parts of the loops, with the other resonances arising from peculiar and constrained locations arising from t-RNA in the native structure. This is supported by the ^{31}P NMR observation of *E. coli* t-RNA^{glu} above the melting temperature when spectral intensity is lost outside the main region indicating the latter to be related to the ordered structure. Substantial effects are found with changes of pD from 6·3 to 8·5, this being unexpected since neither the phosphodiesters nor the unmodified bases titrate in this region. Mg(II) ions are shown to change distinctly only one part of the spectrum, indicating a specific binding by Mg(II) in agreement with previous observations.

In 1974, other workers (243) applied Fourier transform techniques and observed unfractionated yeast t-RNA and yeast t-RNA^{val} at 36·4 MHz but obtained no resolution of peripheral spectral features. However, they found that the melting of t-RNA, as judged by chemical shift changes, occurs at higher temperatures in the presence of Mg(II). Also they were able to follow, by ^{31}P NMR, the degradative effects of ribonuclease enzyme or chemical acetylation. Further work by Guéron and Shulman (244) with *E. coli* t-RNA^{glu} and yeast t-RNA^{phe} at 109 MHz showed many well-resolved ^{31}P resonances with both systems and sufficient sensitivity that individual phosphorus nuclei of the 76 present in yeast t-RNA^{phe} are located. Only one resonance alters its chemical shift and this is assigned to the t-RNA chain terminal phosphate. The effects of Mg(II) addition and temperature have been investigated and used with relative intensities in a discussion of assignments of peaks to regions of the clover-leaf structures. The main ^{31}P group of peaks are assigned to two types of structure which the authors attribute to the double-helical and non-helical portions. The phosphorus resonances are broadened in this work, compared to earlier low field work, by CSA.

Hayashi *et al.* (245) have studied the unfolding of the yeast t-RNA^{phe} clover-leaf (Fig. 26) caused by raising the temperature. The high- and low-frequency parts of the main ^{31}P resonance cluster are distinguished by T_1 and NOE data. The authors support the earlier suggestion as to their assignment in the t-RNA structure. Salemink *et al.* (246) have studied yeast t-RNA^{phe} at 40·5 MHz by the effects of several chemical and enzymatic treatments on the 17 resolved ^{31}P resonances (Fig. 27). By scission of loops

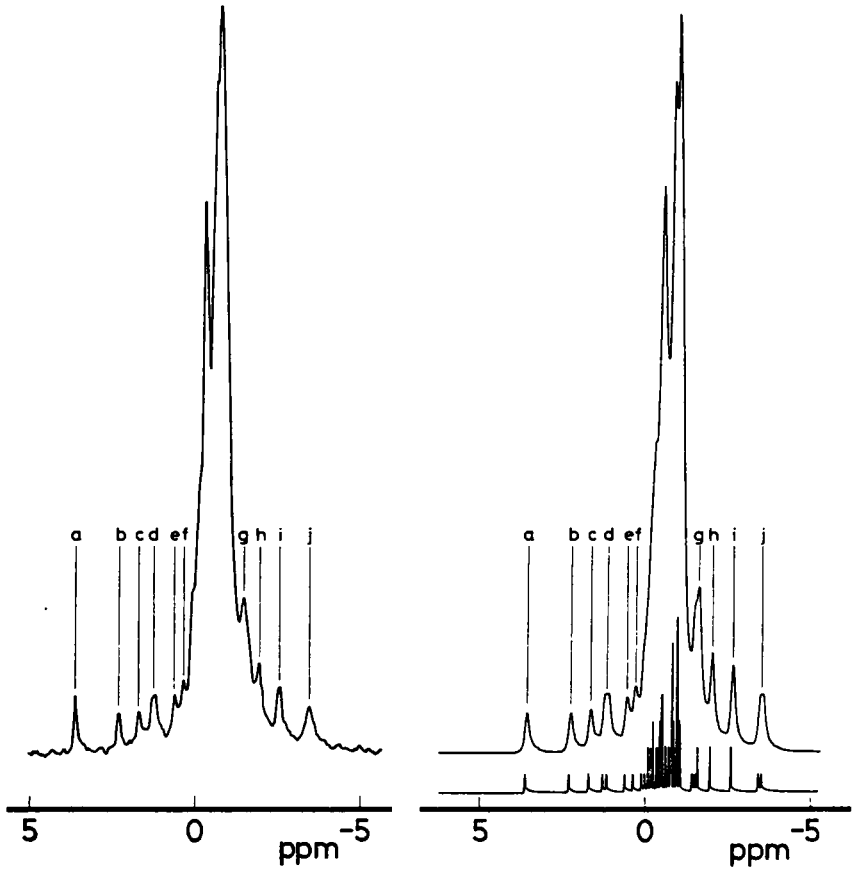

FIG. 27. ^{31}P NMR spectra of intact yeast tRNA^{phe}. Left, at 40·5 MHz; right, simulated spectrum with 76 Lorentzian lines. (246)

and correlation with ^{1}H NMR and X-ray results, the authors conclude that the chemically-shifted phosphodiester groups can be attributed to hydrogen-bonded phosphate groups and those deviating from the normal double-helix conformation.

E. Bacteriophage replication

Two papers have been published on very similar investigations concerning the replication of bacteriophages. Bacteriophages are a class of viruses that infect bacteria and adapt the bacterial double-stranded DNA system for the purpose of replicating their own single-stranded DNA. A small protein (M.W. 9689) from gene 5 of the filamentous bacteriophage M13 had

previously been shown to complex strongly single-stranded DNA. It was known that this gene 5 protein complexed both the single stranded DNA and the single-stranded virus DNA formed after replication. It was also known that the gene 5 protein–DNA interaction involved only approximately four base units of the DNA. Two separate groups used ^{31}P NMR, amongst other techniques, to examine the interaction of gene 5 protein with short synthetic oligonucleotides.

Coleman *et al.* (247) have used a combination of ^{1}H, ^{19}F, and ^{31}P NMR on complexes with tetra- or octa-nucleotides. ^{1}H NMR shows that certain protein aromatic protons are shifted to low frequency. This is interpreted as being due to ring current shifts induced by stacking of the phenyl rings of three of the five tyrosyl residues with the bases of the nucleotides. ^{19}F NMR of *m*-fluorotyrosyl gene 5 protein shows five separate ^{19}F resonances of which three, corresponding to identified tyrosyl units in the protein, appear to be "buried" in the protein–nucleotide complexes. Suspected phosphate–lysine interactions do not produce the expected T_2 effects in the ^{1}H NMR signals of the lysine methylene groups. ^{31}P NMR of the bound nucleotides shows large decreases in T_1 values for the 3′,5′ phosphodiester groups but little distortion of the nucleotide backbone on binding of gene 5 protein. Based on predictions of the secondary structure from the known amino-acid sequence, and tertiary folding dictated by NMR and chemical features of the complex, a three-dimensional model of the gene 5 protein–octanucleotide complex was constructed.

Garssen *et al.* (248) have used ^{1}H and ^{31}P NMR to probe the interaction of gene 5 protein with a self-complementary tetranucleotide double helix. From the ^{1}H NMR spectra of the Watson–Crick base pairs, it was found that the protein is able to unwind the double-helical fragment even at 0 °C. The effect in the ^{31}P NMR spectrum of the tetranucleotide of binding is to broaden the phosphodiester resonances and to shift them to low frequency by 0·3 ppm. The ^{31}P chemical shift change caused by the gene 5 protein is in the opposite direction to that caused by intercalation of actinomycin D as reported by Patel. (235) These observations are used to derive a mechanism of unwinding caused by the gene 5 protein.

F. ^{31}P NMR examination of the immune response

The immune systems of higher animals for defence against infection and foreign substances utilize antibodies that discriminate between chemically different materials to an extraordinary degree. X-ray diffraction studies have been used to probe antibody three-dimensional structures which are believed to be retained in solution. Chemical structural analysis of the antibody immunoglobulins has shown that the combining site consists of amino-acids which are varied in the antibody production so as to provide a

high degree of complementarity with the hapten. The hapten is the chemical function primarily bound by the antibody. Two groups have used phosphorus-containing modifications to known haptens in order to probe the immune response because antibodies have no phosphorus nuclei that can serve this purpose.

Goetze and Richards (249) have studied the interaction of a phosphorylcholine-binding mouse myeloma protein M603 with both phosphorylcholine and methyl-^{13}C-labelled phosphorylcholine. Low frequency chemical shifts of 1·5 and 0·7 ppm are observed for the ^{31}P and ^{13}C nuclei respectively on binding to the antibody. Line-width analysis indicates that some immobilization of the phosphate group occurs but essentially unrestricted rotation exists for the hapten's methyl group. Dissociation rate constants suggest a possibility of differential association by the two opposing ends of the hapten with the antibody. In later work (250) the same authors examined the interaction with phosphorylcholine of four other phosphorylcholine-binding mouse myeloma proteins. Each protein exhibits a unique NMR pattern, although there are extensive similarities in the chemical shift parameters upon binding. Despite a variation in dissociation constants of an order of magnitude for both binding-sites, and the difficulty that phosphate-binding could be stronger than methyl-binding or *vice versa*, the order of net binding effects for the different proteins predicted by NMR is the same as that observed by other methods.

Gettins *et al.* (251) have used both ^{1}H and ^{31}P NMR to investigate the antibody mouse myeloma protein M603. ^{31}P NMR shows that binding of the antibody causes a small change in the pK_a of the phosphorylcholine. Titration of phosphorylcholine on to the antibody, and difference ^{1}H NMR spectroscopy, allows assignment of some of the ^{1}H resonances to amino-acids known to be in the phosphate binding site from X-ray diffraction. Arising from this work, the same authors, in association with another group, (252) used dinitrophenyl (DNP) haptens with phosphorus-containing modifications to study the well-characterized DNP-binding mouse myeloma protein MOPC 315. Haptens were prepared with one, two, or three methylene groups between the phenyl ring and the phosphorus nucleus. ^{1}H NMR titrations were used to measure alterations in the pK_a of histidine residues in one part of the antibody protein and ^{31}P NMR titrations were used to measure the complementary effect upon the phosphorus-containing groups caused by the protein. With previous work the authors concluded that a specific arginine residue in the antibody combining-site is interacting with two of the haptens.

Goetze and Richards (253) determined the pH dependences of the binding affinities for the haptens phosphorylcholine and L-α-glycerophosphorylcholine of three mouse myeloma immunoglobulins. One immunoglobulin is shown to bind at pH 5·5 and to have a net

electronegative character in the phosphate-binding sub-site, whereas the other two bind most strongly at pH 7 and have net electropositive binding sites. Studies with a larger hapten analogue show the first immunoglobulin to have a substantially wider binding cavity. These NMR data indicate the role of various amino-acid residues in defining the differing ligand specificities of these antibodies.

Thus ^{31}P NMR has been used to obtain information both qualitatively and quantitatively unavailable by other methods because of its particular advantages. Nevertheless, as with any other complex scientific problem, other methods must be applied simultaneously and ^{31}P NMR results accord with previous knowledge concerning the immune response.

VIII. ENZYMES AND COENZYMES

A. Introduction

Enzymes are large, complex protein molecules usually having molecular weights in the range 10^3–10^6 daltons, that catalyse biochemical reactions. The catalytic activity of a given enzyme may be specific to a single reaction but is more usually specific to a single type of reaction. Before catalysis can take place, many enzymes require the presence of chemical species in addition to the enzyme and reactants. These species may be simple metal cations or more complex organic molecules and are termed cofactors. The organic cofactors which participate in the catalysed reaction are called coenzymes and undergo a chemical change, e.g. oxidation or reduction. The reactants in enzyme catalysed reactions are often referred to as substrates in biochemical terminology. Other molecules which bear sufficient similarity to a substrate that they interact with the enzyme, but do not undergo the catalysed reaction, are called inhibitors.

Enzymes, like all proteins, consist of carbon, hydrogen, nitrogen, and oxygen but not of phosphorus. Nevertheless ^{31}P NMR is of great importance in enzyme studies because the numerous phosphorylated substrates in the metabolic pathway can be monitored. Also, some enzymes become covalently phosphorylated as an intermediate step in the enzymatic reaction sequence and so can be observed directly by ^{31}P NMR. In addition, many coenzymes contain phosphorus as also do some inhibitors. However, in common with all biological studies, a single technique such as ^{31}P NMR provides information only about the aspects of the biological system best observed by that technique. The view of enzymes as afforded by ^{31}P NMR is necessarily restricted but, although other techniques are also essential, ^{31}P NMR has given crucial information not available from other techniques.

The simplest application of ^{31}P NMR to enzyme reaction systems is to use the technique as just another detection method to monitor the quantities of known reactants and products. In addition to the examples of this method

reported for the individual enzymes, it has been used to observe the hydrolysis of polyphosphates by non-specific phosphatases in two technologically applied studies. The first concerns the bioavailability of phosphate to plants from inorganic pyrophosphate and tripolyphosphate. ^{31}P NMR was used to monitor the rate of their hydrolysis in the presence of corn and soya bean roots. (254) In the second, ^{31}P NMR was used to observe the fate of polyphosphate injected into chicken carcases, a common food processing procedure in the production of frozen chicken. The hydrolysis of the polyphosphate is found to be greatly retarded when the frozen meat is mixed with disodium ethylenediaminetetraacetate (presumably by sequestering of necessary metal ion cofactors), thereby allowing the meat to be thawed without significant further polyphosphate hydrolysis. (255) When chicken carcases subjected to prolonged frozen storage (−18 °C) were examined, it was found that hydrolysis of the injected polyphosphates occurs during storage, (256) thus showing that these substances are not completely immobilized at −18 °C in flesh.

^{31}P (and ^{1}H) NMR were used to help elucidate the structure of an enzyme reaction product. A protein, designated HPr, is an intermediate in the transfer of a phosphoryl group from phosphoenolpyruvate to galactose in the carbohydrate transport pathway of the microorganism *Staphylococcus aureus*. The HPr protein was sequenced by conventional degradation methods (257) but ^{31}P and ^{1}H NMR are needed to locate the phosphorylation site. From chemical shift and pH titration data, the enzymatically prepared phospho-HPr is found to be phosphorylated at the histidine N-1 position, whereas chemically prepared phospho-HPr is phosphorylated at the histidine N-3 position. (258)

Several excellent reviews of experimental and theoretical aspects of NMR enzyme studies have appeared. These are mentioned only briefly and the relevant references given. Foremost amongst these experimental methods is the paramagnetic method of determining internuclear distances. It requires the measurement of the relaxation rate enhancement of particular nuclei due to the effects of a paramagnetic ion. In most cases reported to date, Mn(II) has been used as a substitute for Mg(II), since it can often act as a cofactor for Mg(II)-dependent enzymes. The distances between the enzyme metal-binding site and various enzyme-bound substrate nuclei can thus be determined; this method has been widely applied and aspects of its application are discussed. (259–263)

Johnson (264) has reviewed the general effects of chemical reactions and exchange processes on NMR spectral line-shape and position, and discussions specifically related to enzyme kinetics have been given by Redfield (265) and by Rao and Cohn. (266) Recent comprehensive reviews of the mechanism of enzyme action (267, 268) have incorporated sections with kinetics and results from ^{31}P NMR work.

^{31}P NMR has been used to characterize several types of substrate analogue compounds used in enzyme work. A range of inert transition metal complexes of ADP, ATP, etc. (269, 270) have been used to study the role of active ATP complexes in enzyme reactions. Another group of nucleotide analogues are the nucleoside thiophosphates in which selected oxygen atoms of the phosphate group are replaced by sulphur. (271–276) This substitution is a relatively minor structural change and the thiophosphates are often active substrates.

In order to retain maximum enzyme acceptance one should use analogues with the minimum structural change possible. Perhaps the best technique is to label phosphate groups with another oxygen isotope, usually ^{18}O. The subject of isotope exchange and enzyme mechanism was reviewed by Boyer. (277) Chiral analogues of phosphate monoesters have been prepared using sulphur and oxygen labels; (278) similar reports have appeared for other nucleotides. (279, 280) These analogues have been used to determine the stereochemical course of several enzyme reactions. Applications of these techniques to enzyme studies, in which ^{31}P NMR is the primary method of observation, are reported in the appropriate individual enzyme section.

Many aspects of ^{31}P NMR applications to enzyme reactions have been reviewed by Cohn and Rao subsequent to the preparation of this review. (281)

B. Enzymes

The results obtained from ^{31}P NMR observations on each enzyme reaction are presented individually, with the enzymes listed in the order of their classification according to the recommendations (1964) of the International Union of Biochemistry (282) and its 1972 revision. (283)

1. Transferases

These are enzymes which transfer a group from a donor molecule to an acceptor molecule. The enzymes reported in this section are members of sub-groups EC 2.4 and EC 2.7. In the latter category the transferred group contains phosphorus, and in the former the donor and acceptor molecules are phosphorus-containing.

(a) *Glycogen phosphorylase* (EC 2.4.1.1) catalyses the breakdown of glycogen to glucose-1-phosphate, forming the first reaction step in the glycolytic sequence resulting in the production of glucose from glycogen [3].

$$(\alpha\text{-D-1,4-glucosyl})_n + P_i = (\alpha\text{-D-1,4-glucosyl})_{n-1} + \alpha\text{-D-glucose-1-phosphate} \quad [3]$$

^{31}P NMR has been used to monitor the concentrations of ATP, ADP, P_i, and glucose-1-phosphate in a suspension of rabbit muscle glycogen particles

during transient activation of phosphorylase. This activation occurs with the loss of glucose-6-phosphate from phosphorylase *b* and association of the newly formed phosphorylase *a* with ADP, AMP, or IMP. (284)

The stereospecificity of the glucose-6-phosphate inhibitor's binding site on glycogen phosphorylase *b* has also been studied. (285) In aqueous solution the ^{31}P NMR signals of α- and β-anomers of glucose-6-phosphate are resolved. At pH 7 the integrated intensities of these signals are 40% and 60% respectively, on addition of glycogen phosphorylase *b*; broadening of the α-anomer's resonance only occurs, showing that the β-anomer does not bind.

(b) *UDP-glucuronyltransferase* (EC 2.4.1.17) is found in liver microsomal fractions and it catalyses the transfer of glucuronide to various acceptors including phenols, alcohols, amines, and fatty acids [4].

$$\text{UDP-glucuronate} + \text{acceptor} = \text{UDP} + \text{acceptor-}\beta\text{-glucuronide} \quad [4]$$

When UDP-glucuronic acid is incubated with *p*-nitrophenol in the presence of rabbit liver microsomal fraction, the only products detected by ^{31}P NMR are P_i and UMP. (286) Addition of UDP to the preparation shows a high UDPase activity such that the rate of production of UDP by the transferase reaction is easily exceeded by the rate of UDP hydrolysis. The UDPase activity is inhibited by the addition of EDTA, but this also affects the transferase reaction although UDP is detected.

Attempts to show if UDP-glucuronyltransferase is located on the inner or outer membrane surface of microsomes, by differentiating between the spectra obtained from substrates and products contained within the cells from those outside upon adding lanthanide shift/relaxation agents and by adjusting the external pH, have been unsuccessful.

(c) *Hexokinase* (EC 2.7.1.1) catalyses the phosphorylation of a number of hexoses including D-glucose, D-mannose, and D-fructose to produce the hexose-6-phosphate [5]. This reaction is the initial step in the glucose metabolism of most cells.

$$\text{D-hexose} + \text{ATP} = \text{ADP} + \text{D-hexose-6-phosphate} \quad [5]$$

The catalytic activity is not abolished when the *in vivo* activating metal cation, Mg(II), is replaced by Cd(II) or Co(II), and enzymic activity persists when thiophosphate analogues of ATP are substituted for this substrate. It has been shown that the two diastereoisomers of adenosine-5′-*O*-(2-thiotriphosphate) and their Mg(II) complexes are distinguished by their ^{31}P NMR spectra. (275) Additionally, in adenosine-5′-*O*-(2-thiotriphosphate) and adenosine-5′-*O*-(3-thiotriphosphate) complexes with Cd(II), the metal is bonded via the sulphur atoms, but Mg(II) is bonded via the oxygen atoms

on the thiophosphate group. (287) Consequently the configuration of the Mg(II) chelate of one diastereoisomer of adenosine-5'-*O*-(2-thiotriphosphate) is equivalent to the configuration of the Cd(II) chelate of the opposite diastereoisomer. These are shown [6] using the A and B nomenclature for the diastereoisomers. (274)

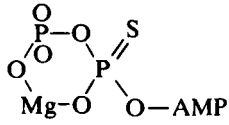

(A)

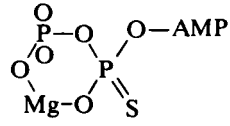

(B)

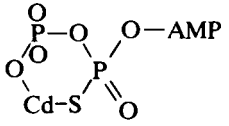

(A)

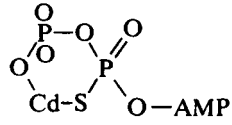

(B)

[6]

Yeast hexokinase reacts with the Mg(II)B isomer and the Cd(II)A isomer at between 1000 and 100 times the rate with Mg(II)A and Cd(II)B isomers. (287) In addition to demonstrating the stereospecificity of the enzyme this shows that the metal complex is the active substrate rather than the free nucleotide with the metal ion associating with the enzyme at some site remote from the catalytic site.

(d) *Pyruvate kinase* (EC 2.7.1.40) is an enzyme of the glycolytic pathway that catalyses the interconversion of ADP and phosphoenolpyruvate to ATP and pyruvate [7]. In addition it can catalyse the partial reaction producing the enolization of pyruvate [8] but without phosphoryl transfer taking place.

$$CH_3\text{–}CO\text{–}COO^- + ATP = CH_2{=}C(OPO_3)\text{–}COO^- + ADP$$

[7]

$$CH_3\text{–}CO\text{–}COO^- = CH_2{=}C(OH)\text{–}COO^-$$

[8]

The enzyme requires the presence of both mono- and di-valent cations for activity which *in vivo* are K^+ and Mg(II). The ease with which these can be substituted by other cations, including for example Na^+, Tl^+, Mn(II), Co(II), Ni(II), has resulted in a number of NMR investigations using various combinations of metals and substrates to form ternary metal·enzyme·substrate or metal·enzyme·inhibitor complexes. Only those investigations involving ^{31}P NMR observations concern us here.

Nowak and Mildvan (288) have determined the correlation times of the methylene protons and phosphate phosphorus of enzyme-bound phosphoglycollate, a competitive analogue of phosphoenolpyruvate, from measurements of the spin–lattice and spin–spin relaxation times. The correlation time of the phosphorus is the same as that calculated for the enzyme molecule as a whole, indicating that the reaction centre of the bound inhibitor is immobilized with respect to the enzyme, thereby permitting orientation or entropy effects to operate in the catalytic reaction. These authors also determined the paramagnetic relaxation enhancement of phosphoglycollate phosphorus in a ternary complex with muscle pyruvate kinase and Mn(II) at a single frequency (40·5 MHz) which yields a Mn–P separation of $3{\cdot}5 \pm 0{\cdot}3$ Å. (289) Although this distance is intermediate between that expected for inner sphere coordination of tetrahedral phosphate to Mn(II) and second sphere coordination in which a small ligand such as water intervenes between the phosphate and Mn(II), it is compatible with a distorted inner sphere complex involving axial oxygen bonding in a 5-coordinate phosphorane structure such as would be expected from an associative (S_N2) mechanism. (267) However, the ESR spectrum of Mn(II) in this complex shows that the NMR data is the averaged result of rapid exchange between inner-sphere coordination (32%) and second-sphere coordination (68%). (290)

In experiments with catalytically active complexes of the enzyme, Mn–P distances of 4·5–6·1 Å are found in the quaternary complex composed of pyruvate kinase·Mn(II)·pyruvate·inorganic phosphate, (291) a Co–P distance of $5{\cdot}0 \pm 0{\cdot}5$ Å in the quaternary enzyme·Co(II)·K^+·phosphoenolpyruvate complex, compared to 2·7 Å in the simple Co(II)·phosphoenolpyruvate complex, (292) and in the quaternary ATP·enzyme·Mn(II)·pyruvate complex the Mn–ATP phosphorus distances are P_α $5{\cdot}1 \pm 0{\cdot}5$, P_β $5{\cdot}0 \pm 0{\cdot}5$, and P_γ $4{\cdot}9 \pm 0{\cdot}6$ Å compared to the binary Mn(II)·ATP complex of P_α $3{\cdot}2 \pm 0{\cdot}3$, P_β $3{\cdot}1 \pm 0{\cdot}3$, and P_γ $3{\cdot}1 \pm 0{\cdot}3$ Å. (293)

These results show that the metal–phosphorus interaction in active enzyme bound complexes is much more predominantly second sphere, that is ~2% inner-sphere and ~98% second-sphere, than is the interaction in inactive substrate analogue enzyme bound complexes. Furthermore, these distances together with those for metal–proton and metal–carbon at various positions in the substrates have been used to construct models of the active site geometry of the substrates in the catalytically active complexes. (294)

Rare earth ions are found to displace Mn(II) from the enzyme·Mn(II) complex and to inhibit enzymatic activity. When Gd(II) is introduced into the enzyme·Na(I)·phosphoenolpyruvate system, the internuclear Gd–P distance is found to be 5·2 Å. (295)

In addition to these paramagnetic ion relaxation effect studies the ^{31}P NMR spectra of enzyme·ATP and enzyme·ADP systems titrated with

Mg(II) were observed by Gupta and Mildvan. (296) They find from the chemical shifts of the nucleoside phosphates that the kinetically active complexes consist of enzyme·Mg(II)·nucleotide·Mg(II); i.e. a second divalent cation is required for enzymatic activity which is bound to the nucleotide substrate. (296) When Cr(III)·ATP, a substitution inert tridentate ATP complex, is substituted for Mg(II)·ATP substrate, the pyruvate kinase catalyses the enolization of pyruvate [8] but not the phosphoryl transfer reaction. Similarly the Cr(III)·ADP complex is an inhibitor of the pyruvate kinase phosphorylation reaction but promotes the Mg(II)·enzyme catalysed enolization of pyruvate. The paramagnetism has been used to determine the Cr–^{1}H and –^{31}P distances of phosphoenolpyruvate in the enzyme·Mg(II)·CrADP·phosphoenolpyruvate complex. These are reported to be $8{\cdot}5 \pm 0{\cdot}6$ and $9{\cdot}6 \pm 1{\cdot}3$ Å for the protons and $5{\cdot}9 \pm 0{\cdot}4$ Å for the phosphorus. (297) The data have been interpreted as indicating van der Waals contact between a phosphoryl oxygen of phosphoenolpyruvate and the hydration sphere of the nucleotide-bound metal. Such molecular contact between the phosphoryl donor (phosphoenolpyruvate) and the phosphoryl acceptor (ADF) is consistent with an associative (S_N2) mechanism (Fig. 28).

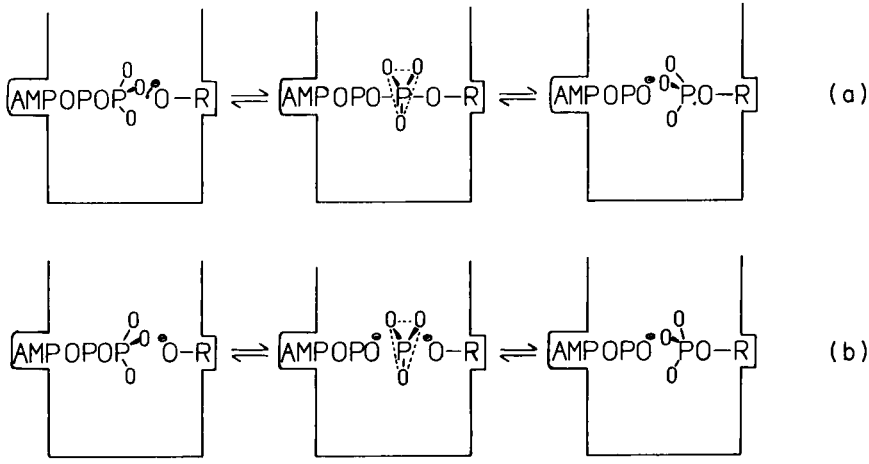

FIG. 28. Two of the possible reaction mechanisms of enzyme catalysed phosphoryl transfer: (a) the associative "in line" mechanism, S_N2; (b) the dissociative "in line" mechanism, S_N1.

However, Lowe and Sproat have presented evidence which strongly supports a dissociative (S_N1) mechanism for the phosphoryl transfer reaction. They incubated rabbit muscle pyruvate kinase, pyruvate, cofactors, and the labelled nucleotide adenosine-5-[$\alpha\beta$-^{18}O, β-$^{18}O_2$]triphosphate and found from the P_γ chemical shift that randomization of ^{16}O,^{18}O in the $\beta\gamma$–O bridge occurs. This is expected of course whatever mechanism operates, but

they also found that the same randomization occurs both in the presence of oxalate, which is an inhibitor of the kinase reaction, and in the absence of pyruvate or a pyruvate analogue. That is, dissociation and recombination of the γ-phosphoryl group occurs in the absence of the receiving substrate which is a necessary participant in the S_N2 mechanism (Fig. 28). (298, 299) Pyruvate kinase behaves towards metal chelates of adenosine-5-*O*-(3-thiotriphosphate) in a similar manner to that reported for hexokinase in that an inversion of the enzyme's stereospecificity is observed between the Cd(II) and Mg(II) chelates. (287)

(e) *3-Phosphoglycerate kinase* (EC 2.7.2.3) catalyses the reversible transfer of a phosphoryl group between ATP and 1,3-diphospho-3-glycerate [9]. This reaction occurs in both fermentation and glycolytic pathways; consequently the enzyme is widely distributed in living matter, being found in plants, yeasts, and animals.

$$COOPO_3^{2-}\text{–}CHOH\text{–}CH_2OPO_3^{2-} + ADP = COO^-\text{–}CHOH\text{–}CH_2OPO_3^{2-} + ATP$$

[9]

The reaction is particularly suited to ^{31}P NMR investigations since both of the substrates and the products contain phosphorus. At 109·3 MHz signals from each are sufficiently resolved for estimates of their concentrations to be made and equilibrium constants derived. (300) At enzyme concentrations greater than substrate concentrations the reverse equilibrium constant for enzyme bound reactants and products is ~0·8 compared to $\sim 3 \times 10^{-4}$ at catalytic enzyme concentrations. The effect of adding sulphate ions is to shift the equilibrium of the enzyme bound substrates in favour of ATP.

The presence of a divalent cation is necessary for enzyme activity, and the spectrum of enzyme bound ATP in the presence of Mg(II) gives rise to two P_β signals of equal area at positions corresponding to MgATP and free ATP, indicating that the enzyme possesses two ATP binding sites, one of which binds Mg(II) weakly, if at all.

(f) *Carbamoyl phosphate synthetase* (EC 2.7.2.5) catalyses the formation of carbamoyl phosphate from ammonium ions in the initial stages of the production of urea for excretion in mammalian liver mitochondria [10].

$$2ATP + HCO_3^- + NH_3 = 2ADP + P_i + NH_2COOPO_3$$

[10]

The enzyme can also utilize glutamine as the nitrogen-containing substrate, this reaction [11] taking place in cell cytoplasm with pyrimidine being a product of the overall biosynthetic route.

$$2ATP + HCO_3^- + COOH\text{–}CH(NH_2)CH_2CH_2CONH_2 =$$
$$2ADP + P_i + NH_2COOPO_3 + COOH\text{–}CH(NH_2)CH_2CH_2COOH$$

[11]

The stereochemistry of this reaction has been investigated by incubating the enzyme and necessary divalent cations and substrates of [11] using adenosine-5'-(2-thiotriphosphate) in place of ATP. (301) Only the A isomer of the two stereoisomers functions as a substrate in the synthesis of carbamoyl phosphate, and only the A isomer is synthesized from adenosine-5-(2-thiodiphosphate) in the reverse reaction [see hexokinase section (c) for absolute stereochemistry of A and B isomers].

(g) *Creatine kinase* (EC 2.7.3.2). Phosphocreatine acts as an energy store in muscle, ready to re-phosphorylate ADP to ATP during periods of intense muscular activity when the rate of ATP hydrolysis exceeds the metabolic production of ATP. During quiescence the surplus ATP re-phosphorylates the free creatine replenishing the energy store. The assay of ATP, ADP, and CP in muscles is described in the "intact tissue" section. Creatine kinase requires the presence of a divalent cation to catalyse the phosphoryl transfer reaction [12].

$$\text{ATP} + \text{creatine} = \text{ADP} + \text{phosphocreatine} \qquad [12]$$

Milner-White and Ryecroft observed that the spectra of MgADP bound to creatine kinase, *in vitro*, in the presence of creatine and nitrate ions, show the presence of two different forms of the enzyme bound nucleotide. (302) They suggest that either the enzyme's two subunits bind MgADP with different affinities and that the chemical shift difference may be due to asymmetry in the transition-state analogue complex, or that the enzyme itself may be heterogeneous with two types of enzyme molecule being present.

The kinetics of the creatine kinase catalysed reaction in intact resting frog tissue skeletal muscle and in perfused beating rat hearts have been studied by a saturation transfer method. The signal of the γ-ATP resonance is selectively irradiated which causes a diminution in the signal observed from phosphocreatine because of the catalysed reaction transfer of the γ-ATP phosphoryl group to creatine. The magnitude of the signal reduction is a function of the chemical exchange rate and the spin–lattice relaxation time of phosphocreatine. Similarly the phosphocreatine signal was irradiated and the diminution of the γ-ATP resonance observed. Values for the forward and reverse reaction rate constants are given and the rate constant for the breakdown of phosphocreatine in the perfused heart ($0{\cdot}35\ s^{-1}$ at 37 °C) is considerably smaller than that reported from measurements made on heart extracts *in vitro* ($0{\cdot}83\ s^{-1}$ at 25 °C). (303) No satisfactory explanation for these rate differences has yet been advanced.

(h) *Arginine kinase* (EC 2.7.3.3). Muscles of invertebrates contain phosphorylated guanidino-compounds (phosphagens) each having its own specific kinase. The arginine specific kinase catalyses the reversible transfer

of a phosphoryl group between ATP and the terminal guanidine nitrogen of L-arginine [13].

$$\text{L-arginine} + \text{ATP} = \text{ADP} + \text{N}^{\omega}\text{-phospho-L-arginine} \quad [13]$$

The ^{31}P NMR spectra of solutions containing lobster muscle arginine kinase at catalytic concentrations (<0·1% substrate concentrations) and stoichiometric concentrations (≥substrate concentrations) give sufficiently resolved signals from all three phosphorus-containing substrates for area measurements to be made. (304) Under the latter conditions the equilibrium constant is ~15 times that under the former, so production of phosphoarginine is favoured at high enzyme concentrations. From an analysis of the line-shapes of the enzyme-bound substrates and products the rate of exchange is found to be faster than the velocity of the overall reaction, therefore the rate of phosphoryl transfer between the enzyme bound substrates is not the rate-determining step of the overall reaction.

The enzyme requires the presence of a divalent cation for activity and this is shown to be complexed by the substrate nucleotides. When EDTA is added to the system sequestering the Mg(II) the uncomplexed nucleotides are observed and the catalysed reaction ceases. The interactions between enzyme, substrates, and cofactors in a series of binary, ternary, and quaternary complexes were studied by Rao and Cohn. (305) They found that when sodium nitrate is added to the quaternary complex E·Mg·ADP·Arg the ADP β resonance shifts in the same manner as if a transition state complex forms, suggesting that planar trigonal monoanions can mimic the phosphoryl group to form a transition state analogue complex E·Mg·ADP·Arg·NO_3.

(i) *Adenylate kinase* (EC 2.7.4.3) catalyses the equilibration of ATP and AMP with ADP, [14], requiring the presence of divalent cations for activity. This requirement is met by Mg(II) *in vivo*. The enzyme tends to be concentrated in those tissues where a high adenosine nucleotide energy turnover occurs; because of its ability to synthesize adenosine nucleotides beyond the monophosphate level, it is extremely widespread in living matter.

$$2\text{ADP} = \text{ATP} + \text{AMP} \quad [14]$$

^{31}P NMR observations have been made on enzyme bound substrates and inhibitors. When the inhibitor diadenosine pentaphosphate is bound to adenylate kinase, its spectrum changes from one consisting of a complex pair of signals situated at −11·1 ppm and −22·8 ppm, due to the two end phosphates and the three middle phosphates respectively of the pentaphosphate chain, to one consisting of five resonances. These, in the absence of Mg(II), are at −10·9, −11·9, −20·5, −22·7, and −24·0 ppm, showing that

the binding to the enzyme is asymmetric. On addition of Mg(II) to the system the signals move to −10·5, −12·5, −18·6, −22·7, and −25·6 ppm, indicating an increase in the bonding asymmetry. (306) A study of enzyme bound substrates (307) has revealed two nucleotide binding sites on the enzyme, one which binds only unchelated nucleotides whereas the other binds ATP or ADP with or without chelated metal. The former also binds AMP and is the ADP donor site. Signals from the donor site ADP (1-P ~ −9·4, 2-P ~ −3·5 ppm) are distinguishable from acceptor site ADP (1-P ~ −11, 2-P ~ −6·5 ppm), and the phosphorus spin–spin coupling constants of ATP (in free solution $J_{1,2} = J_{2,3} \approx 19{\cdot}5$ Hz) become unequal when bound to the enzyme in the absence of Mg(II) ($J_{1,2} = 17{\cdot}6$ Hz, $J_{2,3} = 20{\cdot}5$ Hz), suggesting a conformational change in the phosphate chain. However, in the presence of Mg(II) this inequality is removed ($J_{1,2} \approx J_{2,3} \approx 15$ Hz) which is approximately the same value as found for free ATP·Mg(II) chelate.

From the line-widths of the ADP and ATP signals the rates of phosphoryl transfer on the enzyme are found to be 420 and 690 s^{-1} respectively at pH 7 and 4 °C. (307) Rates of 80 and 43 s^{-1} are reported for the overall reaction. Brown and Ogawa used a modified saturation transfer method. (308, 309) They report interconversion rates of 500 and 1300 s^{-1} from observations made at 15 °C, and a rate of 95 s^{-1} for the overall reaction from AMP. Although there is some disagreement between these values, it is clear that the rate of phosphoryl transfer is not the rate-limiting step of the reaction in either direction.

Using the sulphur nucleotide analogue adenosine-5′-monophosphorothioate as a substrate it has been shown that the adenylate kinase catalysed phosphorylation does not phosphorylate the sulphur atom and that the reaction is stereoselective, producing the A diastereoisomer of adenosine-5′-(1-thiodiphosphate). (310) The stereochemical course of thiophosphoryl group transfer in this reaction has been studied using $ATP_{\gamma}S_{\gamma}{}^{18}O_2$. Although ^{31}P NMR was not used to follow the course of the reaction, which appears to involve net inversion of configuration such as might be expected from a single displacement of the phosphoryl group (Fig. 28), it was used in establishing the configurations of these labelled nucleoside analogues. (280)

(j) *Phosphoglucomutase* (EC 2.7.5.1) catalyses the interconversion of glucose-1-phosphate and glucose-6-phosphate [15]. The former is produced to be ultimately incorporated into glycogen, and the latter is produced when glycogen is being metabolized to produce glucose.

α-D-glucose-1,6-bisphosphate + α-D-glucose-1-phosphate =
α-D-glucose-6-phosphate + α-D-glucose-1,6-bisphosphate

[15]

The ^{31}P NMR resonances of glucose-1-phosphate and glucose-6-phosphate are 2 ppm apart so the activity of this enzyme can be conveniently

assayed by ^{31}P NMR, the main disadvantage being the larger quantities of enzyme and substrates required than for the usual colorimetric methods. (311) The enzyme requires a divalent ion to be active; this is met by Mg(II) in the natural state, and it can be replaced by Mn(II) without complete loss of activity. When glucose-6-phosphate's ^{31}P nucleus is excited by a Carr–Purcell pulse sequence the decay appears in the form of a single exponential, even in the presence of Mn(II) enzyme. Since the ^{31}P NMR signals of α- and β-anomers of glucose-6-phosphate are coincident, these are not expected to decay with the same time constant unless both are equally affected by the Mn(II). Therefore it is concluded that both α- and β-anomers bind to phosphoglucomutase, although enzymatic activity is specific to the α-anomer only. (311)

Observations of the ^{31}P chemical shift, selected ^{1}H–^{31}P decoupling, and NOE effects were made on isolated phosphorylated enzyme containing a phosphate group bound at the active site. These indicate that a serine residue's hydroxyl group is the site of phosphate binding and that the phosphate group is immobilized with respect to the enzyme. Addition of Mg(II) to the phosphoenzyme has no significant effect on the chemical shift, suggesting that direct interaction between phosphate and metal does not occur. (312)

Internuclear distances between enzyme bound substrates, substrate analogues, and various metal forms of phosphoglucomutase have been calculated using paramagnetic relaxation data. The analogue molecule methylphosphonate (CH_3PO_3) binds to the enzyme at two sites with different affinities. The strong binding site is found to be ~10 Å from the metal site and 4·9 Å from the weak binding site in the Mn(II) enzyme, (313) whereas the phosphorus of bound glucose-6-phosphate is 5·8 Å from the Mn(II) site. (311) The covalently bound phosphate enzyme is reported to be 5 ± 1 Å from the Ni(II) binding site. (312)

(k) *RNA polymerase* (EC 2.7.7.6). This enzyme catalyses the production of an RNA transcript from a DNA template when activated by divalent metal cations [16]. It possesses two nucleotide binding sites termed the initiation site, which can bind a dinucleoside monophosphate, and the elongation or polymerization site which binds any of the four RNA constituent nucleoside triphosphates.

$$n \text{ ribonucleoside triphosphate} = n \text{ pyrophosphate} + \text{RNA}_n$$

[16]

The paramagnetic relaxation enhancement due to Mn(II) on the ^{31}P (and ^{1}H) nuclei of adenylyl(3′–5′)uridine [17] both in the binary metal·nucleotide complex and in the ternary complex when both are bound to the enzyme were determined. (314) In the binary complex the metal–phosphorus separation is $3{\cdot}8 \pm 0{\cdot}4$ Å, and in the enzyme bound complex $9{\cdot}3 \pm 0{\cdot}8$ Å.

Adenylyl(3′–5′)uridine binds at the initiation site and the ^{31}P (and ^{1}H) data enabled a model of its conformation to be suggested. Similar ^{1}H data on ATP bound at the elongation site suggest that the metal is located at the latter site.

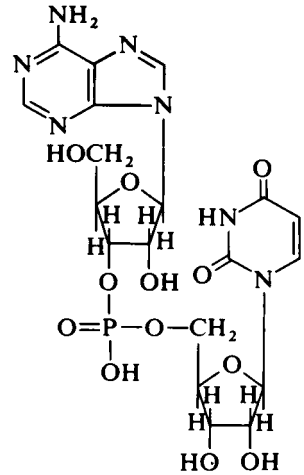

[17]

(l) *DNA polymerase* (EC 2.7.7.7). Those enzymes involved in the synthesis of daughter DNA by copying an existing template are classified as DNA polymerases. The overall reaction is the elimination of pyrophosphate from deoxynucleoside triphosphates [18] with the formation of 3′–5′ phosphodiester bonds.

$$n \text{ Deoxynucleoside triphosphate} = n \text{ pyrophosphate} + DNA_n$$

[18]

E. coli DNA polymerase I is a zinc metalloenzyme which, in the absence of a DNA template, forms non-productive complexes with thymidine-5′-triphosphate and a divalent metal cofactor. Mg(II) and Mn(II) cofactors were used to determine the paramagnetic contribution to the relaxation rates of the three phosphorus nuclei (as well as the proton relaxation rates) of the complexed substrate. (315) From the eight internuclear distances calculated from these observations a unique conformation of the enzyme-bound thymidine-5′-triphosphate is derived with the γ-phosphorus binding directly to the Mn(II) (Mn–P_α 4·2 ± 0·4; Mn–P_β 4·8 ± 0·3; Mn–P_γ 3·2 ± 0·3 Å).

(m) *UDP-glucose pyrophosphorylase* (EC 2.7.7.9). In the biosynthetic pathway from glucose to glycogen, the formation of uridinediphosphate glucose (UDP-glucose) by this enzyme [19] follows the conversion of glucose-6-phosphate into glucose-1-phosphate by phosphoglucomutase.

Glucose-1-phosphate + uridine triphosphate = P_2O_7 + uridinediphosphate glucose

[19]

The mechanism of this reaction was studied using a sulphur substituted uridine nucleotide substrate. Only one of the diastereoisomers of uridine-5′-(1-thiodiphosphate) is found to be active. When the resulting uridine-5′-(1-thiodiphosphate) glucose is hydrolysed under conditions designed to minimize hydrolysis of the aldose phosphate group, the uridine-5′-(1-thiodiphosphate) is of the other diastereoisomeric form. That is, the enzyme reaction proceeds with inversion of the nucleotide, suggesting that a single displacement mechanism operates. (316)

2. Hydrolases

These enzymes catalyse the hydrolysis of various bonds. Those enzymes reported in this review belong to sub-groups EC 3.4 (hydrolysis of ester bonds) and EC 3.6 (hydrolysis of acid anhydrides, i.e. condensed phosphoric acids).

(a) *Alkaline phosphatase* (EC 3.1.3.1) is a zinc metalloenzyme in the native state that catalyses the dephosphorylation of orthophosphate esters [20].

$$ROPO_3^{2-} + H_2O = ROH + HPO_4^{2-}$$

[20]

When a solution of apoenzyme and orthophosphate is titrated with metal ions, it is found that a plot of the line-width of the orthophosphate ^{31}P NMR signal against molar ratio of metal to enzyme shows a distinct change in slope at a metal : enzyme ratio of 2 : 1 for Zn(II), Co(II), and Mn(II), (317) a result that suggests that the enzyme has two tight binding sites for metal ions.

The Mn(II) enzyme has been used to determine the internuclear separation of bound orthophosphate and metal by measuring the paramagnetic enhancement of the ^{31}P relaxation rate, (318) a distance of 7·3 Å being reported. (319)

Observations of the ^{31}P NMR signals of enzyme bound P_i have been made over a wide pH range; over part of this, signals are found at 8·5 ppm, 3·5 ppm, and 0 ppm. The latter is due to unbound P_i; the first two are assigned to covalently bound P_i (E—P_i) and P_i non-covalently bound (E·P_i) at the enzyme active site respectively. (320) The large high frequency shift of the covalently bound P_i is attributed to steric strain imposed on bonding to a serine residue at the active site. These observations have been confirmed, (321) extended to show that 1·5–2·0 mol P_i binds to each dimer of alkaline phosphatase, and that the rate-limiting step in the hydrolysis reaction at alkaline pH is the dissociation of the non-covalently bound phosphate·enzyme complex.

The paramagnetic method has been used to determine the separation between the inhibitor *p*-aminobenzylphosphonate bound at the active site of the Mn(II) enzyme complex. (322) The result of 7·7 Å is in good agreement with that of an earlier study using P_i (319).

These investigators also report that the rotational mobility of P_i in phosphorylated apoenzyme [prepared by demetallating the Cd(II)·enzyme·P_i complex] is much greater than in the Cd(II) phosphoryl enzyme. This result, and others based on the ^{31}P NMR line-widths of Co(II) and Mn(II) phosphorylated enzymes, are interpreted as indicating that the phosphate is bound within the first or second coordination spheres of the metal ion. The result of titrating the Zn(II), Cd(II), Co(II), and Mn(II) metalloenzymes with P_i shows that one equivalent is strongly bound per enzyme dimer; excess phosphate neither exchanges rapidly with the bound phosphate nor associates with the metal ion. (322) Direct observation of the NMR spectra of the metal nuclei and the phosphorus were reported for the cadmium enzyme. (323) Two equivalents of Cd(II) per protein dimer are required to generate the maximum of one equivalent of phosphoryl enzyme as shown by the high frequency shift (~8 ppm) of the ^{31}P signal. The ^{113}Cd spectrum of the cadmium enzyme consists of a single resonance (170 ppm from standard 0·1 m $CdClO_4$) showing that each nucleus is in an identical environment; therefore the enzyme dimer is of at least 2-fold symmetry in the immediate environment of the metal ions. Generation of the phosphorylated cadmium enzyme by adding one equivalent of P_i destroys this symmetry; the ^{113}Cd NMR spectrum now consists of two resonances at 142 ppm and 55 ppm respectively. No further change occurs on addition of more P_i; the latter's NMR signal is indicative of free phosphate.

However, the question of the metal enzyme stoichiometry of the native zinc enzyme has been reopened by Bock and Kowalsky. (324) They report that fully active native enzyme contains four or more Zn(II) atoms per enzyme dimer and two forms of enzyme exist having a stoichiometry of two zinc ions per enzyme dimer. One of these is obtained when zinc is added to the apoenzyme; this form has a lower enzymatic activity than that produced by dialysis of the native enzyme. These results are consistent with the earlier report that the non-covalently bound phosphate metalloenzyme complex exists in two slowly interchanging forms. (321)

In addition to the work described above, designed to discover more about the nature of the enzyme itself, ^{31}P NMR has been employed to investigate the kinetics of alkaline phosphatase catalysed reactions. The formation of phosphorylated enzyme intermediate in the overall reaction sequence can be represented by the scheme [21], where $E{\cdot}HOPO_3^{2-}$ is the non-covalent complex. By using ^{18}O-labelled inorganic orthophosphate, it is found that the exchange of oxygen between the phosphate and water is different when native zinc enzyme or cobalt enzyme (325) catalyses the reaction. The

kinetic pattern with native enzyme indicates that dissociation of $E{\cdot}HOPO_3^{2-}$ is more rapid than formation of $E{-}PO_3^{2-}$ whereas with the cobalt enzyme the opposite appears to be the case.

$$E + HOPO_3^{2-} = E{\cdot}HOPO_3^{2-} = E{-}PO_3^{2-} + H_2O$$

[21]

(b) *Acid phosphatase* (EC 3.1.3.2) catalyses the dephosphorylation of a wide range of orthophosphoric monoesters [22] in a reaction that is thought to proceed by way of an enzyme histidine phosphate intermediate.

$$ROPO_3 + H_2O = ROH + P_i$$

[22]

This enzyme was incubated in the presence of 93% oxygen-18-labelled $KH_2P^{18}O_4$ to determine whether phosphate (oxygen)–water exchange occurs in the absence of complete reaction. Control reactions show no detectable oxygen exchange in the absence of enzyme, and contrary to earlier reports, exchange is catalysed in the presence of enzyme. Although the spectra were obtained at only 40·5 MHz so that there is considerable overlap between resonances of the five individual species $P^{18}O_4$, $P^{18}O_3{}^{16}O$, $P^{18}O_2{}^{16}O_2$, $P^{18}O^{16}O_3$, and $P^{16}O_4$, reaction rate constants and activation energy data are presented. (326)

(c) *Hexosediphosphatase* (EC 3.1.3.11) is an enzyme of the glycolytic pathway which, when activated by a divalent metal ion, catalyses the production of D-fructose-6-phosphate from D-fructose-1,6-bisphosphate [23].

$$\text{Fructose-1,6-bisphosphate} + H_2O = \text{fructose-6-phosphate} + P_i$$

[23]

By substituting Mn(II) for the *in vivo* Mg(II) and using fructose-1-phosphate as the substrate to simplify the ^{31}P NMR spectra, the metal to phosphorus distances are determined in the ternary Mn(II)·enzyme·substrate complex and for the binary Mn(II)·substrate complex. (327) These are $3{\cdot}3 \pm 0{\cdot}3$ Å and $3{\cdot}2 \pm 0{\cdot}1$ Å respectively at pH 7·5, which are interpreted as favouring an S_N2 mechanism for this reaction. (267, 328)

(d) *Guanyloribonuclease* (EC 3.1.4.8) (formerly RNase T_1, EC 2.7.7.26) catalyses the depolymerization of RNA by endonucleolytic cleavage at the 3′-position of guanylate residues [24]. The intermediate RNA fragment terminated by the 2′,3′-cyclophosphodiester is subsequently hydrolysed to a 3′-phosphomonoester [25].

In a combined ^{1}H and ^{31}P NMR study, three histidine proton resonances of the enzyme are assigned and the ^{31}P NMR spectra of the inhibitor, guanosine-3′-monophosphate, reported at various pH values in the absence and presence of the enzyme. (329) It is concluded that the inhibitor binds the

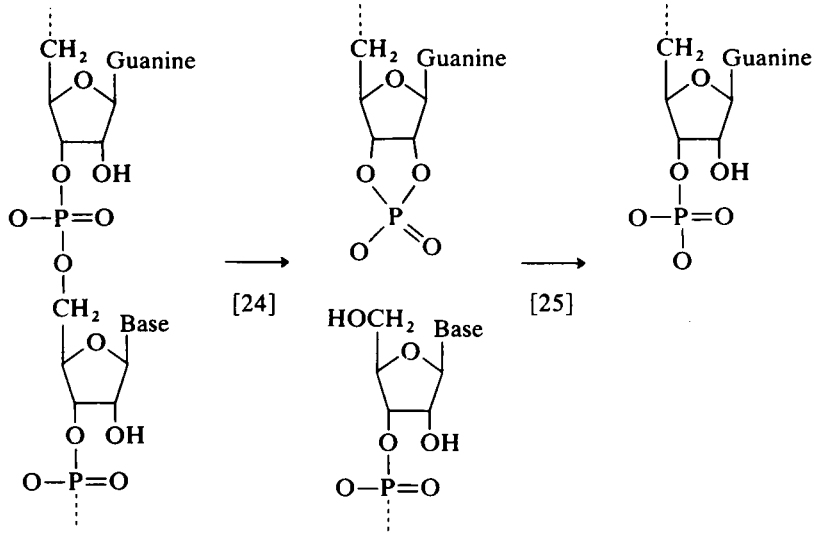

enzyme as the monoanion; a model of the structure of guanylori-bonuclease·guanosine-3′-monophosphate complex is given.

(e) *RNAase I* (EC 3.1.4.22). The overall reaction catalysed by RNAase I (which was formerly classified as EC 2.7.7.16) is the depolymerization of RNA. The hydrolysis reaction proceeds by transfer of the ribose-3′-phosphate of a pyrimidine nucleoside residue from the 5′-position of the adjoining nucleotide to the 2′-position of the pyrimidine itself forming a cyclic phosphodiester. Finally the latter is hydrolysed to a 3′-phosphomonoester ([24], [25] where guanine is replaced by a pyrimidine, i.e. cytosine or uracil).

All the ^{31}P NMR studies reported have used bovine pancreatic RNAase I, which consists of 124 amino-acids in a known sequence, and various pyrimidine nucleoside monophosphate inhibitors. From the pH dependence of the inhibitors' phosphate group signal in free solution and when bound to the enzyme, it is shown that the inhibitors bind as their dianion. (330–332) Furthermore, it is concluded that the results of the first ^{31}P NMR study on this enzyme (333) are unreliable because of paramagnetic ion contamination of the samples.

On the basis of the observed pK values and corresponding ^{1}H NMR results on the enzyme, as well as X-ray data, the inhibitors' phosphate group is thought to bond to the imidazole nitrogens of histidine residues 12 and 119. (332)

(f) *Chymotrypsin* (EC 3.4.21.1). The chymotrypsin enzymes formerly classified as chymotrypsin A (EC 3.4.4.5) and chymotrypsin B (EC 3.4.4.6) both catalyse the hydrolysis of peptides by preferential attack on the carbonyl end of tyrosine, tryptophan, phenylalanine, and leucine residues;

consequently they have been re-classified into the same sub-group. These are enzymes of the mammalian digestive system, being secreted into the duodenum from cells in the pancreas. However, to prevent their proteolytic activity from damaging the cells in which they are synthesized they are produced and secreted as the inactive proenzyme or zymogen, chymotrypsinogen. Only when the latter has reached the duodenum is it activated by another proteolytic enzyme trypsin (EC 3.4.21.4).

Both chymotrypsin and chymotrypsinogen can be phosphorylated at their serine-195 residue by diisopropylfluorophosphate to form stable phosphodiesters. Each derivative has a single ^{31}P NMR resonance, the modified zymogen's signal appearing at 2 ppm to low frequency of that of the modified enzyme, which may be due to changes in the P–O bond angle and hydrogen-bonding differences in each compound. (334) Furthermore, diisopropylphosphoryl chymotrypsin itself is reported to have a ^{31}P NMR spectrum consisting of two resonances again separated by 2 ppm. (335) The intensity ratio of these signals is reported to be pH-dependent and ascribed to two slowly interconverting conformational isomers of the enzyme complex, although the possibility of their being due to transfer of the phosphoryl group between serine-195 and histidine-57 residues is not excluded.

(g) *Inorganic pyrophosphorylase* (EC 3.6.1.1) catalyses the hydrolysis of pyrophosphate [26] thereby maintaining the unidirectional character of other biochemical reactions which have pyrophosphate as their (unwanted) product.

$$P_2O_7^{4-} + H_2O = 2HPO_3^{4-}$$

[26]

The enzyme consists of two identical subunits, each of which possesses two binding sites for Mn(II) ions. Both ^{1}H and ^{31}P NMR were used to study ternary systems consisting of enzyme, Mn(II), and either inorganic orthophosphate or the pyrophosphate analogue hydroxymethane bisphosphonate $Na_2O_3POCH(OH)OPO_3$. Dialysis experiments and relaxation time measurements have been carried out with the result that two phosphate sites per enzyme subunit were discovered, both of which are simultaneously inhibited by the pyrophosphate analogue, suggesting that the sites are close to one another. A separation of 6·2 Å between the tight Mn(II) binding site and the low affinity phosphate site, consistent with outer sphere binding, is reported. In addition the weaker Mn(II) binding site appears to be remote from both phosphate binding sites. (336)

Not unexpectedly, the enzyme has been found to catalyse the exchange of oxygen between orthophosphate and water; (11) at present only a preliminary communication of this work has been made.

(h) *Adenosinetriphosphatase* (EC 3.6.1.3) catalyses the hydrolysis of ATP [27]. Various forms of the enzyme are known, some requiring the presence of Mg(II) or Ca(II) for activity, while others require both ions to be present. Still others are activated by Na^+ and K^+. In addition to ATP some other nucleoside triphosphates, inorganic triphosphate, and adenosine tetraphosphate are hydrolysed by this enzyme. ATPase activity is widespread in organisms, being found associated with cell membranes, microsomes, mitochondria, myosin, and actomyosin.

$$ATP + H_2O = ADP + P_i$$

[27]

Membrane-bound ATPase is intimately associated with the active transport of ions across cell membranes as well as with the synthesis and hydrolysis of ATP. Attempts to study membrane coupling ATPase fractions by ^{31}P NMR are, so far, unsuccessful. Signals from "tightly bound" ATP and ADP (tightly bound in the biological sense of not being removed from the enzyme by other ATP-utilizing enzymes such as hexokinase) are not detected. This failure is attributed to the nucleotides being highly immobilized in the physical sense; (337) if so, this system should be amenable to solid sample methods.

Sheep kidney medulla membrane bound ($Na^+ + K^+$) activated ATPase has been studied by the paramagnetic relaxation method. It possesses a single tight binding site for Mn(II); the effect of this ion on the relaxation rate of methyl phosphonate ($CH_3PO_3^{2-}$) in purified enzyme preparations has been examined. Methyl phosphonate is an inhibitor which binds to the Mn·enzyme complex with a similar affinity as P_i; a Mn–phosphorus separation of $6{\cdot}9 \pm 0{\cdot}5$ Å was found. (338) Thus direct metal–inhibitor bonding does not occur and an intervening first coordination sphere ligand such as hydroxyl between metal and phosphonate is postulated [28].

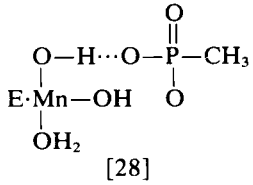

[28]

A kinetic study of myosin ATPase using ^{18}O-labelled orthophosphate has been reported. (339) Myosin subfragment I and Mg(II)ADP were incubated with $P^{18}O_4$ and the rate of $^{16}O/^{18}O$ exchange between the water and inorganic orthophosphate observed. The relative concentrations of $P^{18}O^{16}O_3$, $P^{18}O_2{}^{16}O_2$, $P^{18}O_3{}^{16}O$, and $P^{18}O_4$ do not change with time from their initial ratios, although their absolute concentrations diminish and a concomitant increase in $P^{16}O_4$ concentration occurs. Thus all molecules of $P^{18}O_4$ that experience exchange go completely to $P^{16}O_4$; this behaviour is

explained in the following terms. The overall catalysed reaction of ATPase can be written as a four-step process [29].

$$\underset{(1)}{E + ATP} = \underset{(2)}{E{\cdot}ATP} = \underset{(3)}{E{\cdot}ADP{\cdot}P_i} = \underset{(4)}{E{\cdot}ADP + P_i} = E + ADP + P_i$$

[29]

Considering step 2 in more detail and denoting oxygen-18 by ϕ, [30], if the myosin·ATP complex is in rapid exchange with the myosin·ADP·P_i complex and the release of P_i from this complex is comparatively slow, then all the ^{18}O nuclei are exchanged into the solvent before P_i release.

$$E{\cdot}AOPOPOP\phi + H_2O \rightarrow \left[E{\cdot}AOPOPOH{\cdot}OP\phi_3H\right] \rightarrow E{\cdot}AOPOPOP\phi + H_2\phi$$

[30]

The kinetics of the ATP reaction have also been studied using a saturation transfer method applied *in vivo* to aerobic *E. coli* cells. Selective saturation of the γ-ATP resonance results in a 20% reduction of the P_i signal, which is unchanged when the catalysed reaction is stopped by addition of an inhibitor. This information together with the spin–lattice relaxation time of P_i allows the unidirectional rate constant $P_i \rightarrow$ ATP to be evaluated ($0{\cdot}6 \pm 0{\cdot}15\ s^{-1}$). The reverse reaction rate constant was only estimated because of problems in determining a reliable value of T_1 for the γ-ATP phosphorus. (340)

3. Lyases

These enzymes cleave C–C, C–N, C–O, and other bonds by means other than hydrolysis or oxidation. The two enzymes reported belong to subgroup EC 4.2 and catalyse the breaking of C–O bonds.

(a) *Carbonic anhydrase B* (EC 4.2.1.1) is involved in the respiratory function, catalysing the reversible hydration of carbon dioxide [31]. It is found associated with the red cells in blood. In the native state the apoenzyme is potentiated by Zn(II) ions, and although other metal derivatives of the apoenzyme may be prepared, only the Co(II) compound shows active catalytic activity. Although no phosphorus-containing substrates or products take part in the catalytic reaction, it has been suggested that the proton transfer may involve the buffering medium. Consequently the paramagnetic relaxation effect is used to determine the Co–P separation

$$H_2CO_3\ (\text{or } H^+ + HCO_3^-) = CO_2 + H_2O$$

[31]

between enzyme bound Co(II) and buffer phosphate. (341) Although it was concluded that direct phosphate–Co bonding is present, the calculated distance is impossibly short for any acceptable Co–O–P bonding angle.

(b) *Enolase* (EC 4.2.1.11) is an enzyme of the glycolytic pathway that catalyses the reversible hydration of phosphoenolpyruvate [32].

$$CH_2{=}C(OPO_3^{2-})COO^- + H_2O = CH_2(OH)CH(OPO_3^{2-})COO^-$$

[32]

The paramagnetic relaxation method was used to determine metal to phosphorus (and proton) distances in Mn(II)·enzyme complexes with the substrate analogue compounds phosphoglycollate [33] and α-(dihydroxyphosphinylmethyl)acrylate [34]. Distances of $5{\cdot}47 \pm 0{\cdot}11$ Å and $6{\cdot}23 \pm 0{\cdot}36$ Å respectively are found, suggesting that second sphere phosphate coordination is present; the enzyme bound conformations of the molecules are also reported. (342)

$CH_2(OPO_3^{2-})COO^-$ [33]

$CH_2{=}C(CH_2PO_3^{2-})COO^-$ [34]

4. Isomerases

These enzymes catalyse isomerization within a molecule; the enzyme reported belongs to sub-group EC 5.3 and oxidizes one part and reduces another part of the same molecule.

(a) *Triosephosphate isomerase* (EC 5.3.1.1) is one of the enzymes of the glycolytic pathway that catalyses the interconversion of D-glyceraldehyde-3-phosphate and dihydroxyacetone phosphate (DHAP) [35].

$$CHO{-}CH(OH)CH_2OPO_3H_2 = CH_2(OH)CO{-}CH_2OPO_3H_2$$

[35]

Since DHAP exists in aqueous solution as an equilibrium mixture of keto and hydrated keto forms, and only the former is an active substrate, it is necessary to correct the DHAP concentration parameter when calculating the reaction's kinetic parameters. The phosphorus signals of both forms of DHAP are resolved at 24 MHz, (30) allowing the interaction between each form and the enzyme to be studied. Only the resonance of the keto form broadens in the presence of enzyme, (343, 344) showing that the hydrated DHAP does not bind to the enzyme and thus does not act as a competitive inhibitor.

Further studies have been concerned with the ionization state of enzyme bound inhibitors. The affinity of the enzyme for 2-phosphoglycollate is at a maximum at a pH corresponding to the inhibitor dianion in free solution. Two possible structures may be written for this dianion [36], [37]; knowing the pH dependence of both carbonyl (^{13}C) and phosphate (^{31}P) chemical

shifts, NMR spectra should identify the enzyme bound form. However, the spectrum of the enzyme bound molecule is more consistent with the trianion [38]. (344, 345) To reconcile the conflicting affinity and NMR information it is suggested that 2-phosphoglycollate binds as the trianion and that one enzyme residue is simultaneously protonated.

$^{-}OOCCH_2OPO_3H^{-}$ $HOOCCH_2OPO_3^{2-}$ $^{-}OOCCH_2OPO_3^{2-}$

[36] [37] [38]

5. Ligases

These enzymes catalyse the bonding of two molecules, and involve the hydrolysis of the pyrophosphate bond in a nucleoside triphosphate. The enzyme reported belongs to sub-group EC 6.3 and forms C–N bonds.

(a) *Glutamine synthetase* (EC 6.3.1.2) catalyses the amidation of glutamic acid to form L-glutamine [39]. It is the sole method possessed by microorganisms for the synthesis of glutamine which is an essential constituent amino-acid of proteins.

$$HOOCCH(NH_2)CH_2CH_2COOH + ATP + NH_3 = HOOCCH(NH_2)CH_2CH_2CONH_2 + ADP + P_i$$

[39]

The enzyme isolated from *E. coli* consists of twelve identical subunits whose activity appears to be regulated by three control mechanisms. Two of these mechanisms have been used to study the topography of enzyme·substrates·cofactor complexes. These two control mechanisms are the enzyme's requirement for divalent cations, Mg(II) or Mn(II), to convert its apoenzyme into the active form and the chemical modification of each subunit by adenylylation. The latter reaction is achieved by the action of another enzyme, adenylyltransferase (EC 2.7.7.42), which covalently bonds the adenylyl group of ATP by means of a phosphodiester linkage to the hydroxyl group of a particular tyrosyl residue in the subunit [40].

$$\text{Subunit} + ATP = \text{AMP—subunit} + \text{pyrophosphate}$$

[40]

Relaxation studies of this AMP phosphorus nucleus in fully ($E_{11.5}$; 11·5 adenylyl groups per enzyme molecule) adenylylated enzyme complexes with Mn(II) and Co(II) have been used to determine the metal–phosphorus internuclear separations. These distances are reported to be 10 Å,7 Å and 8 Å,6 Å for each of the two enzyme metal ion binding sites respectively for Co(II) and Mn(II) complexes. From these results, together with ^{13}C NMR and fluorescence data, it is concluded that the most distant metal ion binding site controls the apoenzyme–active enzyme transition and that

the adenylylation site is near to the catalytic reaction site where the second metal binding site is located. (346)

The $^{16}O/^{18}O$ isotopic composition effect of the ^{31}P NMR chemical shift of inorganic phosphate has been used to monitor the reverse of the biosynthetic reaction [39]. Using Mg(II) activated unadenylylated glutamine synthetase ($E_{1\cdot7}$) in the presence of ^{18}O-labelled P_i, ADP, and L-glutamine substrates, it is found that the exchange of ^{18}O from ^{18}O-P_i is approximately 7 times the rate of ATP formation. Detailed analysis of the exchange results indicates that P_i binds and dissociates from the enzyme very much more rapidly than the L-glutamine. (347)

C. Coenzymes

1. Introduction

Coenzymes are organic molecules whose presence is required before certain enzymes are able to catalyse reactions of their substrates. Unless both enzyme and coenzyme are present, no catalysis takes place. In the catalysed reaction the chemical change in the coenzyme counterbalances that taking place in the substrate. For example, in dehydrogenase reactions, for every substrate molecule that is oxidized, one molecule of coenzyme is reduced. The coenzyme behaves in effect as a cosubstrate.

Coenzyme molecules encompass a wide range of organic structures, but the presence of an adenine ring joined to D-ribose and phosphate are common structural elements. All coenzymes are closely related to vitamins, and the biological role of vitamins may be to provide the appropriate structure or structural precursor for coenzyme synthesis.

The ^{31}P NMR work on coenzymes has been mainly concerned with their conformations in free solution and when bound to enzymes and their mode of binding.

2. Coenzyme A

Coenzyme A [41] is an essential cofactor for acetyltransferases and enzymes concerned with the metabolism of fatty acids. Its structure incorporates that of its associated vitamin, pantothenic acid [42].

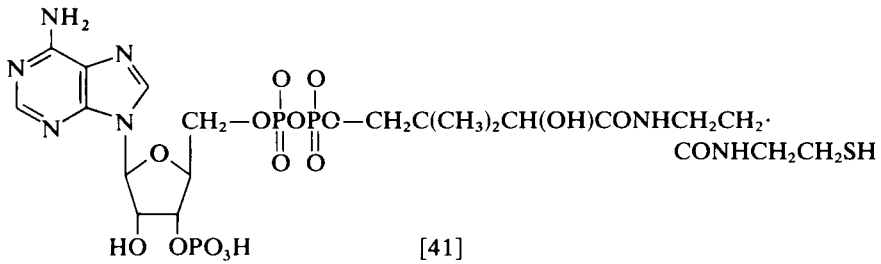

[41]

$$HOCH_2C(CH_3)_2CH(OH)CONHCH_2CH_2COOH$$

[42]

The conformation of CoA in free solution has been described by Lee and Sarma (348, 349) from their extensive ^{1}H NMR observations of the various three bond spin–spin coupling constants and computed spectrum simulations. In addition ^{31}P NMR spectra are used to complement the ^{1}H data for the ribose– and pantetheine–phosphate interfaces.

Possible conformations of propionyl-CoA, when bound to transcarboxylase (EC 2.1.3.1), were determined from the paramagnetic effects of enzyme bound Cu(II) and Co(II) on the ^{1}H and ^{31}P NMR relaxation rates. (350) From the minimum phosphorus–metal distance of $\geq$9 Å it is clear that no direct metal to coenzyme phosphate interaction occurs.

3. Thiamine pyrophosphate

Thiamine pyrophosphate [43] is the coenzyme of a number of decarboxylases and some dehydrogenases. The necessary organic structure for its synthesis is provided by vitamin B_1 (thiamine) [44].

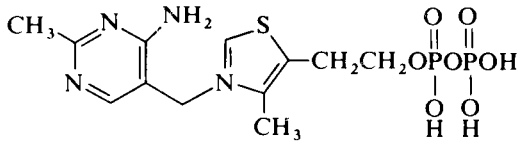

[43]

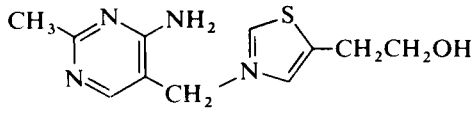

[44]

The conformation of a 1 : 1 Mn(II)·thiamine pyrophosphate complex in free solution is determined from the paramagnetic relaxation effect on its ^{1}H NMR spectrum. (351) This shows that the molecule is folded with the diphosphate group bent over the plane of the thiazolium ring and interacting with the positively charged nitrogen. ^{31}P NMR is used to show that at elevated temperatures the molecule opens with a reduced interaction between phosphate and thiazolium nitrogen; it also shows that no hydrolysis of the diphosphate group occurs during the experiments.

A conformational analysis of thiamine pyrophosphate in the presence and absence of Mg(II) has been carried out from ^{31}P–^{1}H NOE measurements. (352)

4. Pyridoxal phosphate

Pyridoxal phosphate [45] acts as a coenzyme to various racemases, transaminases, decarboxylases, and phosphorylase. Vitamin B_6 [46] (pyridoxine) is the coenzyme's structural precursor. The ^{31}P NMR spectra of both pyridoxal phosphate and pyridoxamine phosphate [47] in free solution

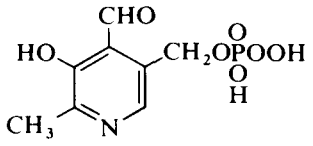

[45]

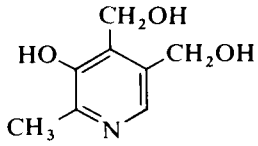

[46]

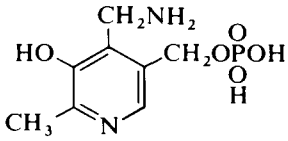

[47]

consist of a triplet, $^3J(^{31}P-^1H) = 6{\cdot}0 \pm 0{\cdot}3$ Hz. Their titration curves show that a single proton titrates in the 3·5–9 pH range with pK values for this dissociation of 6·2 and 5·7 respectively. (353) When either form of the coenzyme is bound to the apoenzyme aspartate transaminase (EC 2.6.1.1) to produce the fully functional holoenzyme, the phosphorus resonance moves to the higher frequency position corresponding to the dianion. The chemical shift of this resonance is practically invariant to pH change over the stability range (5·6–9·2 pH) of the enzyme. It is concluded that the apoenzyme phosphate binding site is probably a positively charged pocket containing lysine and/or arginine residues, and that the coenzyme is bound in the form of a fully ionized monoester. The resonance is also unaffected by the addition of substrates or inhibitors, so participation of the phosphate group in the catalysed reaction seems unlikely. (353)

The interaction of pyridoxal phosphate with glycogen phosphorylase (EC 2.4.2.1) apoenzyme has been the subject of a number of investigations. In the first of these Busby *et al.* found that the ^{31}P NMR resonance of pyridoxal-5′-phosphate bound to phosphorylase *b* consists of more than one component. (354) They tentatively conclude that two ionization states of the coenzyme are present. This result is not confirmed however by Feldmann and Helmreich (355) who observe only a single resonance from pyridoxal-5′-phosphate bound to phosphorylase *b*. The chemical shift of this resonance is invariant over a pH range of 5·8–8·5 showing that deprotonation of the coenzyme–apoenzyme complex or holophosphorylase *b* does not take place under these conditions. Yet when the allosteric effector

(a small molecule that binds to a site distinct from the active site of the enzyme yet activates it) AMP is added to the holophosphorylase *b*, the resulting conformational change allows deprotonation of the phosphate group to occur at pH 7·6. The phosphate group can now participate directly in the catalytic process by acting as a proton source and sink, as well as serving as a structural ligand. The resonances of holoenzyme bound AMP, free AMP, and coenzyme phosphate all overlap, which may be the explanation for the observations of Busby *et al.*

The overlap problem can be overcome by using adenosine-5′-monophosphorothioate which is an effective activator of holophosphorylase *b* and whose signals are 40 ppm to high frequency of the coenzyme phosphate. Using this technique three distinct forms of enzyme bound pyridoxal-5′-phosphate have been detected. (356) These are termed forms (I), (II), and (III) having resonances 0·2, 2–3, and 3·5 ppm respectively to high frequency of a trimethyl phosphate reference signal. Form (I) is the inactive phosphorylase *b* obtained in the absence of an effector. Form (III) is the active phosphorylase *b* effector complex, and form (II) is only observed when the pH is less than 7, but it is not free pyridoxal-5′-phosphate. These results show that conformation changes of the holoenzyme also involve the coenzyme but leave the question of the coenzyme phosphate group participation in acid–base catalysis unanswered.

5. Nicotine adenine dinucleotides

These are coenzymes to various dehydrogenases, epimerases, and hydroxylases. The vitamin niacin (nicotinic acid) [48] provides the essential structural element for the coenzyme [49].

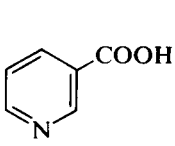

[48]

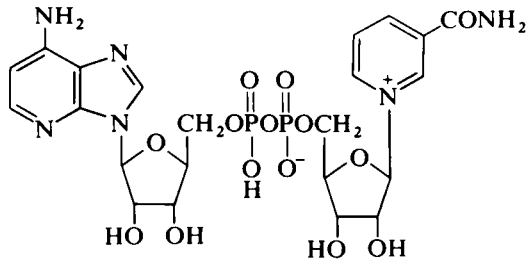

[49]

The conformations of several members of this family of molecules in free solution were studied by Sarma and Mynott. In the main their conclusions are based on $^{3}J(^{1}H–^{1}H)$ and $^{3}J(^{1}H–^{31}P)$ coupling constants obtained from ^{1}H NMR spectra together with computed simulation spectra. Nevertheless ^{31}P NMR spectra and spectrum simulations were also reported. Among the molecules investigated are the oxidized and reduced forms of nicotinamide

mononucleotides (NMN), (357, 358) nicotinamide adenine dinucleotides (NAD^+, NADH), (359, 360) and nicotinamide adenine denucleotide phosphate ($NADP^+$, NADPH). (361)

The interaction of NAD and NADH with beef heart lactate dehydrogenase (EC 1.1.1.27) and with rabbit muscle glyceraldehyde-3-phosphate dehydrogenase (EC 1.2.1.9) has been described by Blumenstein. (362) With lactate dehydrogenase the ^{31}P NMR signal from NADH is ~0·6 ppm to high frequency of its position in free NADH. At high enzyme concentrations an additional signal having a decrease in screening of 1·9 ppm is observed and it is suggested that this is due to coenzyme being bound to an aggregated enzyme species. The spectrum of the coenzyme in the presence of glyceraldehyde-phosphate dehydrogenase consists of a single signal ~0·5 ppm to low frequency of the free coenzyme. The ^{31}P NMR results with NAD^+ and NADH are very similar for each enzyme, suggesting that the environment of both bound oxidized and reduced coenzyme is the same for a given dehydrogenase, although different from one enzyme to another.

Possible conformations of NAD^+ bound to yeast alcohol dehydrogenase (EC 1.1.1.1) were suggested (363) from ^1H and ^{31}P relaxation data obtained with the enzyme bound to a paramagnetic spin-labelled iodoacetamide analogue, which is known to bond covalently to the enzyme cysteine residue 43.

The interaction between $NADP^+$, NADPH, and coenzyme fragments with dihydrofolate reductase (EC 1.5.1.3) from *Lactobacillus casei* are the subject of continuing investigation. (364–366) In free solution the pyrophosphate nuclei of NADPH are accidentally equivalent, giving a single signal at −13·78 ppm, and the 2′-phosphate group a signal at 0·47 ppm (to higher frequency of an orthophosphate reference at pH 8·0). On addition of enzyme the equivalence is removed and an AB quartet signal is obtained ($\delta - 13{\cdot}94$, $-16{\cdot}47$, $^2J(POP) = 20{\cdot}8$ Hz). The 2′-phosphate group signal shifts to higher frequency by 2·66 ppm. $NADP^+$ behaves similarly and it is concluded that the 2′-phosphate binds as its dianion and the local environment of the phosphate group in $NADP^+$ and NADPH are very similar, notwithstanding a 10^3-fold difference in their binding constants. This difference must therefore be localized at sites on the coenzyme remote from the phosphorus nuclei. (364, 365) Further studies of the binding using the coenzyme fragment adenosine-2′-phosphate (2′-AMP), which displays a single ^{31}P NMR resonance whose position changes smoothly over a 0·6 ppm range as the enzyme : 2′-AMP molar ratio is changed, have been reported. (366) This behaviour is analysed in terms of rapid exchange between free and enzyme-bound 2′-AMP, its binding being at a maximum at a pH corresponding to the dianion. In contrast, the binding of 5′-AMP appears to be undetectable by NMR.

IX. PROSPECTS

In a relatively short period, Fourier transform NMR techniques have advanced the practice of ^{31}P NMR into biological areas undreamt of only six years ago. In looking for further advances, one not only trusts in the ingenuity of researchers working with the present generation of NMR equipment, but also that the ends (medical applications) will justify progressively more expensive NMR instruments. While it is traditional at the end of NMR reviews to look forward to more intense NMR magnet fields, with biological ^{31}P NMR probably it will be larger sample volumes that determine progress. The present controversy concerning expensive medical instrumentation in the USA may blight the prospects of techniques such as ^{1}H NMR whole-body imaging and possible ^{31}P NMR ancillary methods, (63, 367) but there are many other medical applications that would not require the ultimate in NMR systems.

Not a large advance in magnet bore size would be needed for human limbs to be studied *in vivo*. In this way, muscular dystrophy and other muscular maladies could be studied directly. Real *in vivo* enzyme kinetics in human tissue could be observed (cf. creatine kinase work in ref. 303). The effects of stress on phosphate metabolites in humans could also be determined; such effects are already known in animals, yet human stress remains a biologically ill-defined condition. ^{31}P NMR as a monitoring aid for open-heart and kidney transplant surgery could be of considerable value as indicated by some of the publications discussed in this review.

Without using larger NMR sample volumes than already possible, there seems to be a variety of medical possibilities in studying phosphorus-containing metabolites. Blood and fertility defects have already been discussed in this review. Biopsies of tissue for diagnostic purposes would seem amenable to ^{31}P NMR although existing biopsy procedures are usually satisfactory. Studies of bone changes in ageing, following reduction of bone samples to stable colloids, (85) could be possible by ^{31}P NMR without the use of magic angle spinning etc. The deposition of calcium phosphate crystals, as in arthritic conditions, should also be amenable to ^{31}P NMR studies. Further animal studies on protection of heart and kidney during surgery would seem likely following the publications mentioned in this review. A variety of ^{31}P NMR publications concerning the effects of pharmaceuticals on tissue components have been reviewed, and it would seem logical to expect studies of their effects on target organs. By the same token, one should expect to have ^{31}P NMR used as a status monitor for the effects of pollutants on tissue, e.g. from lung and gastrointestinal tract. The effects of certain phosphorus-containing food components present in large quantities in human food, i.e. polyphosphates and phytic acid, are already suspected or known to be detrimental to human health

and have proved to be amenable to ^{31}P NMR determination in biological tissue. (255, 368)

^{31}P NMR is limited in direct studies to those molecules containing phosphorus and this is a severe limitation. Phosphorus labelling would expand enormously the applicability of ^{31}P NMR, for example to pharmaceuticals and it would be useful to investigate further phosphonium analogues for substances containing the common *N,N*-dimethyl function. One should expect the greater use of ^{18}O-labelling in reaction kinetic studies, as well as the use of other analogues which permit distinction of natural from introduced materials.

An experimental technique of considerable promise for solid-type materials is magic angle spinning with high-powered decoupling. (86) Although past work has been performed with home-built instruments, commercial equipment is now available. Observation of other nuclei by NMR has also proved to be essential in many of the publications reviewed. With yeasts, (88) the limitations of ^{31}P vis-à-vis ^{13}C observation were demonstrated; probably ^{13}C observation may be superior for those samples with a relatively simple metabolite pattern and without interference by a substantial quantity of relatively mobile lipid as is found in higher organisms. It has been the relative simplicity of ^{1}H-decoupled ^{31}P NMR observation that has been of such great use in biological investigations. However, the spin–spin interaction of ^{31}P with other nuclei has proved useful in many NOE-based publications; a promising new technique for elucidating heteronuclear interactions *in vitro* is two-dimensional NMR. (369)

In the studies of biological materials in this review, practically every publication utilizes the measurements derived from techniques other than ^{31}P NMR. One can predict that many of the advances afforded by ^{31}P NMR will derive from advances in other techniques that make ^{31}P NMR results more meaningful in just the same way as ^{31}P NMR information has made other results more meaningful. Many of the prospects for ^{31}P NMR can only be fulfilled by close collaboration of ^{31}P NMR experts with those in quite disparate fields. This is reflected already in the author listings of publications from the more prolific groups; nevertheless, many workers in biology, medicine, and related areas remain as yet unaware of ^{31}P NMR as a promising tool.

REFERENCES

1. G. Mavel, in "Annual Reports on NMR Spectroscopy", E. F. Mooney (ed.), 1973, **5B**, 1.
2. M. M. Crutchfield, C. H. Dungan, J. H. Letcher, V. Mark and J. R. Van Wazer, in "Topics in Phosphorus Chemistry", M. Grayson and E. J. Griffith (eds.), 1967, **5**, 1.
3. "Specialist Periodical Reports on NMR", Chemical Society, London.
4. "Specialist Periodical Reports on Organophosphorus Chemistry", Chemical Society, London.

5. J. R. Van Wazer, in "Determination of Organic Structures by Physical Methods", F. C. Nachod and J. J. Zuckerman (eds.), Vol. 4, Academic Press, 1971, p. 323.
6. J. S. Cohen, *CRC Critical Reviews in Biochemistry*, 1978, **5**, 25.
7. D. G. Gorenstein, *J. Amer. Chem. Soc.*, 1975, **97**, 898.
8. D. G. Gorenstein and D. Kar, *Biochem. Biophys. Res. Comm.*, 1975, **65**, 1073.
9. A. J. Costello, T. Glonek and J. R. Van Wazer, *Inorg. Chem.*, 1976, **15**, 972.
10. R. B. Moon and J. H. Richards, *J. Biol. Chem.*, 1973, **248**, 7276.
11. M. Cohn and A. Hu, *Proc. Nat. Acad. Sci. USA*, 1978, **75**, 200.
12. O. Lutz, A. Nolle and D. Staschewski, *Z. Naturforsch.*, 1978, **35a**, 380.
13. G. Lowe and B. S. Sproat, *J. Chem. Soc., Chem. Comm.*, 1978, 565.
14. H. S. Kielman and J. C. Leyte, *Ber. Bunsen ges. Phys. Chem.*, 1975, **79**, 1202.
15. T. Glonek and J. R. Van Wazer, *J. Phys. Chem.*, 1976, **80**, 639.
16. P. L. Yeagle, W. C. Hutton and R. B. Martin, *J. Amer. Chem. Soc.*, 1975, **97**, 7175.
17. T. Glonek, *J. Amer. Chem. Soc.*, 1976, **98**, 7090.
18. T. Glonek, R. A. Kleps, E. J. Griffith and T. C. Myers, *Phosphorus*, 1975, **5**, 165.
19. T. Glonek, A. J. R. Costello, T. C. Myers and J. R. Van Wazer, *J. Phys. Chem.*, 1975, **79**, 1214.
20. T. Glonek, *Phosphorus and Sulphur*, 1978, **4**, 235.
21. T. Glonek, M. Lunde, M. Mudgett and T. C. Myers, *Arch. Biochem. Biophys.*, 1971, **142**, 508.
22. N. W. Gabel and V. Thomas, *J. Neurochem.*, 1971, **18**, 1229.
23. T. Glonek, T. O. Henderson, R. L. Hilderbrand and T. C. Myers, *Science*, 1970, **169**, 192.
24. T. O. Henderson, T. Glonek, R. L. Hilderbrand and T. C. Myers, *Arch. Biochem. Biophys.*, 1972, **149**, 484.
25. E. M. Gaydon and J. R. Llinas, *Org. Magn. Resonance*, 1974, **6**, 23.
26. C. Giessner-Prettre and B. Pullman, *J. Theor. Biol.*, 1978, **72**, 751.
27. W. J. Kung, R. E. Marsh and M. Kainosho, *J. Amer. Chem. Soc.*, 1977, **99**, 5471.
28. R. Kluger, P. Wasserstein and N. Nakaoka, *J. Amer. Chem. Soc.*, 1975, **97**, 4298.
29. R. K. Gupta and J. L. Benovic, *Biochem. Biophys. Res. Comm.*, 1978, **84**, 130.
30. G. R. Gray, *Accounts Chemical Res.*, 1976, **9**, 418.
31. A. J. R. Costello, T. Glonek, M. E. Slodki and F. R. Seymour, *Carbohydrate Res.*, 1975, **42**, 23.
32. P. J. Cozzone and O. Jardetzky, *Biochemistry*, 1975, **15**, 4853.
33. P. J. Cozzone and O. Jardetzky, *Biochemistry*, 1975, **15**, 4860.
34. R. J. Labotka, T. Glonek and T. C. Myers, *J. Amer. Chem. Soc.*, 1976, **98**, 3699.
35. Y. F. Lam and G. Kotowycz, *Canad. J. Chem.*, 1977, **55**, 3620.
36. F. F. Brown, I. D. Campbell, R. Henson, C. W. J. Hirst and R. E. Richards, *Eur. J. Biochem.*, 1973, **38**, 54.
37. P. Tanswell, J. M. Thornton, A. V. Korda and R. J. P. Williams, *Eur. J. Biochem.*, 1975, **57**, 135.
38. M. Gabriel, D. Larcher, J. C. Boubel, A. A. Peguy and J. Torreilles, *Inorg. Chim. Acta*, 1978, **26**, 77.
39. L. D. Tuck and J. K. Baker, *Chem. Biol. Interactions*, 1973, **7**, 355.
40. S. Tran-Dinh, M. Roux and M. Ellenberger, *Nucleic Acids Res.*, 1975, **2**, 1101.
41. S. Tran-Dinh and J. M. Neumann, *Nucleic Acids Res.*, 1977, **4**, 397.
42. J. Granot, *FEBS Lett.*, 1978, **88**, 283.
43. J. Granot, *J. Amer. Chem. Soc.*, 1978, **100**, 2886.
44. U. Weser, G. J. Strobel, H. Rupp and W. Voelter, *Eur. J. Biochem.*, 1974, **50**, 91.
45. D. I. Hoult and R. E. Richards, *Proc. Roy. Soc.*, 1975, *A***344**, 311.
46. D. I. Hoult, S. J. W. Busby, D. G. Gadian, G. K. Radda, R. E. Richards and P. J. Seeley, *Nature*, 1974, **252**, 285.

47. M. Bárány, K. Bárány, C. T. Burt, T. Glonek and T. C. Myers, *J. Supramol. Struct.*, 1975, **3**, 125.
48. C. T. Burt, T. Glonek and M. Bárány, *J. Biol. Chem.*, 1976, **251**, 2584.
49. S. M. Cohen and C. T. Burt, *Proc. Nat. Acad. Sci. USA*, 1977, **74**, 4271.
50. J. Dawson, D. G. Gadian and D. R. Wilkie, *J. Physiol.*, 1976, **258**, 82P.
51. P. J. Seeley, S. J. W. Busby, D. G. Gadian, G. K. Radda and R. E. Richards, *Biochem. Soc. Trans.*, 1976, **4**, 62.
52. S. J. W. Busby, D. G. Gadian, G. K. Radda, R. E. Richards and P. J. Seeley, *Biochem. J.*, 1978, **170**, 103.
53. C. T. Burt, T. Glonek and M. Bárány, *Biochemistry*, 1976, **15**, 4850.
54. J. M. Chalovich, C. T. Burt, S. M. Cohen, T. Glonek and M. Bárány, *Arch. Biochem. Biophys.*, 1977, **182**, 681.
55. C. T. Burt, T. Glonek and M. Bárány, *Science*, 1977, **195**, 145.
56. M. J. Dawson, D. G. Gadian and D. R. Wilkie, *J. Physiol.*, 1977, **267**, 703.
57. J. Dawson, D. G. Gadian and D. R. Wilkie, in "NMR in Biology", R. A. Dwek, I. D. Campbell, R. E. Richards and R. J. P. Williams (eds.), Academic Press, 1977, pp. 290–322.
58. K. Yoshizaki, *J. Biochem.* (Tokyo), 1978, **84**, 11.
59. M. J. Dawson, D. G. Gadian and D. R. Wilkie, *Nature*, 1978, **274**, 861.
60. D. G. Gadian, D. I. Hoult, G. K. Radda, P. J. Seeley, B. Chance and C. Barlow, *Proc. Nat. Acad. Sci. USA*, 1976, **73**, 4446.
61. P. B. Garlick, G. K. Radda, P. J. Seeley and B. Chance, *Biochem. Biophys. Res. Comm.*, 1977, **74**, 1256.
62. W. E. Jacobus, G. J. Taylor and R. L. Nunnally, *Nature*, 1977, **265**, 756.
63. D. P. Hollis, R. L. Nunnally, G. J. Taylor, M. L. Weisfeldt and W. E. Jacobus, *J. Magn. Resonance*, 1978, **29**, 319.
64. R. Damadian, *Science*, 1971, **171**, 1151; U.S. Pat. 3,789,832 (1972).
65. W. E. Jacobus, G. J. Taylor, M. L. Weisfeldt, R. L. Nunnally and D. P. Hollis *Biomol. Struct. Funct.* [*Symp.*] (ed. P. F. Agris), Academic Press, 1977, pp. 207–215.
66. G. J. Taylor, W. E. Jacobus, D. P. Hollis, R. L. Nunnally and M. L. Weisfeldt, *Clin. Res.* (*A*), 1977, **25**, 257A.
67. D. P. Hollis, R. L. Nunnally, G. J. Taylor, M. L. Weisfeldt and W. E. Jacobus, *Biomol. Struct. Funct.* [*Symp.*] (ed. P. F. Agris), Academic Press, 1977, pp. 217–224.
68. B. H. Bulkley, R. L. Nunnally and D. P. Hollis, *Lab. Invest.*, 1978, **39**, 133.
69. P. A. Sehr, G. K. Radda, P. J. Bore and R. A. Sells, *Biochem. Biophys. Res. Comm.*, 1977, **77**, 195.
70. B. Chance, Y. Nakase, M. Bond, J. S. Leigh and G. McDonald, *Proc. Nat. Acad. Sci. USA*, 1978, **75**, 4925.
71. J. M. Salhany, S. J. Stohs, L. A. Reinke, G. M. Pieper and J. M. Hassing, *Biochem. Biophys. Res. Comm.*, 1979, **86**, 1077.
72. H. Nishikawa, S. Yamada, K. Yoshizaki and H. Watari, *Proc. Japan Acad.* (*B*), 1978, **54**, 397.
73. A. Colman and D. G. Gadian, *Eur. J. Biochem.*, 1976, **61**, 387.
74. D. G. Gadian, G. K. Radda, R. E. Richards and P. J. Seeley, in "Magnetic Resonance Studies in Biology", R. G. Shulman (ed.), Academic Press.
75. R. Damadian, *Science*, 1971, **171**, 1151.
76. K. S. Zaner and R. Damadian, *Science*, 1975, **189**, 729.
77. K. S. Zaner and R. Damadian, *Physiol. Chem. Phys.*, 1975, **7**, 437.
78. J. A. Koutcher and R. Damadian, *Physiol. Chem. Phys.*, 1977, **9**, 181.
79. L. R. Maxwell and L. H. Bennett, *Physiol. Chem. Phys.*, 1978, **10**, 59.
80. T. Glonek, *Biochem. Med.*, 1978, **19**, 246.

81. P. J. Cozzone, D. J. Nelson and O. Jardetzky, *Biochem. Biophys. Res. Comm.*, 1974, **60**, 341.
82. C. R. Bagshaw and G. H. Reed, *J. Biol. Chem.*, 1976, **251**, 1975.
83. A. Mak, L. B. Smillie and M. Bárány, *Proc. Nat. Acad. Sci. USA*, 1978, **75**, 3588.
84. S. L. Lee, A. Veis and T. Glonek, *Biochemistry*, 1977, **16**, 2971.
85. J. P. Yesinowski, private communication.
86. R. G. Griffin, abstracts of meeting of The Royal Society, London, March 14–15, 1979.
87. J. M. Salhany, T. Yamane, R. G. Shulman and S. Ogawa, *Proc. Nat. Acad. Sci. USA*, 1975, **72**, 4966.
88. M. Kainosho, K. Ajisaka and H. Nakazawa, *FEBS Lett.*, 1977, **80**, 375.
89. G. Navon, S. Ogawa, R. G. Shulman and T. Yamane, *Proc. Nat. Acad. Sci. USA.*, 1977, **74**, 888.
90. R. G. Shulman, G. Navon, S. Ogawa, T. Yamane, T. R. Brown, K. Urgurbil, P. Glynn and H. Rottenberg, *Dev. Bioenerg. Biomembr.*, 1977, **1**, 471.
91. S. Ogawa, R. G. Shulman, P. Glynn, T. Yamane and G. Navon, *Biochim. Biophys. Acta*, 1978, **502**, 45.
92. K. Urgubil, H. Rottenberg, P. Glynn and R. G. Shulman, *Proc. Nat. Acad. Sci. USA*, 1978, **75**, 2244.
93. G. Navon, S. Ogawa, R. G. Shulman and T. Yamane, *Proc. Nat. Acad. Sci. USA*, 1977, **74**, 87.
94. F. E. Evans and N. O. Kaplan, *Proc. Nat. Acad. Sci. USA*, 1977, **74**, 4909.
95. G. Navon, R. Navon, R. G. Shulman and T. Yamane, *Proc. Nat. Acad. Sci. USA*, 1978, **75**, 891.
96. S. M. Cohen, S. Ogawa, H. Rottenberg, P. Glynn, T. Yamane, T. R. Brown, R. G. Shulman and J. R. Williamson, *Nature*, 1978, **273**, 554.
97. S. Ogawa, H. Rottenberg, T. R. Brown, R. G. Shulman, C. L. Castillo and P. Glynn, *Proc. Nat. Acad. Sci. USA*, 1978, **75**, 1796.
98. R. P. Casey, D. Njus, G. K. Radda and P. A. Sehr, *Biochemistry*, 1977, **16**, 972.
99. P. J. Seeley, P. A. Sehr, D. G. Gadian, P. B. Garlick and G. K. Radda, in "NMR in Biology", R. A. Dwek, I. D. Campbell, R. E. Richards and R. J. P. Williams (eds.), Academic Press, 1977, pp. 247–275.
100. H. B. Pollard, H. Shindo, C. E. Creutz, C. J. Pazoles and J. S. Cohen, *J. Biol. Chem.*, 1979, in press.
101. D. Njus, P. A. Sehr, G. K. Radda, G. A. Ritchie and P. J. Seeley, *Biochemistry*, 1978, **17**, 4337.
102. A. F. Horwitz, in "Membrane Molecular Biology", C. F. Fox and A. D. Keith (eds.), Sinauer Associates, Stamford, Conn., 1973, pp. 164–191.
103. D. Chapman and E. Oldfield, *Methods Enzymol.*, 1974, **32**, 198.
104. L. W. Reeves, *Inst. Rev. Sci. Phys. Chem. Series Two*, 1975, Pt. 4, 139.
105. H. Wennerström and G. Lindblom, *Quart. Rev. Biophys.*, 1977, **10**, 67.
106. H. C. Andersen, *Ann. Rev. Biochem.*, 1978, **47**, 359.
107. L. L. M. van Deenen, in "The Molecular Basis of Membrane Function", D. C. Tosteson (ed.), Prentice-Hall, N.J., 1969, p. 47.
108. R. A. Haberkorn, J. Herzfeld and R. G. Griffin, *J. Amer. Chem. Soc.*, 1978, **100**, 1296.
109. E. G. Finer, *J. Magn. Resonance*, 1974, **13**, 76.
110. R. W. Barker, J. D. Bell, G. K. Radda and R. E. Richards, *Biochim. Biophys. Acta.*, 1972, **260**, 161.
111. A. F. Horwitz and M. P. Klein, *J. Supramol. Struct.*, 1972, **1**, 19.
112. V. F. Bystrov, Y. E. Shapiro, A. V. Viktorov, L. I. Barsukov and L. D. Bergelson, *FEBS Lett.*, 1972, **25**, 337.
113. M. P. Sheetz and S. I. Chan, *Biochemistry*, 1972, **11**, 4573.

114. D. G. Davis, *Biochem. Biophys. Res. Comm.*, 1972, **49**, 1492.
115. J. A. Berden, P. R. Cullis, D. I. Hoult, A. C. McLaughlin, G. K. Radda and R. E. Richards, *FEBS Lett.*, 1974, **46**, 55.
116. R. Göldner, W. Gründer and H. Schneider, *Z. Phys. Chem.* (Leipzig), 1975, **256**, 108.
117. M. C. Uhing, *Chem. Phys. Lipids*, 1975, **14**, 303.
118. K. Arnold, W. Gründer, R. Göldner and A. Hofmann, *Z. Phys. Chem.* (Leipzig), 1975, **256**, 522.
119. W. C. Hutton, P. L. Yeagle and R. B. Martin, *Chem. Phys. Lipids*, 1977, **19**, 255.
120. L. D. Bergelson and V. F. Bystrov, in "Biomembranes; Structure and Function", **35**, Proc. F.E.B.S. 9th meeting, Budapest, 1974, G. Gardos and I. Szasz (eds.), Elsevier, 1975, pp. 33–46.
121. L. I. Barsukov, Y. E. Shapiro, A. V. Viktorov, V. I. Volkova, V. F. Bystrov and L. D. Bergelson, *Biochem. Biophys. Res. Comm.*, 1974, **60**, 196.
122. L. I. Barsukov, Y. E. Shapiro, A. V. Viktorov, V. I. Volkova, V. F. Bystrov and L. D. Bergelson, *Chem. Phys. Lipids*, 1975, **14**, 211.
123. H. Grasdalen, L. E. Eriksson, J. Westman and A. Ehrenberg, *Biochim. Biophys. Acta*, 1977, **469**, 151.
124. L. I. Barsukov, V. I. Vokova, Y. E. Shapiro, A. V. Viktorov, V. F. Bystrov and L. D. Bergelson, *Soviet J. Bioorg. Chem.*, 1977, **3**, 991.
125. P. W. Nolden and T. Ackermann, *Biophys. Chem.*, 1976, **4**, 297.
126. A. C. McLaughlin, C. Grathwohl and R. E. Richards, *J. Magn. Resonance*, 1978, **31**, 283.
127. A. McLaughlin, C. Grathwohl and S. McLaughlin, *Biochim. Biophys. Acta*, 1978, **513**, 338.
128. C. A. Pasternak, E. Strachan, K. J. Micklem and J. Duncan, D.H.E.W.Publ.(N.I.H.) (USA) 1974 N.I.H. 75-796 Cell Surf. Malig. Workshop, pp. 147–151.
129. E. Sim, P. R. Cullis and R. E. Richards, *Biochem. J.*, 1975, **151**, 555.
130. E. Sim and C. A. Pasternak, *Biochem. J.*, 1976, **154**, 105.
131. R. G. Edwards and A. R. Hands, *Biochim. Biophys. Acta*, 1976, **431**, 303.
132. E. Sim and P. R. Cullis, *FEBS Lett.*, 1977, **79**, 340.
133. R. F. A. Zwaal, B. Roelofson and C. M. Colley, *Biochim. Biophys. Acta*, 1973, **300**, 159.
134. A. Chrzeszczyk, A. Wishnia and C. S. Springer, *Biochim. Biophys. Acta*, 1977, **470**, 161.
135. C. Huang and J. T. Mason, *Proc. Nat. Acad. Sci. USA*, 1978, **75**, 308.
136. B. de Kruijff, P. R. Cullis and G. K. Radda, *Biochim. Biophys. Acta*, 1975, **406**, 6.
137. P. L. Yeagle, W. C. Hutton, R. B. Martin, B. Sears and C. Huang, *J. Biol. Chem.*, 1976, **251**, 2110.
138. D. M. Michaelson, A. F. Horwitz and M. P. Klein, *Biochemistry*, 1973, **12**, 2637.
139. D. M. Michaelson, A. F. Horwitz and M. P. Klein, *Biochemistry*, 1974, **13**, 2605.
140. J. A. Berden, R. W. Barker and G. K. Radda, *Biochim. Biophys. Acta*, 1975, **375**, 186.
141. F. J. Castellino, *Arch. Biochem. Biophys.*, 1978, **189**, 465.
142. M. Koter, B. de Kruijff and L. L. M. van Deenen, *Biochim. Biophys. Acta*, 1978, **514**, 255.
143. A. Chrzeszczyk, A. Wishnia and C. S. Springer, in "Magnetic Resonance in Colloid and Surface Science", A.C.S., Symposia Series, Amer. Chem. Soc., Washington, USA, 1976, pp. 483–498.
144. P. Palatini, B. de Kruijff and J. de Gier, *Experientia*, 1978, **34**, 1580.
145. M. C. Blok, K. J. Hellingwerf, R. Kapstein and B. de Kruijff, *Biochim. Biophys. Acta*, 1978, **514**, 178.
146. J. E. Rothman and J. Lenard, *Science*, 1977, **195**, 743.
147. B. de Kruijff and P. Baken, *Biochim. Biophys. Acta*, 1978, **507**, 38.
148. M. Liaq and J. H. Prestegard, *Biochim. Biophys. Acta*, 1979, **550**, 157.
149. P. R. Cullis and M. J. Hope, *Nature*, 1978, **271**, 672.

150. A. C. McLaughlin, P. R. Cullis, J. A. Berden and R. E. Richards, *J. Magn. Resonance*, 1975, **20**, 146.
151. A. C. McLaughlin, P. R. Cullis, M. Hemminga, F. F. Brown and J. Brocklehurst, in "NMR in Biology", R. A. Dwek, I. D. Campbell, R. E. Richards, R. J. P. Campbell (eds.), Academic Press, 1977.
152. D. F. Bocian and S. I. Chan, *Ann. Rev. Phys. Chem.*, 1978, **29**, 307.
153. J. Seelig, *Biochim. Biophys. Acta*, 1978, **515**, 105.
154. P. L. Yeagle, *Accounts Chem. Res.*, 1978, **9**, 321.
155. P. R. Cullis and B. de Kruijff, *Biochim. Biophys. Acta*, 1978, **507**, 207.
156. B. J. Forrest, A. K. Grover, R. K. Buchinski and R. J. Cushley, private communication.
157. R. G. Griffin, L. Powers, J. Herzfeld, R. Haberkorn and P. S. Pershan, *Biophys. J.*, 1977, **17**, 84a.
158. R. G. Griffin, L. Powers, J. Herzfeld, R. Haberkorn and P. S. Pershan, Proc. Congr. Ampère 19th Magn. Resonance Relat. Phenom., 1976, pp. 257–260.
159. R. G. Griffin, L. Powers and P. S. Pershan, *Biochemistry*, 1978, **17**, 2718.
160. P. L. Yeagle, "Biomolecular Structure and Function", Academic Press, 1978, pp. 65–70.
161. P. L. Yeagle, W. C. Hutton, C. Huang and R. B. Martin, *Biochemistry*, 1977, **16**, 4344.
162. J. Seelig, H. Gally and R. Wohlgemuth, *Biochim. Biophys. Acta*, 1977, **467**, 109.
163. B. Büldt, H. U. Gally, A. Seelig, J. Seelig and G. Zaccai, *Nature*, 1978, **271**, 182.
164. P. R. Cullis, B. de Kruijff and R. E. Richards, *Biochim. Biophys. Acta*, 1976, **426**, 433.
165. W. Niederberger and J. Seelig, *J. Amer. Chem. Soc.*, 1976, **98**, 3704.
166. H. Gally, W. Niederberger and J. Seelig, *Biochemistry*, 1975, **14**, 3647.
167. P. R. Cullis and B. de Kruijff, *Biochim. Biophys. Acta*, 1976, **436**, 523.
168. M. F. Brown and J. Seelig, *Nature*, 1977, **269**, 721.
169. P. B. Hitchcock, R. Mason, K. M. Thomas and G. G. Shipley, *Proc. Nat. Acad. Sci. USA*, 1974, **71**, 3036.
170. J. Seelig and H. Gally, *Biochemistry*, 1976, **15**, 5199.
171. P. R. Cullis and B. de Kruijff, *Biochim. Biophys. Acta*, 1978, **513**, 31.
172. P. L. Yeagle, W. C. Hutton, C. Huang and R. B. Martin, *Biochemistry*, 1976, **15**, 2121.
173. C. F. Schmidt, Y. Barenholz and T. E. Thompson, *Biochemistry*, 1977, **16**, 2649.
174. P. L. Yeagle, W. C. Hutton and R. B. Martin, *Biochemistry*, 1978, **17**, 5745.
175. S. J. Kohler and M. P. Klein, *Biochemistry*, 1977, **16**, 519.
176. A. C. McLaughlin, P. R. Cullis, M. A. Hemminga, D. I. Hoult, G. K. Radda, G. A. Ritchie, P. J. Seeley and R. E. Richards, *FEBS Lett.*, 1975, **57**, 213.
177. P. R. Cullis and C. Grathwohl, *Biochim. Biophys. Acta*, 1977, **471**, 213.
178. N. F. Moore, E. J. Patzer, R. R. Wagner, P. L. Yeagle, W. C. Hutton and R. B. Martin, *Biochim. Biophys. Acta*, 1977, **464**, 234.
179. B. de Kruijff, P. R. Cullis, G. K. Radda, and R. E. Richards, *Biochim. Biophys. Acta*, 1976, **419**, 411.
180. B. de Kruijff, A. M. H. P. van den Besselaar, P. R. Cullis, H. van den Bosch and L. L. M. van Deenen, *Biochim. Biophys. Acta*, 1978, **514**, 1.
181. A. Stier, S. A. E. Finch and B. Bösterling, *FEBS Lett.*, 1978, **91**, 109.
182. D. G. Davis and G. Inesi, *Biochim. Biophys. Acta*, 1972, **282**, 180.
183. D. F. O'Brien, N. Zumbulyadis, F. M. Michaels and R. A. Ott, *Proc. Nat. Acad. Sci. USA*, 1977, **74**, 5222.
184. P. R. Cullis, *FEBS Lett.*, 1976, **68**, 173.
185. M. F. Brown and J. Seelig, *Biochemistry*, 1978, **17**, 381.
186. P. L. Yeagle, W. C. Hutton, C. Huang and R. B. Martin, *Proc. Nat. Acad. Sci. USA*, 1975, **72**, 3477.
187. P. R. Cullis and B. de Kruijff, *Biochim. Biophys. Acta*, 1978, **507**, 207.

188. P. R. Cullis, P. W. M. van Dijck, B. de Kruijff and J. de Gier, *Biochim. Biophys. Acta*, 1978, **513**, 21.
189. P. F. Mühlradt, V. Wray and V. Lehmann, *Eur. J. Biochem.*, 1977, **81**, 193.
190. V. Lehmann and E. Rupprecht, *Eur. J. Biochem.*, 1977, **81**, 443.
191. P. D. Rick, L. W. Fung, C. Ho and M. J. Osborn, *J. Biol. Chem.*, 1977, **14**, 4904.
192. R. E. Torregrossa, R. A. Makula and W. R. Finnerty, *J. Bacteriol.*, 1977, **131**, 486.
193. I. M. Armitage, D. L. Shapiro, H. Furthmayr and V. T. Marchesi, *Biochemistry*, 1977, **16**, 1317.
194. E. J. J. van Zoelen, A. N. M. van Dijck, B. de Kruijff, A. J. Verkleij and L. L. M. van Deenen, *Biochim. Biophys. Acta*, 1978, **514**, 9.
195. E. J. J. van Zoelen, B. de Kruijff and L. L. M. van Deenen, *Biochim. Biophys. Acta*, 1978, **508**, 97.
196. C. Mombers, A. J. Verkleij, J. de Gier and L. L. M. van Deenen, *Biochim. Biophys. Acta*, 1979, **551**, 271.
197. L. W. Fung, E. A. Pratt and C. Ho, *Biochemistry*, 1979, **18**, 317.
198. R. J. Cushley and B. J. Forrest, *Canad. J. Chem.*, 1977, **55**, 220.
199. J. Frenzel, K. Arnold and P. Nuhn, *Biochem. Biophys. Acta*, 1978, **507**, 185.
200. P. R. Cullis, A. J. Verkleij and P. H. J. T. Ververgaert, *Biochim. Biophys. Acta*, 1978, **513**, 11.
201. H. D. Pierce, A. M. Unrau and A. C. Oehlschlager, *Canad. J. Biochem.*, 1978, **56**, 801.
202. A. Marker, L. G. Paleg and T. M. Stopswood, *Chem. Phys. Lipids*, 1978, **22**, 39.
203. G. L. Jendrasiak and T. N. Estep, *Chem. Phys. Lipids*, 1977, **18**, 181.
204. K. Beyer and M. Klingenberg, *Biochemistry*, 1978, **17**, 1424.
205. W. H. Huestis and M. A. Raftery, *Biochem. Biophys. Res. Comm.*, 1972, **49**, 428.
206. T. O. Henderson, A. J. R. Costello and A. Omachi, *Proc. Nat. Acad. Sci. USA*, 1974, **71**, 2487.
207. R. J. Labotka, T. Glonek, M. A. Hruby and G. R. Honig, *Biochem. Med.*, 1976, **15**, 311.
208. A. J. Costello, W. E. Marshall, A. Omachi and T. O. Henderson, *Biochim. Biophys. Acta*, 1976, **427**, 481.
209. W. H. Huestis and M. A. Raftery, *Biochemistry*, 1975, **14**, 1886.
210. W. E. Marshall, A. J. R. Costello, T. O. Henderson and A. Omachi, *Biochim. Biophys. Acta*, 1977, **490**, 290.
211. E. T. Fossel and A. K. Solomon, *Biochim. Biophys. Acta*, 1976, **436**, 505.
212. R. J. Gupta, *J. Biol. Chem.*, 1976, **251**, 6815.
213. A. J. R. Costello, W. E. Marshall, A. Omachi and T. O. Henderson, *Biochim. Biophys. Acta*, 1977, **491**, 469.
214. R. K. Gupta, J. L. Benovic and Z. B. Rose, *J. Biol. Chem.*, 1978, **253**, 6165.
215. R. K. Gupta, J. L. Benovic and Z. B. Rose, *J. Biol. Chem.*, 1978, **253**, 6172.
216. E. R. P. Zui derweg, G. G. M. van Beek and S. H. de Bruin, *Eur. J. Biochem.*, 1979, **94**, 297.
217. A. J. R. Costello, T. Glonek and T. C. Myers, *Carbohydrate Res.*, 1976, **46**, 159.
218. J. Guo, R. F. Sprecher and N. C. Li, *J. Magn. Resonance*, 1975, **18**, 427.
219. T. Kagimoto, F. Hayashi, M. Yamasaki, Y. Morino, K. Akasaka and S. Kishimoto, *Experientia*, 1978, **34**, 1092.
220. L. C. Smith, H. J. Pownall and A. M. Gotto, *Ann. Rev. Biochem.*, 1978, **47**, 751.
221. G. Assmann, E. A. Sokoloski and H. B. Brewer, *Proc. Nat. Acad. Sci. USA*, 1974, **71**, 549.
222. T. Glonek, T. O. Henderson, A. W. Kruski and A. M. Scanu, *Biochim. Biophys. Acta*, 1974, **348**, 155.
223. T. O. Henderson, A. W. Kruski, L. G. Davis, T. Glonek and A. M. Scanu, *Biochemistry*, 1975, **14**, 1915.

224. E. B. Brasure, T. O. Henderson, T. Glonek, N. M. Pattnaik and A. M. Scanu, *Biochemistry*, 1978, **17**, 3934.
225. P. L. Yeagle, R. G. Landon and R. B. Martin, *Biochemistry*, 1977, **16**, 3487.
226. P. L. Yeagle, R. B. Martin, L. Pottenger and R. G. Langdon, *Biochemistry*, 1978, **17**, 2707.
227. W. S. M. Arrata, C. T. Burt and S. Corder, *Fertil. Steril.*, 1978, **30**, 329.
228. C. T. Burt and J. M. Chalovich, *Biochem. Biophys. Acta*, 1978, **529**, 186.
229. A. L. Olins and D. E. Olins, *Science*, 1974, **183**, 330.
230. S. Hanlon, T. Glonek and A. Chan, *Biochemistry*, 1976, **15**, 3869.
231. R. I. Cotter and D. M. J. Lilley, *FEBS Lett.*, 1977, **82**, 63.
232. N. R. Kallenbach, D. W. Appleby and C. H. Bradley, *Nature*, 1978, **272**, 134.
233. A. Yamada, H. Kaneko, K. Akasaka and H. Hatano, *FEBS Lett.*, 1978, **93**, 16.
234. D. G. Gorenstein, J. B. Findlay, R. K. Momii, B. A. Luxon and D. Kar, *Biochemistry*, 1976, **15**, 3796.
235. D. J. Patel, *Biopolymers*, 1976, **15**, 533.
236. D. J. Patel, *Biopolymers*, 1977, **16**, 1635.
237. K. Akasaka, A. Yamada and H. Hatano, *FEBS Lett.*, 1975, **53**, 339.
238. A. Yamada, K. Akasaka and H. Hatano *Biopolymers*, 1976, **15**, 1315.
239. A. Yamada, K. Akasaka and H. Hatano, *Biopolymers*, 1978, **17**, 749.
240. K. Akasaka, A. Yamada and H. Hatano, *Bull. Chem. Soc. Japan*, 1977, **50**, 2858.
241. T. R. Tritton and I. M. Armitage, *Nucleic Acids Res.*, 1978, **5**, 3855.
242. M. Guéron, *FEBS Lett.*, 1971, **19**, 264.
243. L. M. Weiner, J. M. Backer and A. I. Rezvuhkin, *FEBS Lett.*, 1974, **41**, 40.
244. M. Guéron and R. G. Shulman, *Proc. Nat. Acad. Sci. USA*, 1975, **72**, 3482.
245. F. Hayashi, K. Akasaka and H. Hatano, *Biopolymers*, 1977, **16**, 655.
246. P. J. M. Salomink, T. Swarthof and C. W. Hilbers, *Biochemistry*, in press.
247. J. E. Coleman, R. A. Anderson, R. G. Ratcliffe and I. M. Armitage, *Biochemistry*, 1976, **15**, 5419.
248. G. J. Garssen, C. W. Hilbers, J. G. G. Schoenmakers and J. H. van Boom, *Eur. J. Biochem.*, 1977, **81**, 453.
249. A. M. Goetze and J. H. Richards, *Biochemistry*, 1977, **16**, 228.
250. A. M. Goetze and J. H. Richards, *Proc. Nat. Acad. Sci. USA*, 1977, **74**, 2109.
251. P. Gettins, M. Potter, S. Rudikoff and R. A. Dwek, *FEBS Lett.*, 1977, **84**, 87.
252. S. Wain-Hobson, S. K. Dower, P. Gettins, D. Givol, A. C. McLaughlin, I. Pecht, C. A. Sunderland and R. A. Dwek, *Biochem. J.*, 1977, **165**, 227.
253. A. M. Goetze and J. H. Richards, *Biochemistry*, 1978, **17**, 1733.
254. Y. V. Subbarao, R. Ellis, G. M. Paulsen and J. V. Paukstelis, *Soil Sci. Soc. Amer. J.*, 1977, **41**, 316.
255. I. K. O'Neill and C. P. Richards, *Chem. Ind.*, 1978, 65.
256. M. Douglass, M. P. McDonald, I. K. O'Neill, R. Osner and C. P. Richards, *J. Food Technol.*, 1979, **14**, 193.
257. K. Beyreuther, H. Raufuss, O. Schrecker and W. Hengstenberg, *Eur. J. Biochem.*, 1977, **75**, 275.
258. M. Gassner, D. Stehlik, O. Schrecker, W. Henstenberg and H. Ruterjans, *Eur. J. Biochem.*, 1977, **75**, 287.
259. A. S. Mildvan and M. Cohn, *Adv. Enzymol.*, 1970, **33**, 1.
260. M. Cohn and J. Reuben, *Accounts Chem. Res.*, 1971, **4**, 214.
261. A. S. Mildvan and J. L. Engle, *Methods Enzymol.*, 1972, **26**, 654.
262. P. J. Quilley and G. A. Webb, *Coordination Chem. Rev.*, 1974, **12**, 407.
263. A. S. Mildvan and R. K. Gupta, *Methods Enzymol.*, 1978, **49**, 322.
264. C. S. Johnson, *Adv. Magn. Resonance*, 1965, **1**, 33.

265. A. G. Redfield, *Methods Enzymol.*, 1978, **49**, 359.
266. B. D. N. Rao and M. Cohn, *Biophys. J.*, 1978, **24**, 258.
267. A. S. Mildvan, *Ann. Rev. Biochem.*, 1974, **43**, 357.
268. M. J. Wimmer and I. A. Rose, *Ann. Rev. Biochem.*, 1978, **47**, 1031.
269. R. D. Cornelius, P. A. Hart and W. W. Cleland, *Inorg. Chem.*, 1977, **16**, 2799.
270. R. D. Cornelius and W. W. Cleland, *Biochemistry*, 1978, **17**, 3279.
271. J. Granot, M. M. Werber and A. Danchin, *Bioinorg. Chem.*, 1978, **9**, 81.
272. F. Eckstein, *Angew. Chem. Internat. Edn.*, 1975, **14**, 160.
273. F. Eckstein, V. W. Armstrong and H. Sternbach, *Proc. Nat. Acad. Sci. USA*, 1976, **73**, 2987.
274. F. Eckstein and R. S. Goody, *Biochemistry*, 1976, **15**, 1685.
275. E. K. Jaffe and M. Cohn, *Biochemistry*, 1978, **17**, 652.
276. P. M. Burgers and F. Eckstein, *Biochemistry*, 1979, **18**, 593.
277. P. D. Boyer, *Accounts Chem. Res.*, 1978, **11**, 219.
278. W. A. Blätteer and J. R. Knowles, *J. Amer. Chem. Soc.*, 1979, **101**, 510.
279. J. P. Richard, H. T. Ho and P. A. Frey, *J. Amer. Chem. Soc.*, 1978, **100**, 7756.
280. J. P. Richard and P. A. Frey, *J. Amer. Chem. Soc.*, 1978, **100**, 7757.
281. M. Cohn and B. D. Rao, *Bull. Magn. Resonance*, 1979, **1**, 38.
282. "Enzyme Nomenclature", Recommendations (1964) of the International Union of Biochemistry, Elsevier, 1965.
283. "Enzyme Nomenclature", Recommendations (1972) of the International Union of Pure and Applied Chemistry and the International Union of Biochemistry, Elsevier, 1973.
284. S. J. W. Busby, D. G. Gadian, J. R. Griffiths, G. K. Radda and R. E. Richards, *Eur. J. Biochem.*, 1976, **63**, 23.
285. M. K. Battersby and G. K. Radda, *FEBS Lett.*, 1976, **72**, 319.
286. S. A. E. Finch, T. F. Slater and A. Stier, *Biochem. J.*, 1979, **177**, 925.
287. E. K. Jaffe and M. Cohn, *J. Biol. Chem.*, 1978, **253**, 4823.
288. T. Nowak and A. S. Mildvan, *Biochemistry*, 1972, **11**, 2813.
289. T. Nowak and A. S. Mildvan, *Biochemistry*, 1972, **11**, 2819.
290. G. H. Reed and M. Cohn, *J. Biol. Chem.*, 1973, **248**, 6436.
291. C. H. Fung, A. S. Mildvan, A. Allerhand, R. Komoroski and M. C. Scrutton, *Biochemistry*, 1973, **12**, 621.
292. E. Melamud and A. S. Mildvan, *J. Biol. Chem.* 1975, **250**, 8193.
293. D. L. Sloan and A. S. Mildvan, *J. Biol. Chem.*, 1976, **251**, 2412.
294. A. S. Mildvan, D. L. Sloan, C. H. Fung, R. K. Gupta and E. Melamud, *J. Biol. Chem.*, 1976, **251**, 2431.
295. G. L. Cottam and R. L. Ward, *Biochem. Biophys. Res. Comm.*, 1975, **64**, 797.
296. R. K. Gupta and A. S. Mildvan, *J. Biol. Chem.*, 1977, **252**, 5967.
297. R. K. Gupta and J. L. Benovic, *J. Biol. Chem.*, 1978, **253**, 8878.
298. G. Lowe and B. S. Sproat, *J. Chem. Soc., Chem. Comm.*, 1978, 783.
299. G. Lowe and B. S. Sproat, *J. Chem. Soc., Perkin I*, 1979, 1622.
300. B. D. Nageswara Rao, M. Cohn and R. K. Scopes, *J. Biol. Chem.*, 1978, **253**, 8056.
301. F. M. Raushel, P. M. Anderson and J. J. Villafranca, *J. Biol. Chem.*, 1978, **253**, 6627.
302. E. J. Milner-White and D. S. Rycroft, *Biochem. J.*, 1977, **167**, 827.
303. T. R. Brown, D. G. Gadian, P. B. Garlick, G. K. Radda, P. J. Seeley and P. Styles, in "Frontiers of Biological Energetics", Vol. 2, P. L. Dutton (ed.), Academic Press, 1979, p. 1341.
304. B. D. Nageswara Rao, D. H. Buttlaire and M. Cohn, *J. Biol. Chem.*, 1976, **251**, 6981.
305. B. D. Nageswara Rao and M. Cohn, *J. Biol. Chem.*, 1977, **252**, 3344.
306. B. D. Nageswara Rao and M. Cohn, *Proc. Nat. Acad. Sci. USA*, 1977, **74**, 5355.
307. B. D. Nageswara Rao, M. Cohn and L. Noda, *J. Biol. Chem.*, 1978, **253**, 1149.

308. T. R. Brown and S. Ogawa, *Proc. Nat. Acad. Sci. USA*, 1977, **74**, 3627.
309. T. R. Brown and S. Ogawa, in "Biomolecular Structure and Function", P. F. Agris (ed.), Academic Press, 1978, p. 369.
310. K. F. R. Sheu and P. A. Frey, *J. Biol. Chem.*, 1977, **252**, 4445.
311. D. G. Gadian, G. K. Radda and R. E. Richards, *Biochem. Biophys. Acta*, 1974, **358**, 57.
312. W. J. Ray, A. S. Mildvan and J. B. Grutzner, *Arch. Biochem. Biophys.*, 1977, **184**, 453.
313. W. J. Ray and A. S. Mildvan, *Biochemistry*, 1973, **12**, 3733.
314. B. L. Bean, R. Koren and A. S. Mildvan, *Biochemistry*, 1977, **16**, 3322.
315. D. L. Sloan, L. A. Loeb, A. S. Mildvan and R. J. Feldman, *J. Biol. Chem.*, 1975, **250**, 8913.
316. K. F. R. Sheu and P. A. Frey, *J. Biol. Chem.*, 1978, **253**, 3378.
317. H. Csopak and T. Drakenberg, *FEBS Lett.*, 1973, **30**, 296.
318. R. S. Zukin, D. P. Hollis and G. A. Gray, *Biochem. Biophys. Res. Comm.*, 1973, **53**, 238.
319. R. S. Zukin, D. P. Hollis, G. A. Gray, *Biochem. Biophys. Res. Comm.*, 1973, **53**, 686.
320. J. L. Bock and B. Sheard, *Biochem. Biophys. Res. Comm.*, 1975, **66**, 24.
321. W. E. Hull, S. E. Halford, H. Gutfreund and B. D. Sykes, *Biochemistry*, 1976, **15**, 1547.
322. J. F. Chlebowski, I. M. Armitage, P. P. Tusa and J. E. Coleman, *J. Biol. Chem.*, 1976, **251**, 1207.
323. J. F. Chlebowski, I. M. Armitage and J. E. Coleman, *J. Biol. Chem.*, 1977, **252**, 7053.
324. J. L. Bock and A. Kowalsky, *Biochim. Biophys. Acta*, 1978, **526**, 135.
325. J. L. Bock and M. Cohn, *J. Biol. Chem.*, 1978, **253**, 4082.
326. R. L. Van Etten and J. M. Risley, *Proc. Nat. Acad. Sci. USA*, 1978, **75**, 4784.
327. S. K. Benkovic, J. J. Villafranca and J. J. Kleinschuster, *Arch. Biochem. Biophys.*, 1973, **155**, 458.
328. A. S. Mildvan and C. M. Grisham, *Structure and Bonding* (Berlin), 1974, **20**, 1.
329. Y. Arata, S. Kimura, H. Matsuo and K. Narita, *Biochemistry*, 1979, **18**, 18.
330. D. G. Gorenstein and A. Wyrwicz, *Biochem. Biophys. Res. Comm.*, 1973, **54**, 976.
331. W. Haar, J. C. Thompson, W. Maurer and H. Rüterjans, *Eur. J. Biochem.*, 1973, **40**, 259.
332. D. G. Gorenstein, A. M. Wyrwicz and J. Bode, *J. Amer. Chem. Soc.*, 1976, **98**, 2308.
333. G. C. Y. Lee and S. I. Chan, *Biochem. Biophys. Res. Comm.*, 1971, **43**, 142.
334. G. R. Reeck, T. B. Nelson, J. V. Paukstelis and D. D. Mueller, *Biochem. Biophys. Res. Comm.*, 1977, **74**, 643.
335. D. G. Gorenstein and J. B. Findlay, *Biochem. Biophys. Res. Comm.*, 1976, **72**, 640.
336. D. J. Hamm and B. S. Cooperman, *Biochemistry*, 1978, **17**, 4033.
337. D. A. Harris, *Biochim. Biophys. Acta*, 1978, **463**, 245.
338. C. Grisham and A. S. Mildvan, *J. Supramol. Struct.*, 1975, **3**, 304.
339. M. R. Webb, G. G. McDonald and D. A. Trentham, *J. Biol. Chem.*, 1978, **253**, 2908.
340. T. R. Brown, K. Ugurbil and R. G. Schulman, *Proc. Nat. Acad. Sci. USA*, 1977, **74**, 5551.
341. I. Bertini, C. Luchinat and A. Scozzafava, *FEBS Lett.*, 1978, **93**, 251.
342. T. Nowak, A. S. Mildvan and G. L. Kenyon, *Biochemistry*, 1973, **12**, 1690.
343. M. R. Webb, D. N. Standring and J. R. Knowles, *Biochemistry*, 1977, **16**, 2738.
344. I. D. Campbell, P. A. Kiener, S. G. Waley and R. Wolfenden, *Biochem. Soc. Trans.*, 1977, **5**, 750.
345. I. D. Campbell, R. B. Jones, P. A. Kiener, E. Richards, S. G. Waley and R. Wolfenden, *Biochem. Biophys. Res. Comm.*, 1978, **83**, 347.
346. J. J. Villafranca, S. G. Rhee and P. B. Chock, *Proc. Nat. Acad. Sci. USA*, 1978, **75**, 1255.
347. M. S. Balakrishnan, T. R. Sharp and J. J. Villafranca, *Biochem. Biophys. Res. Comm.*, 1978, **85**, 991.
348. C. H. Lee and R. H. Sarma, in "Structure and Conformation of Nucleic Acids and Protein-Nucleic Acid Interactions", M. Sundaralingam and S. T. Rao (eds.), University Park Press, Baltimore, 1975, p. 631.

349. C. H. Lee and R. H. Sarma, *J. Amer. Chem. Soc.*, 1975, **97**, 1225.
350. C. H. Fung, R. J. Feldmann and A. S. Midlvan, *Biochemistry*, 1976, **15**, 75.
351. H. J. Grande, R. L. Houghton and C. Veeger, *Eur. J. Biochem.*, 1973, **37**, 563.
352. P. A. Hart, private communication.
353. M. Martinez-Carrion, *Eur. J. Biochem.*, 1975, **54**, 39.
354. S. J. W. Busby, D. G. Gadian, G. K. Radda, R. E. Richards and P. J. Seeley, *FEBS Lett.*, 1975, **55**, 14.
355. K. Feldmann and E. J. M. Helmreich, *Biochemistry*, 1976, **15**, 2394.
356. K. Feldmann and W. E. Hull, *Proc. Nat. Acad. Sci. USA*, 1977, **74**, 856.
357. R. H. Sarma and R. J. Mynott, *J. Amer. Chem. Soc.*, 1973, **95**, 1641.
358. R. H. Sarma and R. J. Mynott, "Proceedings of the International Symposium on the Conformation of Biological Molecules and Polymers." Symposia on Quantum Chem. Biochem., Vol. 5, B. Pullmann and E. D. Bergmann (eds.), Academic Press, 1973, p. 591.
359. R. H. Sarma, R. J. Mynott, F. E. Hruska and D. J. Wood, *Canad. J. Chem.*, 1973, **51**, 1843.
360. R. H. Sarma and R. J. Mynott, *J. Amer. Chem. Soc.*, 1973, **95**, 7470.
361. R. H. Sarma and R. J. Mynott, *Org. Magn. Resonance*, 1972, **4**, 577.
362. M. Blumenstein, *Biochemistry*, 1975, **14**, 5004.
363. D. L. Sloan and A. S. Mildvan, *Biochemistry*, 1974, **13**, 1711.
364. J. Feeney, B. Birdsall, G. C. K. Roberts and A. S. V. Burgen, *Nature*, 1975, **257**, 564.
365. J. Feeney, B. Birdsall, G. C. K. Roberts and A. S. V. Burgen, in "NMR in Biology", R. A. Dwek, I. D. Campbell, R. E. Richards and R. J. P. Williams (eds.), Academic Press, 1977, p. 111.
366. B. Birdsall, G. C. K. Roberts, J. Feeney and A. S. V. Burgen, *FEBS Lett.*, 1977, **80**, 313.
367. D. I. Hoult, *J. Magn. Resonance*, 1979, **33**, 183.
368. I. K. O'Neill, M. Sargent and M. L. Trimble, Abstracts of the Ninth International Symposium on Carbohydrate Chemistry, London, April 1978.
369. P. H. Bolton and G. Bodenhausen, *J. Amer. Chem. Soc.*, 1979, **101**, 1080.
370. B. J. Forrest and R. J. Cushley, *Atherosclerosis*, 1977, **28**, 309.

SUBJECT INDEX

*The numbers in **bold** indicate the pages on which the topic is discussed in detail*

D

E

F

G

H

N

T

V

This Page Intentionally Left Blank

Cumulative index of topics covered in Volumes 1 to 10 of this series

Cumulative index of authors who have contributed to Volumes 1–10

This Page Intentionally Left Blank